Identify the transition from a fluid to soil material structure in the fresh state and determine the associated failure criterion based on strength

Versteegh, Linda

Award date:
2023

EINDHOVEN UNIVERSITY OF TECHNOLOGY

Identify the transition from a fluid to soil material structure in the fresh state and determine the associated failure criterion based on strength

Master Thesis

L. (Linda) Versteegh

Supervisors:
Prof. dr. ir. T.A.M. Salet
Dr. ir. R.J.M. Wolfs
Ir. D.H. Bos
Dr. Q. Yu

7K45M0 Graduation Project
Structural Engineering and Design
Eindhoven University of Technology

Eindhoven, 3 May 2023

ABSTRACT

In 3D concrete printing, concrete must flow through the hose but needs to remain static when deposited on the print bed. Two regimes could be distinguished in this process, fluid and soil behavior. Fluid behavior is described by the viscosity of the mixture. Soil behavior is dominated by inter-particle forces, dilatancy, and local frictional effects. A material used for 3D concrete printing could behave as a fluid or soil based on the volume fraction. By increasing the volume fraction of a material with fluid behavior, a transition to soil behavior takes place. The characterizing parameters of the transition point are still unknown in the fresh state of concrete used for 3D printing. Therefore the transition from a fluid to a soil material structure in the fresh state has been identified with the associated failure criterion based on strength.

The transition point has been determined for three different mixtures with varying volume fractions: syrup and glass beads, cement paste, and cement paste with sand aggregates. The mixtures have been tested with two experimental tests, the RAM Extruder and Direct Shear Test. The RAM Extruder is an experimental test based on rheology, where the viscosity of a mixture could be obtained. The Direct Shear Test is a test mainly used in soil mechanics, where the cohesion and angle of internal friction can be obtained.

Based on the results from the RAM Extruder and Direct Shear Test, the transition point from fluid behavior to soil behavior has been observed in two mixtures, cement paste and cement paste with sand aggregates. The mixtures with syrup and glass beads all behave as a fluid, where the viscosity of the mixtures is dominant. The transition point for the cement paste mixture was found between volume fractions 0.53 and 0.56. The mixture with a volume fraction of 0.53 and lower behaved as a Bingham fluid, a fluid with cohesion, where the cement particles formed chemical and physical bonds between each other. The cement paste with a volume fraction of 0.56 behaved as soil, where friction between the cement particles occurred. In the cement paste with sand aggregates mixture, the transition point was found around a volume fraction of 0.50. The volume fraction with a value below 0.50 behaved as a fluid, where cohesion between the cement and sand particles was dominant. For volume fractions higher than 0.50, the friction between the cement and sand particles was dominant, indicating that these mixtures behave as soil.

The transition point can be identified for mixtures in the fresh state. The transition point varies for different mixtures based on particle interactions, particle shape, and particle size.

PREFACE

With this thesis about identifying a transition from a fluid to soil material behavior in fresh concrete suitable for 3D concrete printing, I conclude my time as a student of the master Architecture, Building and Planning, specialization Structural Engineering and Design, at the faculty Built Environment of the Eindhoven University of Technology. Before starting my master's at the TU/e, I developed an interest in structural engineering at the Avans University of applied sciences. After graduating from the Avans, I pursued a master's in structural engineering at the TU/e. For the final project of my master's, I decided on the current research out of interest in the experimental approach in research and the new development of concrete printing. This helped me broaden my knowledge and understanding of concrete and structural design.

The research is carried out under the supervision of the graduation committee, consisting of Prof. dr. ir. T.A.M. Salet, Dr. ir. R.J.M. Wolfs, Ir. D.H. Bos and Dr. Q. Yu. I want to thank my supervisors for sharing their enthusiasm and knowledge of the research content and their guidance through the process. I want to thank Theo Salet and Rob Wolfs for stepping in and supervising the graduation project. I also want to thank Derk Bos for the valuable discussion, it was a great pleasure learning and working with you. Also, thanks to Qingliang Yu for being my third supervisor and providing the materials. Last, I want to thank Freek Bos for the helpful discussion and supervision at the beginning of the graduation project.

Much of the research has been performed in the structural laboratory in Eindhoven. I want to thank the laboratory employees for their guidance, singing, and entertainment while performing the experimental tests.

I am also very grateful for all the support I received during my studies. First, I would really like to thank Ruben Frijns, Rianne Teeuwen, and Jarl Lemmens for prereading my thesis. Second, I want to thank my family for their unconditional support and love. Last, I would like to thank my friends and fellow students, who always supported me and helped me enjoy my student life.

CONTENTS

Contents vii

List of Figures ix

List of Tables xi

List of Symbols xiii

1 Introduction 1

2 Theoretical background 3
2.1 Fluid behavior . . . 3
2.1.1 General Newtonian Fluid models . . . 3
2.1.2 Viscosity . . . 4
2.1.3 Krieger-Dougherty . . . 5
2.2 Solid behavior . . . 6
2.2.1 Inter-particle forces . . . 6
2.3 Soil behavior . . . 8
2.4 Transition . . . 9

3 Method 11
3.1 Material . . . 12
3.2 Direct Shear Test . . . 14
3.3 RAM Extruder . . . 17

4 Results and discussion: Direct Shear Test 21
4.1 Mixture Syrup Glass (SG) . . . 21
4.2 Mixture Cement Paste (CP) . . . 22
4.3 Mixture Cement Sand (CS) . . . 23
4.4 Comparison between mixture compositions . . . 25

5 Results and discussion: RAM Extruder 29
5.1 Mixture Syrup Glass (SG) . . . 30
5.2 Mixture Cement Paste (CP) . . . 31
5.3 Mixture Cement Sand (CS) . . . 33
5.4 Comparison between mixture compositions . . . 35

6 Comparison between Direct Shear Test and RAM Extruder 39

7 Conclusion 43

8 Recommendations 45

Bibliography 47

Appendix 49

A Density 51

B Results DST for mixture SG 55

C Results DST for mixture CP 65

D Results DST for mixture CS **75**

E Results RAM Extruder for mixture SG **85**

F Results RAM Extruder for mixture CP **91**

G Results RAM Extruder for mixture CS **103**

H Development over time **111**

I Results RAM Extruder for the experimental program with varying speeds **115**

J Results DST with varying heights **125**

K Results DST for other mixtures **137**

List of Figures

2.1 Overview of several Generalized Newtonian Fluid models based on [9]. 4
2.2 Krieger-Dougherty graph increase of particles based on [35]. 5
2.3 Flow around particle in liquid [35]. 6
2.4 Krieger-Dougherty graph with maximum packing density. 7
2.5 Elastic particle interaction based on [2]. 8
2.6 Solid friction particle interaction based on [2]. 8
2.7 Collision between two particles based on [2]. 8
2.8 Mohr-Coulomb failure criterion. 8
2.9 Dilatancy effect with particles. 9

3.1 Approach adding water to particles. 11
3.2 Approach adding particles to water. 12
3.3 Microscopic view of glass aggregates [12]. 12
3.4 Microscopic view of sand aggregates [12]. 12
3.5 Particle size distribution curves for glass beads, cement grains, and sand grains. 14
3.6 Test setup of Direct Shear Test. 15
3.7 Abstract test setup of Direct Shear Test based on [12]. 15
3.8 Determination of the effective area in DST. 16
3.9 Typical shear stress versus horizontal displacement for a soil based on [11] and [41]. . . 16
3.10 Determination of maximum shear stress from DST. 17
3.11 Abstract test setup of RAM Extruder. 17
3.12 Test setup of RAM Extruder. 18
3.13 Flow inside the barrel of RAM Extruder based on [33]. 19
3.14 Build-up of material in the barrel of RAM Extruder. 19
3.15 Typical result for experimental program 1 for RAM Extruder. 20
3.16 Typical normal force versus vertical displacement result of RAM Extruder. 20

4.1 Shear stress over normal stress for mixture SG. 22
4.2 Shear stress over normal stress for mixture CP. 23
4.3 Shear stress over normal stress for mixture CS. 24
4.4 Compaction of a loose mixture at sides of the shear box based on [20]. 25
4.5 Shear band evaluation in mixture based on [20]. 25
4.6 Angle of internal friction per volume fraction for different mixtures. 26
4.7 Difference in particle compaction, left mixture CS, right mixture CP (drawing not to scale). 27
4.8 Cohesion per volume fraction for different mixtures. 27

5.1 Typical result for RAM Extruder with varying speed rates (mixture CP, VF 0.48 and die diameter 12mm). 29
5.2 Normal force per volume fraction for mixture SG with different die diameters. 31
5.3 Normal force per volume fraction for mixture CP with different die diameters. 32
5.4 Normal force per volume fraction for mixture CS with different die diameters. 33
5.5 Principle of pressure bleeding based on [8][39]. 34
5.6 Normal force per volume fraction and die diameter for different mixtures. 36

6.1 Normalized static yield stress peak per volume fraction for mixture CP. 40

J.1 Abstract explanation of varied heights in DST. 125

List of Tables

3.1 Relative mix proportions by weight. . . . 13
3.2 Densities of used materials. . . . 13
3.3 Experimental program 1 for RAM Extruder. . . . 18

4.1 Results of DST for mixture SG. . . . 21
4.2 Results of DST for mixture CP. . . . 22
4.3 Results of DST for mixture CS. . . . 24

5.1 Overview of experimental results for mixture SG, volume fraction against die diameter: green: positive results, orange: mediocre results, red: negative results, gray: material not tested. . . . 30
5.2 Overview of experimental results for mixture CP, volume fraction against die diameter: green: positive results, orange: mediocre results, red: negative results, gray: material not tested. . . . 31
5.3 Overview of experimental results for mixture CS, volume fraction against die diameter: green: positive results, orange: mediocre results, red: negative results, gray: material not tested. . . . 33
5.4 Overview of experimental results for mixtures SG, CP, and CS, volume fraction against die diameter: green: positive results, orange: mediocre results, red: negative results, gray: material not tested. . . . 35

B.1 Static yield stress peak values for mixture SG VF0.47 in kPa . . . 55
B.2 Static yield stress peak values for mixture SG VF0.50 in kPa . . . 57
B.3 Static yield stress peak values for mixture SG VF0.53 in kPa . . . 59
B.4 Static yield stress peak values for mixture SG VF0.56 in kPa . . . 61

C.1 Static yield stress peak values for mixture CP VF0.47 in kPa . . . 65
C.2 Static yield stress peak values for mixture CP VF0.50 in kPa . . . 67
C.3 Static yield stress peak values for mixture CP VF0.53 in kPa . . . 69
C.4 Static yield stress peak values for mixture CP VF0.56 in kPa . . . 71

D.1 Static yield stress peak values for mixture CS VF0.47 in kPa . . . 75
D.2 Static yield stress peak values for mixture CS VF0.50 in kPa . . . 77
D.3 Static yield stress peak values for mixture CS VF0.53 in kPa . . . 79
D.4 Static yield stress peak values for mixture CS VF0.56 in kPa . . . 81

E.1 Static yield stress peak values for mixture SG VF0.47 in [N] . . . 85
E.2 Static yield stress peak values for mixture SG VF0.50 in [N] . . . 86
E.3 Static yield stress peak values for mixture SG VF0.53 in [N] . . . 86
E.4 Static yield stress peak values for mixture SG VF0.56 in [N] . . . 87

F.1 Static yield stress peak values for mixture CP VF0.47 in [N] . . . 91
F.2 Static yield stress peak values for mixture CP VF0.50 in [N] . . . 93
F.3 Static yield stress peak values for mixture CP VF0.53 in [N] . . . 96
F.4 Static yield stress peak values for mixture CP VF0.56 in [N] . . . 99

G.1 Static yield stress peak values for mixture CS VF0.47 in [N] . . . 103
G.2 Static yield stress peak values for mixture CS VF0.50 in [N] . . . 106
G.3 Static yield stress peak values for mixture CS VF0.53 in [N] . . . 108

H.1 Starting time of experiment for Direct Shear Test with mixture CP . . . 112
H.2 Starting time of experiment for RAM Extruder with mixture CP . . . 113

H.3 Starting time of experiment for RAM Extruder with mixture CS 114

I.1 Experimental program with varying speeds for RAM Extruder 115
I.2 Relative mix proportions by weight 116

J.1 Varied tested heights of Direct Shear Test. 125

List of Symbols

φ	Angle of internal friction	$^\circ$
σ_0	Bulk yield stress	kPa
μ	Coefficient of friction	-
C	Cohesion	kPa
ρ	Density	kg/m
D	Diameter	mm
D_b	Diameter of barrel	mm
D_d	Diameter of die	m
A_{eff}	Effective area	m^2
V_s	Extrusion speed in the die land	mm/s
δh	Horizontal displacement	mm
$[\eta]$	Intrinsic viscosity	dL/g
L	Length of die	mm
m	Mass	kg
ϕ_{max}	Maximum solid fraction in a suspension	-
F_N	Normal force	kN
σ_N	Normal stress	kPa
α	Parameter characterizing speed in the die entry	$kPa \cdot s/mm$
β	Parameter characterizing speed in the die land	$kPa \cdot s/mm$
η_r	Relative viscosity	$kPa \cdot s$
F_S	Shear force	kN
$\dot{\gamma}$	Shear rate	s^{-1}
γ	Shear strain	-
τ	Shear stress	kPa
τ_0	Shear yield stress	kPa
ϕ	Solid fraction in a suspension	-
ΔP	Total pressure drop	kPa
η_0	Viscosity of liquid	$kPa \cdot s$
η	Viscosity of suspension	$kPa \cdot s$
V	Volume	m^3
τ_0	Yield stress	kPa

1

INTRODUCTION

The extrusion process of materials in 3D concrete printing (3DCP) is a complex combination of required characteristics for printability and buildability [5] [23]. For describing the physics of deformation and flow of matter in 3D concrete printing, more attention is required on material rheology [23][27]. Also, the material behavior under loading is a critical parameter that directly influences the buildability of the 3D printed concrete in the fresh state [27]. Therefore, two different behavior can be distinguished in the fresh state of 3D printed concrete, fluid and soil behavior. Fluid behavior for the flowability of the material, and soil behavior to retain its shape after several layers have been deposited onto each other [27]. Nonetheless, little is known about the experimental methods for identifying the transition between fluid and soil behavior [5]. Different material failure criteria can describe the fluid and soil regimes. The fluid regime is mostly described by rheology, whereas soil mechanics describe the soil regime [32]. The suitable failure criterion should be applied to define the properties of a mixture in the transition regime from fluid to soil behavior. In this state, the characterizing parameters are unknown, and not every experimental test is applicable in both regimes.

Browne and Bamforth [8] already made an approach that described the three regimes, fluid, transitional, and soil behavior, based on the influence of water-cement ratio and flow resistance. Their approach was for conventional concrete, where the printability and buildability of 3DCP were not considered. This approach causes blocking in a pipeline during pumping. Because of a lack of additional analyses for 3DCP, this research identifies the fluid, transition, and soil regime in the fresh state and determines the associated failure criterion based on strength. This leads to the research objective:

"*To identify the transition from a fluid to a soil material structure in the fresh state and determine the associated failure criterion based on strength.*"

To identify the transition regime, material compositions in the fresh state are analyzed with two different experimental tests to obtain the mechanical material properties. The first is a rheological test, the RAM extruder, whereas the second test, the Direct Shear Test (DST), is mainly used in soil mechanics [3] [33].

The remainder of this thesis elaborates more on how these tests help with this characterization. Chapter 2 describes the theoretical background of the different material models and characteristics in the fluid, solid and soil regimes. In Chapter 3, the method is described to obtain the material characteristics from the DST and RAM Extruder for the fluid, transition, and soil regime with the used mixtures. Subsequently, the results of the DST and RAM Extruder are presented and discussed in Chapters 4 and 5. The used mixtures are evaluated for the fluid, transition, and soil regime in Chapter 6. Conclusions from the experimental tests and evaluation are given in Chapter 7. Last, recommendations for follow-up of the research and for the development of 3D concrete printers are given in Chapter 8.

2

THEORETICAL BACKGROUND

The mechanical properties are essential to determine the printability and buildability of the mixture used in 3D concrete printing [5]. While printing, the material needs to flow inside the hose, but after deposition, the material needs to remain stable. The material used in 3DCP is mainly characterized as a visco-plastic material [39]. A visco-plastic material could behave as a fluid, solid or soil material. In this chapter, the different material behaviors are described by their study, applicable material model, and dominating effect.

2.1 Fluid behavior

The fluid behavior of a material structure is described in rheology. Different Generalized Newtonian Fluid (GNF) models can be applied to describe the material. With one of the GNF models, the viscosity of the material could be determined, which is the dominating effect in a fluid.

2.1.1 General Newtonian Fluid models

In rheology, concrete is considered a viscoelastic material [33]. To describe a viscoelastic material, different Generalized Newtonian Fluids (GNF) models could be used as a material model due to the wide variety of viscoelastic materials, given in Figure 2.1. The models are all based on constitutive relations and can only fit the observed behavior of shear stress and shear rate relation [12] [33]. The simple Newtonian fluid has a constant viscosity based on the linear relation between the shear stress and shear rate. This relation is given in Equation 2.1.

$$\tau = \eta \cdot \dot{\gamma} \tag{2.1}$$

Where τ is the shear stress in $[kPa]$, η is the viscosity in $[kPa \cdot s]$ and $\dot{\gamma}$ is the shear rate in $[s^{-1}]$.

Besides the Newtonian fluid, shear thinning or shear thickening could occur due to viscous dissipation, which is modified by the flow [33]. The Power-law model describes both effects, shear thinning, and shear thickening. The Newtonian fluid and power-law models are independent of the yield stress.

The Bingham fluid and Herschel Bulkley models differ from the Newtonian and Power-law models by introducing additional yield stress, τ_0. The applied pressure on the material needs to exceed the yield stress to make the material flow [12] [24] [39]. The equation for the Bingham model to determine the shear stress is given in Equations 2.2.

$$\tau = \tau_0 + \eta \cdot \dot{\gamma} \tag{2.2}$$

Where τ_0 is the yield stress in $[kPa]$.

Besides the GNF models, the Benbow-Bridgwater model could be used to quantify the rheological parameters of different materials. This model is mainly used for fluids, such as molten plastics, clay suspensions, and cementitious materials [10]. The model describes a material that undergoes a converging flow [12]. The Benbow-Bridgwater model is given in Equation 2.3, 2.4 and 2.5 [4]. In the model, $P1$ describes the pressure required to extrude the paste through the die based on converging flow, where $P2$ represents the shear yield stress in the die of the RAM Extruder [4] [12].

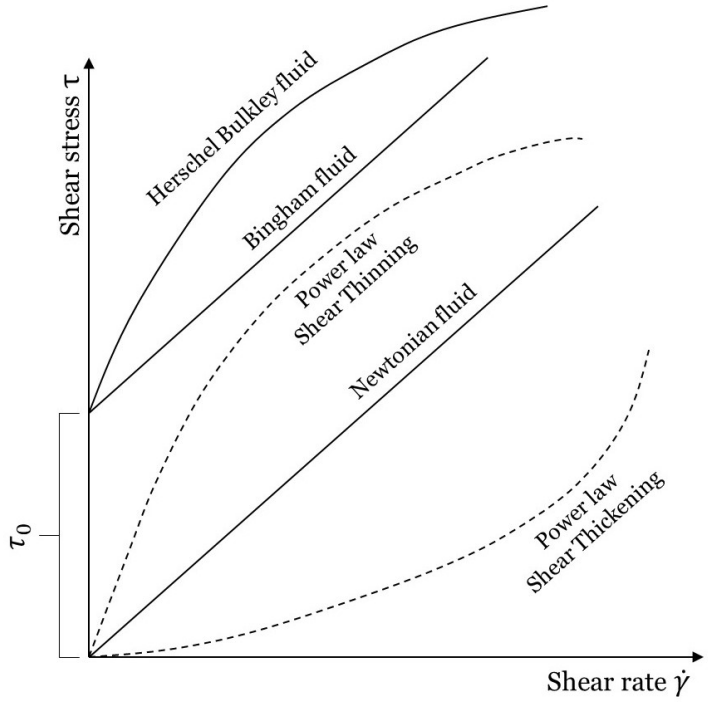

Figure 2.1: Overview of several Generalized Newtonian Fluid models based on [9].

$$\Delta P = P_1 + P_2 \tag{2.3}$$

$$P_1 = 2\left(\sigma_0 + \alpha V_s^m\right) ln\left(\frac{D_b}{D_d}\right) \tag{2.4}$$

$$P_2 = \frac{4L}{D_d}\left(\tau_0 + \beta V_s^n\right) \tag{2.5}$$

Where:

ΔP	=	Total pressure drop	$[kPa]$
σ_0	=	Bulk yield stress	$[kPa]$
α	=	Parameter characterizing speed in the die entry	$[kPa \cdot s/mm]$
V_s	=	Extrusion speed in the die land	$[mm/s]$
D_b	=	Diameter of barrel	$[mm]$
D_d	=	Diameter of die	$[mm]$
τ_0	=	Shear yield stress	$[kPa]$
β	=	Parameter characterizing speed in the die land	$[kPa \cdot s/mm]$
L	=	Length of die	$[mm]$

2.1.2 Viscosity

Fluid behavior is described in rheology, where viscosity is a dominating parameter [33], as found in Equations 2.1 and 2.2. A study of the relative viscosity in suspensions has been performed by Einstein [13]. The found theory is only valid for low volume fractions and in the case of uniform-sized spherical particles. Einstein found that the relative viscosity relates to the volume concentration of spheres in the relation given in Equation 2.6.

$$\eta_r = \frac{\eta}{\eta_0} = 1 + 2.5\phi \tag{2.6}$$

In which η_r is the relative viscosity in $[kPa \cdot s]$, and ϕ is the concentration of spheres. The equation is only valid for low volume fractions below $\phi = 0.05$ [37]. The theory of Einstein does not hold for suspensions with a non-uniform sphere distribution, as observed by Ward and Whitmore [42]. They found that the relative viscosity depends on the size distribution of the spheres. Roscoe [37] and Brinkman [6] found independently a theoretical expression for the relative viscosity. This expression is presented in Equation 2.7, which is valid for all concentrations, with uniform and non-uniform sphere distribution [37].

$$\eta_r = (1-\phi)^{2.5} \tag{2.7}$$

2.1.3 Krieger-Dougherty

Krieger and Dougherty [26] developed a model which describes the impact of an increasing volume fraction on the apparent viscosity, where the volume fraction is the number of particles added to a liquid. The model is validated for the theory of Einstein, as given by Equation 2.6. The model of Krieger-Dougherty was found for spherical particles and is presented in Figure 2.2 and 2.4. The numbers presented on the X-axis in the figure have been found for spherical particles, as presented by the rectangular boxes above, where ϕ_{max} is reached at a value of 0.64 [7]. For non-spherical particles, the model of Krieger-Dougherty is also applicable, but other values for ϕ could be found. The model is valid for low and high shear rates [26]. The viscosity, as presented in Figure 2.2, is obtained by Equation 2.8 [26].

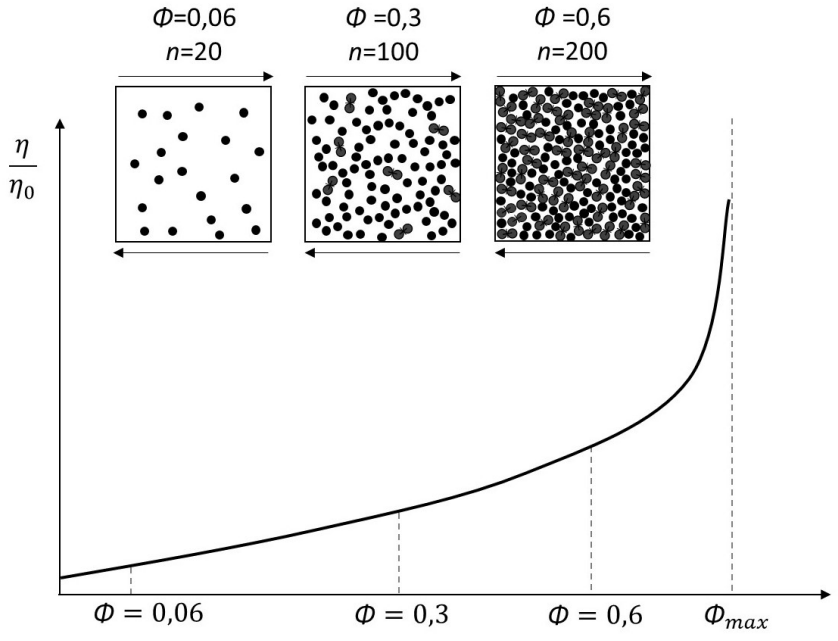

Figure 2.2: Krieger-Dougherty graph increase of particles based on [35].

$$\eta = \eta_0(1 - \frac{\phi}{\phi_{max}})^{-[\eta]\phi} \tag{2.8}$$

Where η_0 is the viscosity of the liquid in $[mPa \cdot s]$, ϕ is the volume fraction presenting the number of particles in the suspending liquid, ϕ_{max} is the maximum packing density, and $[\eta]$ is the intrinsic viscosity in $[dL/g]$, which is 2.5 for spherical particles. The intrinsic viscosity represents the true viscosity independent of the concentration in the suspension. The shear stress of a fluid can be determined with the viscosity in relationship with the shear rate, which is given in Equation 2.1.

When particles are added to a fluid, they act as obstacles, which hinder the flow of the fluid and increase the flow resistance, as presented in Figure 2.3. These particles influence the viscosity of the total suspension.

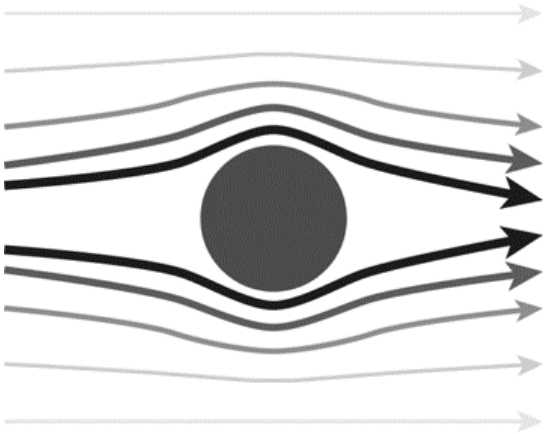

Figure 2.3: Flow around particle in liquid [35].

2.2 Solid behavior

Solid behavior can be described in the fluid and soil regime, which depends on the yield stress. In Equation 2.2, the yield stress is included. The material transitions from fluid to solid behavior when this parameter becomes significant. This transition from fluid to solid behavior is also found in the model of Krieger-Dougherty, Figure 2.2. The transition is at ϕ_{cr}, where the critical packing density is reached. The critical packing density is not a well-defined parameter but depends on the particles' distribution and shape [39]. The yield stress occurs due to inter-particle forces, which is the dominating effect in the solid behavior.

2.2.1 Inter-particle forces

Inter-particle forces could occur when particles interact with each other. At the grain level, frictional interactions occur between smaller particles, also described as local friction. At the cement paste scale, colloidal interactions take place [45]. The different inter-particle forces at the cement paste scale can affect the behavior of a paste [12]. Such forces are dispersion forces, often called Van der Waals forces, electrostatic forces, and steric forces [16] [19]. The forces are the main cause of the agglomeration of cement particles in concrete and result in poor flow properties. Additional materials, such as a superplasticizer, could be added to the mixture to encounter these forces.

Between the particles, attractive and repulsive forces can be found. Dispersion forces between identical particles are always attractive [16]. Electrostatic and steric forces are both repulsive. The electrostatic and steric forces are not great enough to overcome the attractive Van der Waals forces between cement particles, causing the clustering of the particles [17].

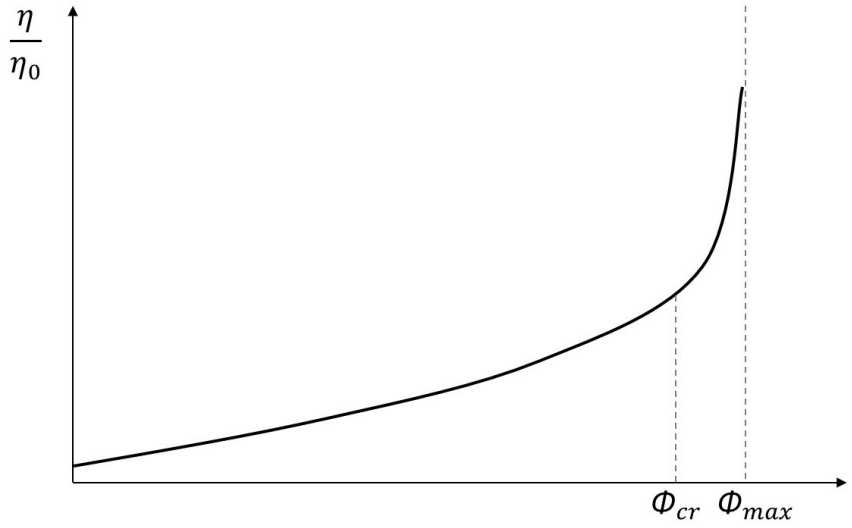

Figure 2.4: Krieger-Dougherty graph with maximum packing density.

When larger aggregates are added to a cement paste, the cement paste could be considered homogeneous, where only the frictional interactions between the aggregates are considered. In the case of dry aggregates, the contact between the solid aggregates is dominant over the other types of inter-particle contact, such as electrostatic contact with adhesive forces, capillary cohesion, and solid bridges. The contact force of solid particles at a macroscopic level is dominated by elastic repulsion, often called Hertz contact, and friction, also named Coulomb's law. The Hertz contact, given in Figure 2.5, is based on particles that interact by an external normal force, F_N.

Besides the normal force, also a tangential component occurs when particles at the grain level interact since particles are packed randomly. This interaction is the friction between particles, as given in Figure 2.6. Besides these inter-particle effects at the grain level, another particle interaction in the flow case should be considered, collision. The collision occurs when two particles with a velocity interact, as shown in Figure 2.7 [2].

A model to predict the yield stress was developed by Flatt [18]: YODEL. In this model, inter-particle forces, suspension microstructure, and particle size distribution have been considered by the parameter m_1. For determining this parameter, G_{max}, the maximum attractive interparticle force, takes into account the Van der Waals attraction forces, with the Hamaker constant, A_0 [18].

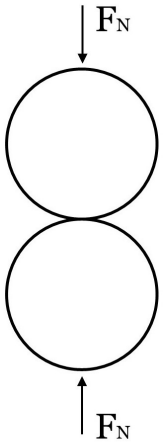

Figure 2.5: Elastic particle interaction based on [2].

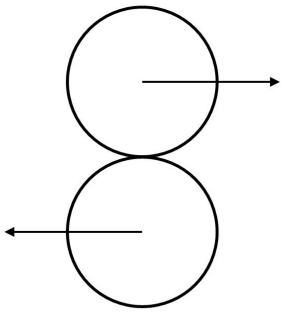

Figure 2.6: Solid friction particle interaction based on [2].

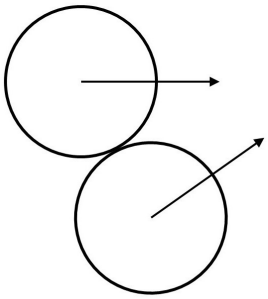

Figure 2.7: Collision between two particles based on [2].

2.3 Soil behavior

Soil behavior is described by soil mechanics, which is the science of equilibrium and motion of soil bodies [41]. The shear stress is mainly addressed with the Mohr-Coulomb failure criterion. the failure criterion of Mohr-Coulomb is based on two principal stresses [41]. The Mohr-Coulomb model is visually presented in Figure 2.8. The equation for the Mohr-Coulomb model is given in Equation 2.9.

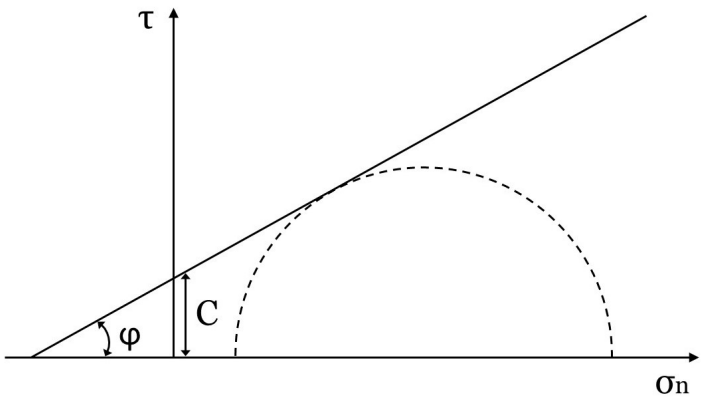

Figure 2.8: Mohr-Coulomb failure criterion.

$$\tau = C + \sigma_N \cdot \mu \tag{2.9}$$

Where C is the cohesion in $[kPa]$, σ_N is the normal stress in $[kPa]$, and μ is the coefficient of friction. The cohesion indicates that a certain shear stress is necessary for a shear failure, even when the normal stress is zero [41], indicating that soil behavior is yield stress dependent.

In the model of Krieger-Dougherty, Figure 2.4, the soil behavior is observed from ϕ_{max}. Here dilatancy and local friction become the dominating effects. Dilatancy is the effect where particles cannot move anymore without moving away from each other, and the volume increases with Δh, see Figure 2.9.

Besides dilatancy, also local friction occurs in the soil behavior, where particles slide over each other and cause friction, which is also affected by the particle shape. The black arrows present this effect in Figure 2.9. The angle of internal friction in the Mohr-Coulomb failure criterion includes the effects of dilatancy and local friction. The angle of internal friction could be determined with the shear stress and the normal stress by Equation 2.10.

$$\varphi = arctan(\frac{\tau}{\sigma_N}) \tag{2.10}$$

Where τ is the shear stress in $[kPa]$ and σ_N is the normal stress in $[kPa]$.

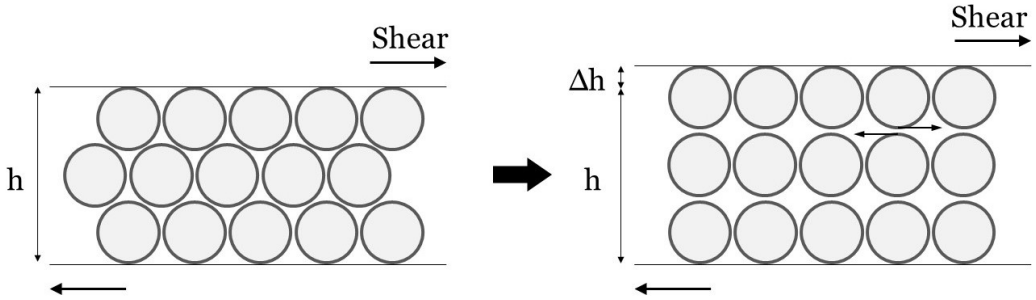

Figure 2.9: Dilatancy effect with particles.

2.4 Transition

Material can be described by rheological behavior, which is a regime dominated by hydrodynamic interactions, namely the viscosity, by solid behavior, dominated by the inter-particle forces or the soil behavior, dominated by the friction, including dilatancy and local friction effects [45].

Solid behavior can be observed in the fluid and soil regime. In the fluid regime, a Bingham fluid can have cohesion and stresses below the critical yield stress, where it behaves as a solid but is not pressure-dependent. Solid behavior can be observed in the soil regime when the material is pressure-dependent. Considering the two regimes, fluid and soil, where the solid regime is in either one, means a transition point exists between the fluid and soil regimes. This is in line with the regimes found by Browne and Bamforth [8]. They observed the soil behavior, which is dominated by friction between particles and requires a significantly higher pressure to displace the concrete than the fluid regime referred to as a hydrodynamic stress transfer. The transition in behavior from fluid to soil could also be found by combining Equation 2.2, for materials in the fluid regime, and Equation 2.9, for the soil regime, into Equation 2.11.

$$\tau = \tau_0 + \mu \cdot \sigma_N + \eta \cdot \dot{\gamma} \tag{2.11}$$

Here τ is the shear stress in $[kPa]$, τ_0 is the static yield stress in $[kPa]$, μ is the coefficient of friction, σ_N is the normal stress in $[kPa]$, η is the apparent viscosity in $[kPa \cdot s]$ and $\dot{\gamma}$ is the shear rate in $[s^{-1}]$. Combining the formulas for determining the shear stress for a Bingham fluid and a soil mixture, shear stress could be found. Also, the dominating regime could be found. If parameters μ and σ_N are the most significant values for the overall shear stress, τ, the mixture behaves as soil. If the parameters η and $\dot{\gamma}$ influence the overall shear stress, τ, the most, the mixture is in the fluid regime. The parameter τ_0 can be significant in the fluid and soil behavior, as it presents the static yield stress, which is the stress required for initiating flow before the structure of a material is broken down, which is also referred to as yield stress or cohesion [36].

3

METHOD

The influence of the material's structure on the identification of the behavior of a material could be determined by two different approaches. The first approach is to start with a fluid and add particles until the material behaves like soil, as visually presented in Figure 3.1. The other approach starts with only particles, where water is added. In this method, first, the voids between the cement particles will be filled with water. When all voids are filled, the particles will be enveloped by water, making the mixture more fluid and eventually behaving like a liquid. This approach is visually presented in Figure 3.2. For simplification, no distinction is made between the water to fill the voids and the water to envelop the water. The approach of this research is to start with a liquid and add particles until soil behavior is observed, the approach presented in 3.1.

To observe the transition regime in a material based on strength, two different experimental tests have been performed, the RAM Extruder and the Direct Shear Test (DST). Different mixtures have been tested, with varying water-to-cement ratios and varying amounts of aggregates. All mixtures are related to volume fractions, where the tested volume fractions are: 0.47, 0.50, 0.53, and 0.56. The mixtures which have been used in this research are first described. After that, the experimental program of the DST has been explained. Last, the experimental program used in this research for the RAM Extruder has been described.

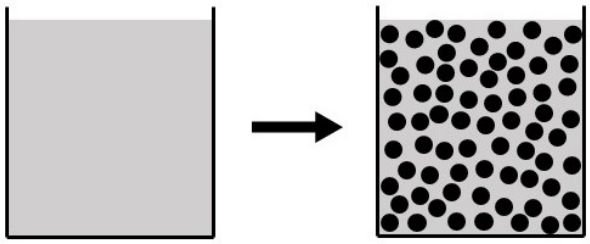

Figure 3.1: Approach adding water to particles.

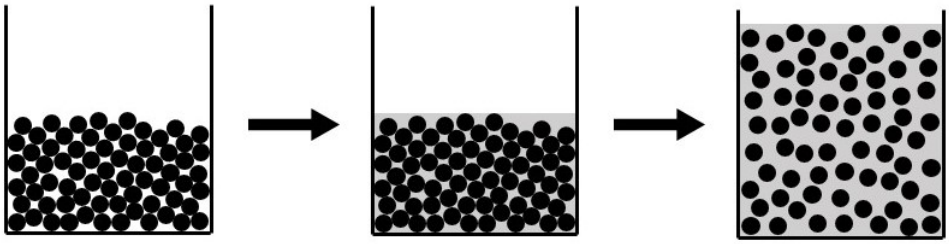

Figure 3.2: Approach adding particles to water.

3.1 Material

Three different material compositions have been used, as presented in Table 3.1 as mixtures SG, CP, and CS. Mixture SG consists of glass beads and syrup. Glass beads have an almost perfect spherical shape, as presented in Figure 3.3. The syrup used is Van Gilse Schenkstroop, which is more viscous than water and gives a homogeneous mixture with the glass aggregates. Mixture CP (cement paste) consists of cement in combination with water. The cement used is CEM III/C, which is composed of 5-19% of Portland cement clinker and 81-95% of blast-furnace slag. Due to the high level of blast-furnace slag, the cement has a slow strength development compared to other cement types [14]. The slow strength development has also been researched and presented in Appendix H. In mixture CS, cement is combined with water, with a water-to-cement ratio of 0.43, and sand aggregates. Sand has an irregular shape, as given in Figure 3.4, which causes extra colloidal effects. The cement paste in this mixture is assumed as a fluid, where the sand aggregates have been considered as the particles for the calculation of the volume fraction (ϕ), according to Equation 3.1. The relative mixing proportions of the three different mixtures have been presented in Table 3.1.

$$\phi = \frac{\frac{m_p}{d_p}}{\frac{m_p}{d_p} + \frac{m_f}{d_f}} \tag{3.1}$$

Where m_p is the mass of the particles in $[kg]$, d_p is the density of the particle in $[kg/m^3]$, m_f is the mass of the fluid in $[kg]$ and d_f is the density of the fluid in $[kg/m^3]$.

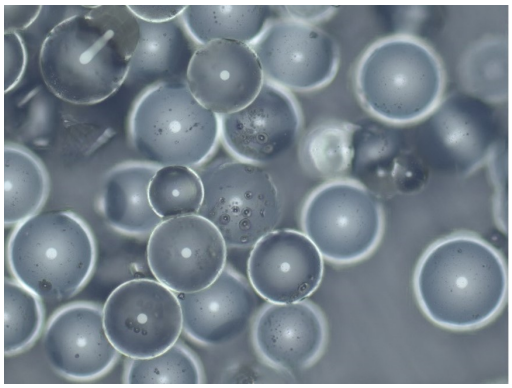

Figure 3.3: Microscopic view of glass aggregates [12].

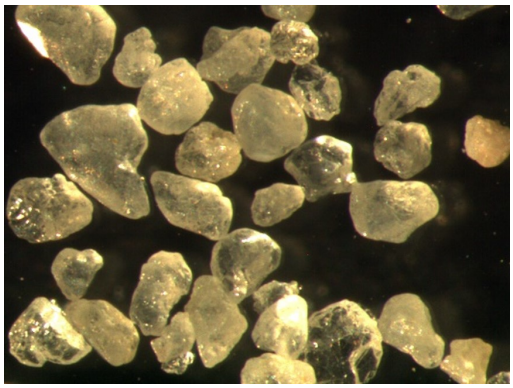

Figure 3.4: Microscopic view of sand aggregates [12].

Three different type of particles have been used, glass beads, cement grains, and sand grains. The particle size distribution of all three type of particles is given in Figure 3.5. The cement particles have

Table 3.1: Relative mix proportions by weight.

Mixture	Volume fraction	w/c ratio	Proportions				
			Cement	Sand aggregates	Glass aggregates	Water	Syrup
SG	0.47				1.44		1
	0.50				1.62		1
	0.53				1.83		1
	0.56				2.07		1
CP	0.47	0.38	2.64			1	
	0.50	0.34	2.98			1	
	0.53	0.30	3.36			1	
	0.56	0.26	3.79			1	
CS	0.47	0.43	2.33	4.1		1	
	0.50	0.43	2.33	4.6		1	
	0.53	0.43	2.33	5.2		1	
	0.56	0.43	2.33	5.9		1	

a particle size range of 106 to 180 μm, with a mean diameter of 140 μm. The sand particles have a particle size range of 600 to 1400 μm, with a mean diameter of 1 mm. The particle size of glass beads ranges between 150 and 200 μm, with a mean diameter of 195 μm.

The densities have been used to determine the volume fractions of the mixtures presented in Table 3.1, according to Equation 3.1. The densities of the dry particles, cement grains, sand aggregates, and glass aggregates have been determined with a Micromeritics AccuPyc II 1340 gas pycnometer and presented in Appendix A. The fluid materials, water and syrup, have been determined by Equation 3.2 with the measured volume, V, in $[m^3]$ and weight of three samples, m, in $[kg]$. The densities of the materials are given in Table 3.2.

$$\rho = \frac{m}{V} \tag{3.2}$$

Table 3.2: Densities of used materials.

Material	Density $[kg/m]$
CEM III/C	2969.7
Sand aggregates	2640.2
Glass aggregates	2434.7
Water	997.0
Syrup	1500.0

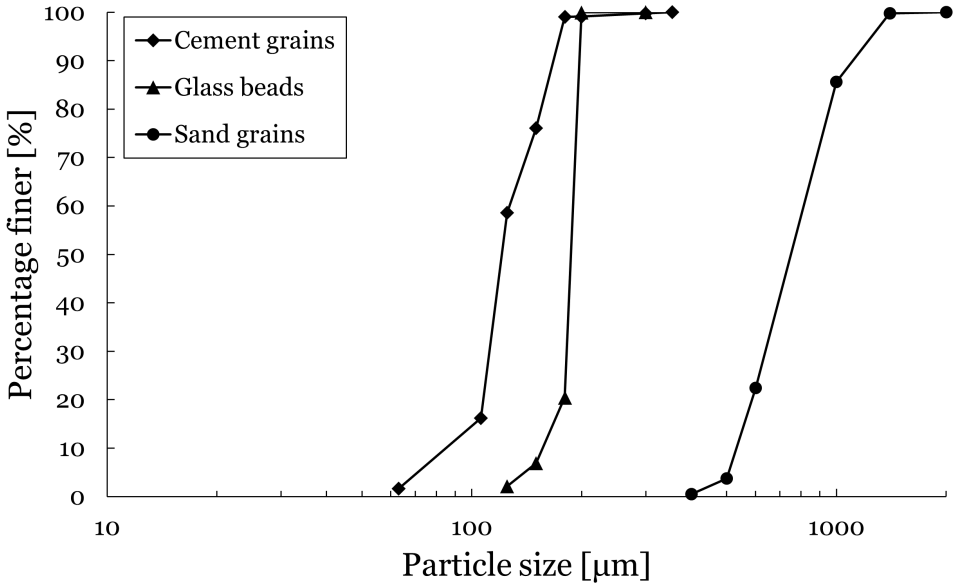

Figure 3.5: Particle size distribution curves for glass beads, cement grains, and sand grains.

3.2 Direct Shear Test

The Direct Shear Test (DST) is mainly used in soil mechanics to determine the mechanical properties of soil [20] [24] [25]. The test setup is designed according to ASTM D3080 [1] and contains two plates with a circular opening with a diameter of 70 mm and, when placed on top of each other, giving a sample height of 36 mm, a pulley, and a steel rope, presented in Figure 3.6 and 3.7. The setup was placed in a Schenck RM100 test rig with a 5 kN load cell. The test is performed by pulling the steel rope via the pulley, with a constant speed of 15 mm/min, where the top plate is moved with respect to the bottom plate. The friction between the two plates is minimized by grooves in the bottom plate and steel balls in the top plate sliding in the grooves of the bottom plate. By moving the top plate, a shear plane is formed in the fresh concrete, which is forced by the movement of the test setup [34]. The experimental test has been performed a minimum of three times for each unique combination of applied normal force and mixture composition. The shear stress τ in $[kPa]$ could be calculated from the applied shear force F_S in $[kN]$ and effective area A_{eff} in $[m^2]$ by Equation 3.3.

$$\tau = \frac{F_S}{A_{eff}} \tag{3.3}$$

Besides the applied shear force, three different external normal forces were applied on the samples, 0 N, 4.220 N, and 12.536 N, resulting in the normal loads: 1.5 N, 5.720 N, and 14.036 N, where the self-weight of the sample has been included [44]. From the resulting normal force F_N in $[kN]$ and effective area A_{eff} in $[m^2]$, the normal stress σ_N in $[kPa]$ could be calculated with Equation 3.4.

$$\sigma_N = \frac{F_N}{A_{eff}} \tag{3.4}$$

In Equation 3.3 and Equation 3.4, a force is divided by the effective area. The effective area decreases with an increasing horizontal displacement, as was found by Kozicki et al. [25], therefore Equation 3.5 is applied to calculate the effective area A_{eff}, where D is the diameter of the box in $[m]$, in this research 0.07 m, and Δh is the horizontal displacement in $[m]$ [43], as also visually presented in Figure 3.8.

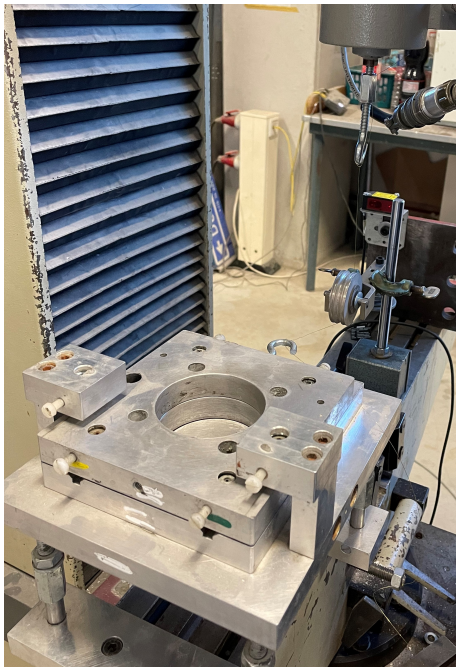

Figure 3.6: Test setup of Direct Shear Test.

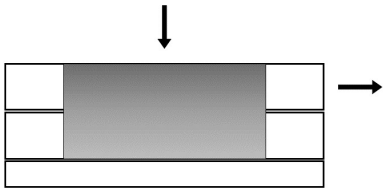

Figure 3.7: Abstract test setup of Direct Shear Test based on [12].

$$A_{eff} = \frac{1}{2}D^2 \left[cos^{-1}\left(\frac{\Delta h}{D}\right) - \left(\frac{\Delta h}{D}\right)\sqrt{1-\left(\frac{\Delta h}{D}\right)^2} \right] \tag{3.5}$$

A typical test result for a mixture considered in the soil regime of the DST is presented in Figure 3.9. The shear stress first increases linearly, after which the shear stress decreases and becomes constant. These could also be named the static and dynamic phases, as visually presented in Figure 3.9. Here the static phase takes place in the first 10% of the shear strain (γ), where the static yield stress can be obtained, and the dynamic phase takes place when the shear stress reaches a plateau value and is close to the dynamic yield stress with an increasing horizontal displacement [31] [39].

In soil mechanics, also another effect is considered, which influences the development of the shear stress over the horizontal displacement and the packing of the material. Dense and loose packed are considered in soil mechanics, where the typical test results are presented in Figure 3.10. The loosely packed material has no dilatancy effect but has the same local friction effect if the particles are considered equal. Dilatancy and local friction between particles are effects of the densely packed material, which are effects of the static phase, whereas, in the dynamic phase, only local friction effects are present. For a fluid mixture, no dilatancy effects are visible, which leads to almost constant shear

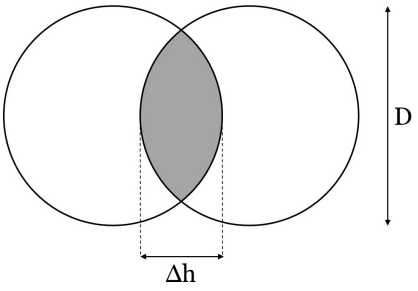

Figure 3.8: Determination of the effective area in DST.

stress over horizontal displacement, as also presented in Figure 3.10.

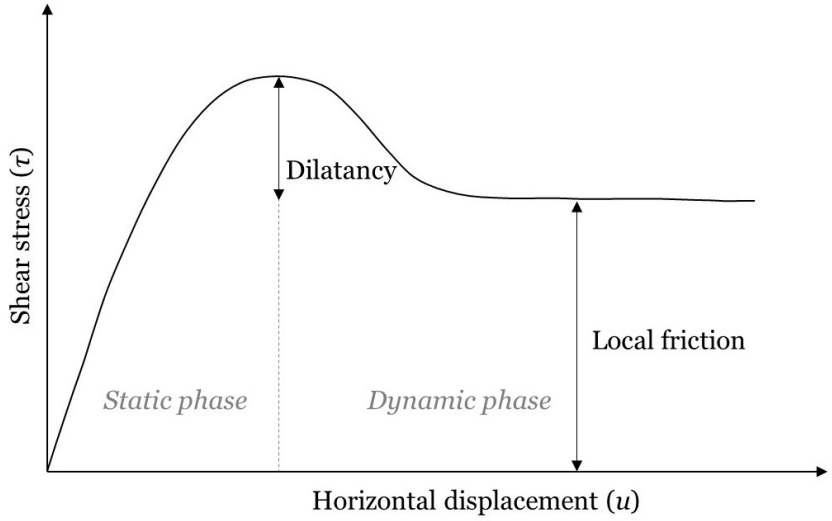

Figure 3.9: Typical shear stress versus horizontal displacement for a soil based on [11] and [41].

From the test results of the DST, the static yield stress peak could be established. The static yield stress peak is visually presented by a cross in Figure 3.10, which occurs in the first 7 mm of horizontal displacement, which is a shear strain, γ, of 10%. The found static yield stress peak, based on a minimum of three individual experimental tests, is a shear stress, τ, which is plotted against the normal stress, σ_N. The normal stress, σ_N, is determined by the applied normal forces. With the application of various normal forces, with a minimum of two different applied normal forces, and the corresponding static yield stress peak, a fit could be made with a trend line. The trend line is a linear relationship, which describes the Mohr-Coulomb behavior, mainly used to describe the shear failure of rock and soil [29]. The cohesion, C, is the shear stress found with a normal stress of zero, and the angle of internal friction, φ, is found by taking the inverse tangent of the slope of the trend line, as presented in Equation 2.10.

The DST is meant to establish a local shear plane failure. However, due to the sample height of 36 mm, global shear stress could be measured. Therefore the sample height was varied to study the influence of a global and local shear effect. These results are presented in Appendix J.

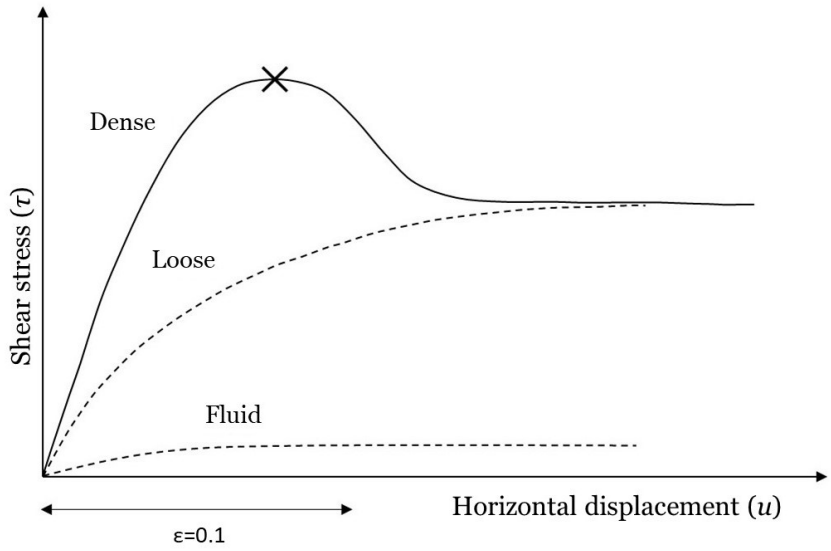

Figure 3.10: Determination of maximum shear stress from DST.

3.3 RAM Extruder

The RAM Extruder is based on extruding from a larger diameter through a smaller diameter, which is also common in 3D printing. In a 3D concrete printer, the concrete goes via a hose through a nozzle, where it is deposited on a print bed. The RAM Extruder also follows the principle from a larger to a smaller area. The RAM Extruder is an experiment that is mainly used in rheology and is called a capillary, mostly used to calculate the viscosity of polymer blends [33].

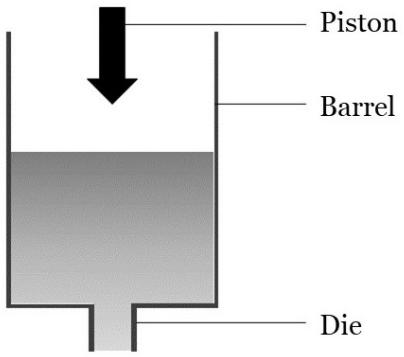

Figure 3.11: Abstract test setup of RAM Extruder.

The RAM Extruder consists of different elements, a large container, the barrel, and the die, a smaller circular container, as presented in Figure 3.11 and 3.12. The material flows from the barrel into the die by pushing with the piston. The displacement-controlled piston measures the force needed to push the material through the die. Here the RAM Extruder has a principle of converging flow from a larger to a smaller area [12]. The test setup has been placed in an Instron 5985. The barrel has a diameter

of 36 mm and a length of 300 mm. The piston is pushed from the entry of the barrel to 230 mm of vertical displacement. Two different programs have been performed. The first program is given in Table 3.3, here the piston is pushed with different speed rates. The second program pushes the piston at a constant speed rate of 5 mm/s. Different die's have been used, with a constant length of 15 mm and a varying diameter of 12, 18, 24, or 30 mm. This results in length over diameter (L/d) values of 1.25, 0.83, 0.63, and 0.5. The experiment has been performed with a minimum of three repetitions of a unique combination of mixture composition and die diameter.

Figure 3.12: Test setup of RAM Extruder.

Table 3.3: Experimental program 1 for RAM Extruder.

Speed rate $[mm/s]$	Vertical displacement $[mm]$
2	0-30
1	30-80
0.5	80-130
0.25	130-180
2	180-230

Inside the barrel of the RAM Extruder, a unidirectional converging flow occurs, where the material slides along the surface of the barrel to the entry of the die. Inside the barrel, the shear rate is not constant. The shear rate in the middle of the barrel is higher than at the barrel's walls, as visually presented in 3.13. The shear rate distribution over the cross-section of the barrel could vary, which is dependent on the material in the barrel [33].

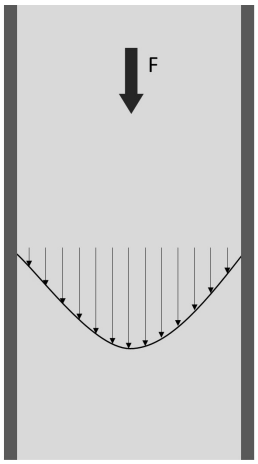

Figure 3.13: Flow inside the barrel of RAM Extruder based on [33].

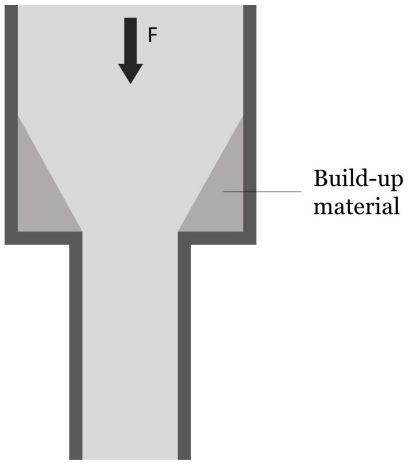

Figure 3.14: Build-up of material in the barrel of RAM Extruder.

Due to the effect of the varying shear rate in the barrel and the converging flow due to the transition from the barrel, with a diameter of 36 mm, to the die, with a smaller diameter (12, 18, 24, or 30 mm), the material could build-up around the die entry, as visually presented in Figure 3.14. The build-up around the die entry could vary per mixture. For fluid mixtures, the particles slide along each other. For very stiff materials, the build-up could cause blockage due to remaining particles, where water is pushed out. This also leads to an inhomogeneous mixture.

The RAM Extruder is mainly used to calculate the viscosity of mixtures and to describe a mixture by a model, for instance, the Benbow-Bridgwater model [4] [12]. To calculate the viscosity and obtain the parameters for the Benbow-Bridgwater model, different experiments and corrections to the data need to be performed. To obtain these parameters, a displacement-controlled and force-controlled program should be executed. The displacement-controlled experiment should be performed for a variation of piston speeds, leading to a variation of die speeds, to obtain the shear yield stress and a variation of die diameters to obtain the bulk yield stress [4]. Experimental program 1 could be used to obtain these results, where a typical result of this program is given in Figure 3.15. The force-controlled experiment should be performed to make a correction for the wall slip, which occurs between the piston and the barrel, to obtain the correct measured shear rate. Besides this correction, two other corrections should be made to obtain the viscosity: a correction for the entrance pressure since the material is undergoing a converging flow. This pressure could be obtained from a Bagley plot. And the Weissenberg-Rabinowitch correction should be made, which corrects the shear rate for the velocity profile, which shape depends on the material, as presented in Figure 3.13 [12] [33].

Besides obtaining the parameters for the Benbow-Bridgwater model, a static yield stress peak could be obtained from the experimental results of the RAM Extruder. A typical result of the RAM Extruder for one applies speed rate is given in Figure 3.16. The static yield stress peak describes the force required to initiate flow.

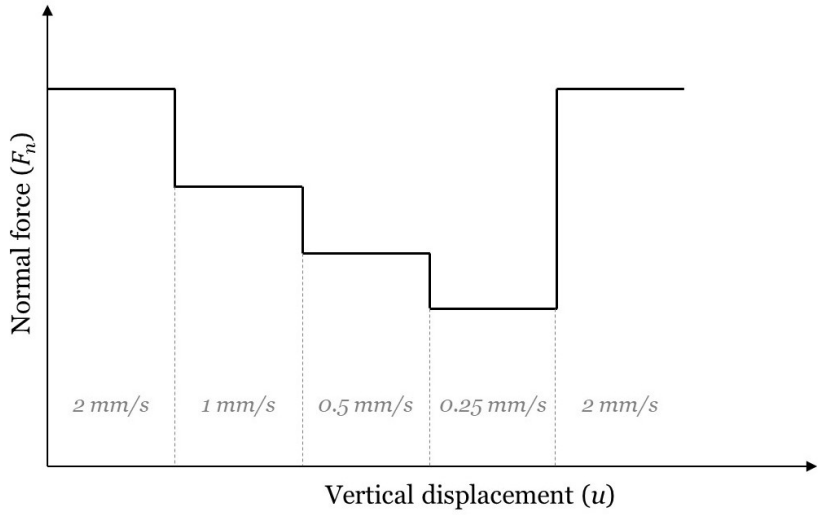

Figure 3.15: Typical result for experimental program 1 for RAM Extruder.

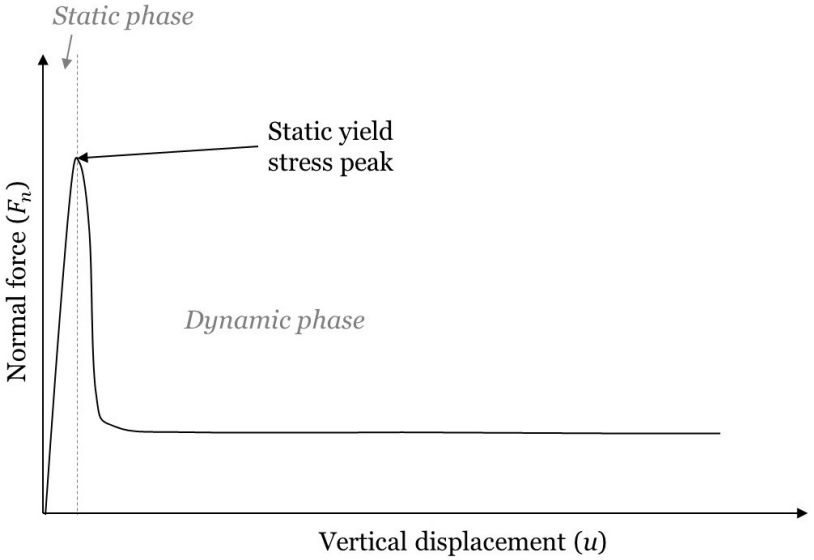

Figure 3.16: Typical normal force versus vertical displacement result of RAM Extruder.

4

Results and discussion: Direct Shear Test

The Direct Shear Test (DST) has been performed, with the experimental program presented in Section 3.2, for different material compositions with the equipment shown in Figure 3.6. The tests have been performed with four different shear boxes. The shear boxes have a small friction contribution, which has been subtracted from the presented results. The results have been presented and discussed below. The individual results of these experimental tests are presented in Appendices B, C, D, and K.

4.1 Mixture Syrup Glass (SG)

The results of mixture SG are presented in Figure 4.1 and Table 4.1. The trend line of the mixtures with a volume fraction of 0.47, 0.53, and 0.56 lie close to each other. The trend line of volume fraction 0.50 has a negative slope resulting in a negative angle of internal friction. Also, the individual experimental results, presented in Appendix B, do not show a typical test result for soil, as presented in Figure 3.9. The individual results have almost constant shear stress over horizontal displacement.

The negative slope of the trend line of volume fraction 0.50 could be caused by the minimal experimental tests resulting in a larger spread in the results, or an error in the test setup could have caused it. The almost constant shear stress over horizontal displacement of the individual experimental results could occur due to the test setup or by not forming a horizontal shear zone, as was found by Grabowski and Nitka [20] for samples with a larger void ratio. Here the particles start to compact in the upper plate and become an inhomogeneous mixture. This could indicate that the mixture for all volume fractions is in the fluid regime. So, the determination of the static yield stress is unreliable for determining the Mohr-Coulomb values.

Table 4.1: Results of DST for mixture SG.

Volume fraction	**Slope**	**Cohesion** $[kPa]$	**Angle of internal friction** $[^\circ]$	$\mathbf{R^2}$
0.47	0.1173	0.4907	6.6902	0.4495
0.50	-0.0427	0.4508	-2.4450	0.6922
0.53	0.0985	0.6229	5.6255	0.6058
0.56	0.1323	0.3498	7.5365	0.9833

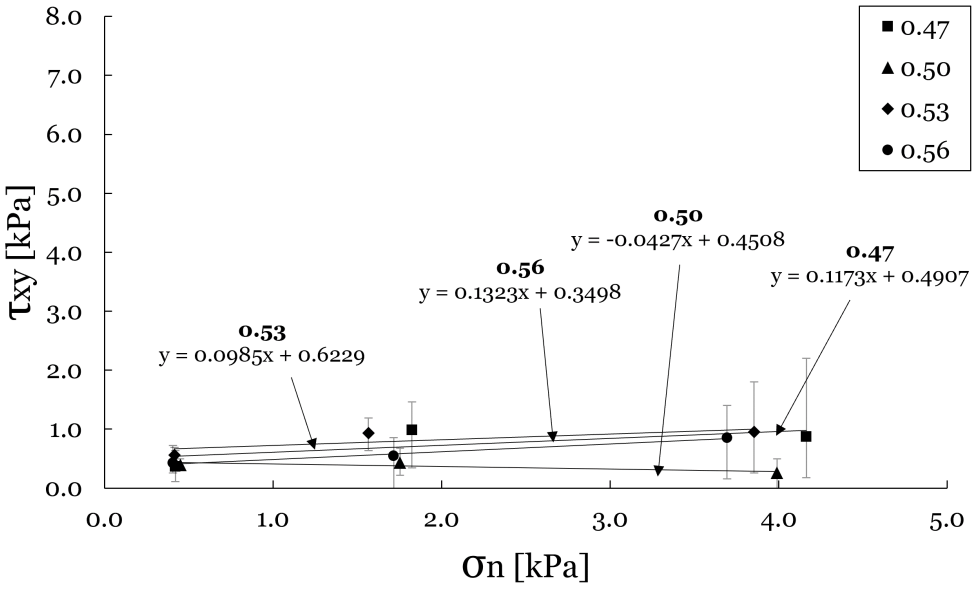

Figure 4.1: Shear stress over normal stress for mixture SG.

4.2 Mixture Cement Paste (CP)

In Figure 4.2 and Table 4.2, the results of mixture CP are given. The mixtures with volume fractions of 0.47, 0.50, and 0.53 lie close to each other, and the highest volume fraction of the three gives the highest cohesion. However, the coefficient of friction, in Table 4.2 presented as slope, decreases with an increasing volume fraction for these volume fractions. The individual experimental results, presented in Appendix C, also give this trend. Volume fractions 0.47 and 0.50 show almost constant shear stress over horizontal displacement, and the externally applied normal forces do not influence the shear stress. The individual experimental results of volume fraction 0.53 show an increase of shear stress over horizontal displacement but do not show a normal pressure dependency based on the different applied normal forces. The trend line of volume fraction 0.56 has a higher shear stress, based on Figure 4.2. The cohesion value is more than twice as high as the value of volume fraction 0.53, and the friction coefficient is higher than the friction coefficients of lower volume fractions, leading to a higher internal friction angle. The individual experimental results, presented in Appendix C, also show that the mixture, with a volume fraction of 0.56, is pressure-dependent. The self-weight (1.5N) has the lowest peak value, whereas the sample with 14.036 N applied normal force has the highest static yield stress.

Table 4.2: Results of DST for mixture CP.

Volume fraction	**Slope**	**Cohesion** $[kPa]$	**Angle of internal friction** $[^\circ]$	$\mathbf{R^2}$
0.47	0.1440	0.1517	8.1943	0.9382
0.50	0.0752	0.6944	4.3005	0.4187
0.53	0.0392	0.9428	2.2448	0.2635
0.56	0.2616	2.5914	14.6601	0.8064

The decreasing slope with an increasing volume fraction, between volume fraction 0.47 to 0.53, is not in correspondence with the newly predicted model by Lu and Wang [29], in which it is assumed the angle of internal friction has no significant influence for a cement paste and only the cohesion increases with the increase of the volume fraction of a cement paste. This could have been caused by the small experimental test program, with a minimum of three test, or by an error in the test setup

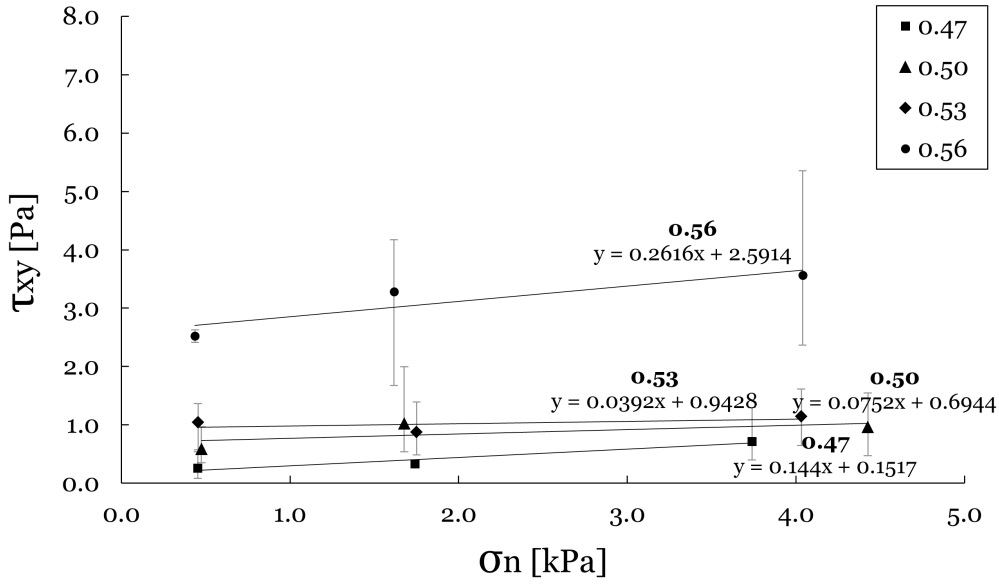

Figure 4.2: Shear stress over normal stress for mixture CP.

causing variation in the angle of internal friction. The increase of cohesion with an increasing volume is in correspondence with the newly predicted model of Lu and Wang [29], but still more than twice as low as the mixture with a volume fraction of 0.56, which could indicate that these mixtures with lower volume fractions are in the fluid regime.

The higher angle of internal friction for volume fraction 0.56 is also not in correspondence with the results found by Lu and Wang [29], in which the angle of internal friction does not significantly change due to a change in volume fraction. However, the tested mixtures by Lu and Wang have a lower w/c ratio than the mixture with a volume fraction of 0.56. Therefore, the mixtures of Lu and Wang could lay in a fluid regime based on a comparison between volume fractions 0.47, 0.50, and 0.53 and mixtures of Lu and Wang. Also, the individual experimental results, where volume fraction 0.56 shows pressure dependency is in correspondence with the findings of Lu and Wang [29], who concluded that normal stress has a significant effect on the maximum shear resistance of mortars with low flowability. In these mortars, sand aggregates were added to a cement paste, resulting in soil behavior. Also, the typical peak and constant dynamic phase, as presented in Figure 3.9, is observed. Therefore, mixture CP with a volume fraction of 0.56 can be considered as soil, whereas the other tested volume fraction can be considered a fluid. The transition regime has not specifically been found with these volume fractions but will be between volume fractions 0.53 and 0.56 based on these results.

4.3 Mixture Cement Sand (CS)

The results for the DST of the mixture with sand aggregates, mixture CS, are presented in Figure 4.3 and Table 4.3. The mixtures with a volume fraction of 0.47 and 0.50 originate close to each other, which is also the case for the mixtures with a volume fraction of 0.53 and 0.56. However, the mixture with a volume fraction of 0.50 has a steeper slope than the mixture with a volume fraction of 0.47. The individual experimental results also do not show a pressure dependency, based on the individual experimental results presented in Appendix D.

The mixtures with a volume fraction of 0.53 and 0.56 have a cohesion value that is around twice as high as the values of volume fractions 0.47 and 0.50. Also, the coefficient of friction is higher for volume fractions 0.53 and 0.56 compared to the lower volume fractions. The individual experimental

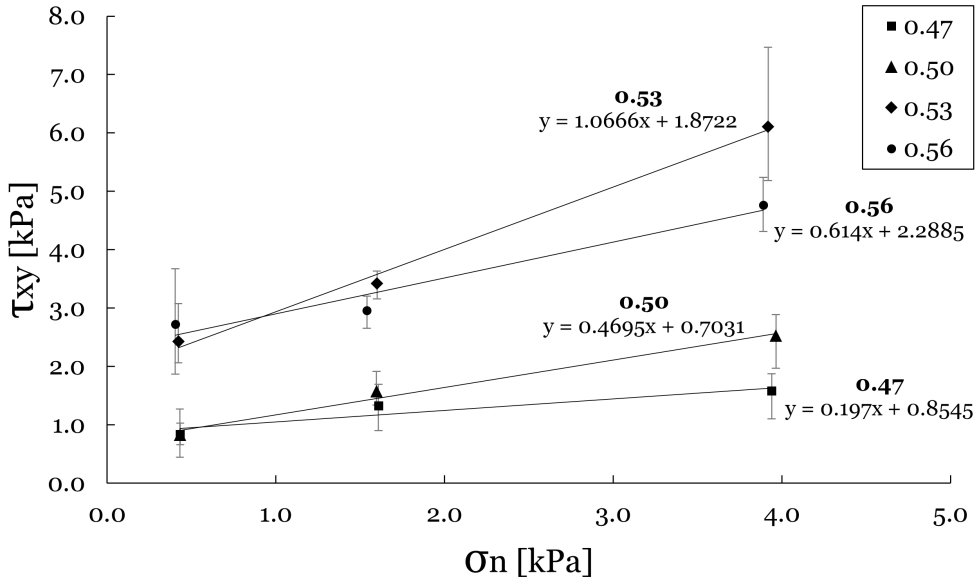

Figure 4.3: Shear stress over normal stress for mixture CS.

Table 4.3: Results of DST for mixture CS.

Volume fraction	**Slope**	**Cohesion** $[kPa]$	**Angle of internal friction** $[^\circ]$	$\mathbf{R^2}$
0.47	0.1970	0.8545	11.1446	0.8693
0.50	0.4695	0.7031	25.1501	0.9846
0.53	1.0666	1.8722	46.8458	0.9948
0.56	0.6140	2.2885	31.5499	0.9523

results, given in Appendix D, show the typical static yield stress peak and dynamic yield stress.

The steeper slope for volume fraction 0.50 compared to volume fraction 0.47 indicates that volume fraction 0.50 is pressure-dependent. Higher friction between particles and interlocking of particles during shearing takes place, as was also found by Assaad et al. [3]. Besides this effect, both mixtures do not show the typical solid behavior as presented in Figure 3.9, which indicates that these mixtures both are in the fluid regime. Also, the particles in the mixtures with volume fractions of 0.47 and 0.50 are more loosely packed than those with volume fractions of 0.53 and 0.56, which could cause compaction of the particles near the sides of the shear box, as was found by Grabowski and Nitka [20], and visually presented in Figure 4.4. Also, the more loosely packed mixture of Grabowski and Nitka showed a lower internal friction angle, as was also found by mixtures with a volume fraction of 0.53 and 0.56.

The relation for cohesion and angle of internal friction of volume fraction 0.53 and 0.56 compared to volume fractions 0.47 and 0.50 was also found by Lu and Wang [29] for mortars, where the cohesion and internal friction angle increase with the increase of volume fraction. The static and dynamic yield stress which has been found for volume fractions 0.53 and 0.56 indicates that both mixtures behave as soil. Besides, both mixtures show a pressure dependency, where the samples with the highest applied external normal force (14.036 N) give the highest peak of shear stress. For volume fraction 0.56, the static yield stress peak is lower for the applied normal force of 5.72 N than for the applied normal force of 1.5 N (self-weight). This could be caused by the relatively small sample size, causing larger deviations, as one experiment gives different output than the other two repetitions.

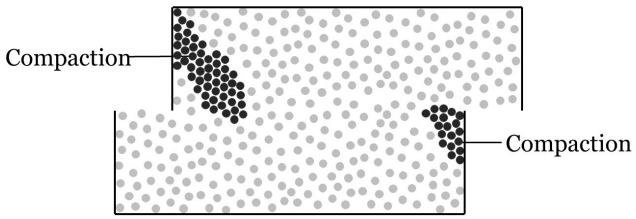

Figure 4.4: Compaction of a loose mixture at sides of the shear box based on [20].

Another remark is that a higher angle of internal friction has been found for the mixture with a volume fraction of 0.53 than the mixture with a volume fraction of 0.56. Also, a higher shear stress capacity has been found for the mixture with a volume fraction of 0.53 for normal stress around 1.6 kPa and 3.9 kPa compared to the mixture with a volume fraction of 0.56. Different effects could cause this. First, the experimental setup could have caused any unwanted effects, leading to a higher shear stress for a volume fraction of 0.53 or a lower shear stress for a volume fraction of 0.56. This could be eliminated by performing more experiments and randomizing the experimental program. Second, a plateau value could have been reached, where the maximum shear stress fluctuates around. This was also found by Heymann et al. [21], where they found a plateau at low shear rates, which affects the apparent yield stress. This could indicate that the dilatancy and frictional effects are not increasing anymore with an increasing volume fraction. This could be an effect due to the particle size diameter, which is equal in both experiments. This can be investigated by performing more experimental tests. Two variations in additional experimental tests can be made: performing more than three repetitions per volume fraction and applied normal force and additional experimental tests with volume fractions around 0.53 and 0.56. Last, the forming of the horizontal shear band could influence the peak shear stress. The shear band forms in the first few millimeters of displacement from an s-shaped shear zone into a horizontal shear zone, as was found by Grabowski and Nitka [20] [34] and Kozicki et al. [25], and visually presented in Figure 4.5. This could be further investigated by creating an analytical model and focusing on the forming of the horizontal shear band in the post-peak shear stress phase.

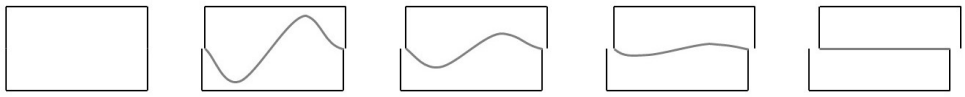

Figure 4.5: Shear band evaluation in mixture based on [20].

Concluding from the results of mixture CS, the mixtures with a volume fraction lower than 0.50 can be considered a fluid, whereas mixtures with a volume fraction and higher than 0.50 can be considered a mixture in the soil regime. The transition regime of mixture CS is around volume fraction 0.50, based on the experimental results.

4.4 Comparison between mixture compositions

Combining the results of mixtures SG, CP, and CS in one graph gives the results presented in Figure 4.6. Here the angles of internal friction are presented over the volume fraction. The angle of internal friction gives information about the dilatancy and local friction effects, as presented in Figure 3.9. Mixture SG has an overall lower angle of internal friction compared to the mixtures CP and CS, with a deviation at volume fraction 0.53, where mixture SG has a higher angle of internal friction compared

to mixture CP. The lower angle of internal friction for mixture SG compared to mixture CP has been caused by the particle shape since both particles are in the same particle size regime. The glass beads in mixture SG are perfectly spherical, whereas the cement grains are irregularly shaped, causing higher local frictional effects. Also, the angle of internal friction decreases for mixtures SG and CP. Mixture SG decreases between volume fractions 0.47 and 0.50, after which the angle of internal friction only increases. For mixture CP, the angle of internal friction decreases from volume fraction 0.47 to 0.53, after which it increases with a larger slope. The decreases could be caused due to the fluid regime where the mixtures fall, and as was stated by Lu and Wang [29], the angle of internal friction should not significantly vary in the fluid regime for a cement paste.

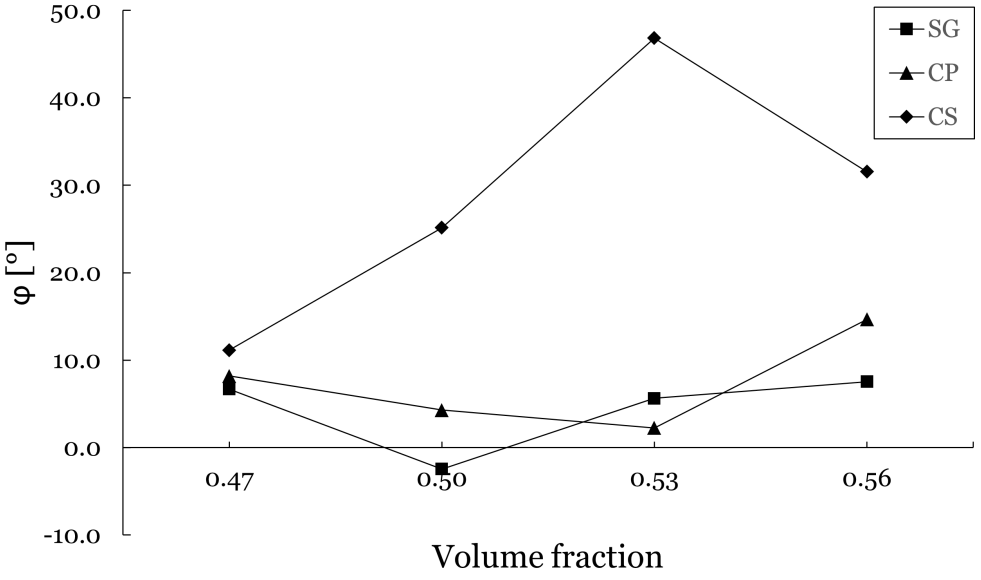

Figure 4.6: Angle of internal friction per volume fraction for different mixtures.

Mixture CS has the highest increase of internal friction angle from volume fractions 0.47 to 0.53 compared to the other mixtures. This indicates that the dilatancy and local frictional effects have also been increasing with the increase of volume fraction. The dilatancy and local frictional effects are more dominant than for the other mixtures. This could be caused by the size and distribution of the aggregates [38]. The average aggregate size of the sand is 1 mm, combined with the cement particles, with an average size of 140 μm. The glass aggregates have an average particle size of 195 μm. The sand particles are seven to ten times larger than the cement and glass particles, causing a larger dilatation effect. However, also the combination of sand particles and cement particles contributes to this effect. The difference between the mixtures CS and CP is presented in simplified Figure 4.7, where the voids between the sand aggregates have been filled with cement grains, and in the cement paste the voids have been filled with water. The decrease between volume fractions 0.53 and 0.56 for mixture CS could be caused by reaching a plateau, which was also found by Heymann et al. [21], as also presented in Section 4.3.

Besides the angles of internal friction, the cohesion values are visually presented together in Figure 4.8. The cohesion value represents the shear failure without normal stress, where dilatancy and local frictional effects occur. Mixture SG has an almost constant cohesion value, which is the result of the glass beads. The glass beads have no bonding, where no additional forces between the particles occur. Mixture CP has particles in the same particle size regime, however, the particles have an increasing cohesion with the increase of volume fraction. This is caused by physical or chemical interactions, such as Van der Waals forces, as described in Subsection 2.2.1. Also, the inter-particle forces occur in

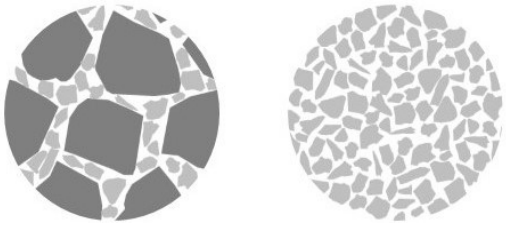

Figure 4.7: Difference in particle compaction, left mixture CS, right mixture CP (drawing not to scale).

mixture CS, which has an increasing cohesion value from volume fraction 0.50 to 0.56.

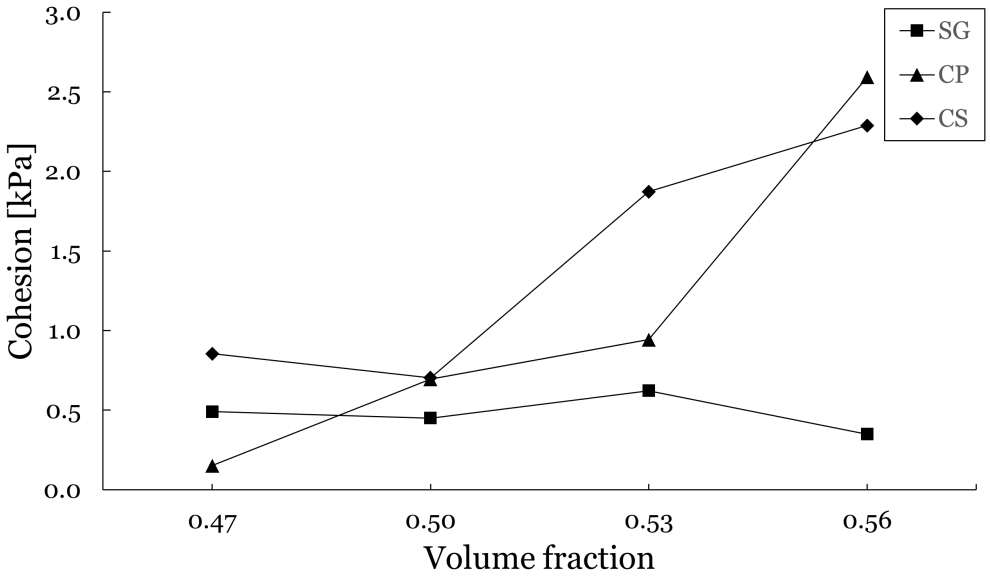

Figure 4.8: Cohesion per volume fraction for different mixtures.

5

Results and discussion: RAM Extruder

The RAM Extruder experiments have been performed according to the program described in Section 3.3. The program has been performed with a vertical displacement rate of 5 mm/s for mixtures SG, CP, and CS. Also, the program with varying speeds has been performed for mixture CP and CS, but with different volume fractions as mentioned in Section 3.1. Other researchers also performed the experiment with various speeds varying between 0.25 mm/s to 2 mm/s [10] [12]. A typical result of the experimental program with varying speeds is given in Figure 5.1. The other results of this experimental program are given in Appendix I. From these test results, no shear rate dependency has been found, as was found by Chaves Figueiredo [10] and Dorresteijn [12]. Therefore, the results have not been elaborated extensively since the Bingham properties and Benbow-Bridgwater parameters can not be obtained from the experimental results. The results from the experimental program with a vertical displacement rate of 5 mm/s have been elaborated more extensively and will be discussed in this chapter for mixtures SG, CP, and CS.

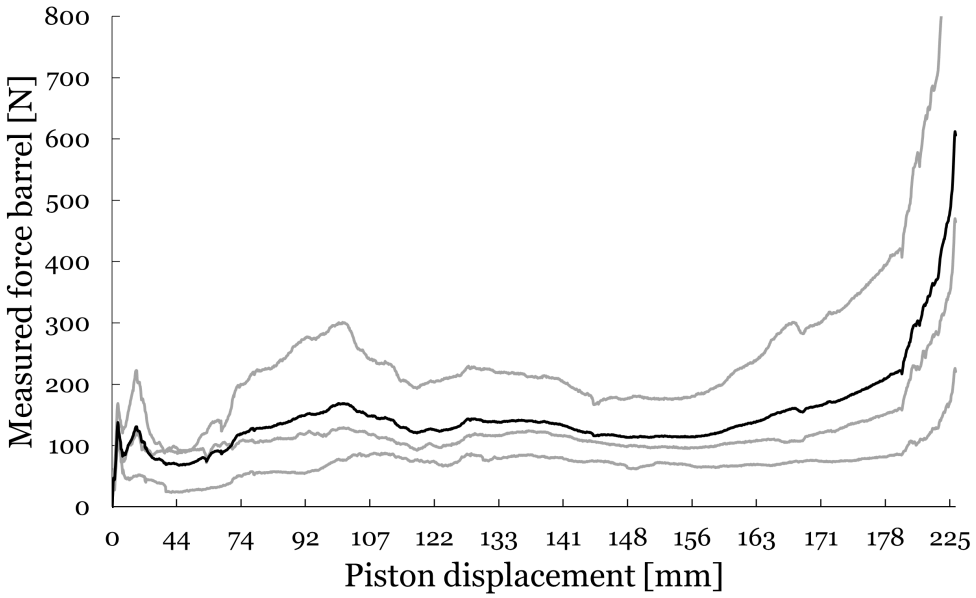

Figure 5.1: Typical result for RAM Extruder with varying speed rates (mixture CP, VF 0.48 and die diameter 12mm).

The die's which have been used in this research differs from the original setup, which has been used by Chaves Figueiredo [10] and Dorresteijn [12]. The die's, that also have been used for the results presented in Appendix I, consist of the same diameter size, 12 mm, and a varying length, resulting in different lengths over diameter (L/d) ratios. However, most mixes in the experimental program did not perform with these diameters because the mixes were too stiff, resulting in blocking in the barrel.

Therefore, die's with a constant length of 15 mm and varying diameters have been used, as given in Section 3.3. With this adjustment, the mixtures presented in Section 3.1 have been tested.

5.1 Mixture Syrup Glass (SG)

The results of the extrudability of mixture SG in the RAM Extruder are given in 5.1. In the table, positive results represent an extrudable mixture composition, and mediocre results present mixture compositions that are extrudable but with a deviation. Negative results represent mixture compositions that have been tested but do not extrude in the RAM Extruder.

Table 5.1: Overview of experimental results for mixture SG, volume fraction against die diameter: green: positive results, orange: mediocre results, red: negative results, gray: material not tested.

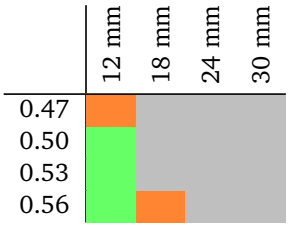

Volume fractions 0.47, 0.50, and 0.53 have not been tested in the RAM Extruder with a diameter of 18, 24, and 30 mm because the mixture was too liquid and did not remain static in the barrel before applying pressure with the piston. Volume fraction 0.47 in combination with a die diameter of 12 mm and volume fraction 0.56 in combination with a die diameter of 18 mm gave mediocre results, the combinations did remain static inside the barrel but ran out through the die faster than the displacement of the piston.

The static yield stress peak represents the force that initiates flow of the material, as presented in Section 3.3 in Figure 3.16. The static yield stress peak is observed for the positive and mediocre results presented in Table 5.1 and presented in Figure 5.2. The individual experimental results are presented in Appendix E. The values for the different volume fractions are all between 0.42 kN and 0.70 kN.

The static yield stress peak of all volume fractions with a die diameter of 12 mm and for volume fraction 0.56 with a die diameter of 18 mm are all around the same value indicating that all volume fractions are in the same regime.

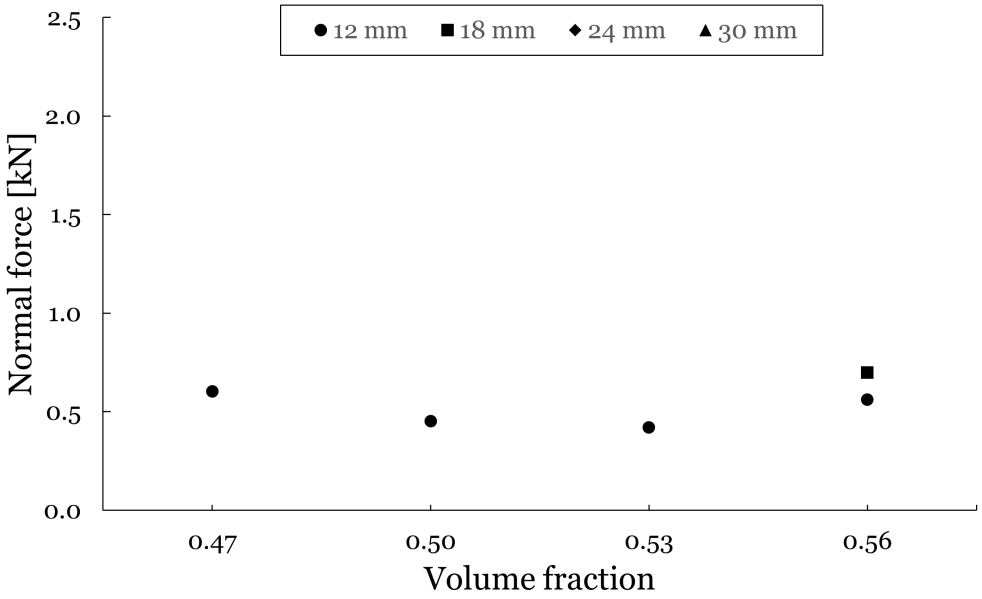

Figure 5.2: Normal force per volume fraction for mixture SG with different die diameters.

5.2 Mixture Cement Paste (CP)

The results of the peak values of normal force per volume fraction for mixture CP are given in Figure 5.3, the results of the individual experimental tests are presented in Appendix F. Not all volume fractions for mixture CP were suitable to test in the RAM Extruder for all die diameters. An overview is given in Table 5.2. Volume fraction 0.47 was stiff enough to fill up the barrel. After filling up the barrel, the material started running out through the die due to the self-weight. This is the same effect as found for mixture SG with a volume fraction of 0.47 and a die diameter of 12 mm and a volume fraction of 0.56 for a die diameter of 18 mm. Also, volume fraction 0.56 with a die diameter of 24 mm and 30 mm gave mediocre results. This is caused by blocking, where the material becomes too stiff inside the barrel. The program is not fully completed and stopped at a maximum applied force of 10 kN.

Table 5.2: Overview of experimental results for mixture CP, volume fraction against die diameter: green: positive results, orange: mediocre results, red: negative results, gray: material not tested.

	12 mm	18 mm	24 mm	30 mm
0.47				
0.50				
0.53				
0.56				

The mixtures with a volume fraction of 0.47, 0.50, and 0.53 were suited for testing with the given die diameters in Table 5.2. These mixtures did flow well in the barrel through the die of the RAM Extruder. This could indicate that the mixtures are saturated, as described by Feys [39] and Yammine [45]. They distinguish mixtures as saturated and unsaturated concrete. Saturated concrete has a sufficient lubricate layer around the particles, in this case, cement particles, which cause a hydrodynamic stress transfer. This is the movement of concrete depending on the shear rate in the interstitial liquid between the particles. Unsaturated concrete movement is dominated by a frictional stress transfer, which is the particles colliding with each other. As volume fractions 0.47, 0.50, and 53 are indicated

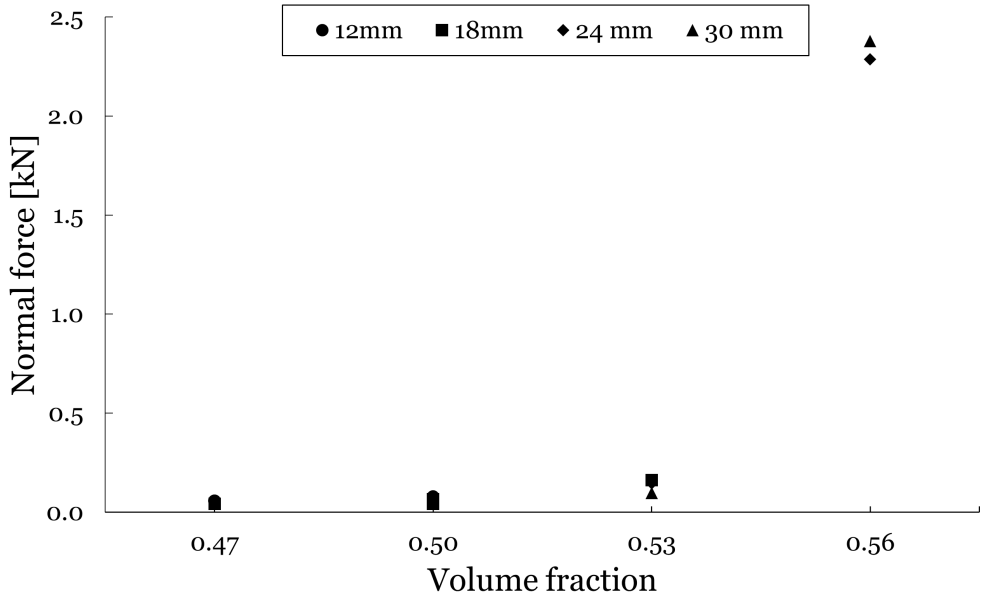

Figure 5.3: Normal force per volume fraction for mixture CP with different die diameters.

as saturated, it would mean that the movement can be indicated as a hydrodynamic stress transfer, which is dependent on the shear rate. However, based on results presented in Appendix I, mixture CP does not show a shear rate dependency. This could be due to the test program which is applied, with varying piston speeds in one program. To exclude this effect, individual tests with one shear rate can be performed for various shear rates, which could be related to the flow rate of the concrete in the hose of the 3D concrete printer. With this addition, the shear yield stress could be obtained for the Benbow-Bridgewater model [4]. The mixtures with a volume fraction of 0.47, 0.50, and 0.53 show all the same maximal normal force, independently of the die diameter, compared to the volume fraction of 0.56.

The blocking of the mixture with a volume fraction of 0.56 has occurred during the pushing of the piston, where the material starts compacting, and the particles are packed closer to each other. A side effect of this is that the material starts becoming inhomogeneous, and the cement particles are separated from the water. After a certain time of applying force, only water is running through the die instead of a homogeneous mixture as also been described by Feys [39] and Yammine [45] for saturated and unsaturated concrete. Browne and Bamforth [8] performed tests within a pipe for saturated and unsaturated concretes, and they found that unsaturated concrete was far less pumpable than saturated concrete. The unsaturated concrete exceeds the pump pressure required to move the concrete, which causes blocking. According to Browne and Bamforth [8], the blocking in the pipe is caused by dewatering of the mixture, which could happen in a relatively short length of a pipe. This means that the concrete must have a low permeability to avoid blockage. Based on the results of volume fraction 0.56 presented in Figure 5.3 and the dewatering during the experiment, the mixture can be classified as unsaturated, which has a too-high permeability indicating that mixture CP with a volume fraction of 0.56 is in the soil regime.

Since there is not a significant difference between the volume fractions 0.47, 0.50, and 0.53, independent of the die diameter, and a significant difference with volume fraction 0.56, which was considered in the soil regime, it indicates that the mixtures with a volume fraction of 0.47, 0.50, and 0.53 are in the fluid regime even though no shear rate dependency was found. The transitional regime in mixture CP would be between volume fractions 0.53 and 0.56, based on these results.

5.3 Mixture Cement Sand (CS)

The RAM Extruder is a suitable test for two combinations of volume fractions with die diameter for mixture CS: for a volume fraction of 0.47 with a die diameter of 24 mm and a volume fraction of 0.50 with a die diameter of 30 mm, according to Table 5.3. The mixture with a volume fraction of 0.47 and a die diameter of 30 mm has been tested. However, the mixture was not stiff enough to fill up the barrel without material running through the die.

Table 5.3: Overview of experimental results for mixture CS, volume fraction against die diameter: green: positive results, orange: mediocre results, red: negative results, gray: material not tested.

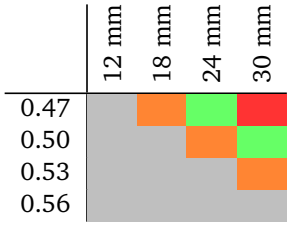

The mixtures with a combination of volume fraction 0.47 with a die diameter of 18 mm, volume fraction 0.50 with a die diameter of 24 mm, and volume fraction 0.53 with a die diameter of 30 mm gave mediocre results. During the program, with an increasing vertical displacement, the normal force increased up to 10 kN, after which the experiment was stopped for safety. However, a static yield stress peak has still been observed in these mixture compositions in the first 7 mm of vertical displacement. The results of the static yield stress peak per volume fraction and die diameter are given in Figure 5.4. The individual experimental results for mixture CS are presented in Appendix G.

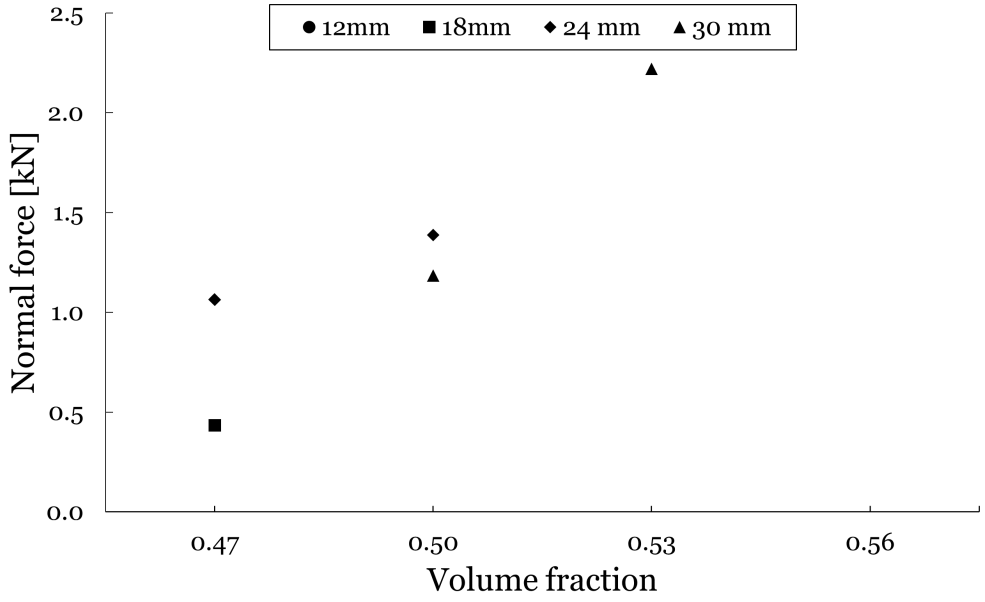

Figure 5.4: Normal force per volume fraction for mixture CS with different die diameters.

In Figure 5.4, the normal force increases with the increase of volume fraction. The mixture becomes stiffer and needs a higher force to set in motion. The peak of the static yield stress is higher. Besides

the increasing normal force with increasing volume fraction, also the normal force increases with a smaller die diameter. This effect is observed for volume fractions 0.47 and 0.50, where two different die diameters have been used.

The effect when the normal force increases up to 10 kN has been caused by pressure bleeding, visually presented in Figure 5.5. Here particles, in this case, sand and cement particles, are starting to interlock within the barrel. The particles build-up and only the paste or water is pushed out. In the case of mixture CS, sand particles and cement particles have been segregated from the water. The segregated water runs through the die. The effect of pressure bleeding depends on the type of mixture. The mixture can be saturated, but due to pressure, the mixture can become unsaturated, and the force on the piston rapidly increases due to the particle interlocking [8]. This can only occur if the mixture has an internal resistance to the flow of mixed water while under pressure, which is not the case for mixtures with a volume fraction of 0.47 in combination with 18 mm die, a volume fraction of 0.50 with a die diameter of 24 and with a volume fraction of 0.53 with a die diameter of 30 mm, which was also found for mixture CP with a volume fraction of 0.56. The effect could be avoided by adding an anti-segregation and anti-bleeding agent, like Nanometric Silica slurry Rhoximat CS 60 SL [40]. This effect does not occur immediately after the test program has started. Therefore the results of the static yield stress peak, which occurs in the first 7 mm of vertical displacement, can still be considered valid.

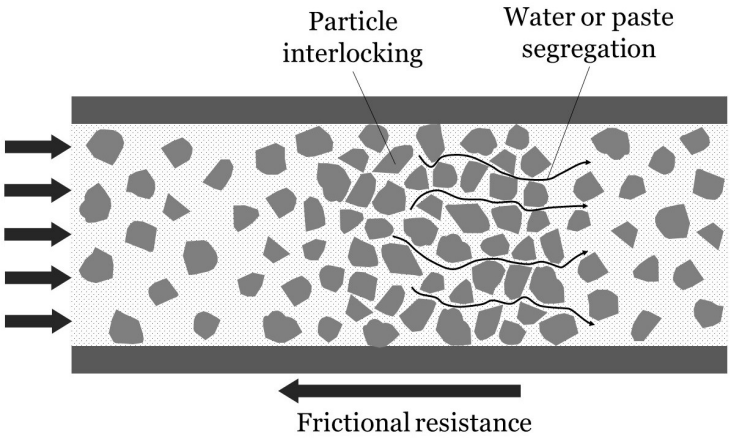

Figure 5.5: Principle of pressure bleeding based on [8][39].

To overcome the problem of pressure bleeding, the tested mixtures could all be chosen in the saturated regime. However, according to Browne and Bamforth [8], a saturated concrete mixture could still transform into an unsaturated concrete mixture, which still causes pressure bleeding. The pressure bleed test could be performed to measure the dewatering characteristics of the mixture [8]. However, with this method, still, not all mixtures could be tested with the RAM Extruder. To obtain the properties for a Bingham fluid, Equation 2.2, a different experimental test could be performed with the same mixtures.

A possible suitable test to obtain the Bingham properties is the Vane Rotational Rheometer. This test has first been used in soil mechanics to measure the shear strength of soils, which would be suited for the mixtures that behave as soil. Nowadays, it has become a standard technique in rheometry in which the parameters of the Bingham fluid, Equation 2.2, can be defined [15] [33]. Therefore, this experimental test could be suitable for the fluid and soil regime to determine the yield stress and viscosity via regression analysis [39] and identify and characterize the transition regime.

Other rheometers could also suitable to determine the properties of a Bingham fluid but not for a mixture with aggregates of 1 mm. For instance, the parallel plate test has a gap of 1 mm. To test a mixture with aggregates, the gap must be five to ten times larger than the maximum particle size in the mixture [39]. Also, in the research of Dorresteijn [12], the parallel plate test gave an error in the experiment for mixtures with glass and sand particles due to the particle size. The Vane Rotational Rheometer gave mediocre results for these mixtures because these materials created a shear plane next to the vane, which would indicate that the internal friction was too high, and only the yield stress could be determined. Toutou and Roussel [40] also used a Vane Rotational Rheometer for a cement paste and mortar, by which they successfully obtained the yield stress. It is recommended to use a Vane Rotational Rheometer for the mixtures presented in Section 3.1 to obtain the parameters for a Bingham fluid.

5.4 Comparison between mixture compositions

Combining the results of the extrudability for all mixtures gives Table 5.4. The mixtures with the lowest volume fraction, 0.47, show different extrudability options. Mixture CS is the only mixture suitable to test with a die diameter of 24 mm, caused by the internal friction between the sand particles.

For volume fraction 0.50, mixture CP has been tested for all die diameters, compared to mixture SG, this is caused by the cohesion between the cement particles, which has not been found for mixture SG. Mixture CS has only been tested for die diameters of 24 and 30 mm, compared to mixture CP where all die diameters were possible. This is caused by a different effect than cohesion, which was found for mixture CP. For mixture CS the friction between the sand particles causes this effect based on the limited possible die diameters.

Table 5.4: Overview of experimental results for mixtures SG, CP, and CS, volume fraction against die diameter: green: positive results, orange: mediocre results, red: negative results, gray: material not tested.

		12 mm	18 mm	24 mm	30 mm
0.47	SG				
	CP				
	CS				
0.50	SG				
	CP				
	CS				
0.53	SG				
	CP				
	CS				
0.56	SG				
	CP				
	CS				

The same effect was observed for the mixtures with a volume fraction of 0.53. Here mixture CP shows positive results for die diameters 18, 24, and 30 mm, whereas mixture SG only shows positive results for die diameter 12. This indicates that for mixture SG there is limited to no cohesion or friction between the glass particles. The large variety of suitable die diameters for mixture CP indicates that the cohesion value is high, where the cement particles bond based on chemical or physical interactions. Mixture CS has only been tested for a die diameter of 30 mm, which gave mediocre results, as was also found for volume fraction 0.50, it indicates that it has beencaused by the friction between the sand aggregates.

For volume fraction 0.56, mixture SG has been suitable for die diameter of 12 mm and gave mediocre results for die diameter of 18 mm. The die diameter of 12 mm has also been suitable for lower volume fractions, which indicates that cohesion and friction between the glass particles do not play a role for volume fractions of 0.56 and lower. Mixture CP shows mediocre results for die diameters 24 and 30 mm, here the friction between the cement grains is dominant, causing pressure bleeding. The friction between the sand particles has been estimated as too high for mixture CS, based on volume fraction 0.53, to perform the RAM Extruder.

Combining the results of the static yield stress peaks of mixtures SG, CP, and CS gives a normal force over volume fraction graph, presented in Figure 5.6. Here the average normal force per different mixture, die diameter, and volume fraction is given based on the static yield stress peak. Mixture SG has the most constant values for the normal force, where all volume fractions are in the same regime.

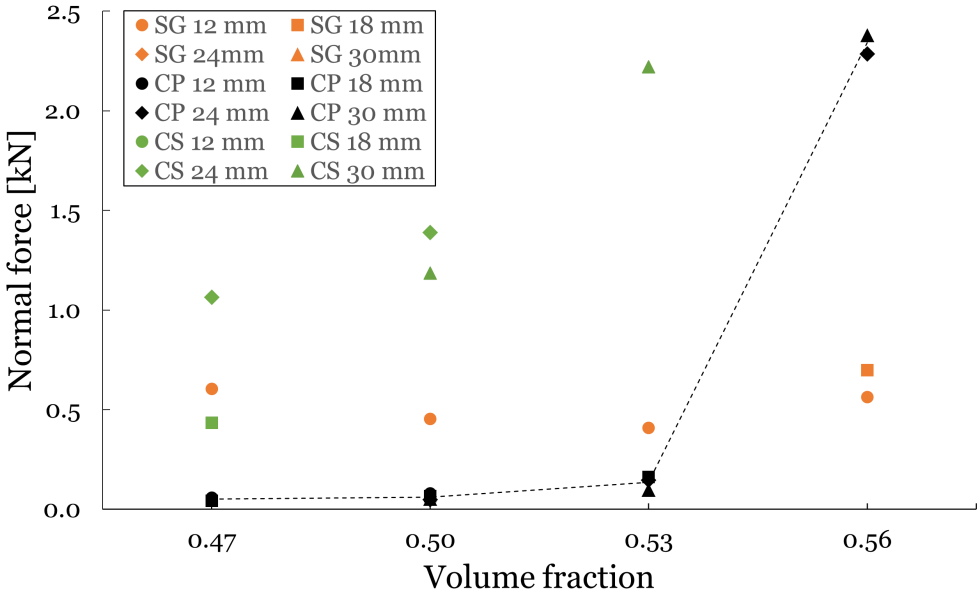

Figure 5.6: Normal force per volume fraction and die diameter for different mixtures.

Mixture CP shows an increase in average normal force after volume fraction 0.53, where the normal force is higher than 1.0 kN. This indicates that this mixture has transitioned from the fluid to soil behavior between volume fractions 0.53 and 0.56. Also, the values of volume fractions 0.47 to 0.53 with different die diameters do not show a significant difference. This could indicate that the cohesion between the cement particles is dominant and friction between the particles is less dominant based on the principle of converging flow and build-up, as in Figure 3.14. Another remark is that the static yield stress peaks of mixture CP with volume fractions 0.47 to 0.53 are lower compared to the results obtained for mixture SG for the same volume fractions. Since both mixtures with volume fractions between 0.47 and 0.53 are in the fluid regime, this could be influenced by the particle size distribution, as presented in Figure 3.5.

The last mixture, mixture CS, has an increase of normal force with the increase of volume fraction. However, the slope depends on the die diameter. The die diameter has a significant influence on the normal force for mixture CS. This has been caused by the friction between the sand particles in combination with the converging flow, which creates build-up around the die entry, as presented in Figure 3.14. The largest difference is found for volume fraction 0.47, between die diameters 18 and 24 mm, indicating that the friction between particles is dominant for the normal force. For a die diameter of

18 mm, mixture CS with a volume fraction of 0.47 is in the fluid regime, as was also found for mixture SG and mixture CP, for volume fraction 0.47 to 0.53. For a die diameter of 24 mm, mixture CS with a volume fraction of 0.47 is in the same region as volume fraction 0.50 for die diameters 24 and 30 mm. The normal force of volume fraction 0.53 is in the same region as mixture CP with a volume fraction of 0.56, indicating that mixture CS, with a volume fraction of 0.53, also behaves as soil. This indicates that volume fraction 0.47 with a die diameter of 24 mm and volume fraction 0.50 are around the transition point from fluid to soil behavior.

To study the rheological behavior of the mixtures with more widely possible mixtures in the fluid and solid regime, a different experimental test could be used. The Vane Rotational Rheometer is proposed as another experimental test setup, which is used in different researches [12] [15] [40], to determine the Bingham parameters. The experimental test uses the principle of simple shear flow and can be displacement or force-controlled [12] [33].

6

Comparison between Direct Shear Test and RAM Extruder

Two experimental tests have been performed, namely the Direct Shear Test (DST) and RAM Extruder. The DST is used to obtain the properties for the Mohr-Coulomb model, as presented by Equation 2.9. The RAM Extruder is a rheometer that is used to obtain the properties of a Bingham fluid, as presented in Equation 2.2. These formulas are combined into Equation 2.11 presented in Section 2.4. The obtained parameters by the DST and RAM Extruder could be filled into the equation, and significant parameters can be found. Either the friction coefficient and normal stress or the apparent viscosity and shear rate are dominant. This indicates if a material behaves as soil, with the Mohr-Coulomb model, or behaves as a fluid, with the Bingham model. However, the viscosity and shear rate could not be obtained with the experimental program performed for the RAM Extruder. The shear rate could not be obtained since only one displacement rate has been applied. Therefore, only the static yield stress peaks and the behavior of the results of the DST and RAM Extruder have been compared.

First, the behavior of the different mixtures in both experimental tests. Mixture SG has a low angle of internal friction in the DST caused by the perfect spherical shape of the glass beads. Also, in the DST, a low cohesion value was found for mixture SG. No chemical or physical bonds arise between the glass beads. Frictional effects could occur when higher volume fractions are being tested when particles interact. A similar result has been found in the RAM Extruder. The normal force remained almost constant with an increase in volume fraction, indicating that no bonds between the glass beads occur. Also, in the RAM Extruder, it is expected that the normal force increases with a higher volume fraction, above 0.56, where the glass beads interact based on friction.

For mixture CP, different behavior has been observed than for mixture SG. In the DST, mixture CP shows the effects of chemical and physical bonds between the cement grains. The cohesion value increases with the increase of volume fraction, indicating the bonds between the cement grains. The angle of internal friction, including deviations, is around the same value for volume fraction 0.47 to 0.53, as was found Lu and Wang [28]. These volume fractions behave as a fluid, which could explain the difference with volume fraction 0.56. Here the angle of internal friction is a dominant factor caused by the additional effect of friction between the cement grains. The effect of friction between cement grains for a volume fraction of 0.56 has also been observed in the RAM Extruder. In this experimental test, the effect of pressure bleeding occurred when the water was segregated from the cement grains. The effect of friction between cement grains for volume fraction 0.47 to 0.53 is not dominant in the RAM Extruder, based on the small differences between the die diameters. The small differences between the die diameters for mixture CP are caused by the cohesion between the cement particles, where chemical and physical bonds have been created. This is in correspondence with the cohesion found in the DST.

Mixture CS has an increasing angle of internal friction between volume fractions 0.47 to 0.53, caused by the friction between the sand particles. The particle shape and size are important factors causing friction between the particles. Also, an increasing cohesion with the increase of volume fraction has been found, which is the effect of chemical and physical bonds between the particles, sand and cement, in the mixture. Frictional effects between the sand particles have also been found for mixture CS in the RAM Extruder. In the experimental test, pressure bleeding occurred when particles started to interlock in the barrel and water was segregated from the sand and cement particles.

Second, the static yield stress peak is discussed. The static yield stress peak is the stress required for initiating flow [36]. This applies to both experimental tests, where a flow is initiated by shear, for DST, or normal force, for RAM Extruder. The output of the DST is a shear stress, whereas the output of the RAM Extruder is a normal force. The shear stress is normalized to the highest found cohesion value for a specific mixture, where the normal stress is zero. The normal force found in the RAM Extruder is normalized to the highest found normal force for a specific mixture in the results of the RAM Extruder. For the normalized values, only a trend could have been found for mixture CP since the die diameters do not influence the normal force due to the cohesion of the mixture. The trend of mixture CP for the RAM Extruder and DST is given in Figure 6.1.

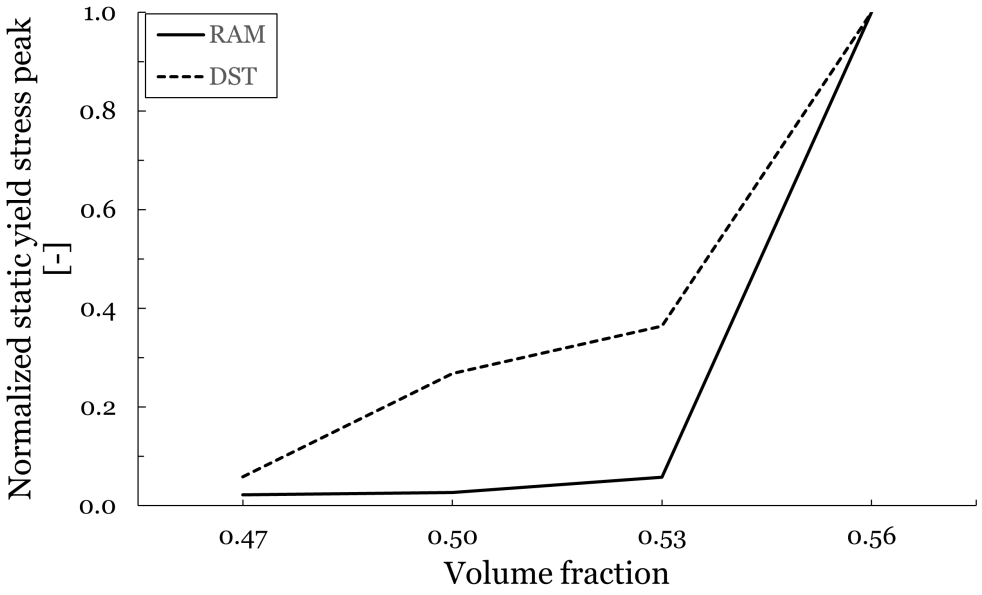

Figure 6.1: Normalized static yield stress peak per volume fraction for mixture CP.

The normalized values in Figure 6.1 show a similar course for the DST and RAM Extruder. For volume fractions 0.47 to 0.53, a difference has been observed between the two experimental tests. The cohesion value increases in the DST, whereas in the RAM Extruder, the effect of cohesion between cement particles is less dominant. After volume fraction 0.53, the normalized static yield stress peak increases. In the DST and RAM Extruder, frictional effects occur between the cement grains, causing the higher static yield stress peak compared to the lower volume fractions.
Ma et al. [30] also investigated the effect of increasing the volume fraction of cement paste. They found that the static yield stress increases with the volume fraction. This is mainly affected by the strength of colloidal interactions between the cement particles. Also, in the research of Ma et al. [30], the highest increase of static yield stress peak was between volume fraction of 47.5% to 49.41%. However, no higher volume fractions have been researched. Therefore no comparison between the research of Ma et al. [30] and the found data in this research could be made since, in this research, higher volume fractions have been taken.

Lu and Wang [28] also compared results from a direct shear test and a rheometer for a cement paste with different w/c ratios based on the static yield stress. They found that the static yield stress increases rapidly from a water-cement ratio of 0.35 and lower. Where in this research, an increase in static yield stress is found for mixtures with a lower water-cement ratio than 0.30. This difference could be influenced by the cement type and temperature during mixing and testing or mixing procedures.

Heymann et al. [22] investigated the transition from a liquid to a solid state for spherical particles. They found that at low shear rates, a plateau can be seen, which affects the apparent yield stress. This was also observed for mixture CS between volume fractions 0.53 and 0.56. This indicates that if a material behaves as soil, a plateau occurs, where the static yield stress is not increasing anymore with an increase in volume fraction.

More research has been done on the transition from a fluid to a solid regime on fresh concrete by Heymann et al. [21], Yuan et al. [46] and Roussel et al. [38]. Here variations such as time dependency, shear rate, and admixtures were taken into account, influencing the transition from a fluid to a solid regime. They found that the static yield stress peak also depends on the shear rate. Therefore, additional research on the shear rate dependency on the static yield stress peak could be useful for a more detailed description of the transition from a fluid to a solid regime.

7

CONCLUSION

In this study, three different mixture compositions have been studied on their rheological and soil-like behavior to identify and characterize the transitional regime. An experimental program was set up and performed to obtain the material properties. The experimental method consists of the Direct Shear Test (DST) and RAM Extruder, mainly used in soil mechanics and rheology studies. With this experimental program, the structure of a material has been identified and characterized in three different regimes: fluid, transition, and soil. These regimes are related to specific failure mechanisms based on strength properties.

The transition between fluid and soil behavior depends on the type of mixture, where particle interactions, particle shape, and particle size are important factors. The interaction between particles can occur in chemical or physical interactions, dominated by cohesion or dilatancy and local frictional effects. The particle shape can cause the interlocking of particles, resulting in a higher cohesion. The particle size can cause various dilatancy effects, where a larger particle has a larger effect.

Three different mixture compositions have been tested to find a transition point from fluid to soil behavior. First, mixture SG (syrup and glass beads), where the transition point has not been found. This aligns with the literature, where the transition point is around a volume fraction of 0.64 for perfect spherical particles. The tested volume fractions for mixture SG are lower than 0.64 and, found by the DST and RAM Extruder, in the fluid regime. In this regime, viscosity is the dominant parameter.

Second, Mixture CP (cement paste) has the transition point from fluid to soil behavior between volume fractions 0.53 and 0.56. The volume fraction where the transition occurs in mixture CP is lower than for mixture SG. This is caused by the chemical and physical interactions in the mixture, such as the Van der Waals connections. The cohesion found for volume fractions 0.47 to 0.53 can be related to solid behavior, where inter-particle forces dominate. However, the friction angle does not dominate for volume fractions 0.47 to 0.53, indicating the solid behavior in the fluid regime. Between volume fractions 0.53 and 0.56, frictional effects become more dominant, caused by the particle shape and interlocking of particles. This leads to a dilatancy effect and local friction, a characteristic of soil behavior. Therefore the transition point for mixture CP is between volume fractions 0.53 and 0.56.

Last, the transition point of mixture CS has been found around a volume fraction of 0.50. The angle of internal friction increases between volume fractions 0.47 and 0.50, indicating that the material is becoming more pressure-dependent, a characteristic of the soil regime. Volume fraction 0.47 behaves as a solid in the fluid regime, where the angle of internal friction is lower because of less pressure dependency than volume fraction 0.50. Volume fractions above 0.50, 0.53, and 0.56 behave as soils, where friction between particles is dominant. This results in larger dilatancy and local frictional effects than a volume fraction of 0.50.

From this research, it can be concluded that with the material structure, a transition between fluid and soil behavior in the fresh state can be identified, where the transition is influenced by particle interactions, particle shape, and particle size.

8

RECOMMENDATIONS

This research gives insight into identifying the transition from fluid to soil behavior in the fresh state based on experimental test results and the associated failure mechanism for 3D concrete printing. More insight into the transition could be obtained through further research. Therefore, in this chapter, suggestions have been made which improve the insight into the transition between fluid and soil behavior. Besides these suggestions for further research, some suggestions have been made for 3D concrete printer developers.

First, the suggestions to improve insight into fluid to soil behavior transition will be discussed. The Bingham properties could be obtained, where all parameters of Equation 2.11 could be filled in to find the dominant regime of the mixture, either fluid or soil behavior. The Bingham properties could probably be obtained by an adjustment of the RAM Extruder or an adjustment to the material. No shear rate dependency was found with the setup used in this research. Adjusting the RAM Extruder to a larger barrel, where the diameter is enlarged, the parameters could be obtained when the experiment is performed for different vertical displacement rates. One vertical displacement rate per test is recommended to exclude the effects of the transition to different vertical speed rates. Also, an anti-segregation admixture could be added to the mixture, excluding the effect of pressure bleeding.

An analytical model could be made to obtain more knowledge about a mixture's behavior inside the RAM Extruder's barrel. The converging flow, in combination with the angle of the build-up material at the die entry, could be observed with an analytical model, and blockage inside the barrel could be described.

Besides adjusting the RAM Extruder, other experimental tests could also be performed to obtain the Bingham properties. The Vane Rotational Rheometer is a possible test to obtain these properties. This is an experimental test based on rheology. However, it has also been used in soil mechanics research. The experimental test uses the principle of simple shear flow. A remark to this test is that only the yield stress could be obtained for specific materials because a shear plane could occur next to the vane. Therefore, close attention should be paid to forming a shear plane to obtain the Bingham parameters. Besides the Vane Rotational Rheometer, also the DST could be used to obtain the Bingham parameters. The Bingham properties could be obtained by performing the DST with different shear rates. Close attention should be paid to the static yield stress peak. The peak could increase with an increasing shear rate. Also, the possibilities with the current experimental setup of the DST at the SED laboratory of the Eindhoven University of Technology should be investigated. The current experimental setup could be unsuitable for applying a variation of displacement rates.

Also, the vertical displacement of the sample in the DST could be measured. The volumetric strain could be found by obtaining the vertical displacement of the sample. With the volumetric strain, the dilatancy effect could be described individually. This research only describes the dilatancy effect in the static yield stress peak, which combines the dilatancy and local friction effects.

The experimental program could be extended for the individual mixtures in this research. For mixture SG, additional tests could be performed with higher volume fractions, within a range of 0.56 to 0.70, to validate that ϕ_{max} for round particles is around 0.64, as was found in other research and to validate the model of Krieger-Dougherty. With volume fractions higher than 0.64 for round particles, behavior

related to the soil regime should be observed. Also, the experimental program for mixture CS could be extended. The results observed a plateau at volume fractions 0.53 and 0.56. For more insight into this plateau and to obtain a specific value after which it occurs, it is recommended to perform more experimental tests in the range of volume fractions 0.52 to 0.60. During the testing, attention should be paid to randomizing the experiments to avoid errors in the experimental setup. Also, more repetitions are recommended to exclude uncertainties.

Second, suggestions for developers in 3D concrete printing. To obtain more insight into the relationship between the 3D concrete printer and the experimental results, other, more complex mixtures could be used, or the experiments could be scaled up. The mixture could be made more complex by adding plasticizers, VMA, fibers, and various particle-size aggregates to the cement paste. Additions to the cement paste could influence the failure criterion used to describe the material in a specific regime. By scaling up the experiments to the scale of the 3D concrete printer, a comparison could be made between the experimental results and the behavior of mixtures in the 3D concrete printer.

Besides more insight into the relationship between the 3D concrete printer and the experimental results, recommendations have been made for developing 3D concrete printers. If the mixture behaves like soil, a shorter hose is recommended. The soil behavior is dominated by dilatancy and local frictional effects, where the friction causes blocking, as observed in the RAM Extruder. The shorter the hose, the less likely blocking occurs due to friction between particles. Also, it is recommended to make the nozzle smaller than the diameter of the hose. In the RAM Extruder, it has been observed that materials that behave as soil or as a fluid fall through the die when the diameter of the die is too large. Therefore the applied pressure from the pump is more difficult to control and the printing trial can be less constant.

BIBLIOGRAPHY

[1] Standard Test Method for Direct Shear Test of Soils Under Consolidated Drained Conditions ASTM D3080, 2004. 14

[2] Bruno Andreotti, Yoël Forterre, and Olivier Pouliquen. *Granular Media*. Cambridge University Press, 2013. ix, 7, 8

[3] Joseph J. Assaad, Jacques Harb, and Yara Maalouf. Measurement of yield stress of cement pastes using the direct shear test. *Journal of Non-Newtonian Fluid Mechanics*, 214:18–27, 2014. 1, 24

[4] J. J. Benbow, E. W. Oxley, and J. Bridgwater. The extrusion mechanics of pastes-the influence of paste formulation on extrusion parameters. *Chemical Engineering Science*, 42(9):2151–2162, 1987. 3, 19, 32

[5] F. P. Bos, P. J. Kruger, S. S. Lucas, and G. P.A.G. van Zijl. Juxtaposing fresh material characterisation methods for buildability assessment of 3D printable cementitious mortars. *Cement and Concrete Composites*, 120(March):104024, 2021. 1, 3

[6] H.C. Brinkman. the Viscosity of Concentrated Suspensions. *The Journal of Chemical Physics*, 20(571):273–288, 1952. 5

[7] H.J.H. Brouwers. Viscosity of a concentrated suspension of rigid monosized particles. *Physical Review E - Statistical, Nonlinear, and Soft Matter Physics*, 81(051402), 2010. 5

[8] Roger D. Browne and Phillip B. Bamforth. Tests To Establish Concrete Pumpability. *J Am Concrete Inst*, 74(5):193–203, 1977. ix, 1, 9, 32, 34

[9] D. Burt. *Improved Design of Settling Tanks Using an Extended Drift Flux Model*. PhD thesis, 2010. ix, 4

[10] Stefan Chaves Figueiredo, Claudia Romero Rodríguez, Zeeshan Y. Ahmed, D. H. Bos, Yading Xu, Theo M. Salet, Oğuzhan Çopuroğlu, Erik Schlangen, and Freek P. Bos. An approach to develop printable strain hardening cementitious composites. *Materials and Design*, 169, 2019. 3, 29

[11] Muawia A. Dafalla. Effects of clay and moisture content on direct shear tests for clay-sand mixtures. *Advances in Materials Science and Engineering*, 2013, 2013. ix, 16

[12] Evelien Dorresteijn. *The applicability of different characterization methods to determine the mechanical material properties of 3D printable pastes with various aggregates and fibers*. PhD thesis, Eindhoven University of Technology, 2022. ix, 3, 6, 12, 15, 17, 19, 29, 35, 37

[13] Albert Einstein. Eine neue Bestimmung der Moleküldimensionen. pages 289–306, 1906. 4

[14] ENCI. Hoogovencement. *Hoogovencement*, pages 0–1, 2006. 12

[15] Patrice Estellé, Christophe Lanos, Arnaud Perrot, and Sofiane Amziane. Processing the vane shear flow data from Couette analogy. *Applied Rheology*, 18(3), 2008. 34, 37

[16] Robert J. Flatt. Dispersion forces in cement suspensions. *Cement and Concrete Research*, 34(3):399–408, 2004. 6

[17] Robert J. Flatt and Paul Bowen. Electrostatic repulsion between particles in cement suspensions: Domain of validity of linearized Poisson-Boltzmann equation for nonideal electrolytes. *Cement and Concrete Research*, 33(6):781–791, 2003. 6

[18] Robert J. Flatt and Paul Bowen. Yodel: A yield stress model for suspensions. *Journal of the American Ceramic Society*, 89(4):1244–1256, 2006. 7

[19] Robert J Flatt, Paul Bowen, Yves F Houst, and Heinrich Hofmann. Modelling Interparticle Forces and Yield Stress of Cement Suspensions. *11th International Congress on the Chemistry of Cement.*, (May):618–628, 2003. 6

[20] Aleksander Grabowski and Michał Nitka. 3D DEM simulations of basic geotechnical tests with early detection of shear localization. *Studia Geotechnica et Mechanica*, 43(1):48–64, 2020. ix, 14, 21, 24, 25

[21] Lutz Heymann and Nuri Aksel. Transition pathways between solid and liquid state in suspensions. *Physical Review E - Statistical, Nonlinear, and Soft Matter Physics*, 75(2):1–9, 2007. 25, 26, 41

[22] Lutz Heymann, Sigrid Peukert, and Nuri Aksel. On the solid-liquid transition of concentrated suspensions in transient shear flow. *Rheologica Acta*, 41(4):307–315, 2002. 41

[23] Y. Jacquet, V. Picandet, and A. Perrot. Characterization of Tensile Behavior of Fresh Cementitious Materials. *ACI Materials Journal*, 118(6):217–226, 2021. 1

[24] Roshan Jayathilakage, Jay Sanjayan, and Pathmanathan Rajeev. Direct shear test for the assessment of rheological parameters of concrete for 3D printing applications. *Materials and Structures/Materiaux et Constructions*, 52(1):1–13, 2019. 3, 14

[25] J. Kozicki, M. Niedostatkiewicz, J. Tejchman, and H. B. Muhlhaus. Discrete modelling results of a direct shear test for granular materials versus FE results. *Granular Matter*, 15(5):607–627, 2013. 14, 25

[26] Irvin M. Krieger and Thomas J. Dougherty. A Mechanism for Non-Newtonian Flow in Suspensions of Rigid Spheres. *Transactions of the Society of Rheology*, 3(1):137–152, 1959. 5

[27] Jacques Kruger, Stephan Zeranka, and Gideon van Zijl. 3D concrete printing: A lower bound analytical model for buildability performance quantification. *Automation in Construction*, 106(June):102904, 2019. 1

[28] Gang Lu and Kejin Wang. Investigation into yield behavior of fresh cement paste: Model and experiment. *ACI Materials Journal*, 107(1):12–19, 2010. 39, 40

[29] Gang Lu and Kejin Wang. Theoretical and experimental study on shear behavior of fresh mortar. *Cement and Concrete Composites*, 33(2):319–327, 2011. 16, 22, 23, 24, 26

[30] Siwei Ma, Cihang Huang, Prince Baah, Tommy Nantung, and Na Lu. The influence of water-to-cement ratio and superabsorbent polymers (SAPs) on solid-like behaviors of fresh cement pastes. *Construction and Building Materials*, 275, 2021. 40

[31] Fabien Mahaut, Samir Mokéddem, Xavier Chateau, Nicolas Roussel, and Guillaume Ovarlez. Effect of coarse particle volume fraction on the yield stress and thixotropy of cementitious materials.pdf. *Cement and Concrete Research*, 38(11):1276–1285, 2008. 15

[32] V. Mechtcherine, F. P. Bos, A. Perrot, W. R.Leal da Silva, V. N. Nerella, S. Fataei, R. J.M. Wolfs, M. Sonebi, and N. Roussel. Extrusion-based additive manufacturing with cement-based materials – Production steps, processes, and their underlying physics: A review. *Cement and Concrete Research*, 132(March):106037, 2020. 1

[33] Faith A. Morrison. *Understanding Rheology*. Oxford University Press, 2001. ix, 1, 3, 4, 17, 18, 19, 34, 37

[34] M. Nitka and A. Grabowski. Shear band evolution phenomena in direct shear test modelled with DEM. *Powder Technology*, 391:369–384, 2021. 14, 25

[35] Anton Paar. The influence of particles on suspension rheology, 2023. ix, 5, 6

[36] Ye Qian and Shiho Kawashima. Distinguishing dynamic and static yield stress of fresh cement mortars through thixotropy. *Cement and Concrete Composites*, 86:288–296, 2018. 9, 40

[37] R. Roscoe. The viscosity of suspensions of rigid spheres. *British Journal of Applied Physics*, 3(8):267–269, 1952. 5

[38] N. Roussel, H. Bessaies-Bey, S. Kawashima, D. Marchon, K. Vasilic, and R. Wolfs. Recent advances on yield stress and elasticity of fresh cement-based materials. *Cement and Concrete Research*, 124(August):105798, 2019. 26, 41

[39] Nicolas Roussel. *Understanding the Rheology of Concrete*. Woodhead Publishing Limited, Cambridge, 1st edition, 2012. ix, 3, 6, 15, 31, 32, 34, 35

[40] Z. Toutou and N. Roussel. Multi scale experimental study of concrete rheology: From water scale to gravel scale. *Materials and Structures/Materiaux et Constructions*, 39(2):189–199, 2006. 34, 35, 37

[41] Anton Verruijt and Stefan van Baars. *Soil Mechanics*. VSSD, 1 edition, 2007. ix, 8, 16

[42] S. G. Ward and R. L. Whitmore. Studies of the viscosity and sedimentation of suspensions Part 1. - The viscosity of suspension of spherical particles. *British Journal of Applied Physics*, 1:286–290, 1950. 5

[43] Eric W. Weisstrein. Vesica Piscis. 14

[44] R. J.M. Wolfs, F. P. Bos, and T. A.M. Salet. Early age mechanical behaviour of 3D printed concrete: Numerical modelling and experimental testing. *Cement and Concrete Research*, 106(May 2017):103–116, 2018. 14, 111

[45] Joumana Yammine, Mohend Chaouche, Michel Guerinet, Micheline Moranville, and Nicolas Roussel. From ordinary rhelogy concrete to self compacting concrete: A transition between frictional and hydrodynamic interactions. *Cement and Concrete Research*, 38(7):890–896, 2008. 6, 9, 31, 32

[46] Qiang Yuan, Dajun Zhou, Kamal H. Khayat, Dimitri Feys, and Caijun Shi. On the measurement of evolution of structural build-up of cement paste with time by static yield stress test vs. small amplitude oscillatory shear test. *Cement and Concrete Research*, 99:183–189, 9 2017. 41

A

Density

AccuPycII 1340 V2.00
Serial Number: 1076
Density and Volume Report

Sample ID: Glass Beads
Sample Mass: 25.9120 g
Temperature: 22.4 ?C
Number of Purges: 10
Cell Volume: 37.7887 cm3

Started: 06/02/23 11:39:21
Completed: 06/02/23 11:58:09
Equilibration Rate: 0.0050 psig/min
Expansion Volume: 73.9736 cm3

Cycle#	Volume cm3	Deviation cm3	Density g/cm3	Deviation g/cm3	Elapsed Time	Temperature ?C
1	10.6413	-0.0016	2.4350	0.0004	0:05:35	22.2
2	10.6383	-0.0046	2.4357	0.0011	0:07:05	22.2
3	10.6389	-0.0040	2.4356	0.0009	0:08:33	22.2
4	10.6408	-0.0021	2.4352	0.0005	0:09:57	22.2
5	10.6433	0.0004	2.4346	-0.0001	0:11:24	22.3
6	10.6444	0.0015	2.4343	-0.0003	0:12:53	22.3
7	10.6431	0.0002	2.4346	-0.0001	0:14:21	22.3
8	10.6451	0.0022	2.4342	-0.0005	0:15:47	22.4
9	10.6457	0.0028	2.4340	-0.0006	0:17:11	22.3
10	10.6482	0.0053	2.4335	-0.0012	0:18:40	22.3

Average Volume: 10.6429 cm3
Average Density: 2.4347 g/cm3

Standard Deviation: 0.0030 cm3
Standard Deviation: 0.0007 g/cm3

AccuPycII 1340 V2.00
Serial Number: 1076
Density and Volume Report

Sample ID: Sand
Sample Mass: 32.2937 g
Temperature: 20.9 ?C
Number of Purges: 10
Cell Volume: 37.7887 cm3
Started: 13/12/22 11:05:01
Completed: 13/12/22 11:24:55
Equilibration Rate: 0.0050 psig/min
Expansion Volume: 73.9736 cm3

Cycle#	Volume cm3	Deviation cm3	Density g/cm3	Deviation g/cm3	Elapsed Time	Temperature ?C
1	12.2331	0.0015	2.6399	-0.0003	0:05:31	20.5
2	12.2266	-0.0050	2.6413	0.0011	0:07:13	20.6
3	12.2317	0.0001	2.6402	-0.0000	0:08:45	20.6
4	12.2270	-0.0046	2.6412	0.0010	0:10:24	20.6
5	12.2324	0.0009	2.6400	-0.0002	0:11:53	20.7
6	12.2327	0.0012	2.6399	-0.0003	0:13:24	20.7
7	12.2371	0.0056	2.6390	-0.0012	0:14:49	20.7
8	12.2303	-0.0012	2.6405	0.0003	0:16:25	20.8
9	12.2317	0.0002	2.6402	-0.0000	0:18:07	20.8
10	12.2329	0.0013	2.6399	-0.0003	0:19:46	20.9

Average Volume: 12.2315 cm3
Standard Deviation: 0.0029 cm3
Average Density: 2.6402 g/cm3
Standard Deviation: 0.0006 g/cm3

B

Results DST for mixture SG

Volume fraction 0.47

Table B.1: Static yield stress peak values for mixture SG VF0.47 in kPa

	1	2	3	Average
1.5 N	0.110	0.634	0.350	0.365
5.72 N	1.149	1.465	0.341	0.985
14.036 N	0.176	2.201	0.245	0.874

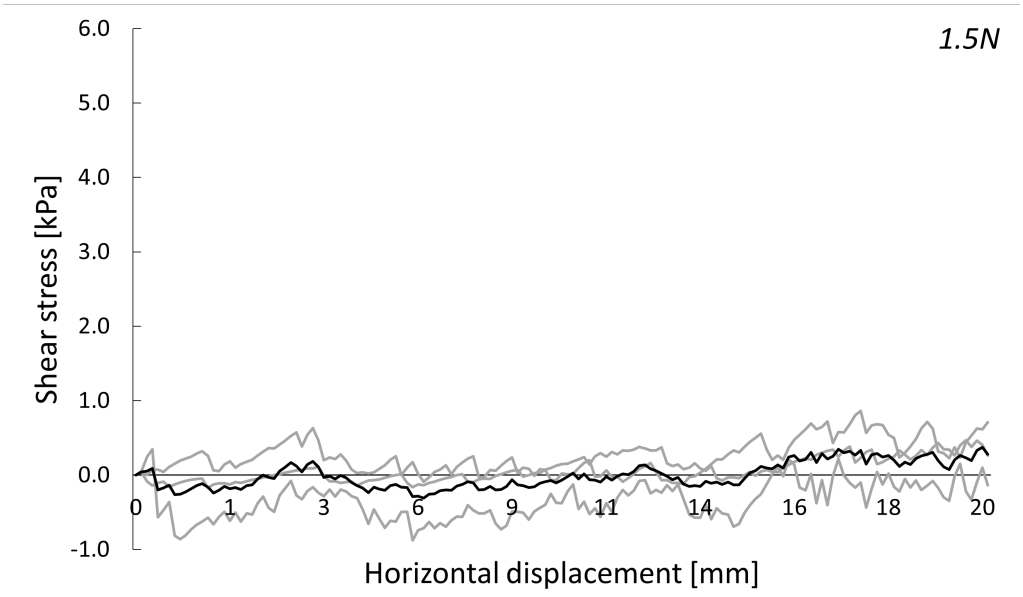

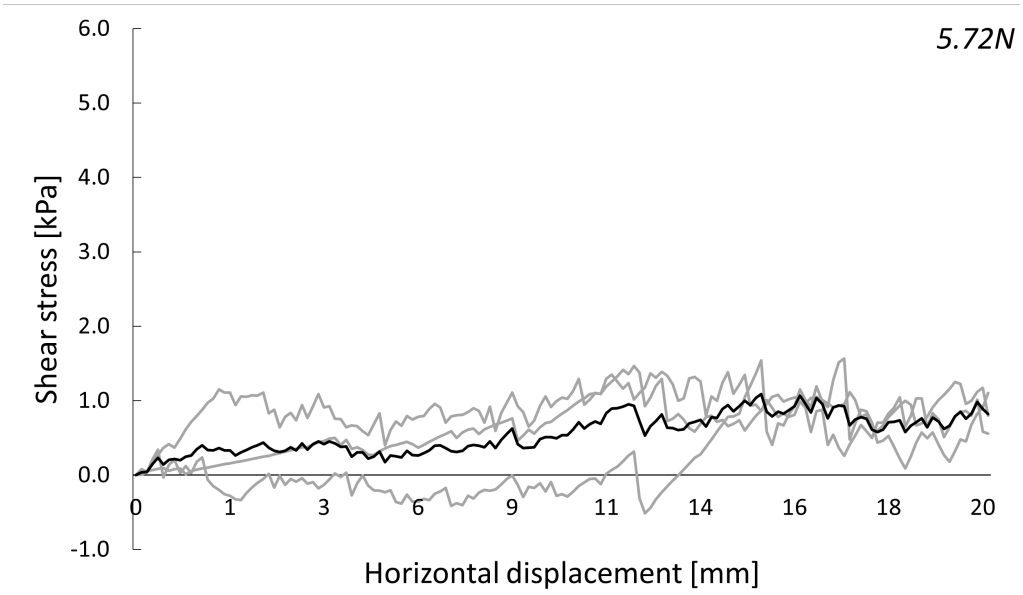
5.72N
Shear stress [kPa]
6.0
5.0
4.0
3.0
2.0
1.0
0.0
-1.0
0
1
3
6
9
11
14
16
18
20
Horizontal displacement [mm]

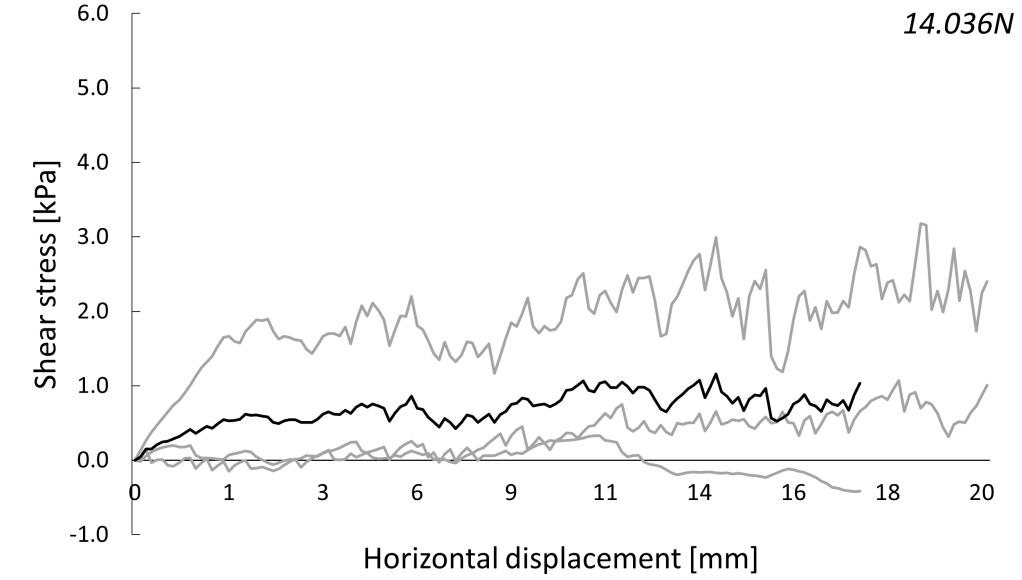
14.036N
Shear stress [kPa]
6.0
5.0
4.0
3.0
2.0
1.0
0.0
-1.0
0
1
3
6
9
11
14
16
18
20
Horizontal displacement [mm]

Volume fraction 0.50

Table B.2: Static yield stress peak values for mixture SG VF0.50 in kPa

	1	2	3	Average
1.5 N	0.493	0.355	0.336	0.395
5.72 N	0.407	0.220	0.675	0.434
14.036 N	0.497	0.000	0.280	0.259

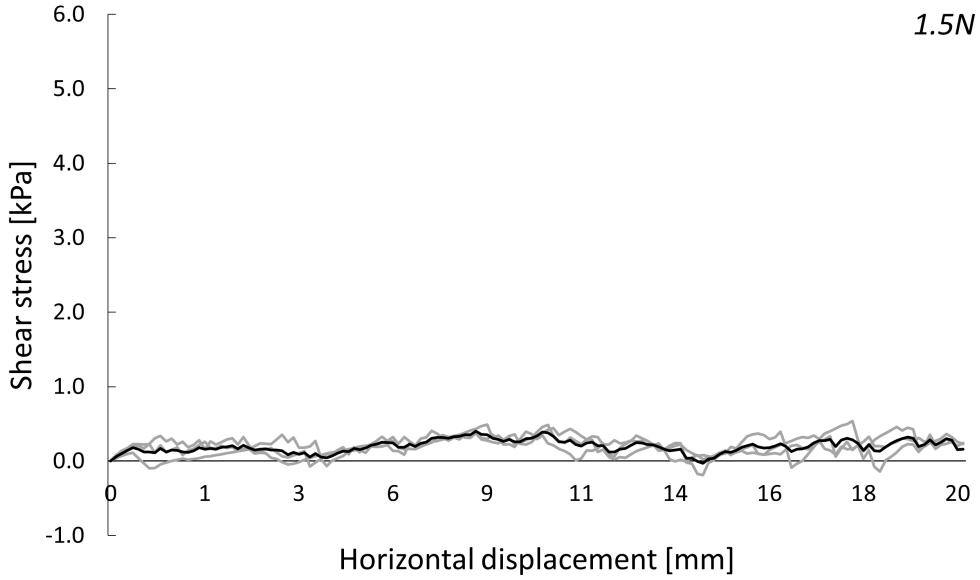

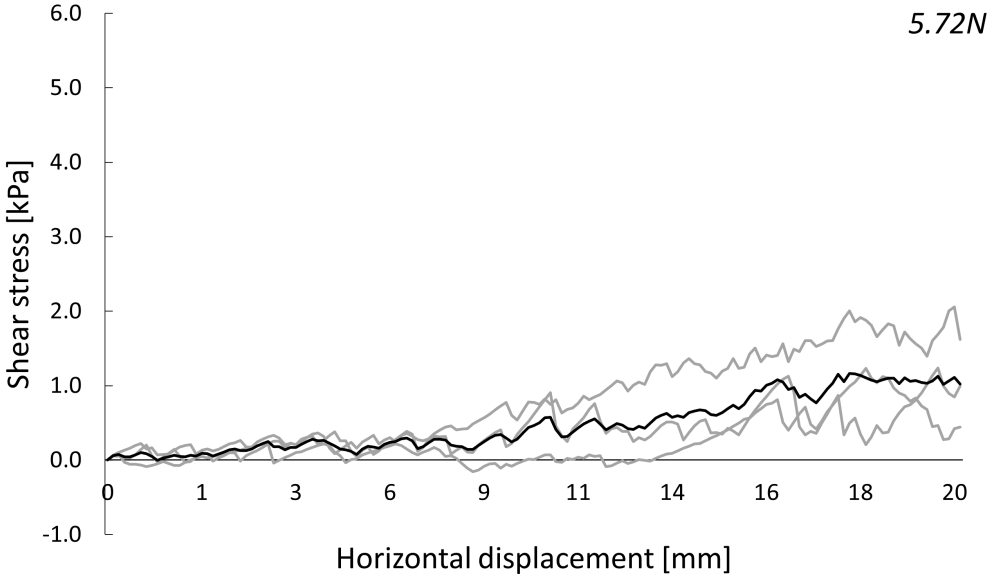
5.72N
6.0
5.0
4.0
3.0
2.0
1.0
0.0
-1.0
Shear stress [kPa]
0
1
3
6
9
11
14
16
18
20
Horizontal displacement [mm]

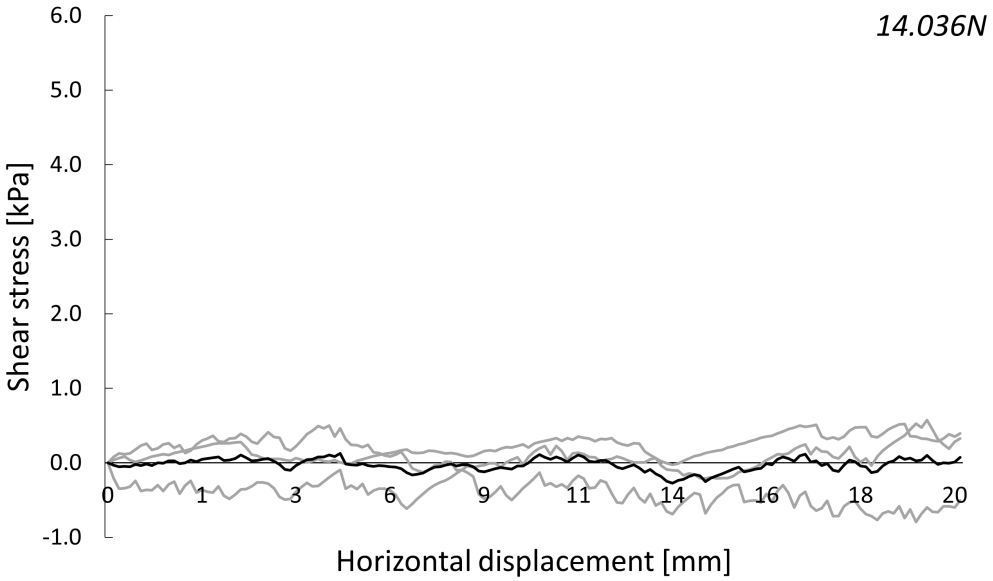
14.036N
6.0
5.0
4.0
3.0
2.0
1.0
0.0
-1.0
Shear stress [kPa]
0
1
3
6
9
11
14
16
18
20
Horizontal displacement [mm]

Volume fraction 0.53

Table B.3: Static yield stress peak values for mixture SG VF0.53 in kPa

	1	2	3	Average
1.5 N	0.339	0.689	0.648	0.559
5.72 N	0.979	0.640	1.186	0.935
14.036 N	1.801	0.791	0.258	0.950

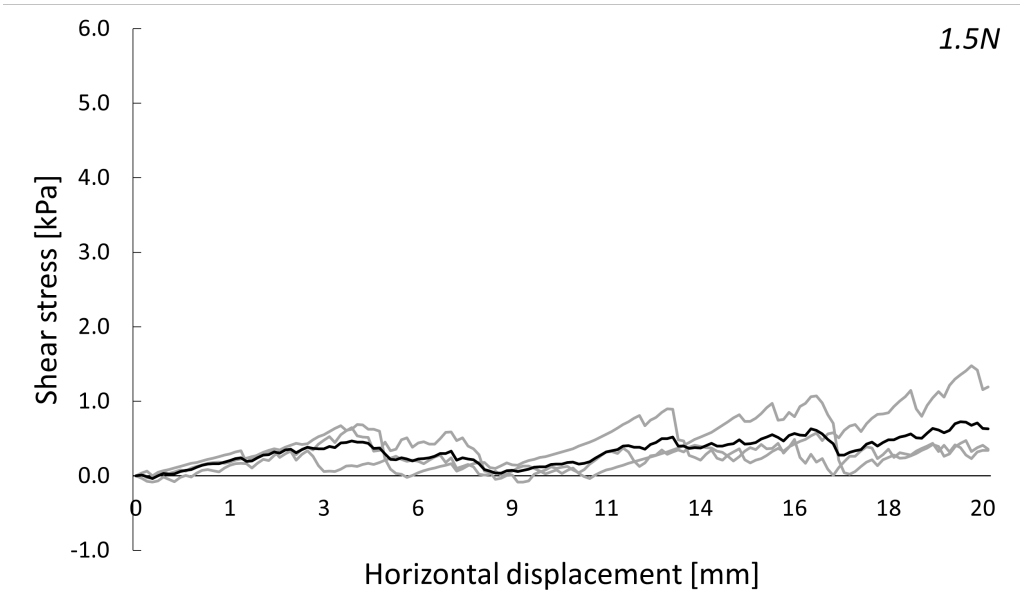

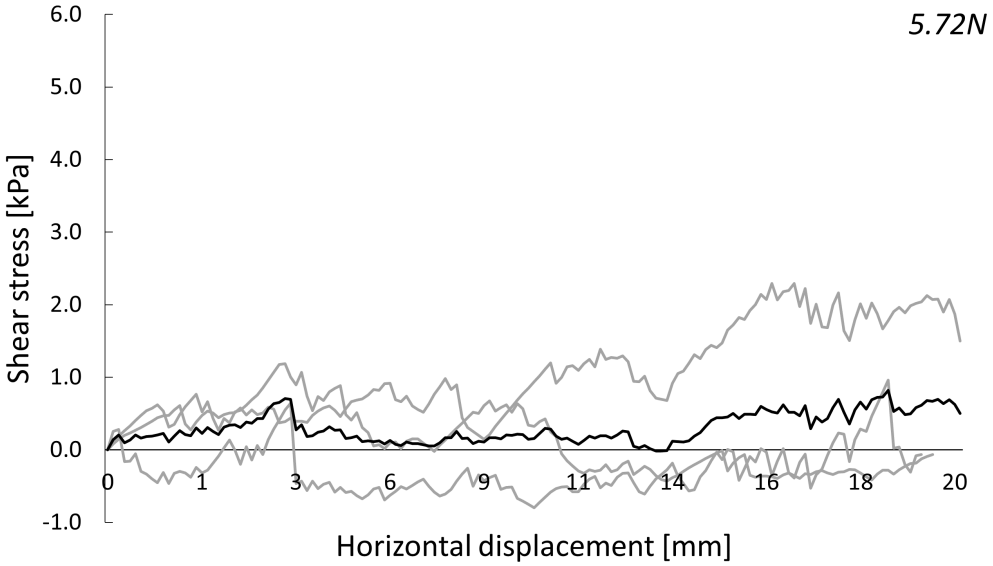
5.72N
6.0
5.0
4.0
3.0
2.0
1.0
0.0
-1.0
Shear stress [kPa]
0
1
3
6
9
11
14
16
18
20
Horizontal displacement [mm]

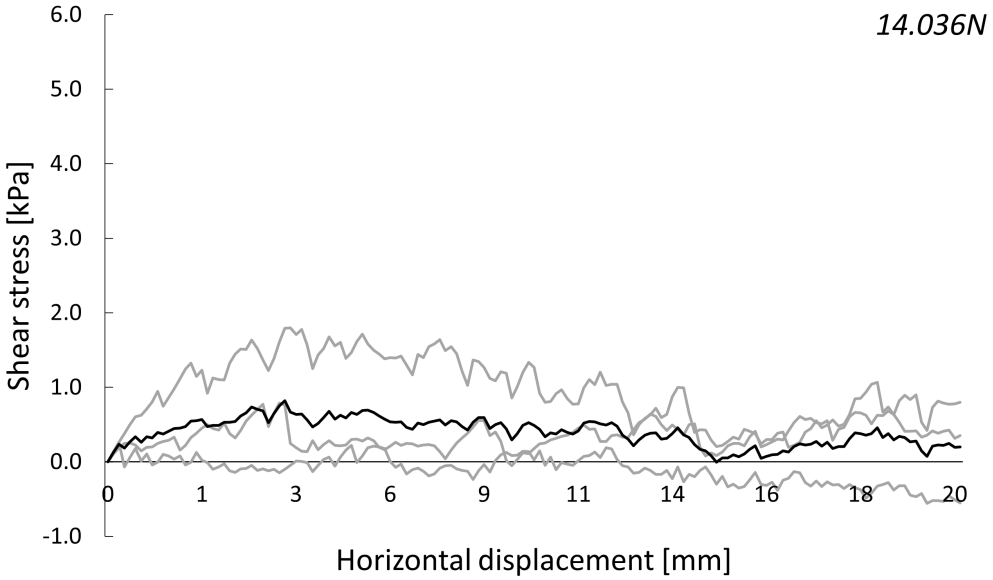
14.036N
6.0
5.0
4.0
3.0
2.0
1.0
0.0
-1.0
Shear stress [kPa]
0
1
3
6
9
11
14
16
18
20
Horizontal displacement [mm]

Volume fraction 0.56

Table B.4: Static yield stress peak values for mixture SG VF0.56 in kPa

	1	2	3	Average
1.5 N	0.254	0.724	0.291	0.423
5.72 N	0.857	0.000	0.776	0.544
14.036 N	0.999	0.154	1.402	0.852

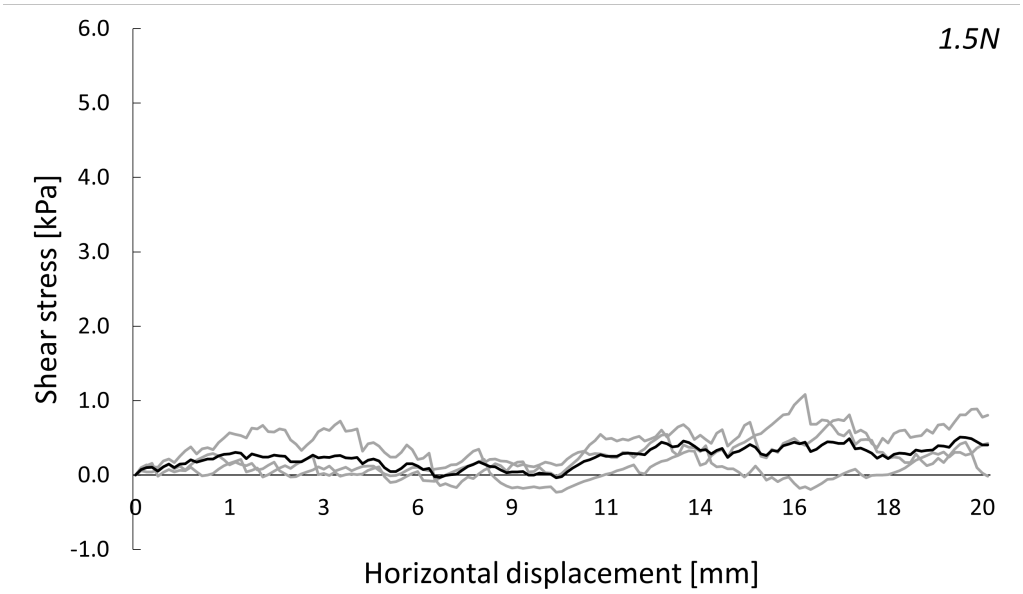

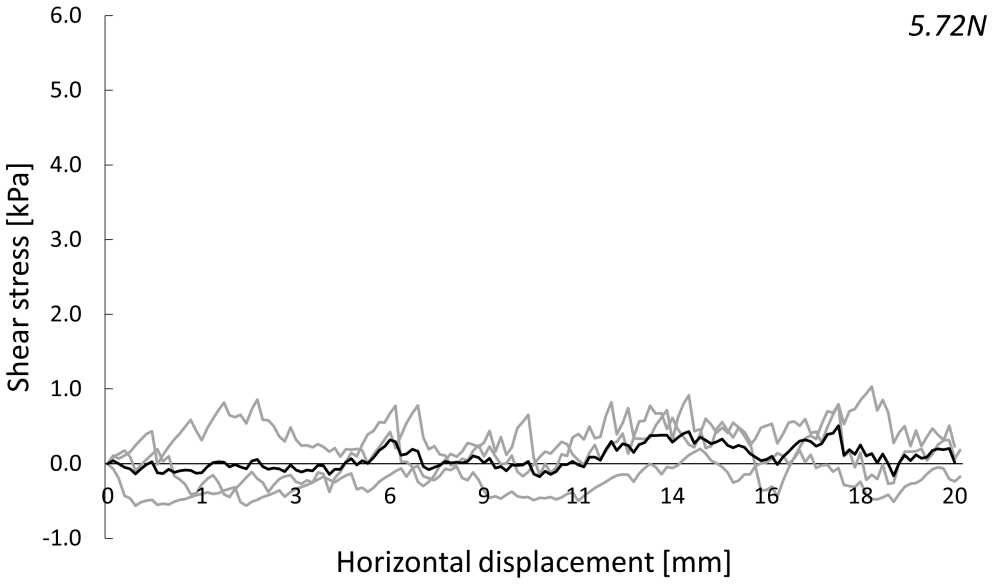
5.72N
Shear stress [kPa]
6.0
5.0
4.0
3.0
2.0
1.0
0.0
-1.0
0
1
3
6
9
11
14
16
18
20
Horizontal displacement [mm]

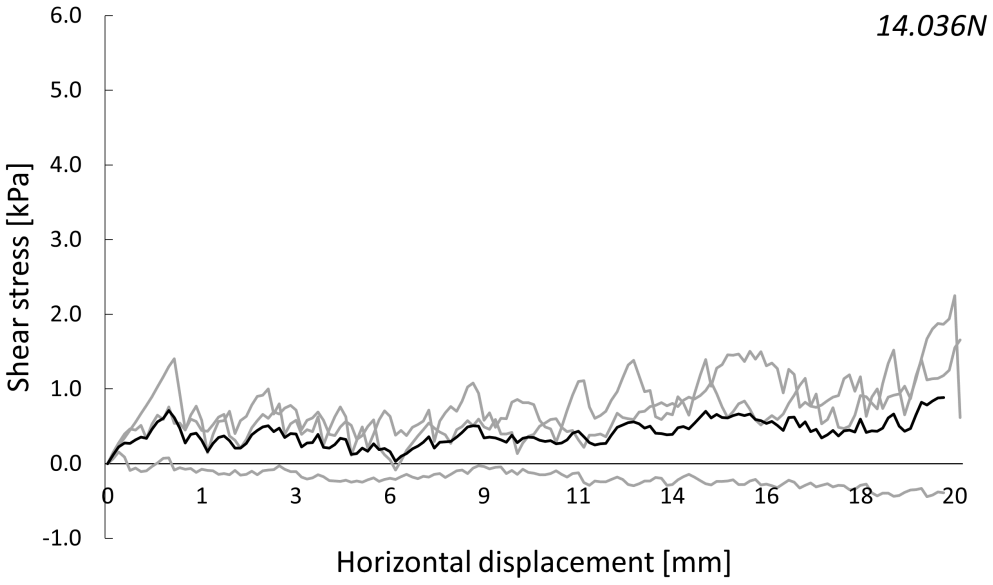
14.036N
Shear stress [kPa]
6.0
5.0
4.0
3.0
2.0
1.0
0.0
-1.0
0
1
3
6
9
11
14
16
18
20
Horizontal displacement [mm]

Combination

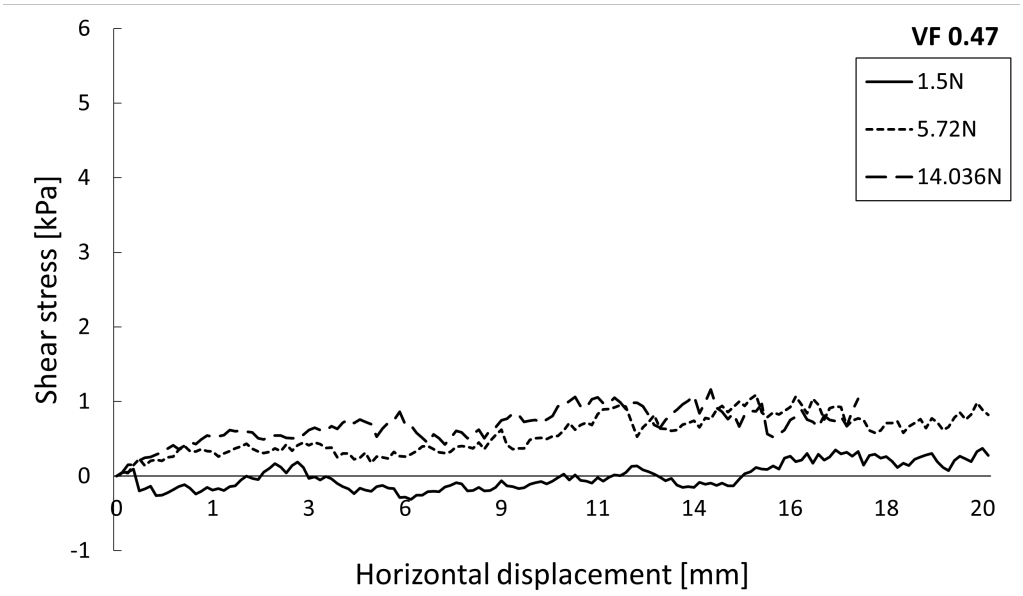

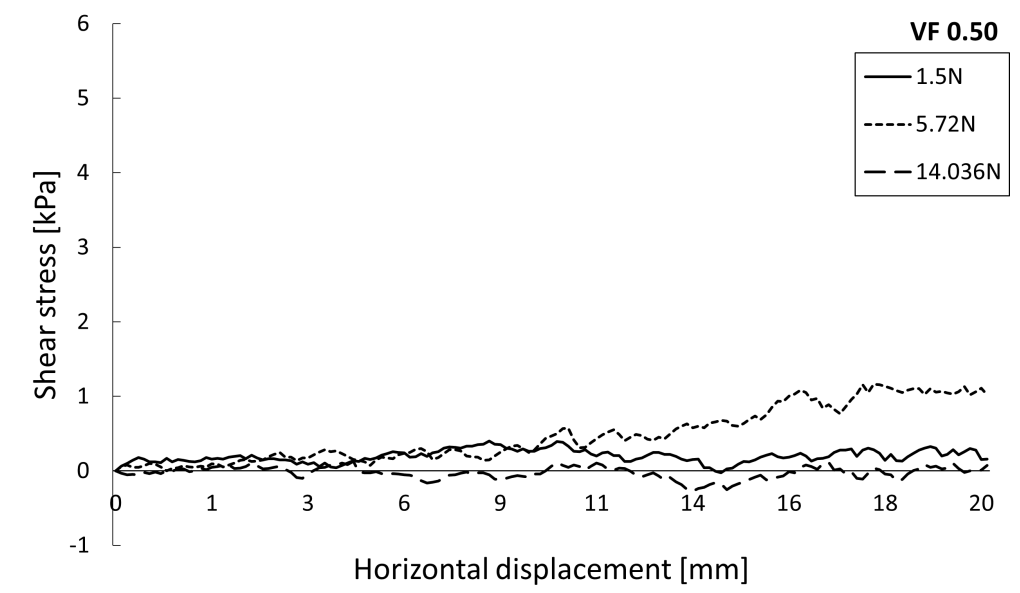

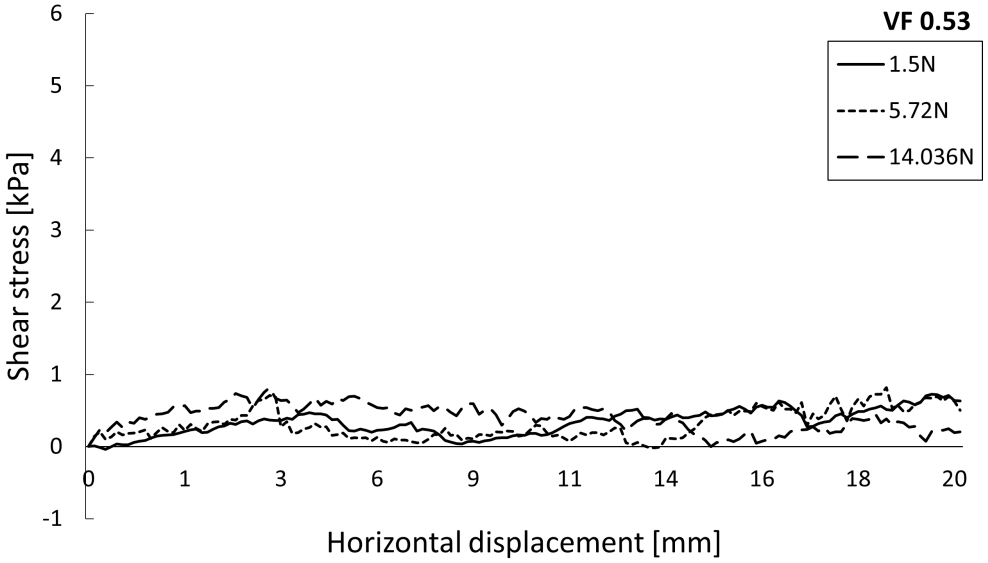
VF 0.53
1.5N
5.72N
14.036N
Shear stress [kPa]
6
5
4
3
2
1
0
-1
0
1
3
6
9
11
14
16
18
20
Horizontal displacement [mm]

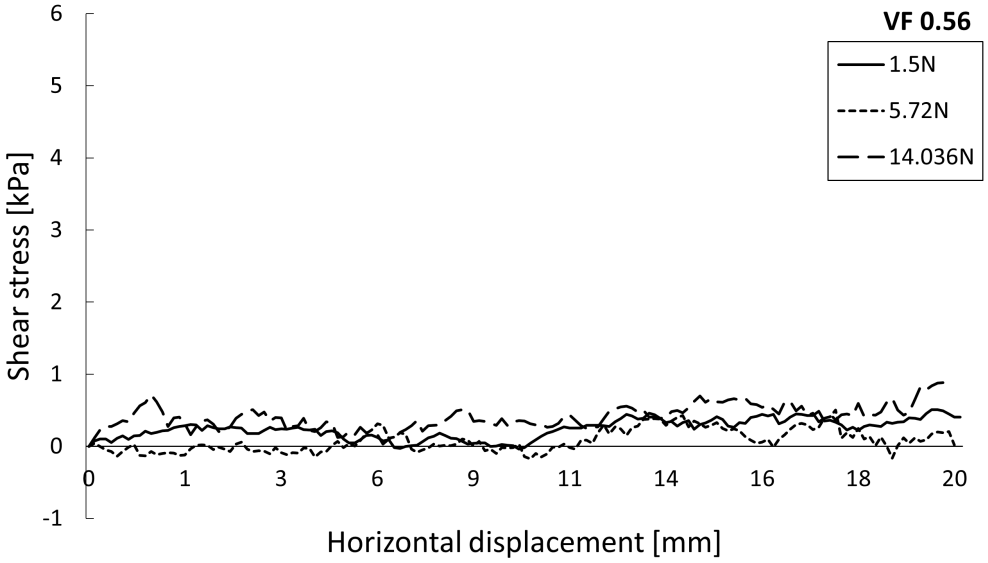
VF 0.56
1.5N
5.72N
14.036N
Shear stress [kPa]
6
5
4
3
2
1
0
-1
0
1
3
6
9
11
14
16
18
20
Horizontal displacement [mm]

C

Results DST for mixture CP

Volume fraction 0.47

Table C.1: Static yield stress peak values for mixture CP VF0.47 in kPa

	1	2	3	4	Average
1.5 N	0.081	0.541	0.231	0.186	0.260
5.72 N	0.337	0.297	0.362	-	0.332
14.036 N	0.397	1.297	0.459	-	0.718

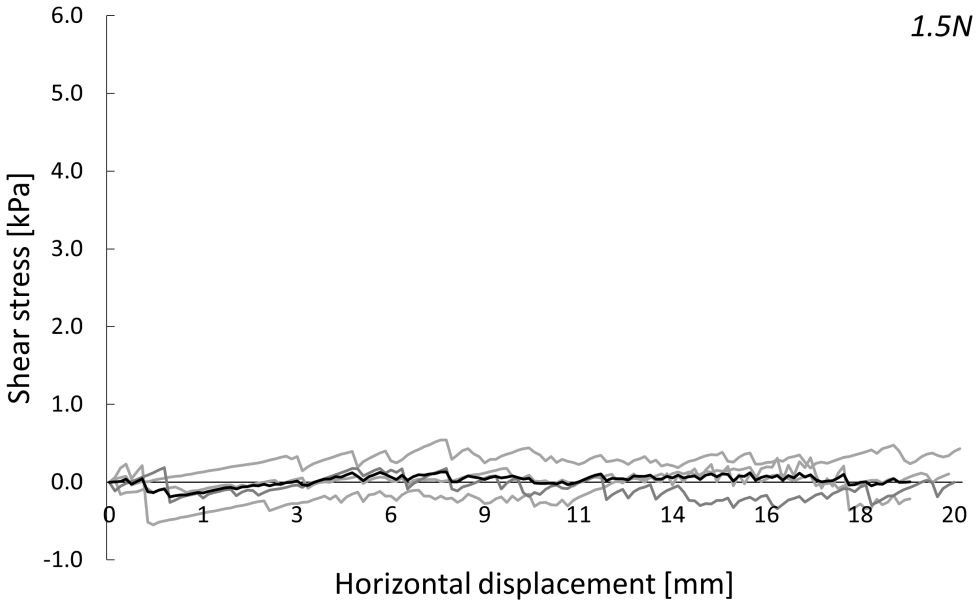

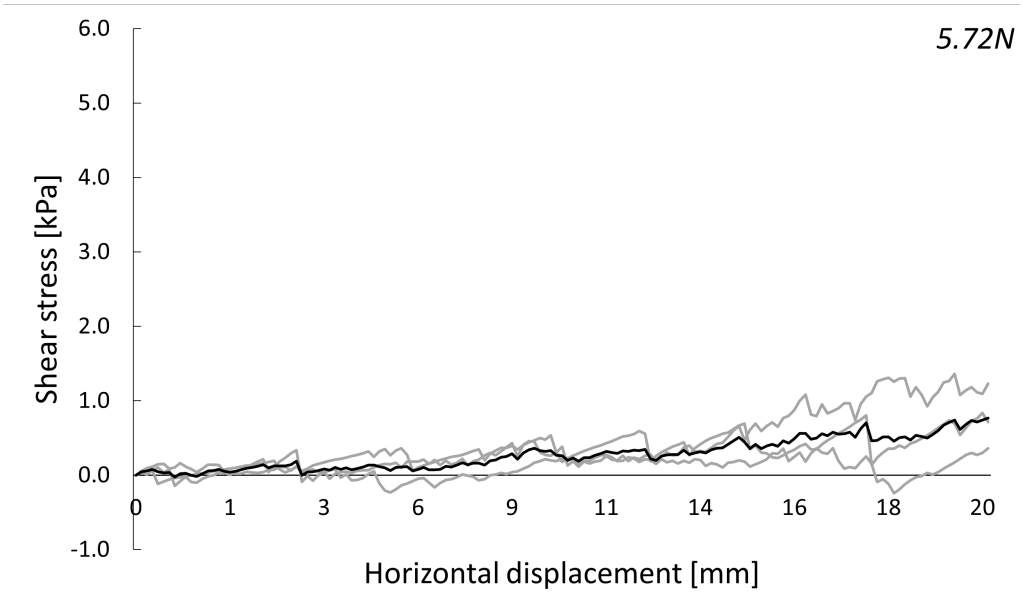
5.72N
6.0
5.0
4.0
3.0
2.0
1.0
0.0
-1.0
Shear stress [kPa]
0
1
3
6
9
11
14
16
18
20
Horizontal displacement [mm]

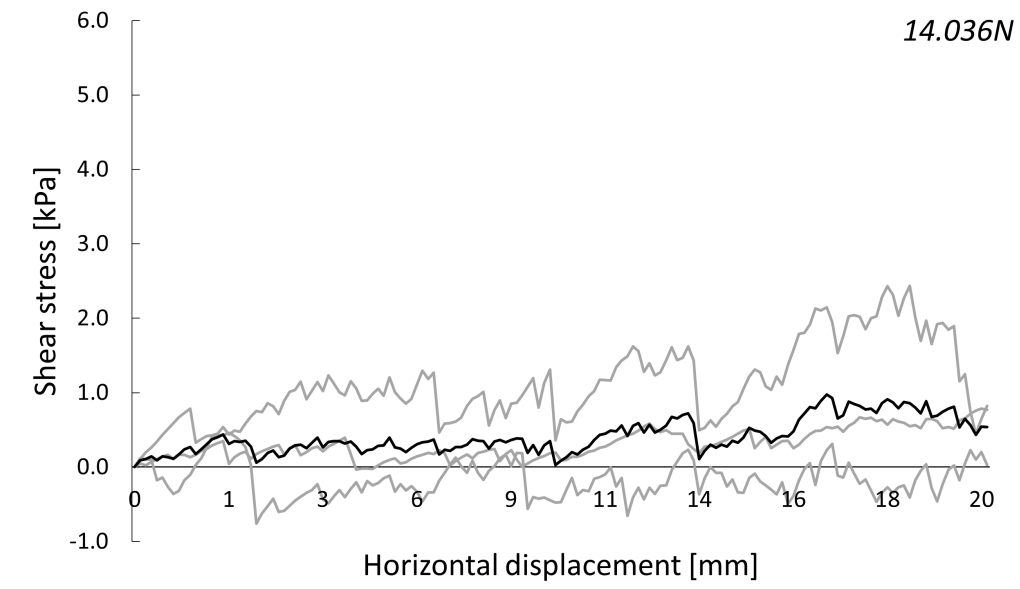
14.036N
6.0
5.0
4.0
3.0
2.0
1.0
0.0
-1.0
Shear stress [kPa]
0
1
3
6
9
11
14
16
18
20
Horizontal displacement [mm]

Volume fraction 0.50

Table C.2: Static yield stress peak values for mixture CP VF0.50 in kPa

	1	2	3	4	Average
1.5 N	0.451	0.349	0.968	-	0.590
5.72 N	0.751	0.803	0.538	1.999	1.023
14.036 N	0.473	1.548	0.877	-	0.966

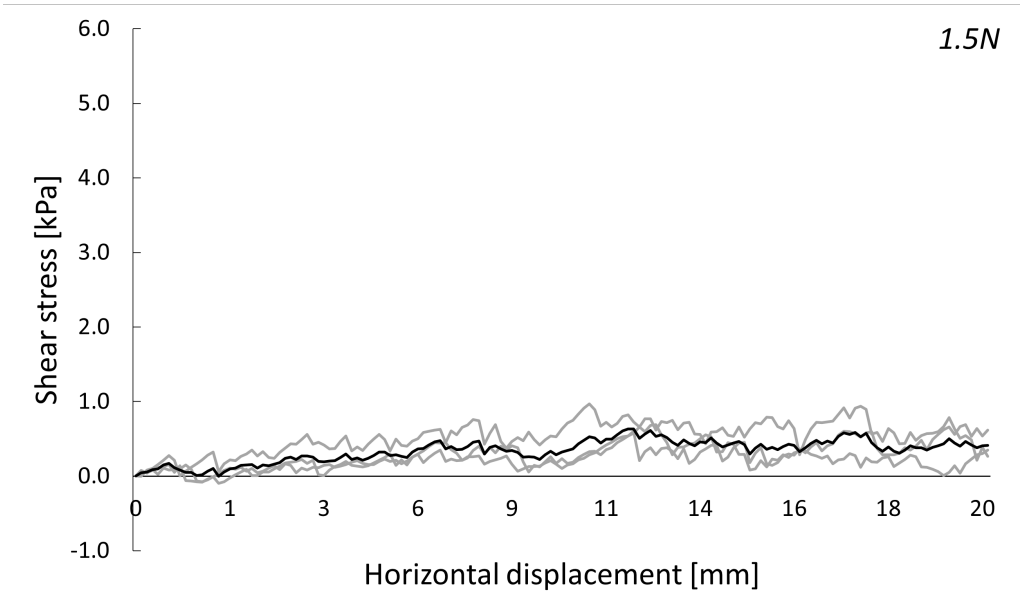

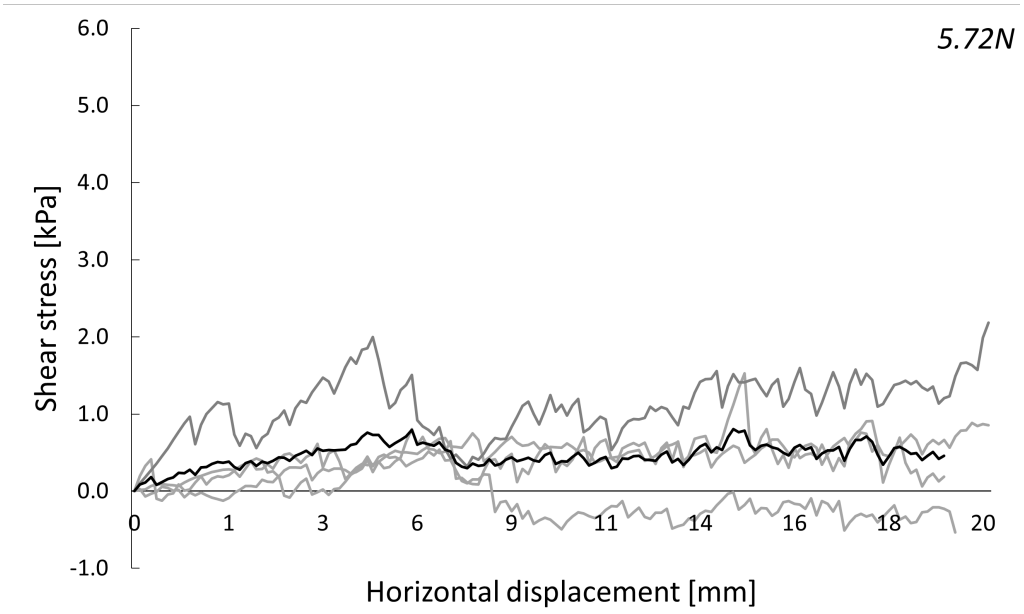
5.72N
Shear stress [kPa]
6.0
5.0
4.0
3.0
2.0
1.0
0.0
-1.0
0
1
3
6
9
11
14
16
18
20
Horizontal displacement [mm]

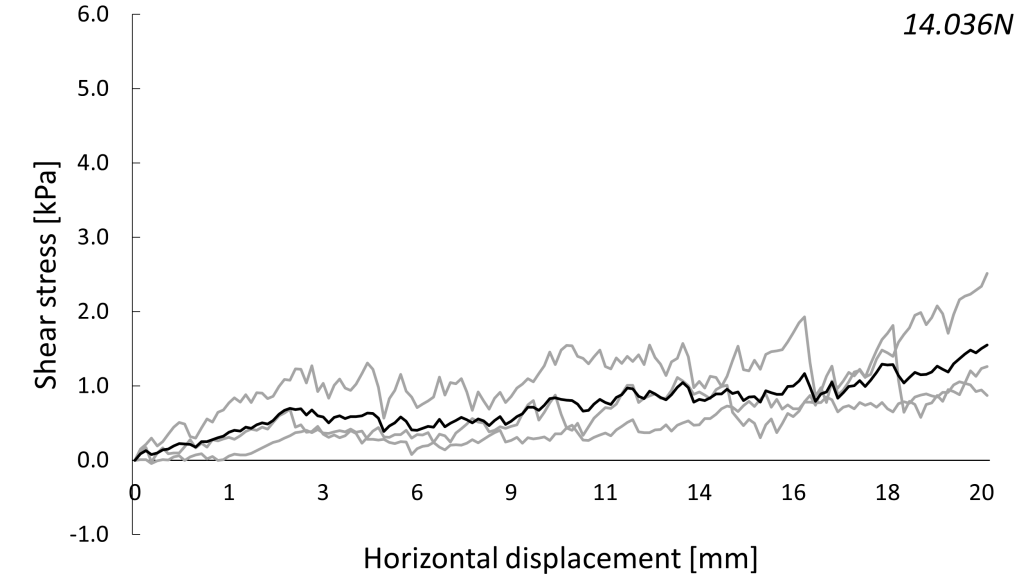
14.036N
Shear stress [kPa]
6.0
5.0
4.0
3.0
2.0
1.0
0.0
-1.0
0
1
3
6
9
11
14
16
18
20
Horizontal displacement [mm]

Volume fraction 0.53

Table C.3: Static yield stress peak values for mixture CP VF0.53 in kPa

	1	2	3	4	Average
1.5 N	1.203	0.573	1.365	-	1.047
5.72 N	0.485	1.390	1.1014	0.614	0.876
14.036 N	1.615	1.191	0.644	-	1.150

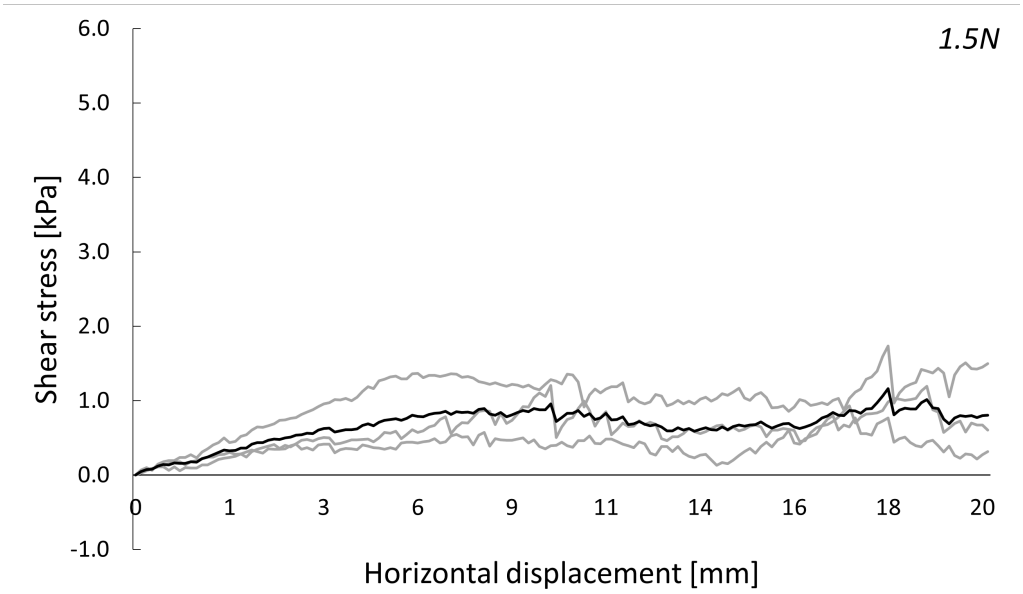

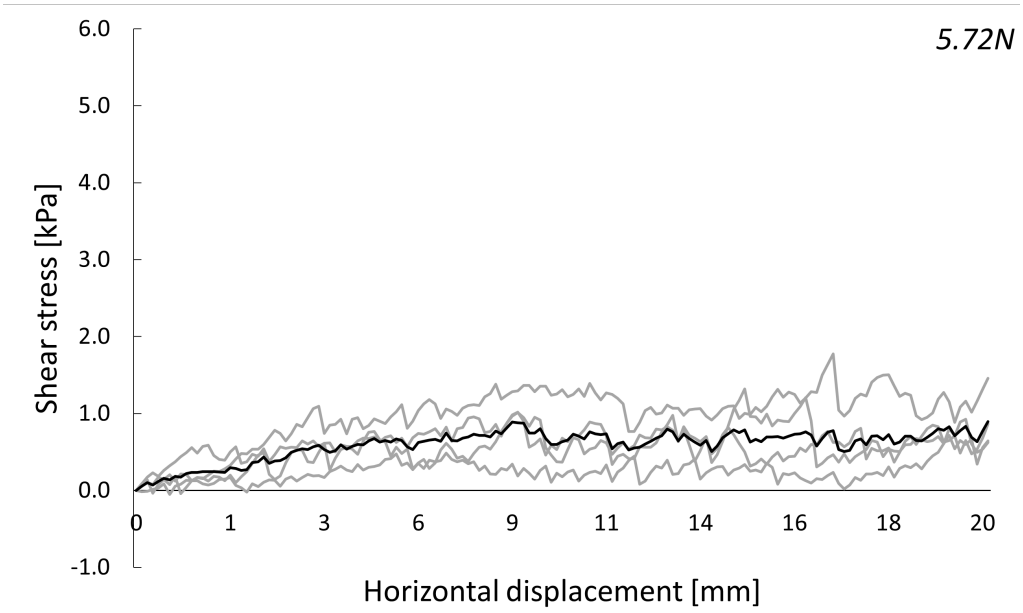
5.72N
Shear stress [kPa]
6.0
5.0
4.0
3.0
2.0
1.0
0.0
-1.0
0
1
3
6
9
11
14
16
18
20
Horizontal displacement [mm]

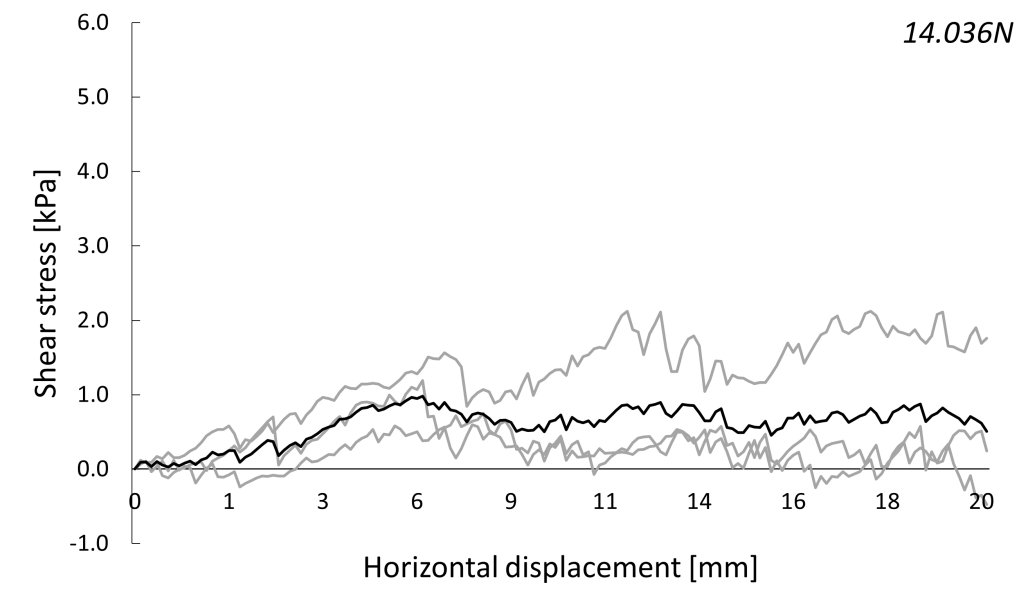
14.036N
Shear stress [kPa]
6.0
5.0
4.0
3.0
2.0
1.0
0.0
-1.0
0
1
3
6
9
11
14
16
18
20
Horizontal displacement [mm]

Volume fraction 0.56

Table C.4: Static yield stress peak values for mixture CP VF0.56 in kPa

	1	2	3	4	Average
1.5 N	2.629	2.537	2.413	-	2.526
5.72 N	1.672	4.170	3.326	3.955	3.281
14.036 N	2.963	2.366	5.535	-	3.561

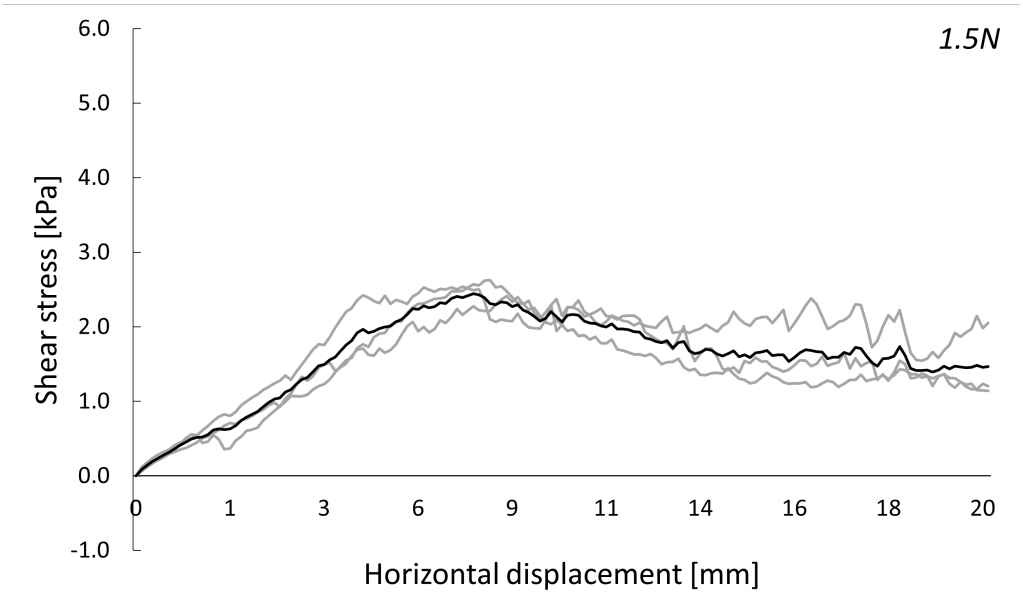

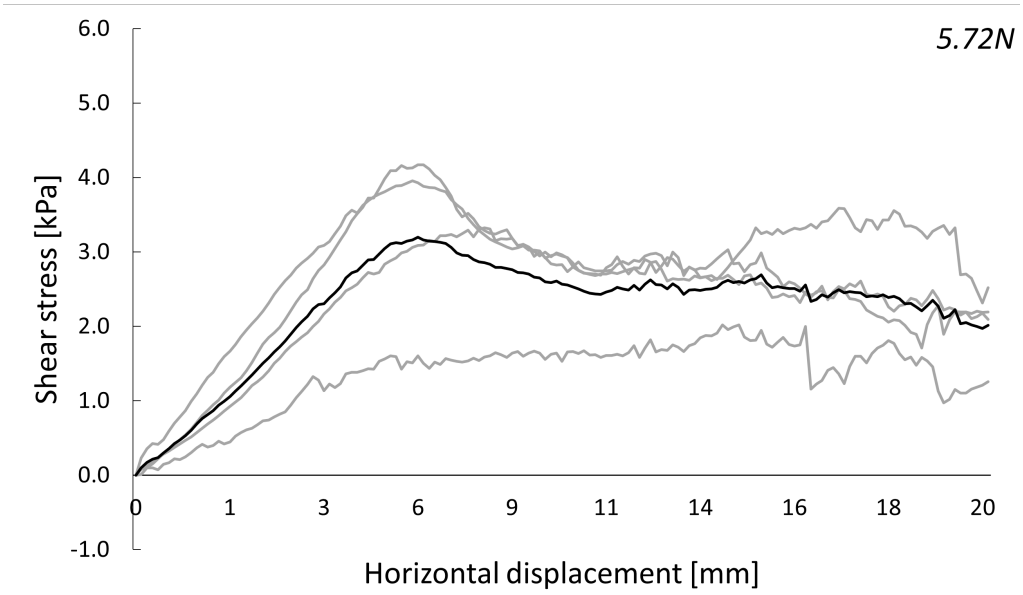
5.72N
Shear stress [kPa]
6.0
5.0
4.0
3.0
2.0
1.0
0.0
-1.0
0
1
3
6
9
11
14
16
18
20
Horizontal displacement [mm]

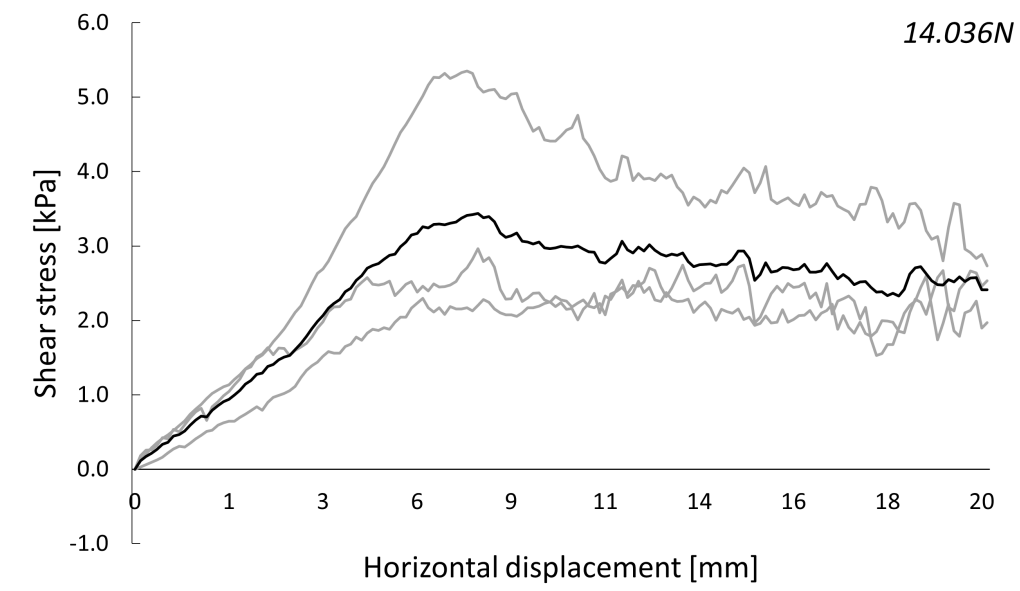
14.036N
Shear stress [kPa]
6.0
5.0
4.0
3.0
2.0
1.0
0.0
-1.0
0
1
3
6
9
11
14
16
18
20
Horizontal displacement [mm]

Combination

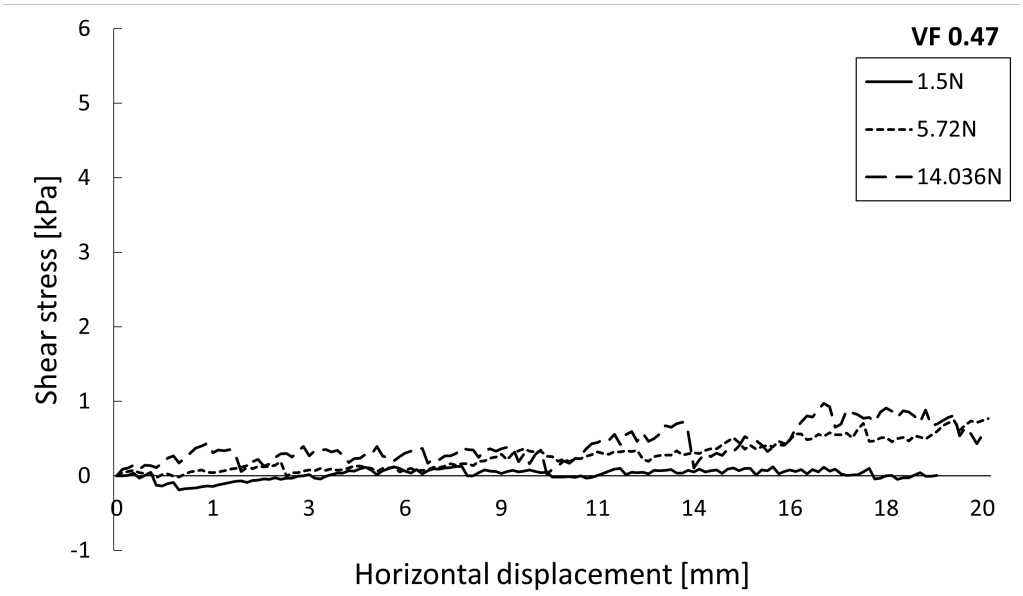

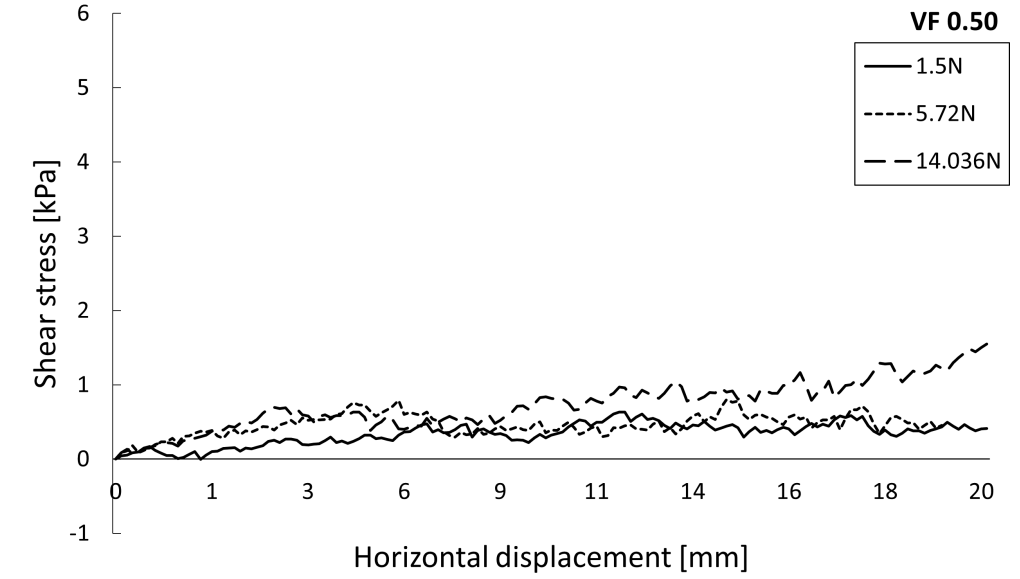

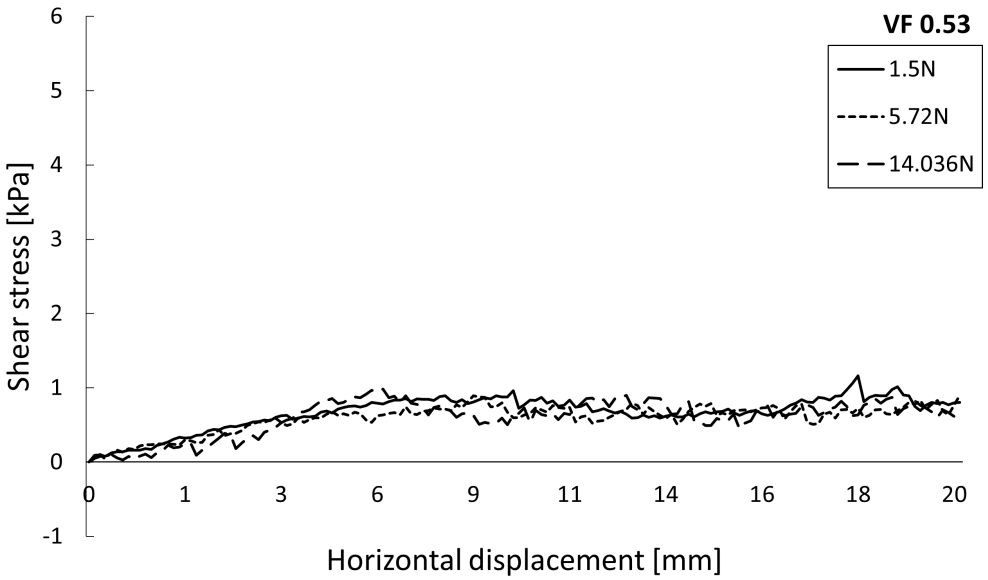
VF 0.53
1.5N
5.72N
14.036N
Shear stress [kPa]
6
5
4
3
2
1
0
-1
0
1
3
6
9
11
14
16
18
20
Horizontal displacement [mm]

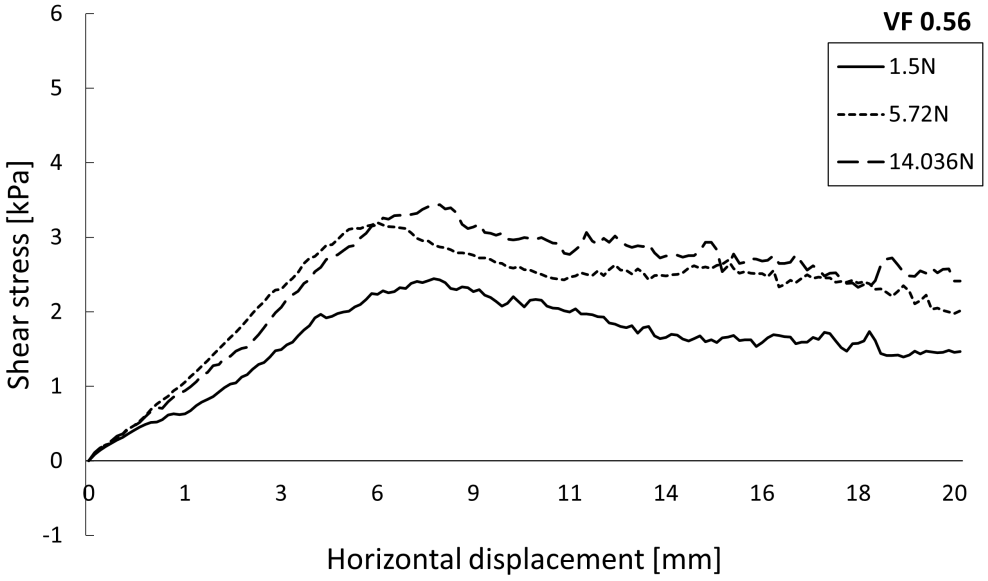
VF 0.56
1.5N
5.72N
14.036N
Shear stress [kPa]
6
5
4
3
2
1
0
-1
0
1
3
6
9
11
14
16
18
20
Horizontal displacement [mm]

D

Results DST for mixture CS

Volume fraction 0.47

Table D.1: Static yield stress peak values for mixture CS VF0.47 in kPa

	1	2	3	4	5	Average
1.5 N	0.446	1.269	0.857	1.1015	0.596	0.837
5.72 N	0.897	1.693	1.488	-	-	1.360
14.036 N	1.098	1.764	1.874	1.226	-	1.490

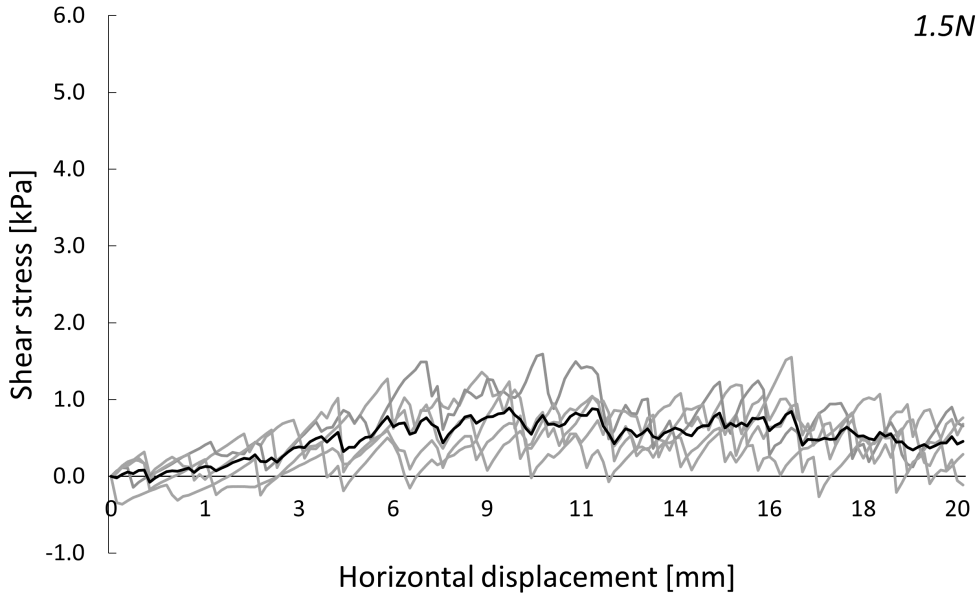

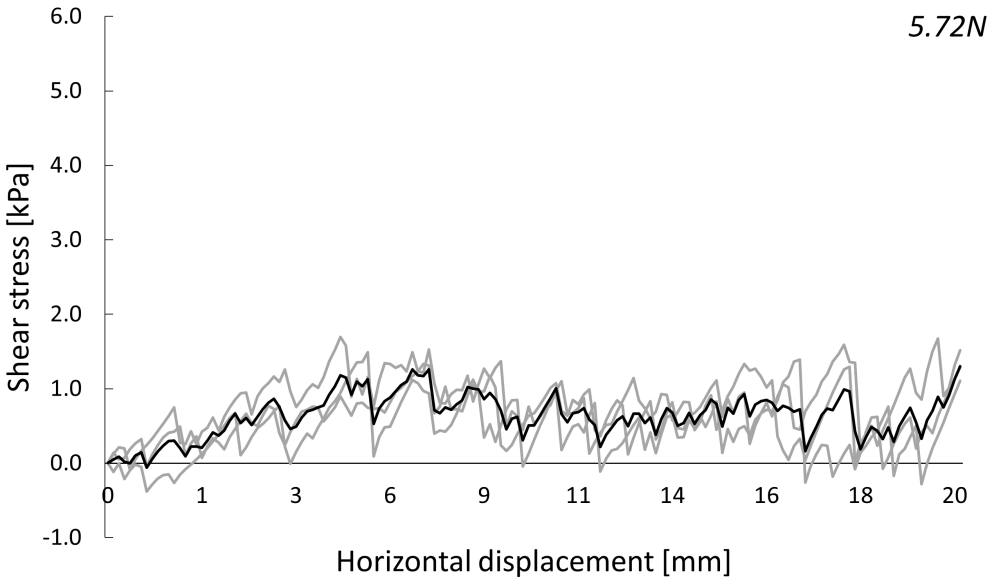
5.72N
Shear stress [kPa]
6.0
5.0
4.0
3.0
2.0
1.0
0.0
-1.0
0
1
3
6
9
11
14
16
18
20
Horizontal displacement [mm]

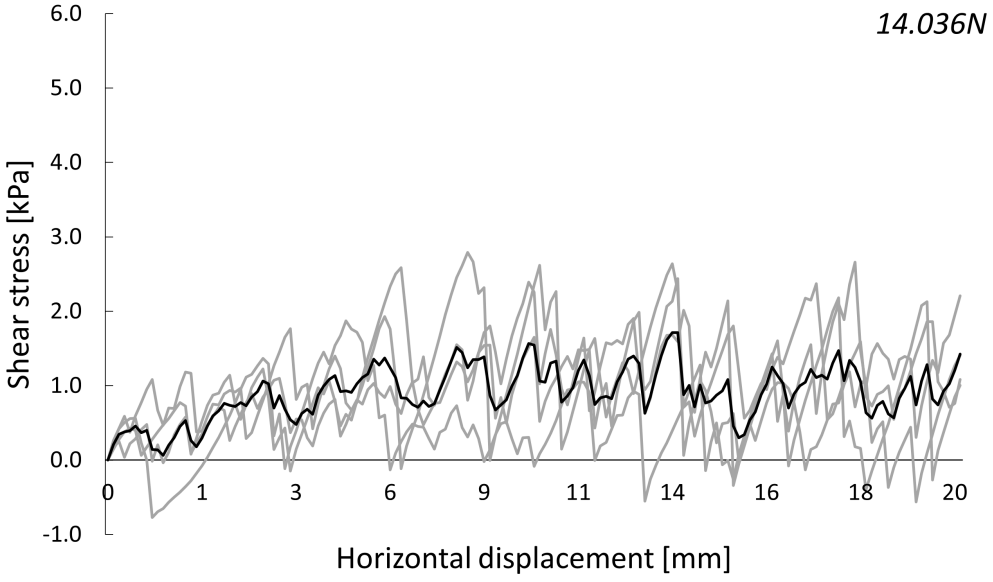
14.036N
Shear stress [kPa]
6.0
5.0
4.0
3.0
2.0
1.0
0.0
-1.0
0
1
3
6
9
11
14
16
18
20
Horizontal displacement [mm]

Volume fraction 0.50

Table D.2: Static yield stress peak values for mixture CS VF0.50 in kPa

	1	2	3	Average
1.5 N	0.793	0.659	1.027	0.826
5.72 N	1.471	1.334	1.913	1.573
14.036 N	2.877	2.722	1.966	2.525

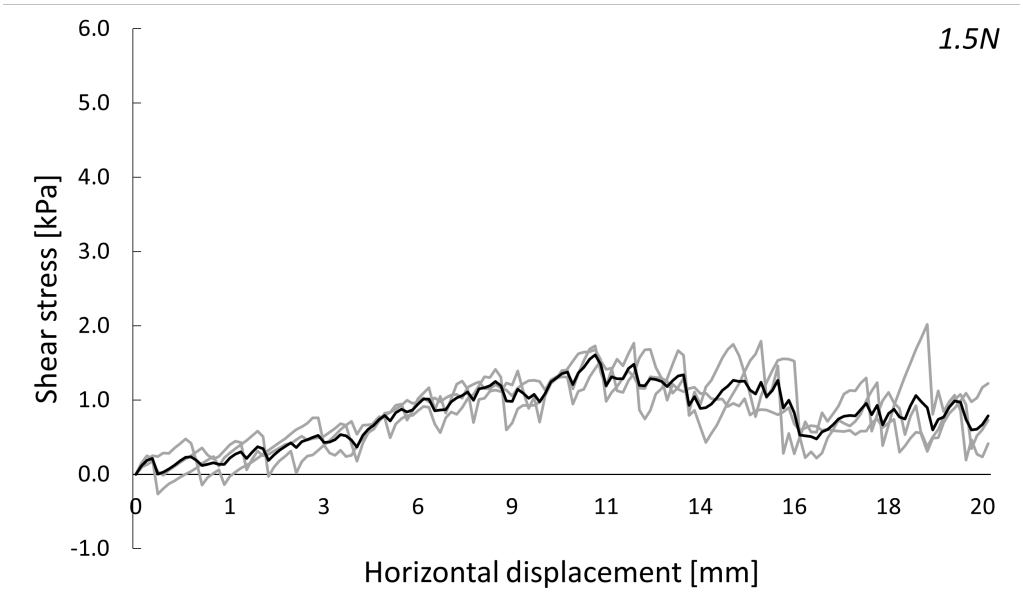

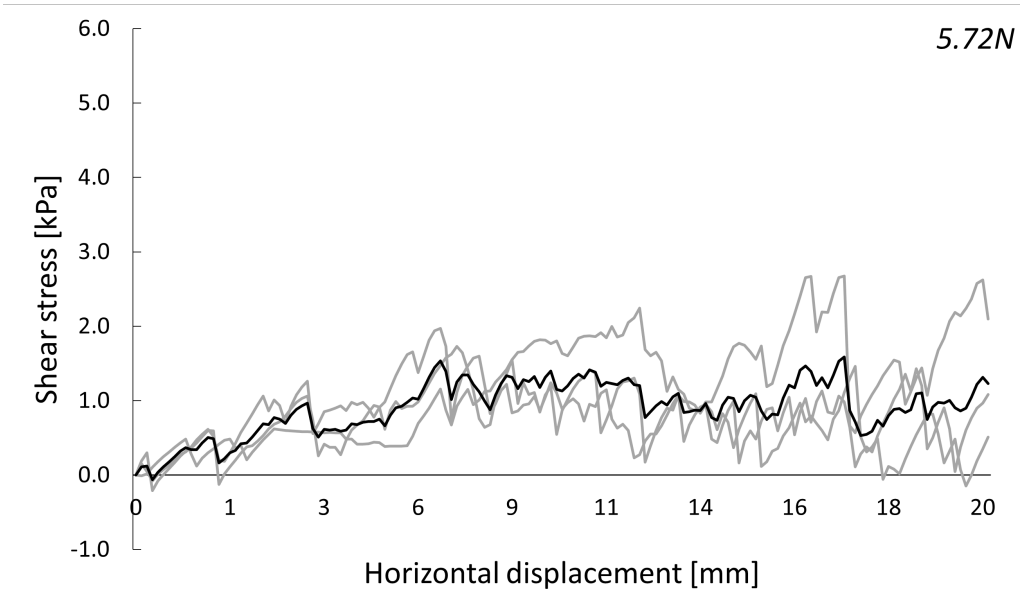
5.72N
Shear stress [kPa]
6.0
5.0
4.0
3.0
2.0
1.0
0.0
-1.0
0
1
3
6
9
11
14
16
18
20
Horizontal displacement [mm]

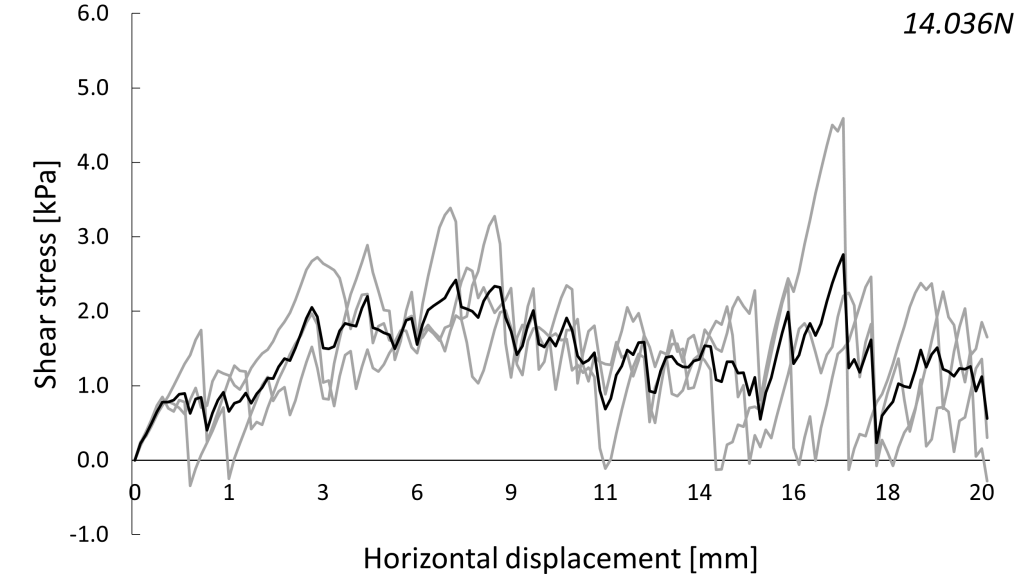
14.036N
Shear stress [kPa]
6.0
5.0
4.0
3.0
2.0
1.0
0.0
-1.0
0
1
3
6
9
11
14
16
18
20
Horizontal displacement [mm]

Volume fraction 0.53

Table D.3: Static yield stress peak values for mixture CS VF0.53 in kPa

	1	2	3	Average
1.5 N	2.141	2.059	3.077	2.426
5.72 N	3.480	3.634	3.155	3.423
14.036 N	5.183	7.468	5.661	6.104

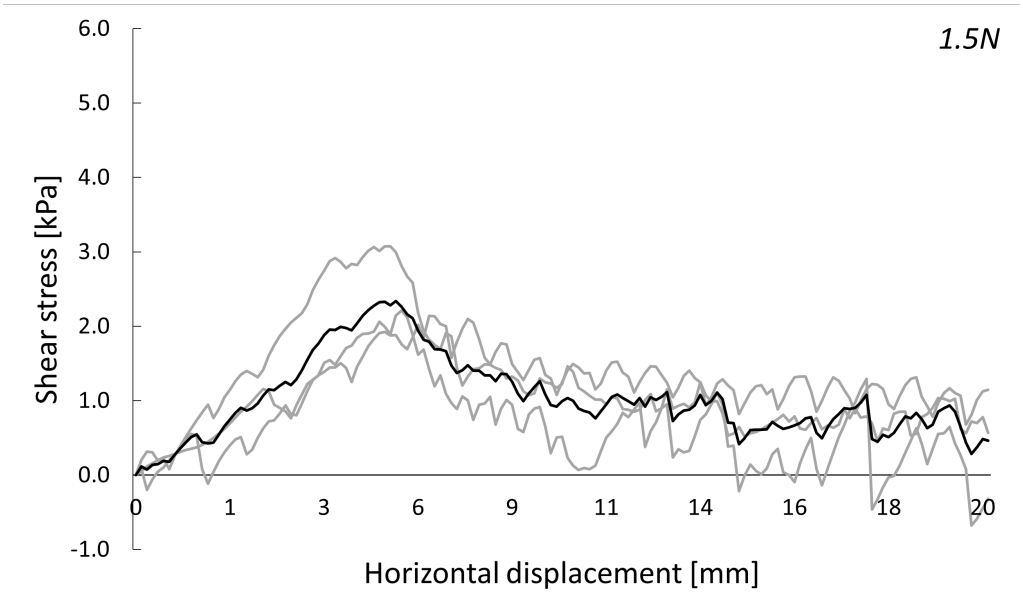

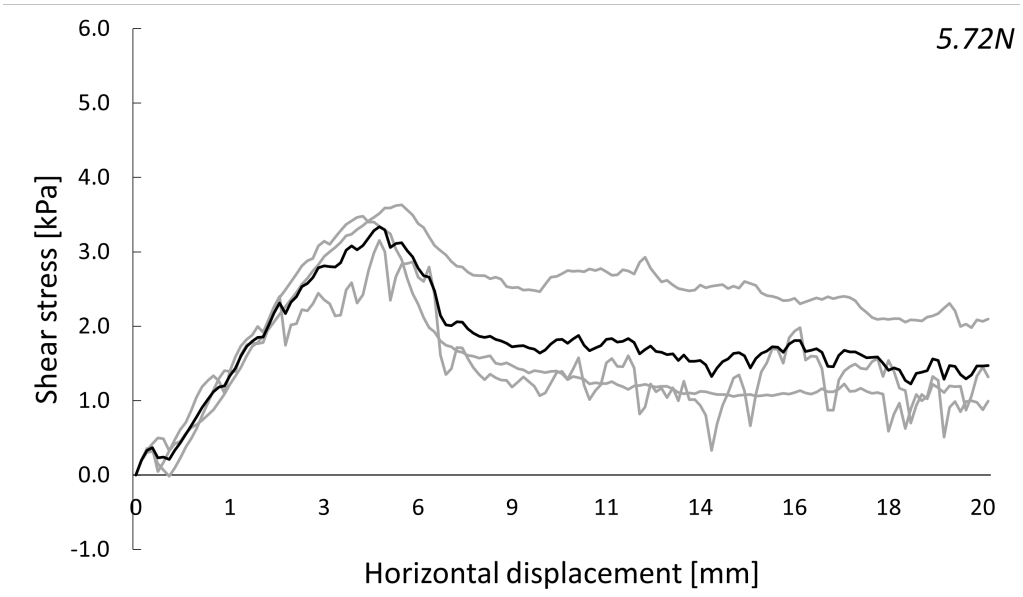
5.72N
Shear stress [kPa]
6.0
5.0
4.0
3.0
2.0
1.0
0.0
-1.0
0
1
3
6
9
11
14
16
18
20
Horizontal displacement [mm]

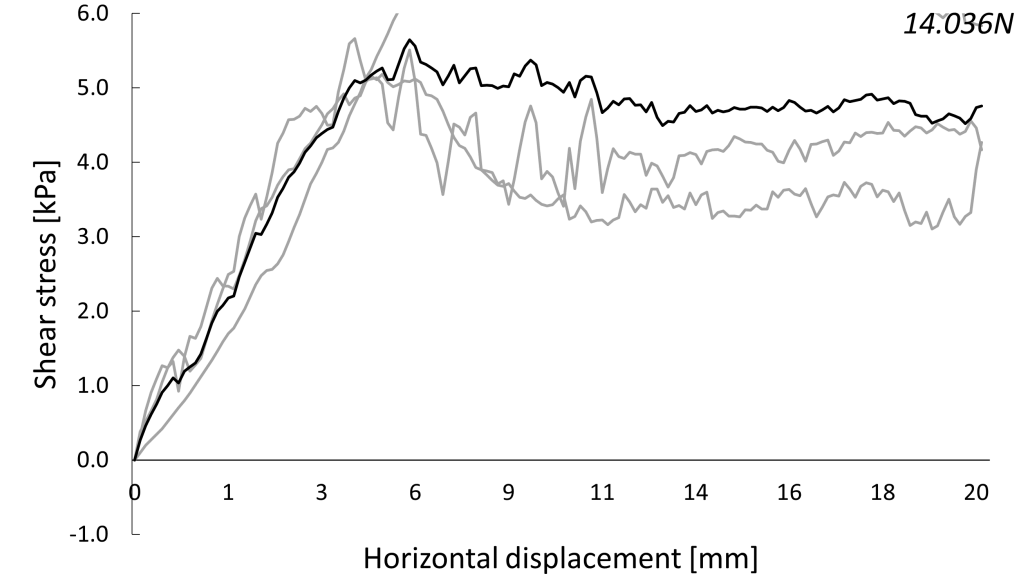
14.036N
Shear stress [kPa]
6.0
5.0
4.0
3.0
2.0
1.0
0.0
-1.0
0
1
3
6
9
11
14
16
18
20
Horizontal displacement [mm]

Volume fraction 0.56

Table D.4: Static yield stress peak values for mixture CS VF0.56 in kPa

	1	2	3	Average
1.5 N	1.867	3.674	2.629	2.723
5.72 N	3.202	2.653	3.015	2.957
14.036 N	4.751	5.239	4.311	4.767

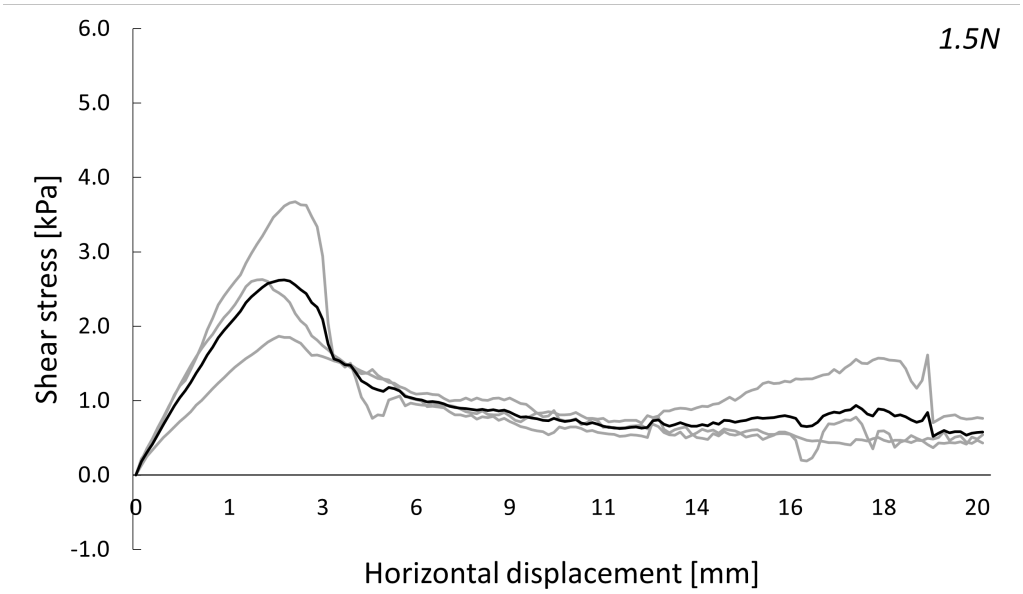

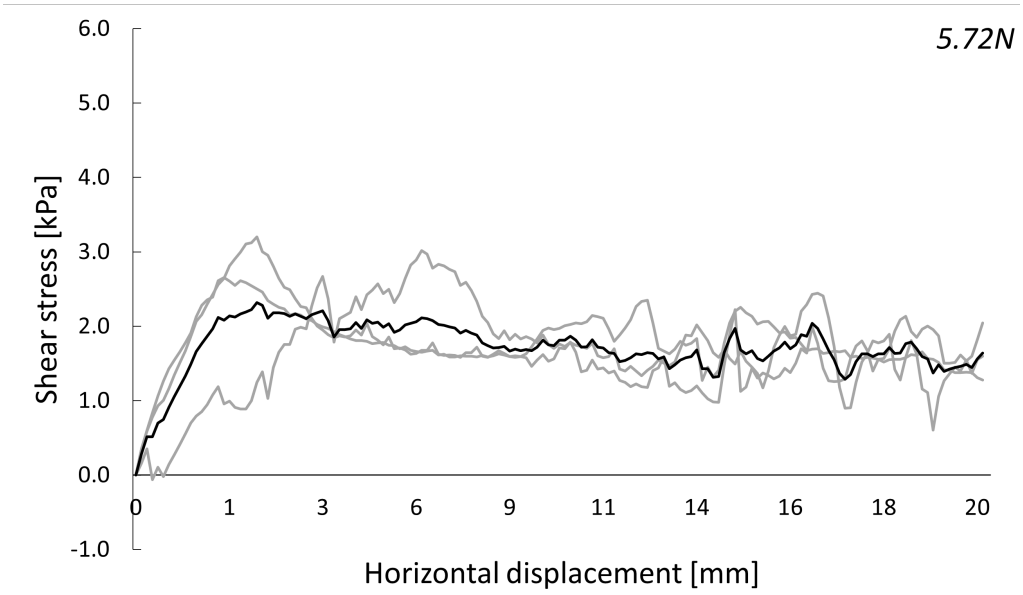
5.72N
Shear stress [kPa]
6.0
5.0
4.0
3.0
2.0
1.0
0.0
-1.0
0
1
3
6
9
11
14
16
18
20
Horizontal displacement [mm]

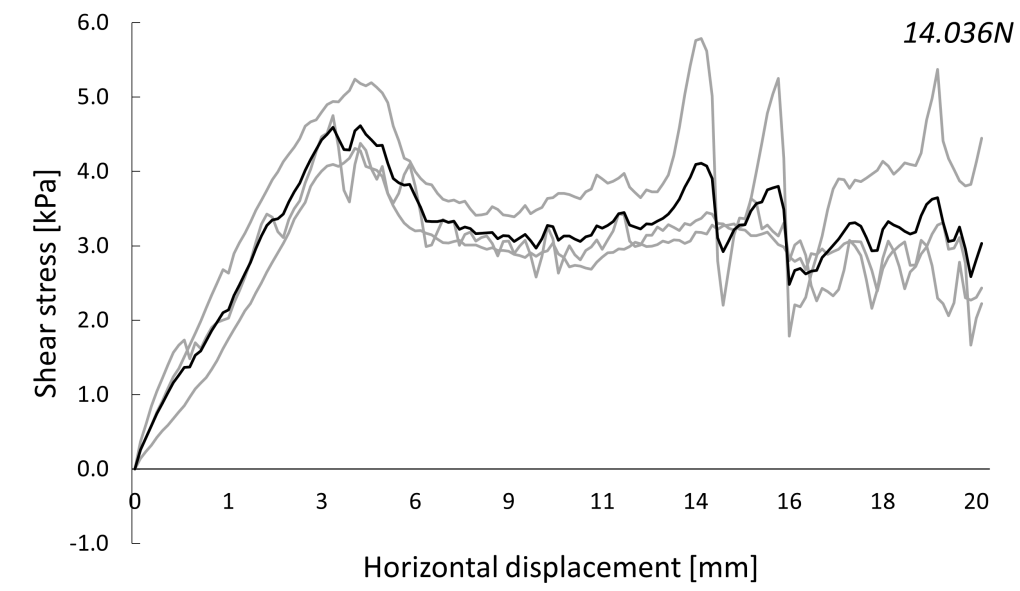
14.036N
Shear stress [kPa]
6.0
5.0
4.0
3.0
2.0
1.0
0.0
-1.0
0
1
3
6
9
11
14
16
18
20
Horizontal displacement [mm]

Combination

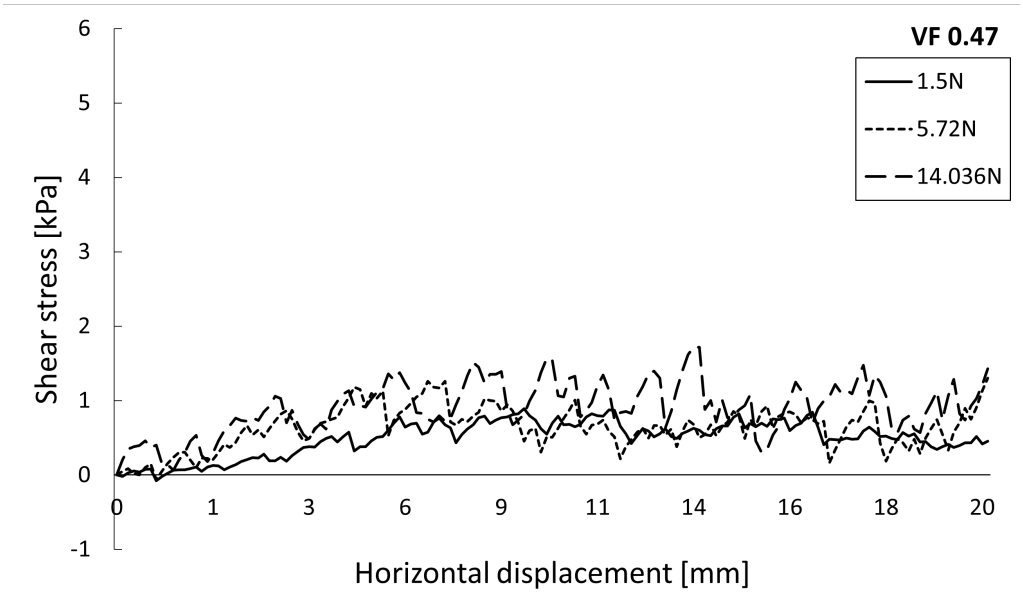

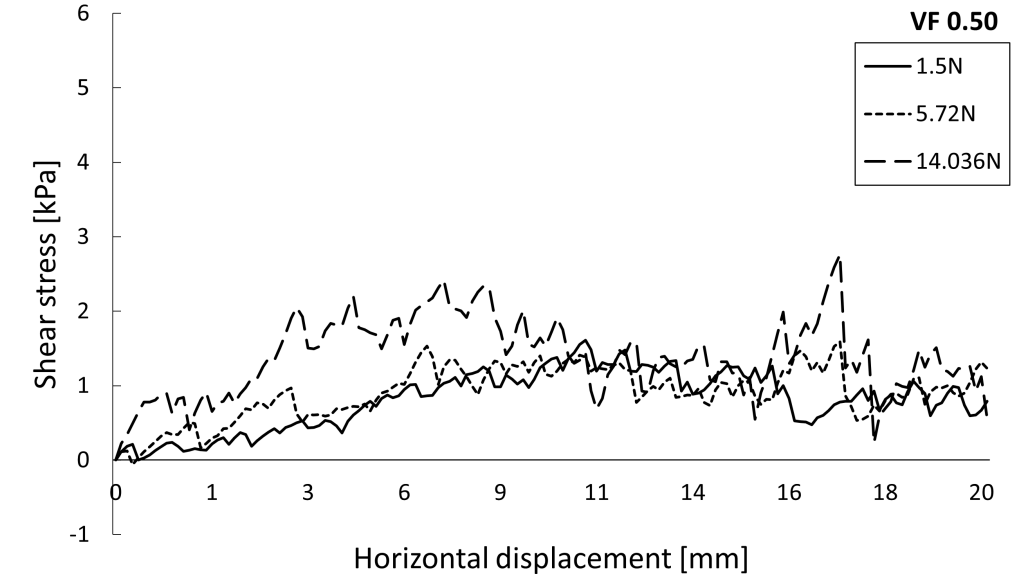

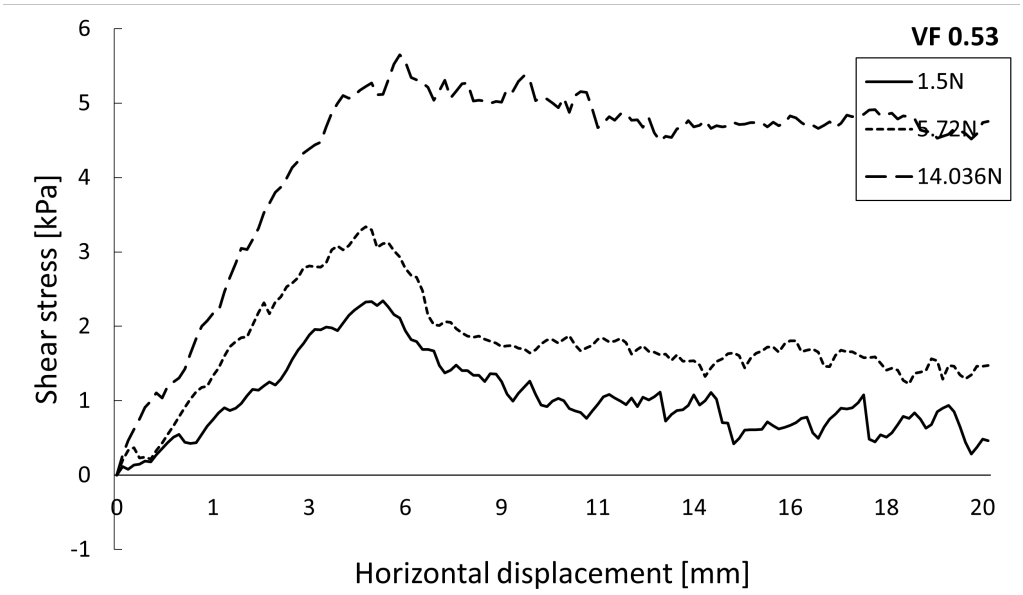
VF 0.53
1.5N
5.72N
14.036N
Shear stress [kPa]
Horizontal displacement [mm]
6
5
4
3
2
1
0
-1
0
1
3
6
9
11
14
16
18
20

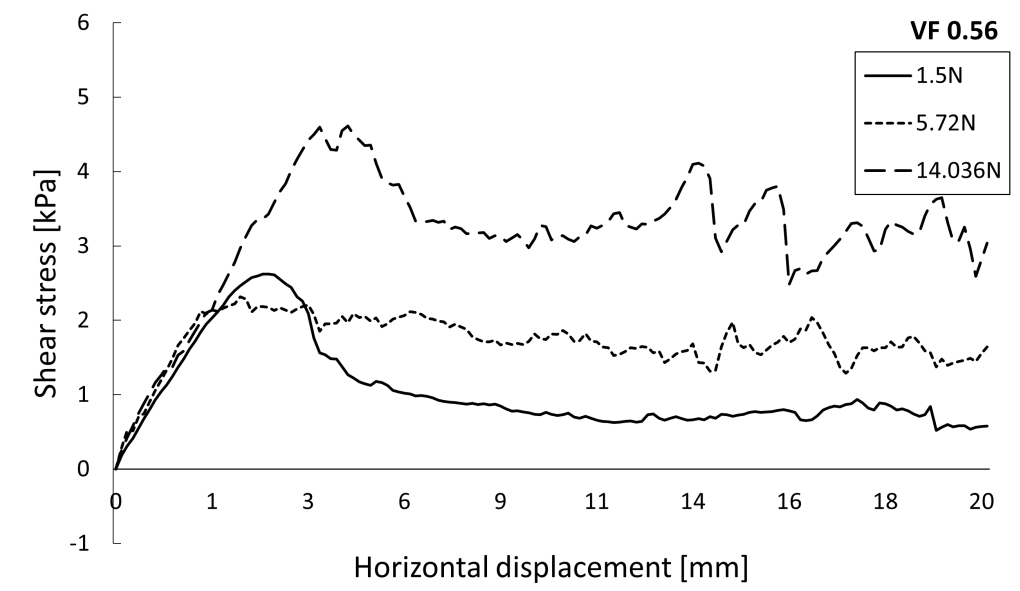
VF 0.56
1.5N
5.72N
14.036N
Shear stress [kPa]
Horizontal displacement [mm]
6
5
4
3
2
1
0
-1
0
1
3
6
9
11
14
16
18
20

E

Results RAM Extruder for mixture SG

Volume fraction 0.47

Table E.1: Static yield stress peak values for mixture SG VF0.47 in [N]

	12 mm	18 mm	24 mm	30 mm
1	727.29	-	-	-
2	566.81	-	-	-
3	517.59	-	-	-
Average	603.90	-	-	-

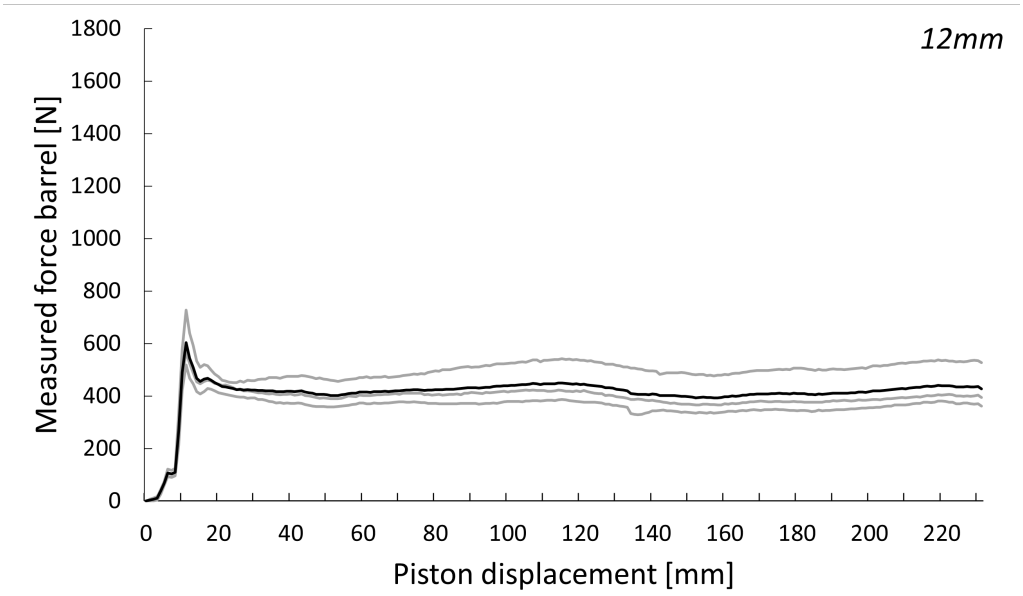

Volume fraction 0.50

Table E.2: Static yield stress peak values for mixture SG VF0.50 in [N]

	12 mm	18 mm	24 mm	30 mm
1	457.82	-	-	-
2	424.04	-	-	-
3	436.32	-	-	-
4	495.30	-	-	-
Average	453.37	-	-	-

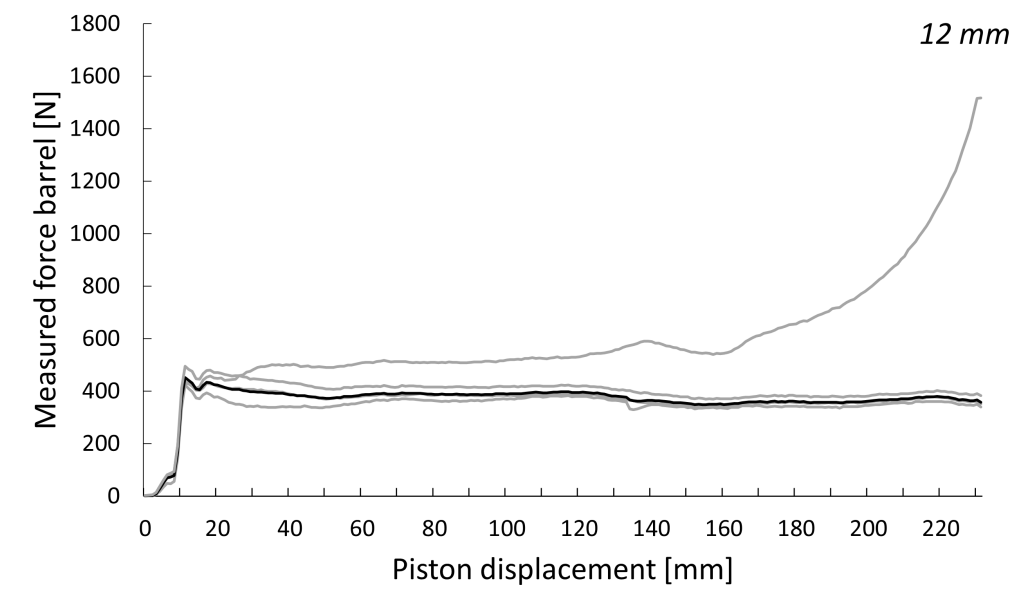

Volume fraction 0.53

Table E.3: Static yield stress peak values for mixture SG VF0.53 in [N]

	12 mm	18 mm	24 mm	30 mm
1	418.08	-	-	-
2	384.52	-	-	-
3	457.03	-	-	-
Average	419.88	-	-	-

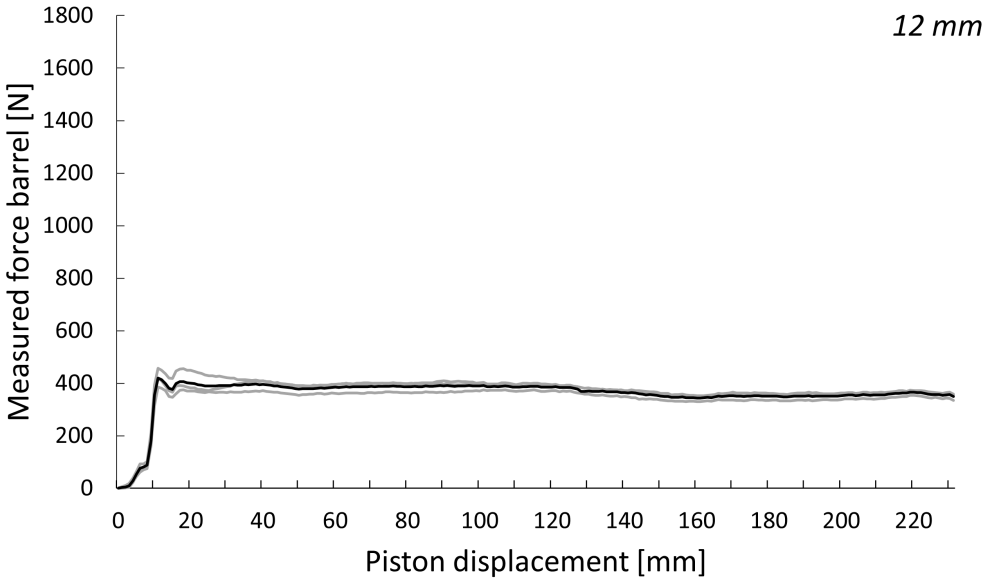

Volume fraction 0.56

Table E.4: Static yield stress peak values for mixture SG VF0.56 in [N]

	12 mm	18 mm	24 mm	30 mm
1	367.68	885.83	-	-
2	663.87	630.25	-	-
3	656.34	578.99	-	-
Average	562.63	698.36	-	-

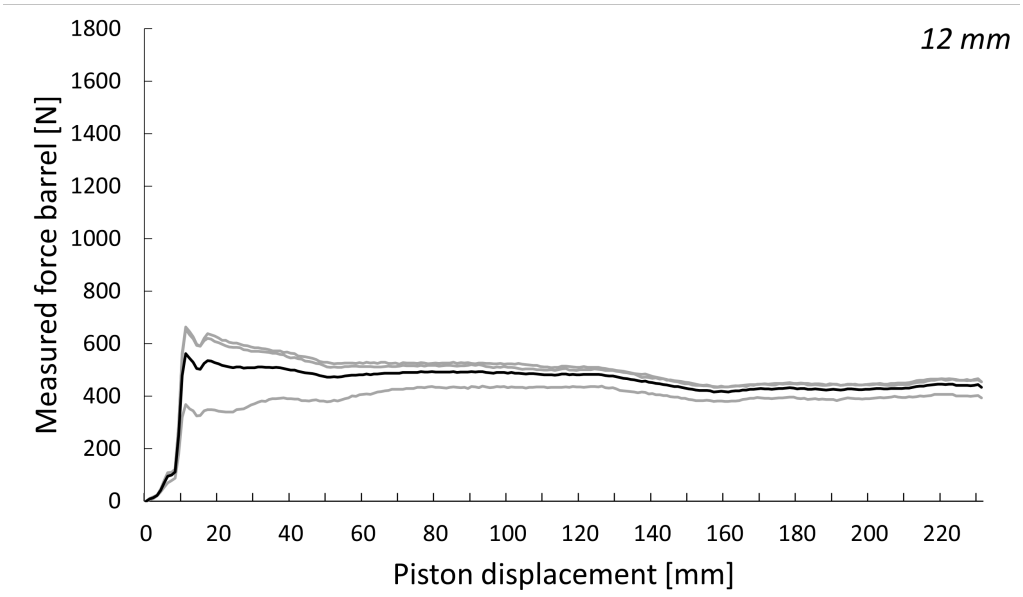
12 mm
Measured force barrel [N]
1800
1600
1400
1200
1000
800
600
400
200
0
0
20
40
60
80
100
120
140
160
180
200
220
Piston displacement [mm]

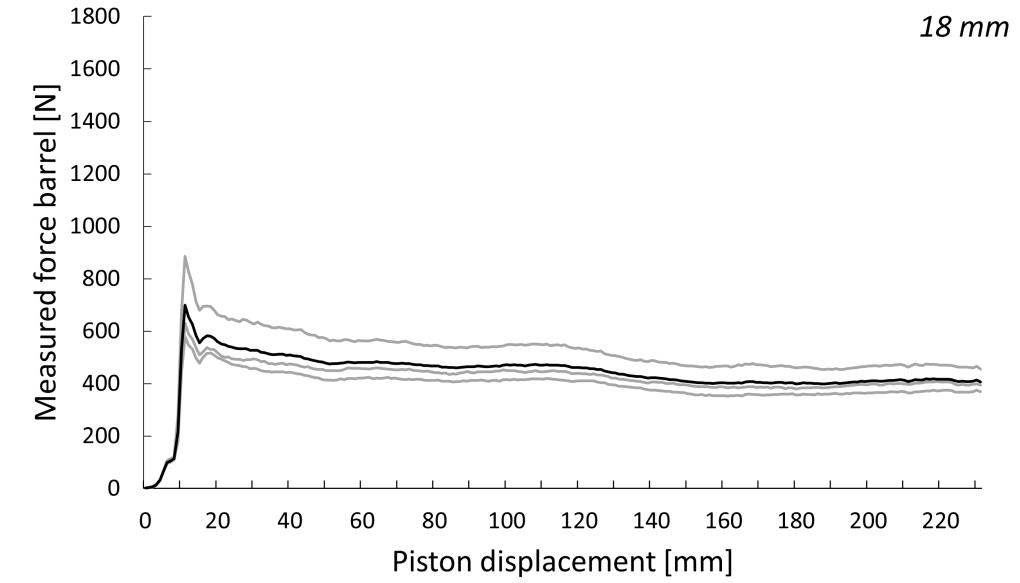
18 mm
Measured force barrel [N]
1800
1600
1400
1200
1000
800
600
400
200
0
0
20
40
60
80
100
120
140
160
180
200
220
Piston displacement [mm]

Combination

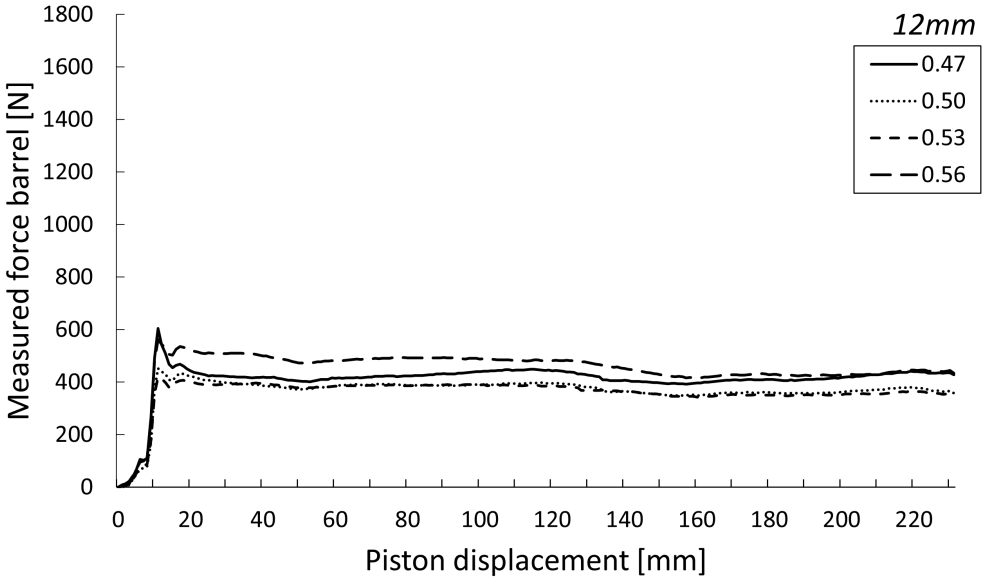

F

Results RAM Extruder for mixture CP

Volume fraction 0.47

Table F.1: Static yield stress peak values for mixture CP VF0.47 in [N]

	12 mm	18 mm	24 mm	30 mm
1	46.87	43.93	-	-
2	68.44	40.28	-	-
3	57.71	-	-	-
Average	57.67	42.11	-	-

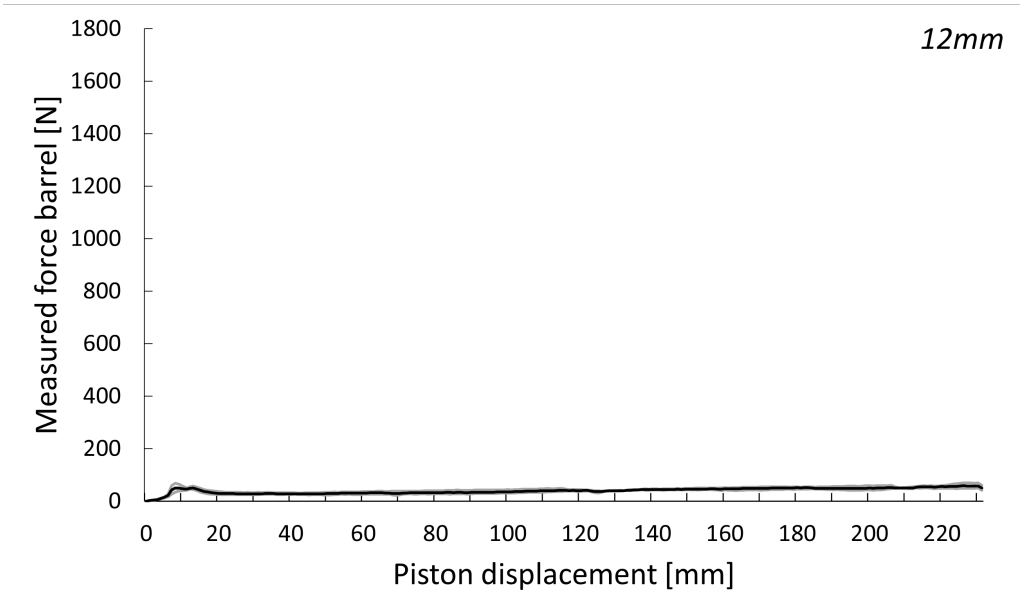

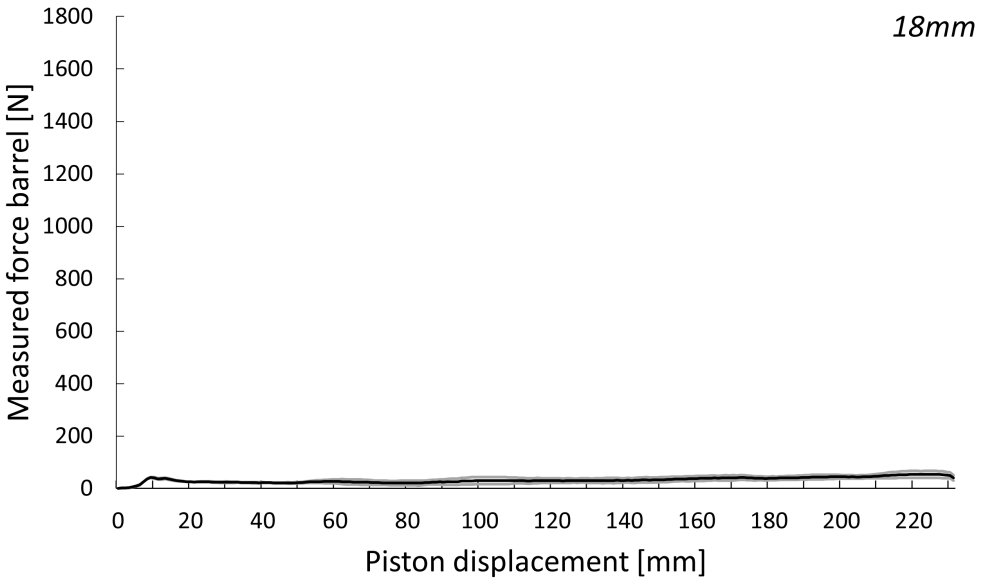
18mm
Measured force barrel [N]
1800
1600
1400
1200
1000
800
600
400
200
0
0
20
40
60
80
100
120
140
160
180
200
220
Piston displacement [mm]

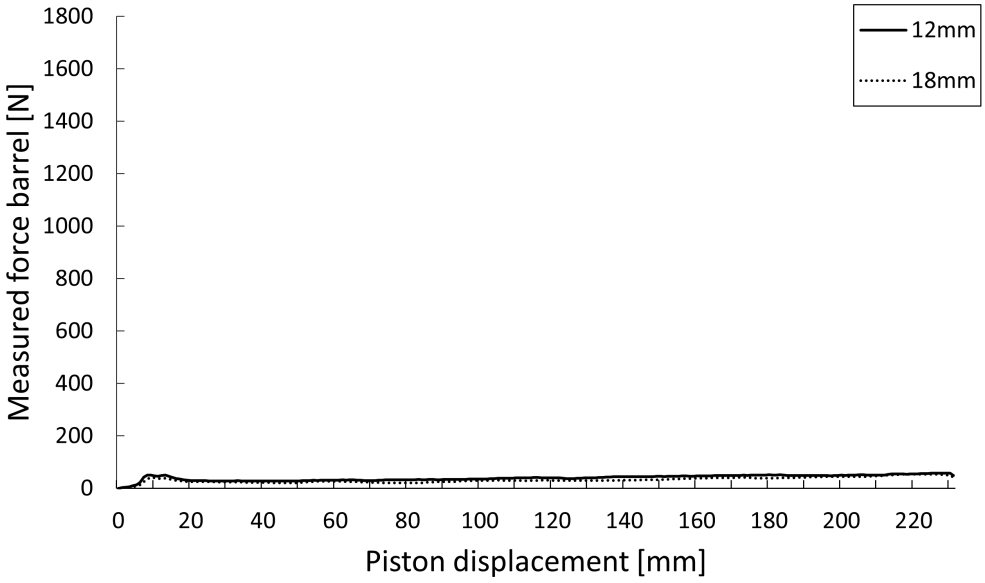
12mm
18mm
Measured force barrel [N]
1800
1600
1400
1200
1000
800
600
400
200
0
0
20
40
60
80
100
120
140
160
180
200
220
Piston displacement [mm]

Volume fraction 0.50

Table F.2: Static yield stress peak values for mixture CP VF0.50 in [N]

	12 mm	18 mm	24 mm	30 mm
1	102.37	70.19	48.91	35.98
2	78.54	58.40	36.39	67.85
3	58.51	68.53	57.45	53.55
Average	79.81	65.71	47.58	52.46

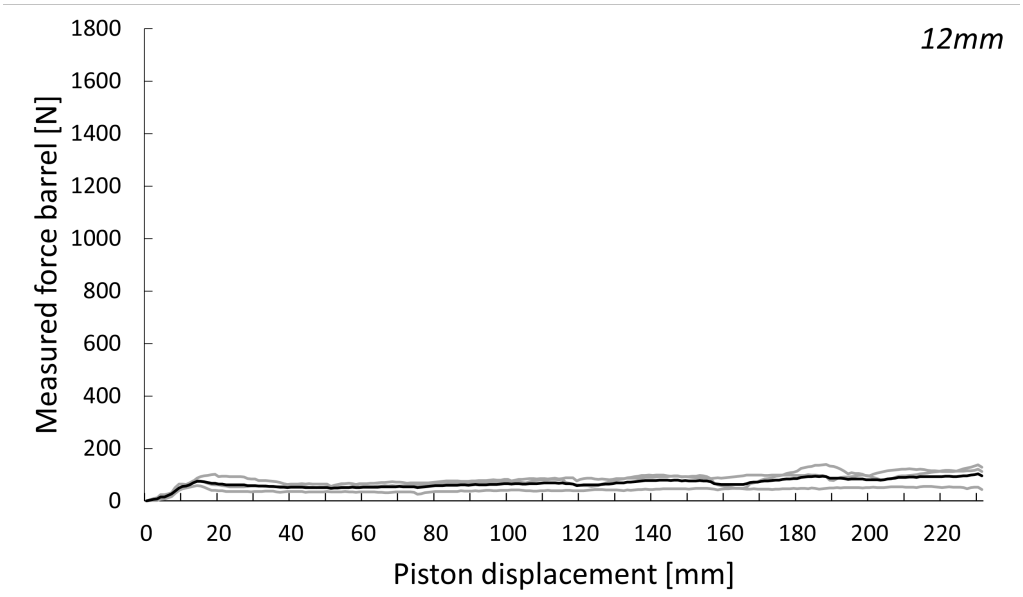

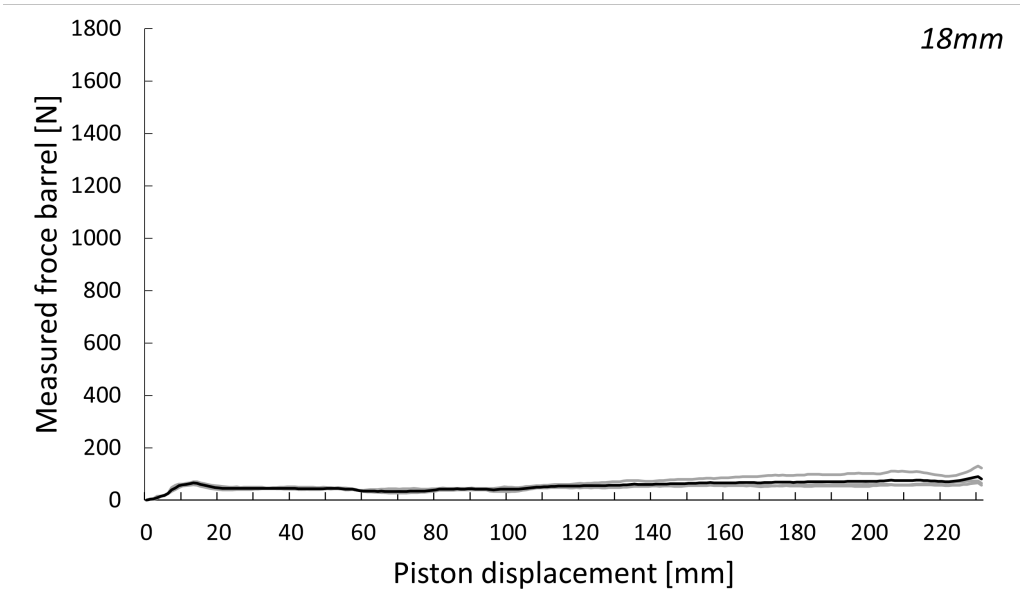
18mm
Measured froce barrel [N]
1800
1600
1400
1200
1000
800
600
400
200
0
0
20
40
60
80
100
120
140
160
180
200
220
Piston displacement [mm]

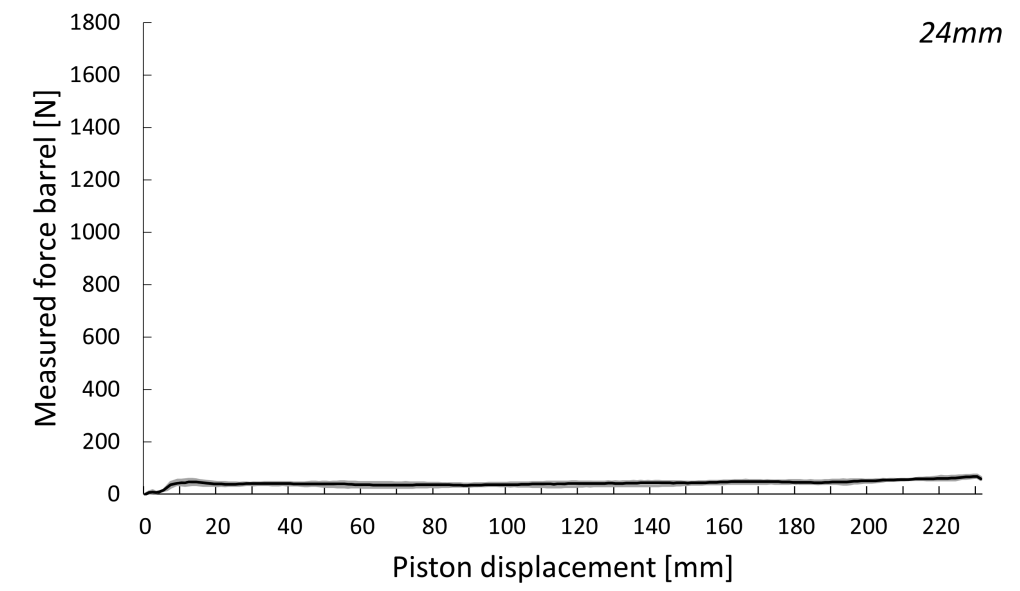
24mm
Measured force barrel [N]
1800
1600
1400
1200
1000
800
600
400
200
0
0
20
40
60
80
100
120
140
160
180
200
220
Piston displacement [mm]

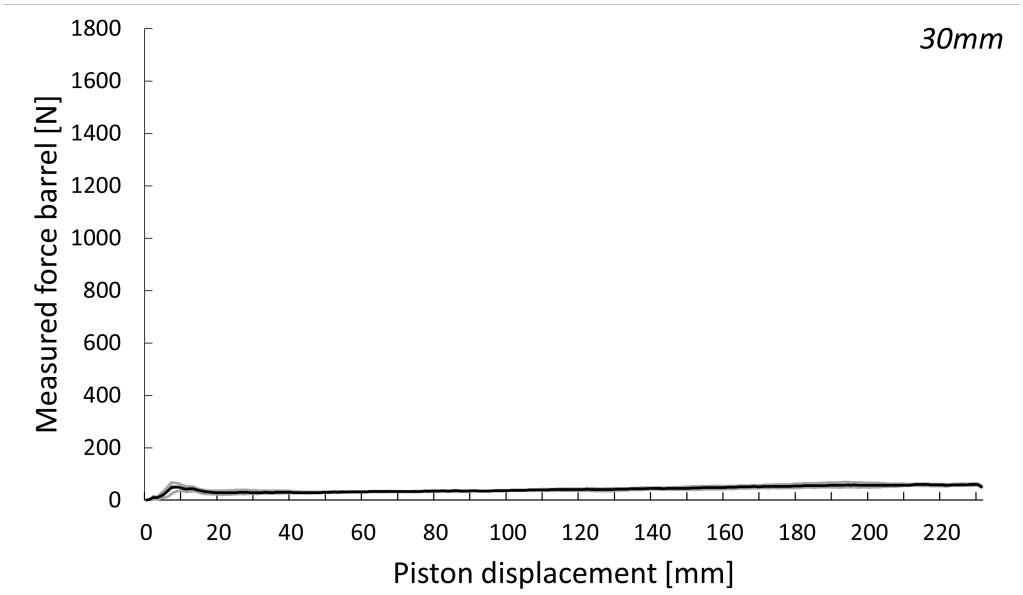
30mm
Measured force barrel [N]
1800
1600
1400
1200
1000
800
600
400
200
0
0
20
40
60
80
100
120
140
160
180
200
220
Piston displacement [mm]

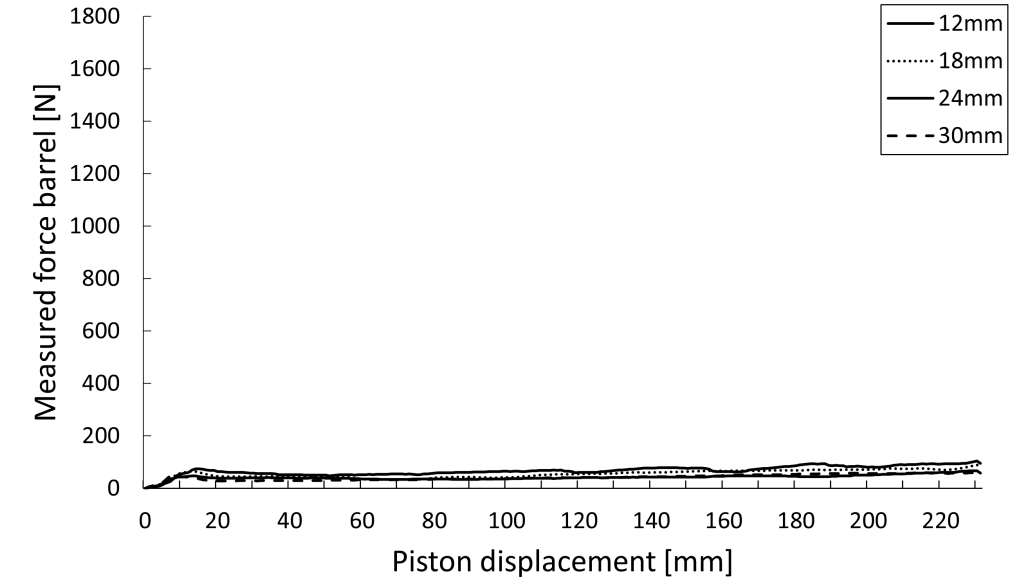
12mm
18mm
24mm
30mm
Measured force barrel [N]
1800
1600
1400
1200
1000
800
600
400
200
0
0
20
40
60
80
100
120
140
160
180
200
220
Piston displacement [mm]

Volume fraction 0.53

Table F.3: Static yield stress peak values for mixture CP VF0.53 in [N]

	12 mm	18 mm	24 mm	30 mm
1	-	261.1	196.75	120.47
2	-	199.47	116.34	73.90
3	-	23.35	123.23	98.29
Average	-	161.31	145.44	97.55

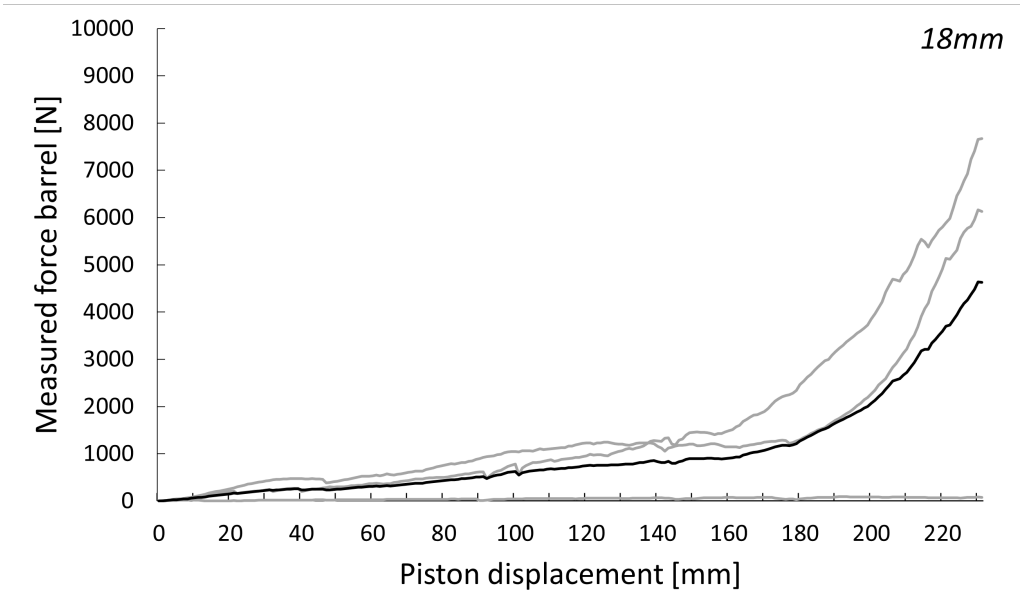

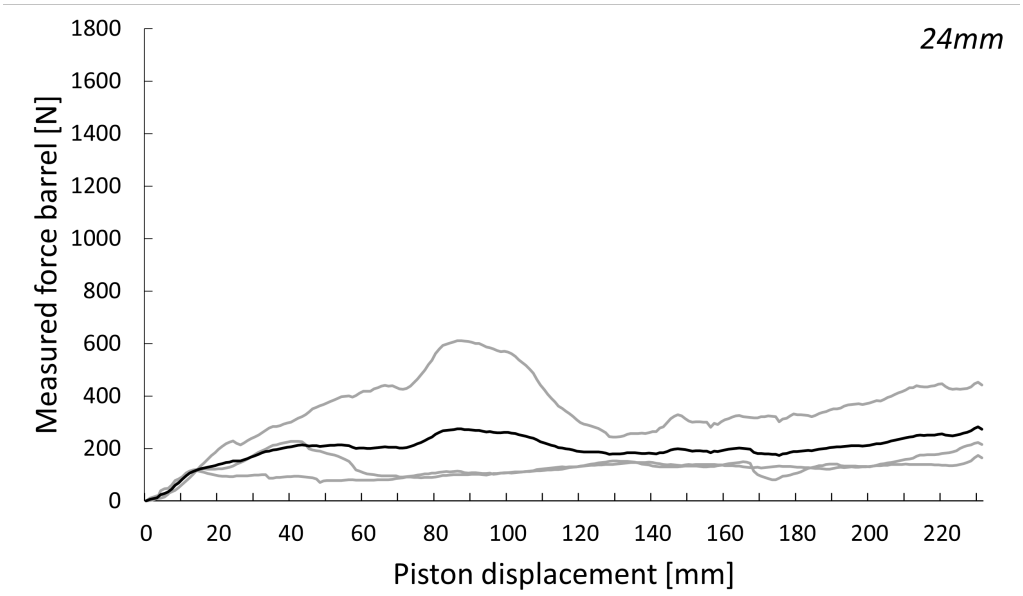
24mm
Measured force barrel [N]
1800
1600
1400
1200
1000
800
600
400
200
0
0
20
40
60
80
100
120
140
160
180
200
220
Piston displacement [mm]

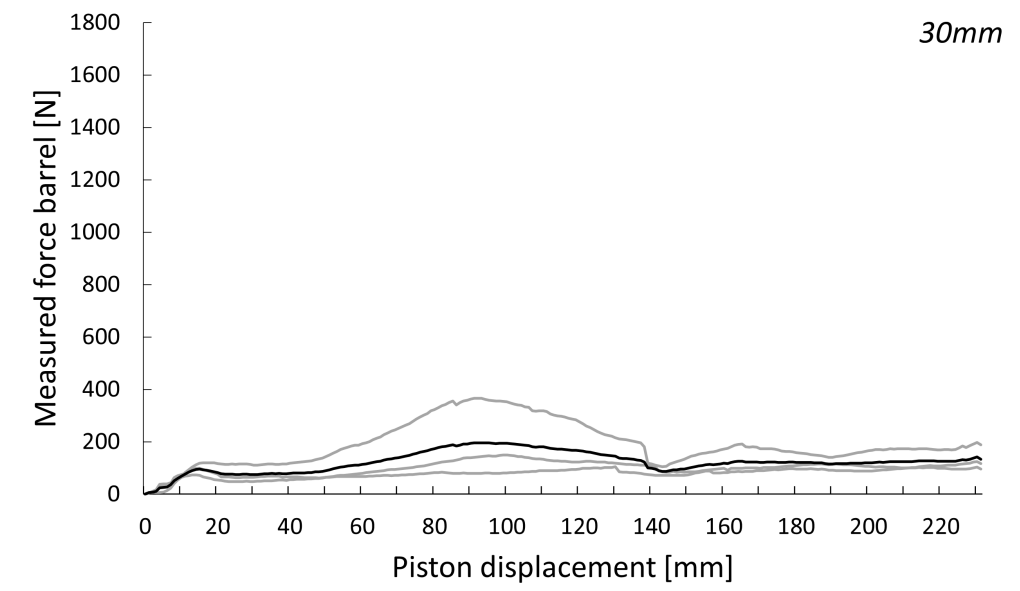
30mm
Measured force barrel [N]
1800
1600
1400
1200
1000
800
600
400
200
0
0
20
40
60
80
100
120
140
160
180
200
220
Piston displacement [mm]

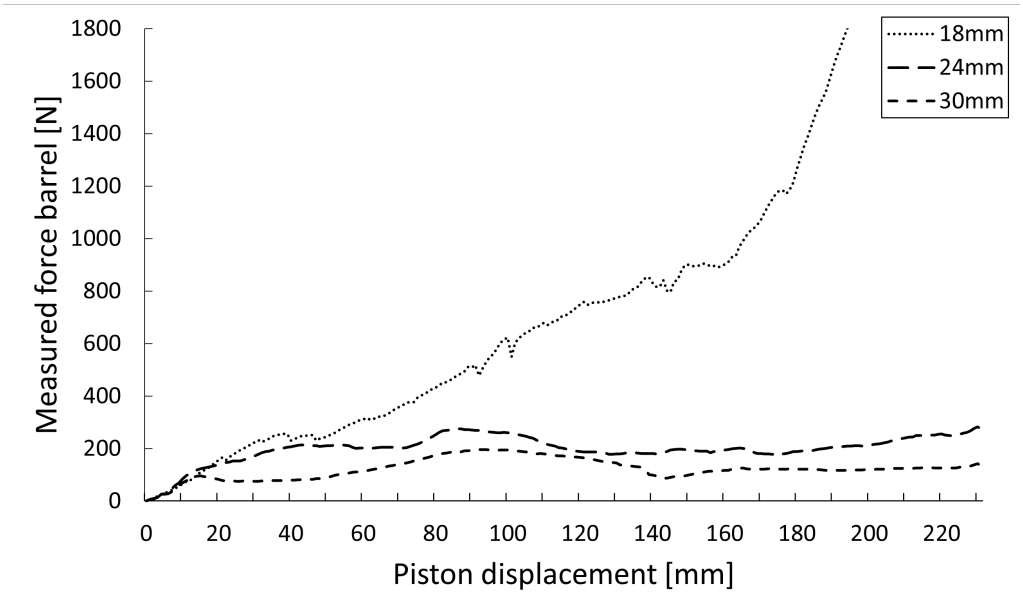
Measured force barrel [N]
1800
1600
1400
1200
1000
800
600
400
200
0
0
20
40
60
80
100
120
140
160
180
200
220
Piston displacement [mm]
18mm
24mm
30mm

Volume fraction 0.56

Table F.4: Static yield stress peak values for mixture CP VF0.56 in [N]

	12 mm	18 mm	24 mm	30 mm
1	-	-	3686.80	4839.61
2	-	-	883.41	1148.11
3	-	-	-	1148.17
Average	-	-	2285.11	2378.63

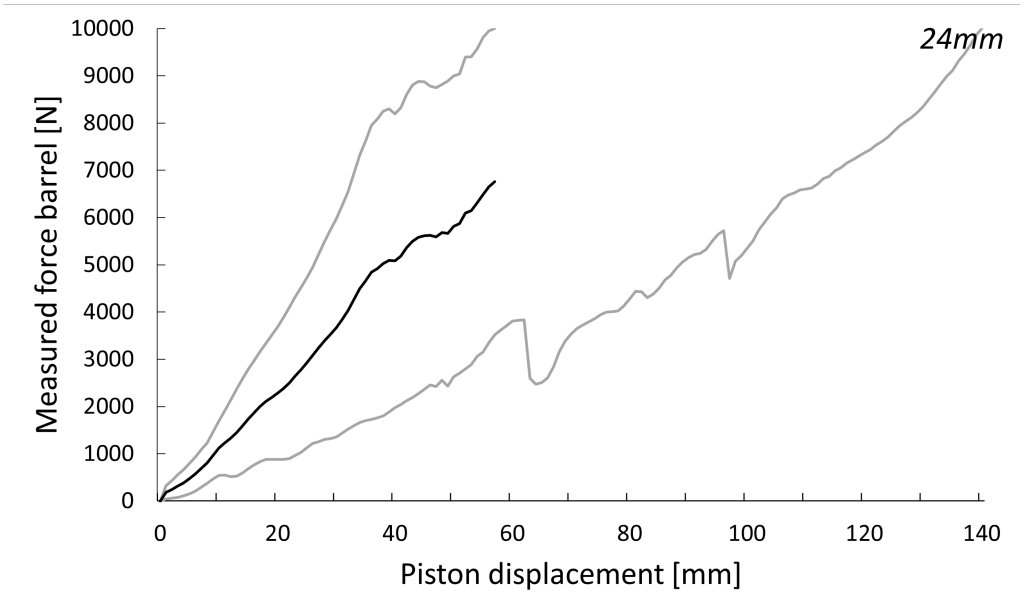

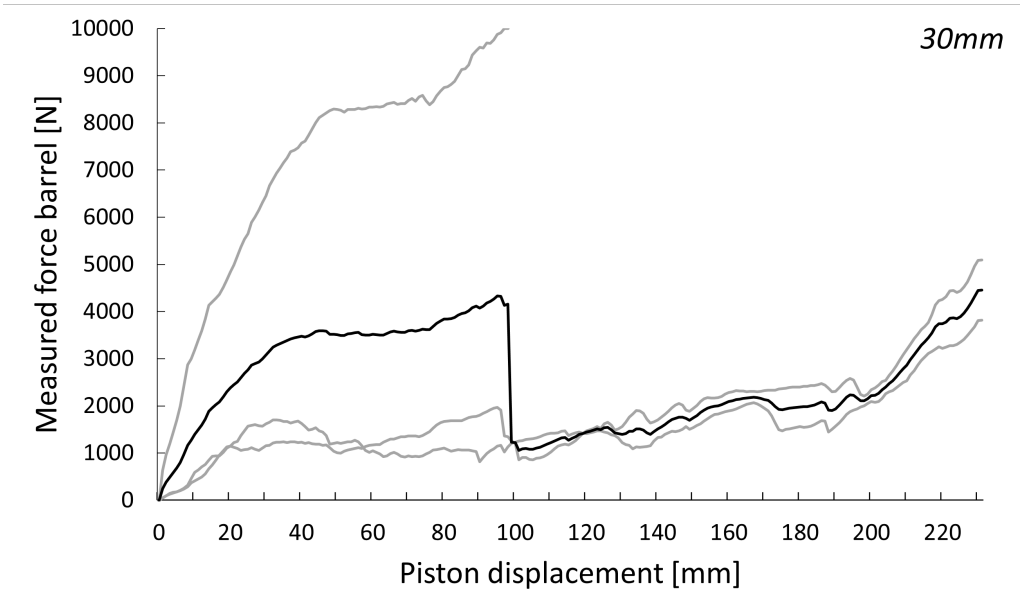
30mm
Measured force barrel [N]
10000
9000
8000
7000
6000
5000
4000
3000
2000
1000
0
0
20
40
60
80
100
120
140
160
180
200
220
Piston displacement [mm]

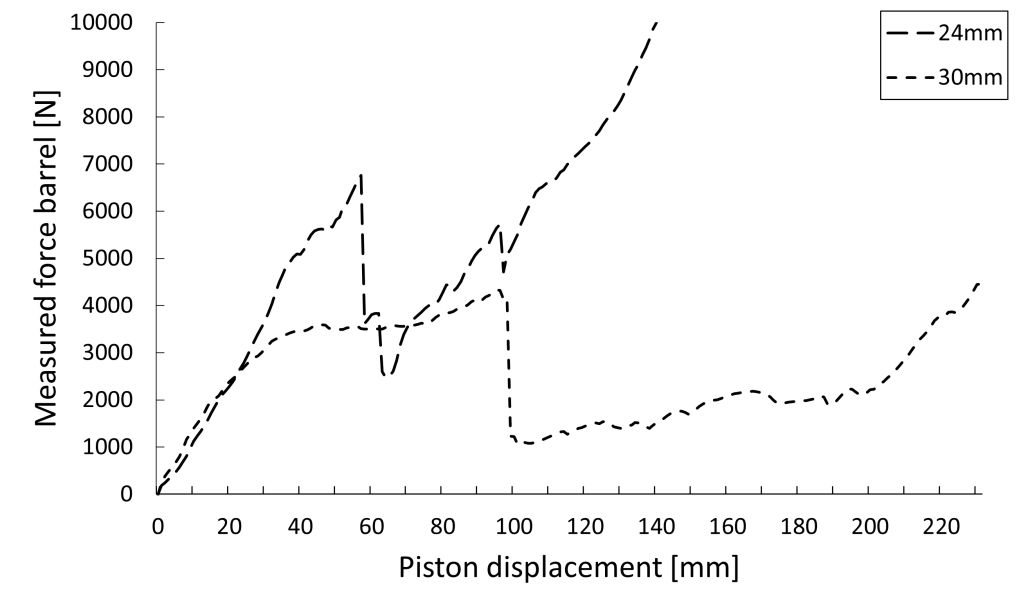
24mm
30mm
Measured force barrel [N]
10000
9000
8000
7000
6000
5000
4000
3000
2000
1000
0
0
20
40
60
80
100
120
140
160
180
200
220
Piston displacement [mm]

Combination

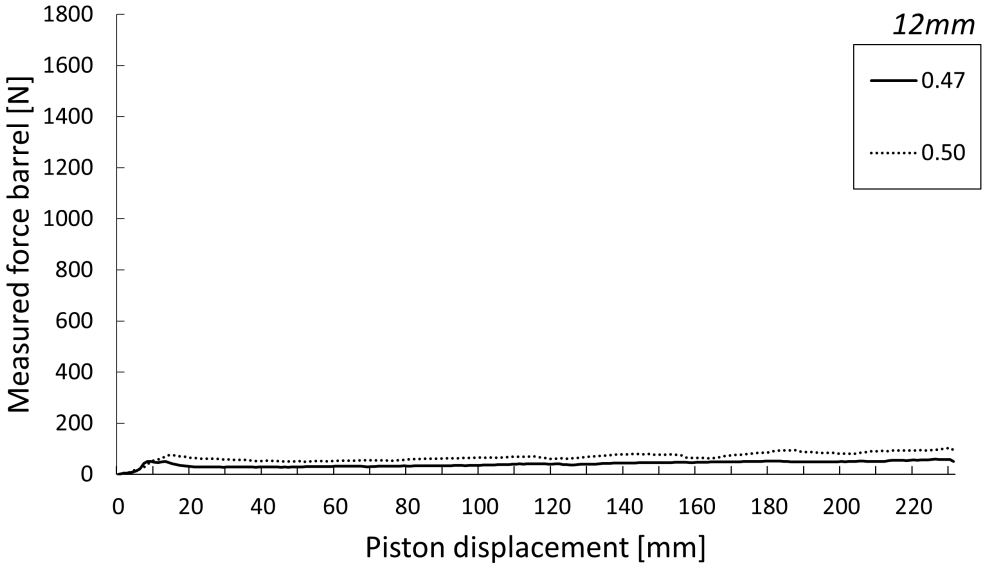

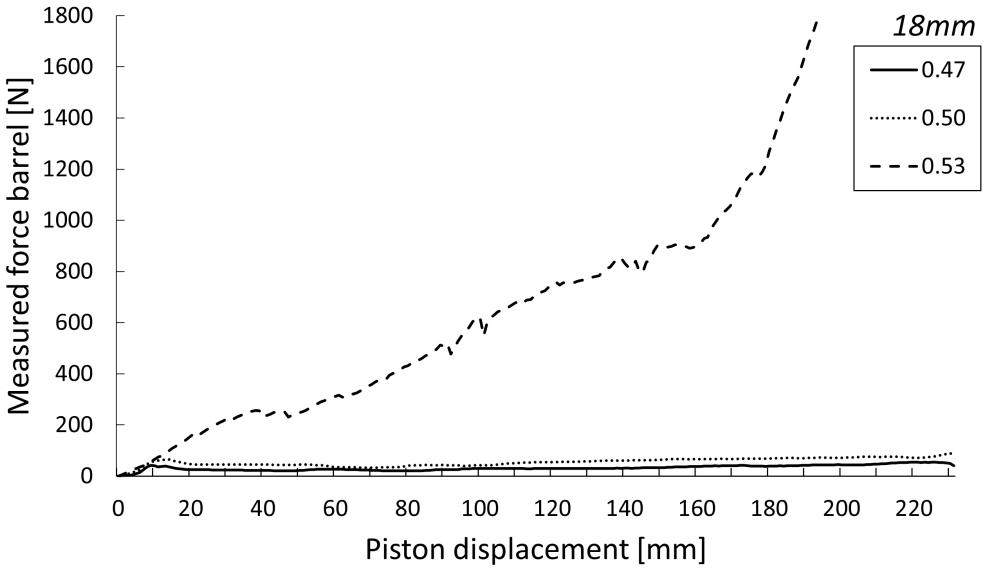

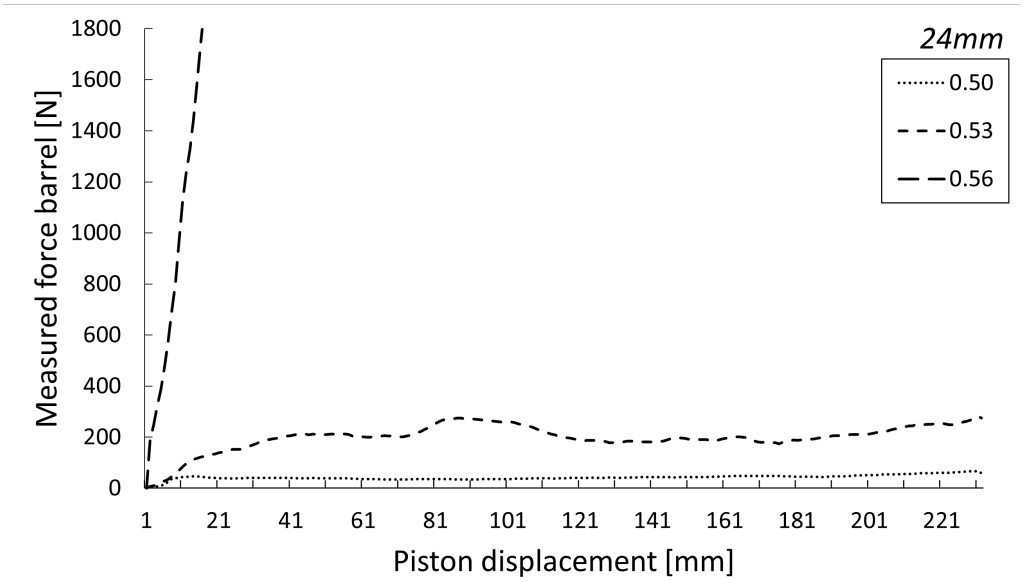
24mm
0.50
0.53
0.56
Measured force barrel [N]
1800
1600
1400
1200
1000
800
600
400
200
0
1
21
41
61
81
101
121
141
161
181
201
221
Piston displacement [mm]

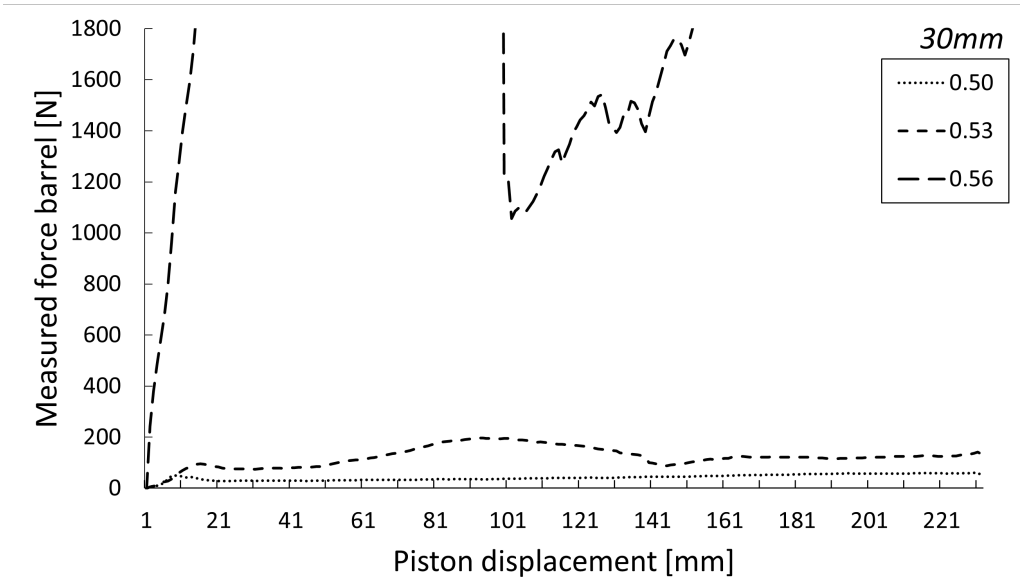
30mm
0.50
0.53
0.56
Measured force barrel [N]
1800
1600
1400
1200
1000
800
600
400
200
0
1
21
41
61
81
101
121
141
161
181
201
221
Piston displacement [mm]

G

Results RAM Extruder for mixture CS

Volume fraction 0.47

Table G.1: Static yield stress peak values for mixture CS VF0.47 in [N]

	12 mm	18 mm	24 mm	30 mm
1	-	287.86	822.50	92.62
2	-	516.35	696.11	-
3	-	497.15	1671.37	-
Average	-	433.787	1063.33	92.62

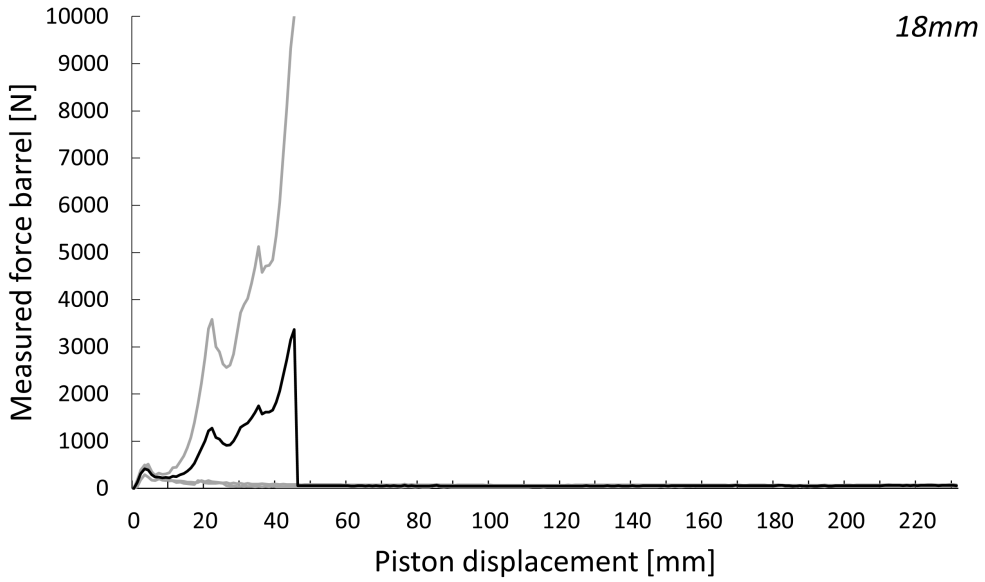

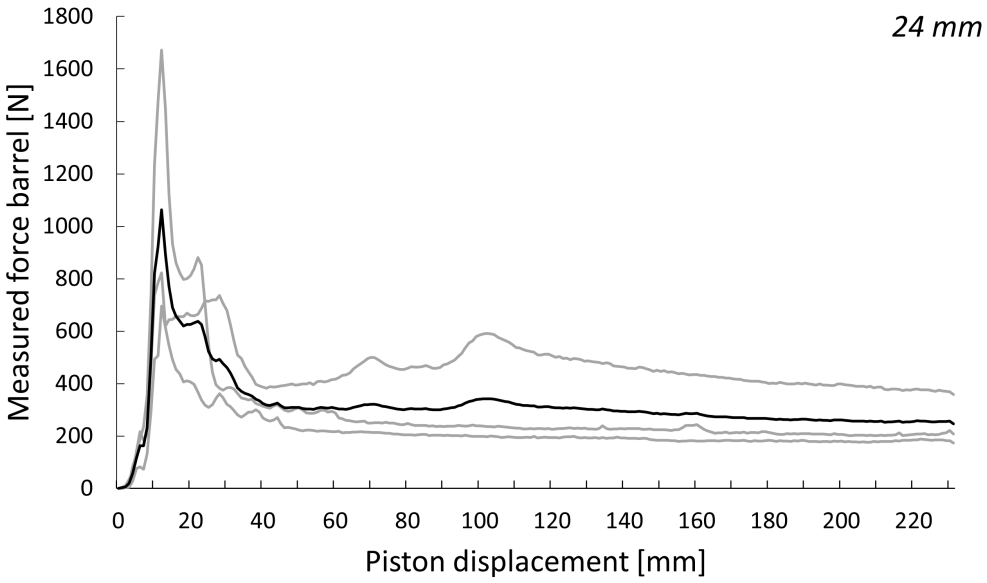
24 mm
Measured force barrel [N]
1800
1600
1400
1200
1000
800
600
400
200
0
0
20
40
60
80
100
120
140
160
180
200
220
Piston displacement [mm]

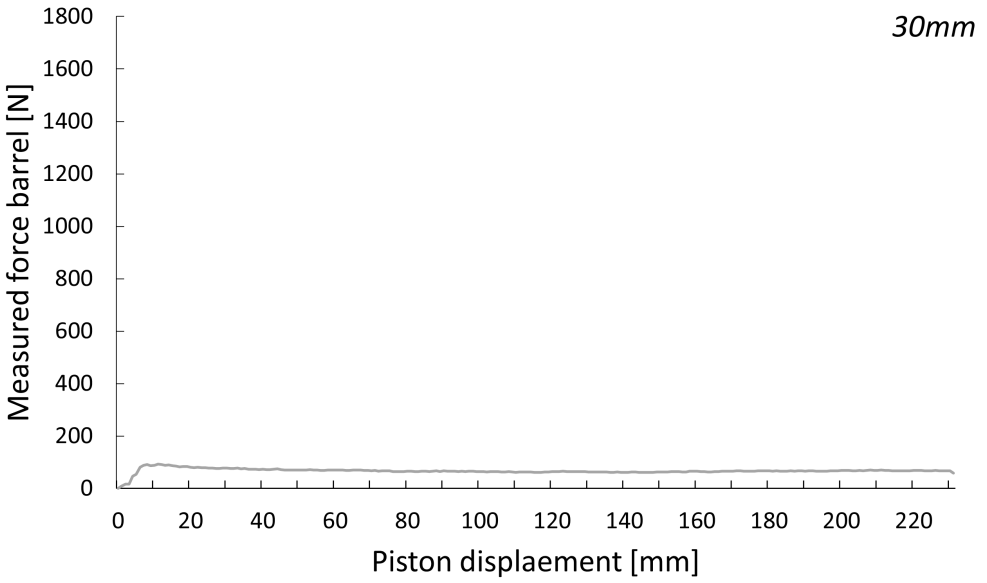
30mm
Measured force barrel [N]
1800
1600
1400
1200
1000
800
600
400
200
0
0
20
40
60
80
100
120
140
160
180
200
220
Piston displaement [mm]

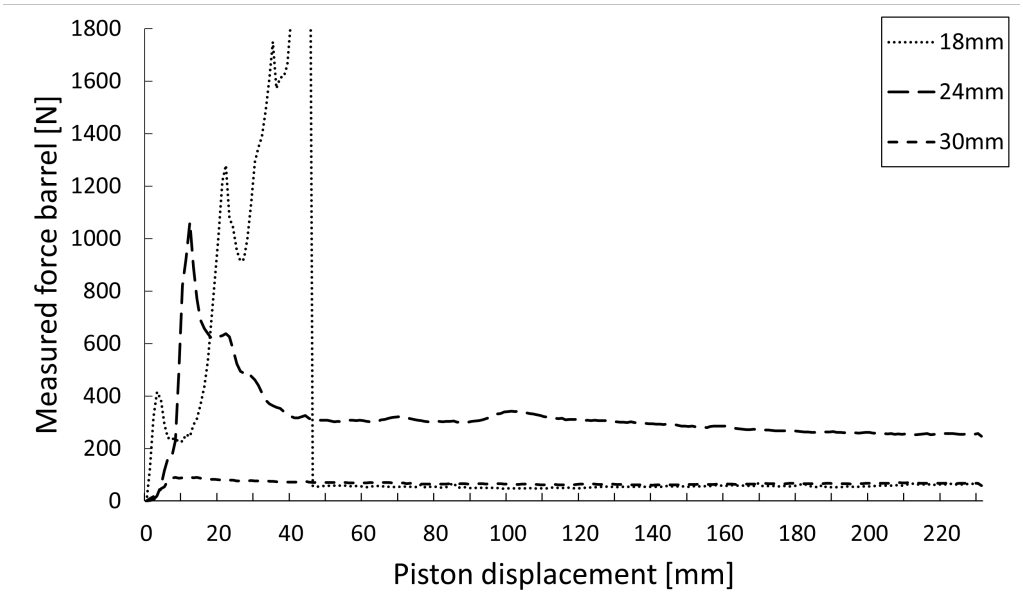
Measured force barrel [N]
1800
1600
1400
1200
1000
800
600
400
200
0
0
20
40
60
80
100
120
140
160
180
200
220
Piston displacement [mm]
18mm
24mm
30mm

Volume fraction 0.50

Table G.2: Static yield stress peak values for mixture CS VF0.50 in [N]

	12 mm	18 mm	24 mm	30 mm
1	-	-	1485.68	979.21
2	-	-	1213.43	1283.09
3	-	-	1465.35	1290.55
Average	-	-	1388.15	1184.28

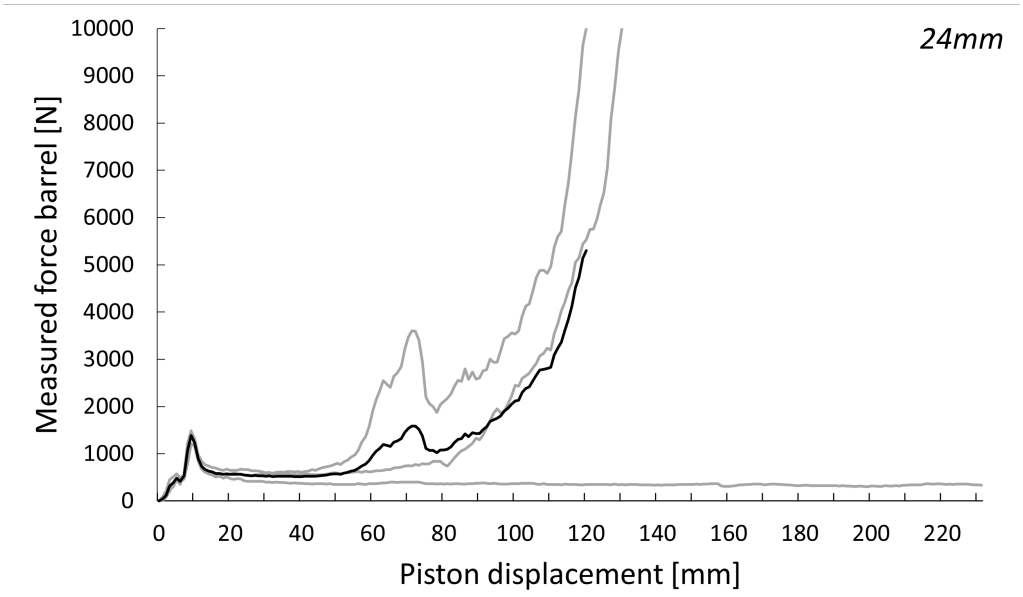

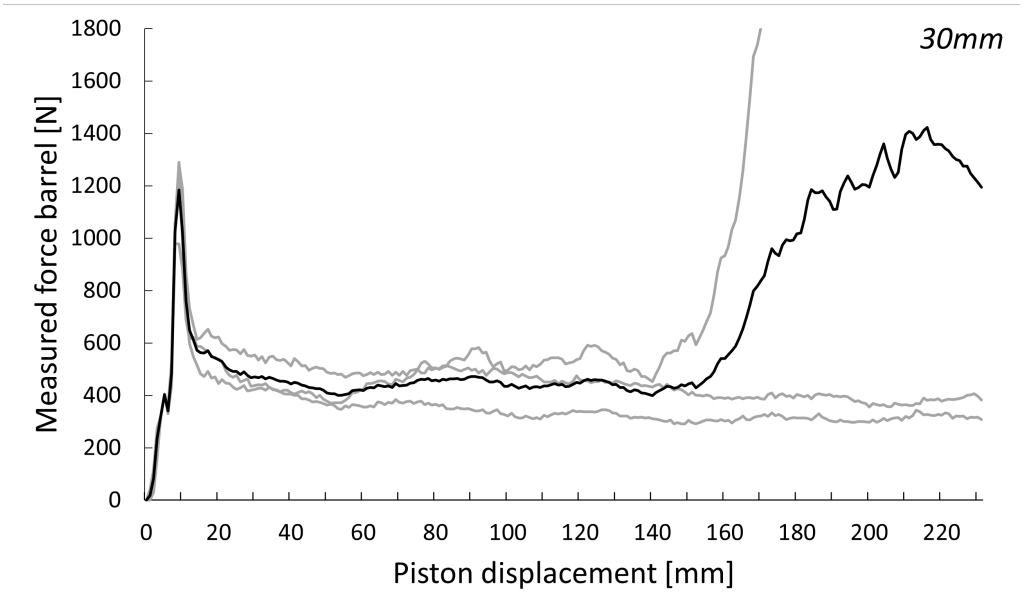
30mm
Measured force barrel [N]
Piston displacement [mm]
0
200
400
600
800
1000
1200
1400
1600
1800
0
20
40
60
80
100
120
140
160
180
200
220

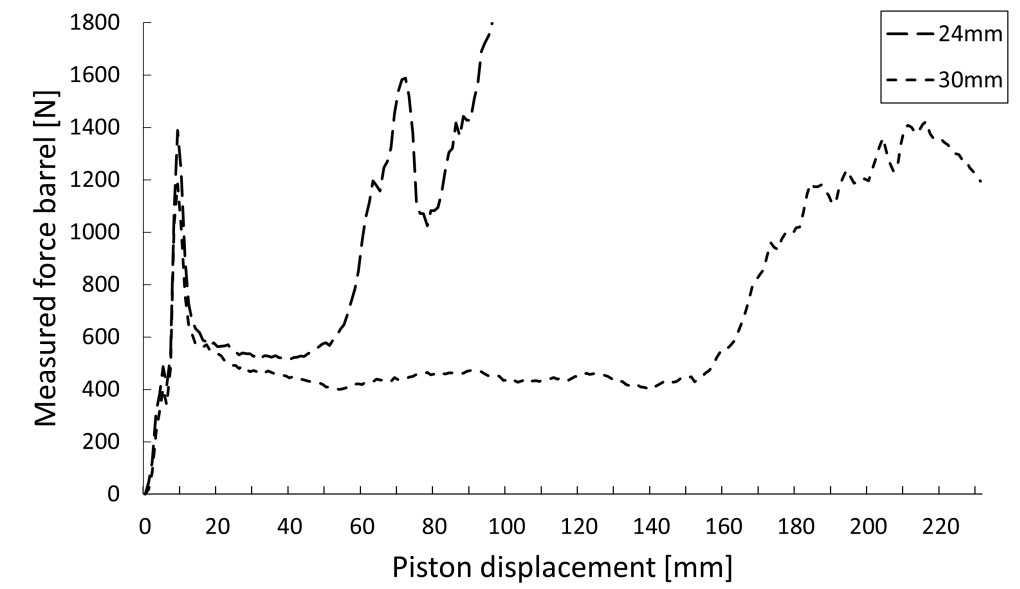
24mm
30mm
Measured force barrel [N]
Piston displacement [mm]
0
200
400
600
800
1000
1200
1400
1600
1800
0
20
40
60
80
100
120
140
160
180
200
220

Volume fraction 0.53

Table G.3: Static yield stress peak values for mixture CS VF0.53 in [N]

	12 mm	18 mm	24 mm	30 mm
1	-	-	-	1783.15
2	-	-	-	2657.04
3	-	-	-	-
Average	-	-	-	2220.10

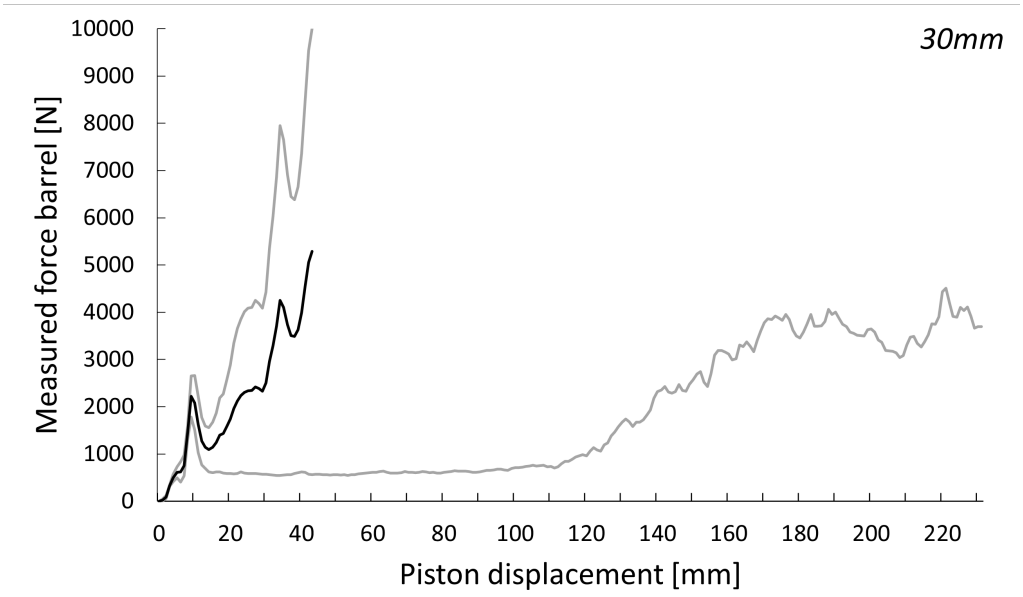

Combination

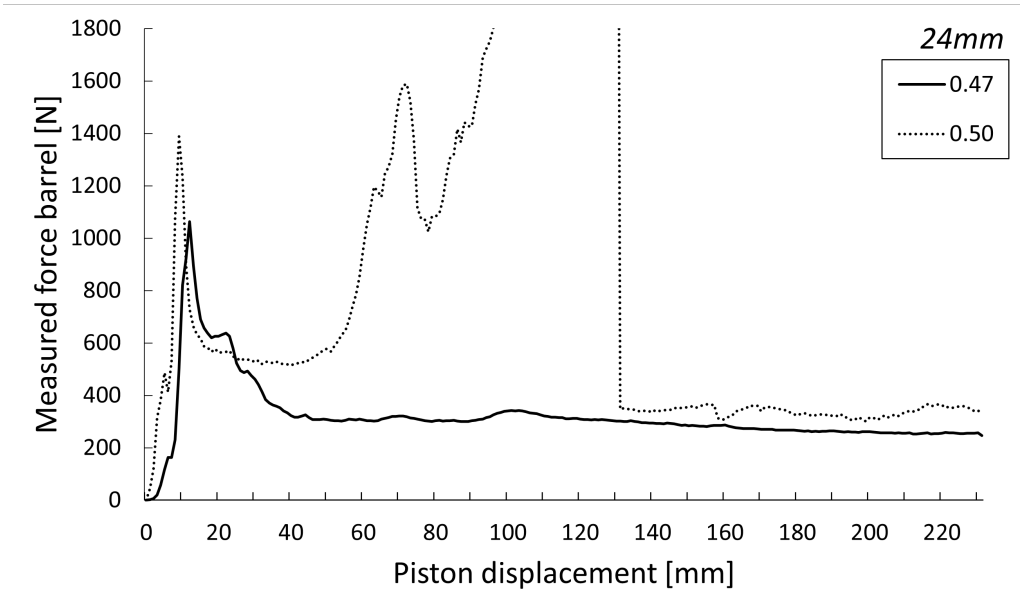
24mm
0.47
0.50
Measured force barrel [N]
Piston displacement [mm]
0
200
400
600
800
1000
1200
1400
1600
1800
0
20
40
60
80
100
120
140
160
180
200
220

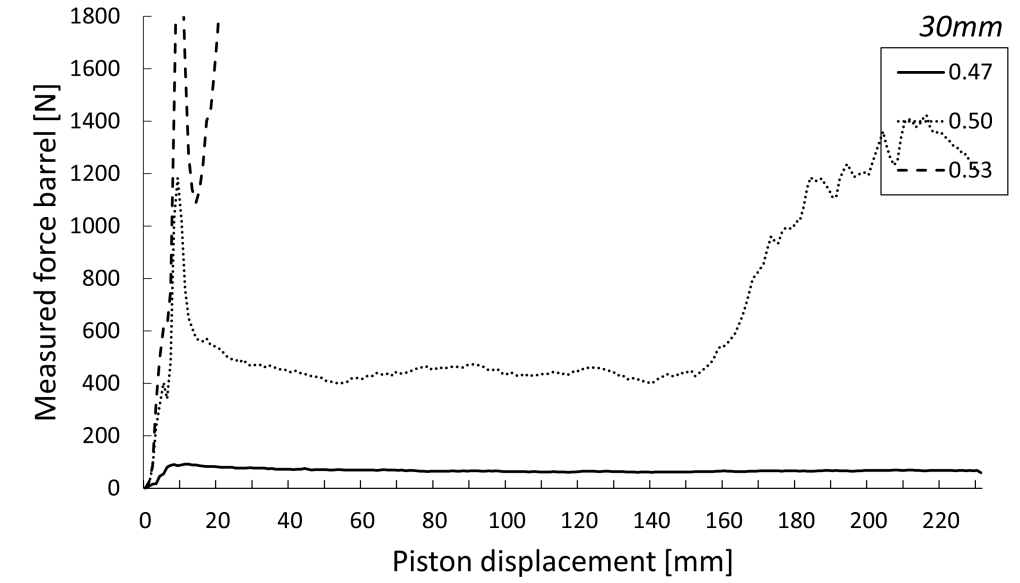
30mm
0.47
0.50
0.53
Measured force barrel [N]
Piston displacement [mm]
0
200
400
600
800
1000
1200
1400
1600
1800
0
20
40
60
80
100
120
140
160
180
200
220

H

Development over time

In Section 3.1, it has been stated that the used cement, CEM III/C, has a slow strength development compared to other cement types over time. Wolfs [44] found time can have a significant influence on the strength development. Therefore, the time when the experimental test started has been tracked. The time started when the water was added to the dry mix, in this research, cement with possibly sand particles, and has been noted when the experimental test started. The time was tracked for mixture CP in the DST and RAM Extruder and for mixture CS in the RAM Extruder. Based on the static yield stress peaks with the time indication in Tables H.1, H.2 and H.3, no time dependency was found in the first 30 minutes after water and cement came in contact.

Table H.1: Starting time of experiment for Direct Shear Test with mixture CP

Volume fraction	Normal force [N]	τ [kPa]	Time
0.47	1.5	0.08	7:29
		0.54	4:59
		0.23	2:18
		0.19	5:28
0.47	5.72	0.34	9:56
		0.30	11:22
		0.36	2:26
0.47	14.036	0.40	2:55
		1.30	5:31
		0.46	8:07
0.50	1.5	0.45	7:20
		0.35	9:39
		0.97	2:15
0.50	5.72	0.75	2:48
		0.80	5:16
		0.54	7:27
		2.00	4:37
0.50	14.036	0.47	10:24
		1.55	2:17
		0.88	4:44
0.53	1.5	1.20	7:21
		0.57	9:48
		1.36	2:54
0.53	5.72	0.49	11:13
		1.39	2:49
		1.01	5:06
		0.61	5:47
0.53	14.036	1.61	3:11
		1.19	5:36
		0.64	8:38
0.56	1.5	2.63	3:14
		2.54	5:38
		2.41	7:56
0.56	5.72	1.67	10:22
		4.17	3:08
		3.33	5:45
		3.96	6:46
0.56	14.036	2.96	8:41
		2.37	11:21
		5.35	3:50

Table H.2: Starting time of experiment for RAM Extruder with mixture CP

Volume fraction	Die diameter [mm]	F_N [N]	Time
0.47	12	46.87	4:37
		68.44	14:52
		57.71	24:02
0.47	18	43.93	4:53
		40.28	3:58
0.50	12	102.37	5:32
		78.54	17:10
		58.51	28:14
0.50	18	70.19	5:37
		58.40	16:14
		68.53	26:18
0.50	24	48.91	5:41
		36.39	14:29
		57.45	25:11
0.50	30	35.98	5:50
		67.85	14:54
		53.55	24:25
0.53	18	261.10	6:19
		199.47	7:36
		23.35	19:01
0.53	24	196.75	7:18
		116.34	18:14
		123.23	28:45
0.53	30	120.47	6:02
		73.90	15:07
		98.29	23:37
0.56	24	3686.80	5:35
		883.41	22:59
0.56	30	4839.61	6:24
		1148.11	19:09
		1148.17	25:44

Table H.3: Starting time of experiment for RAM Extruder with mixture CS

Volume fraction	Die diameter [mm]	F_N [N]	Time
0.47	18	287.86	4:07
		516.35	9:17
		497.15	14:06
0.47	24	822.50	3:39
		696.11	7:07
		1671.37	14:05
0.47	30	92.62	3:36
0.50	24	1485.68	3:43
		1213.43	9:18
		1465.35	23:33
0.50	30	979.21	4:20
		1283.09	9:28
		1290.55	14:47
0.53	30	1783.15	4:47
		2657.04	11:32

I

Results RAM Extruder for the experimental program with varying speeds

The experimental test RAM Extruder has been performed with a program with varying speeds, as presented in Table I.1. The program consists of two types of barrels, where only the large barrel was used for the experimental program presented in Chapter 5. This appendix presents the results of an experimental program with the short and long barrels. The short barrel (SB) has a diameter of 36 mm, equal to the long barrel (LB). The SB has a length of 120 mm. The test has also been performed with different die's. The diameter of all die's is 12 mm, where the length varies. The used lengths are: 15 mm, 60 mm, and 120 mm. The experimental program has been performed for different mixture compositions than presented in Section 3.1, but with the same materials, cement, sand, and glass beads. The glass beads have an average diameter of 1 mm, which differs from the material presented in Section 3.1. The glass beads are mixed with a cement paste, similar to the combination of sand with cement paste. The volume fractions of the mixtures are presented in Table I.2.

Table I.1: Experimental program with varying speeds for RAM Extruder

Speed rate [mm/s]	Vertical displacement for long barrel [mm]	Vertical displacement for short barrel [mm]
2	0-30	0-10
1	30-80	10-30
0.5	80-130	30-50
0.25	130-180	50-70
2	180-230	70-90

Table I.2: Relative mix proportions by weight

Mix-ture	Volume fraction	w/c ratio	Proportions			
			Cement	Sand aggregates	Glass aggregates	Water
CP-2	0.42	0.46	2.16			1
	0.44	0.43	2.34			1
	0.48	0.36	2.71			1
	0.52	0.31	3.23			1
	0.55	0.27	3.64			1
CS-2	0.27	0.37	2.70	1.85		1
	0.35	0.37	2.70	2.37		1
	0.40	0.37	2.70	2.50		1
	0.47	0.37	2.70	2.78		1
	0.55	0.43	2.33	5.81		1
CG-2	0.42	0.37	2.70		1.85	1
	0.44	0.37	2.70		2.08	1
	0.48	0.32	3.17		2.70	1

Mixture CP-2

Volume fraction 0.42

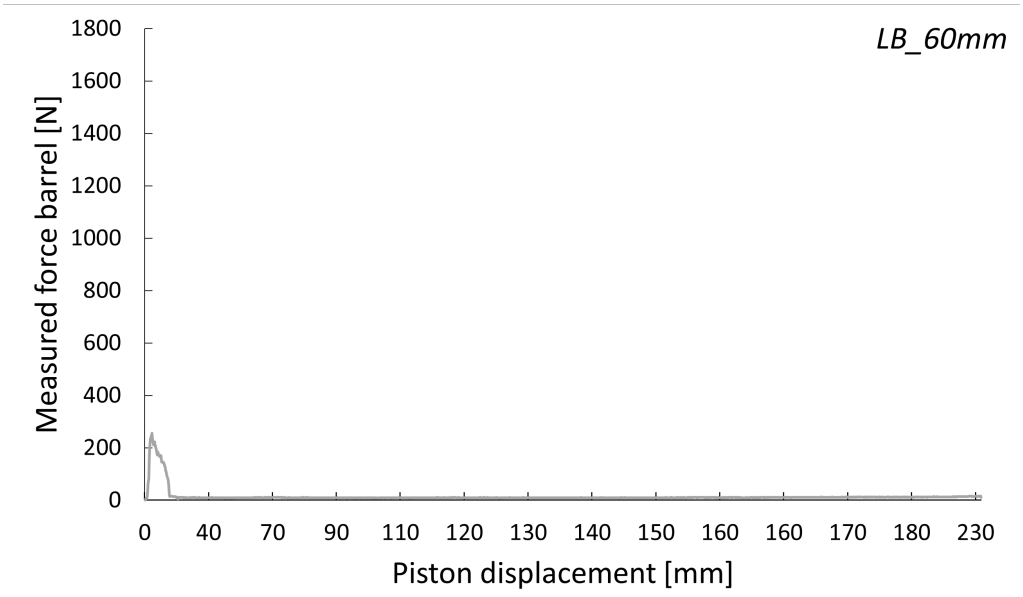

Volume fraction 0.48

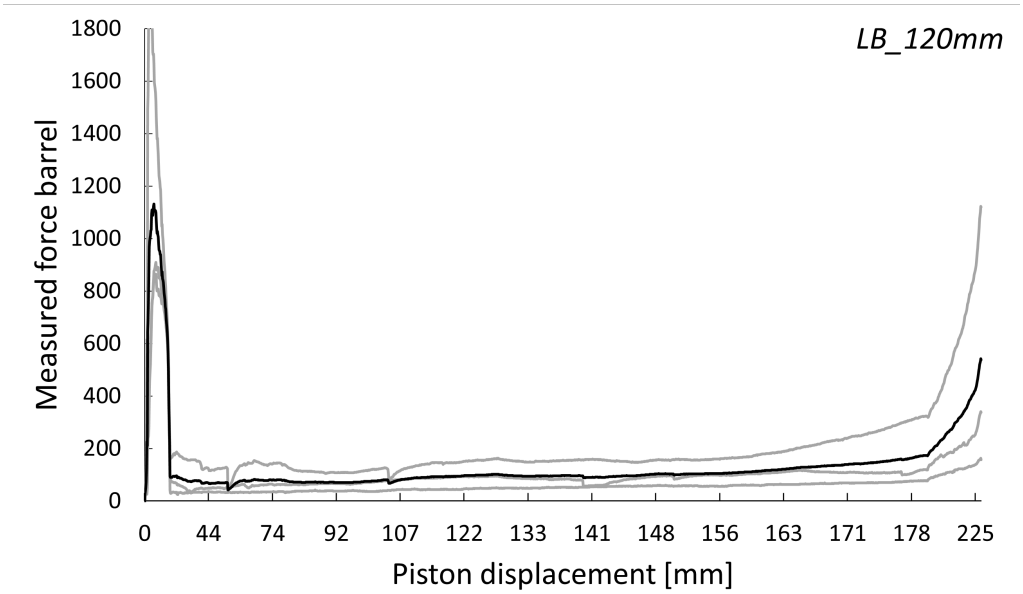

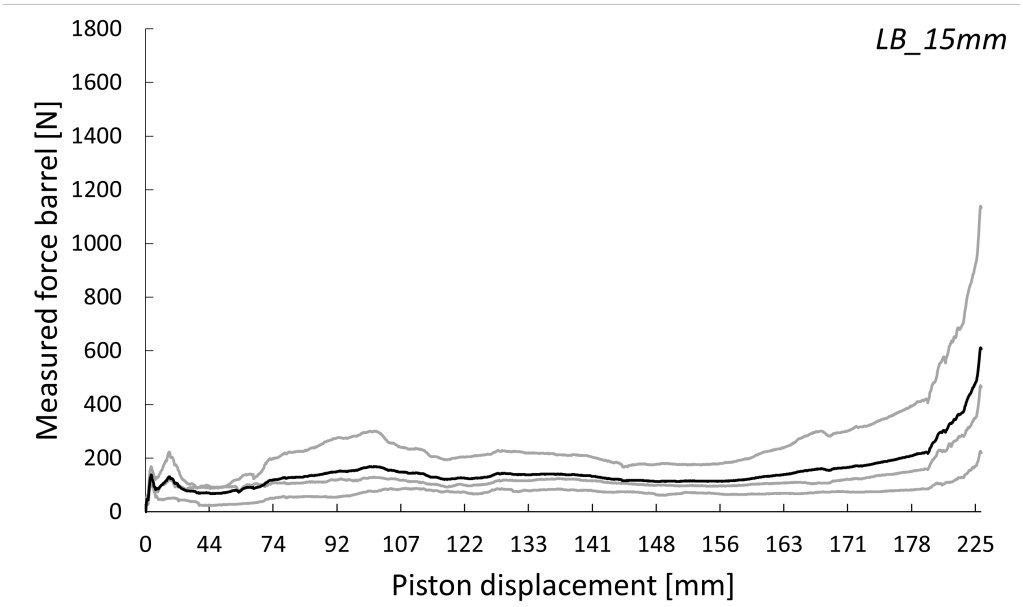

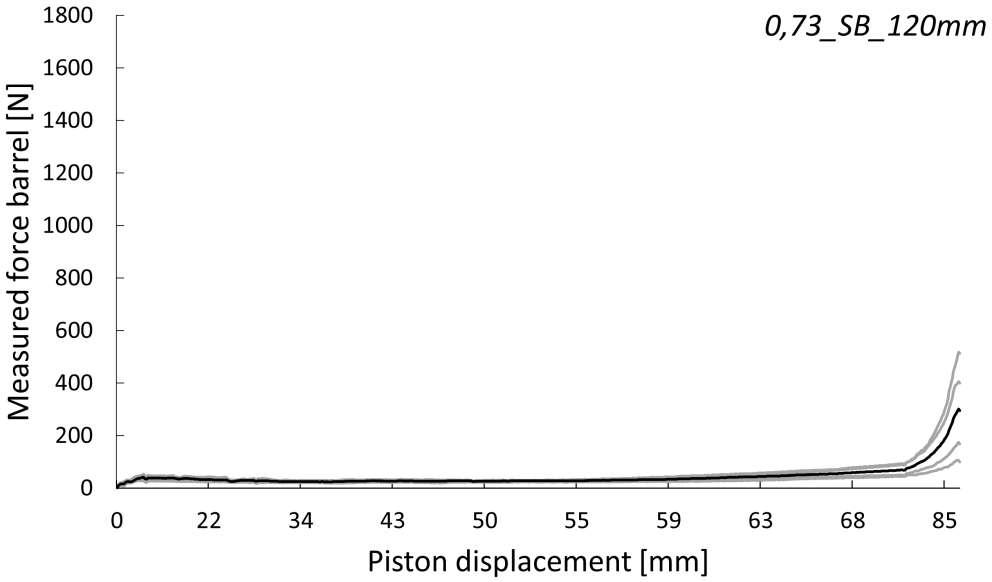
0,73_SB_120mm
Measured force barrel [N]
1800
1600
1400
1200
1000
800
600
400
200
0
0
22
34
43
50
55
59
63
68
85
Piston displacement [mm]

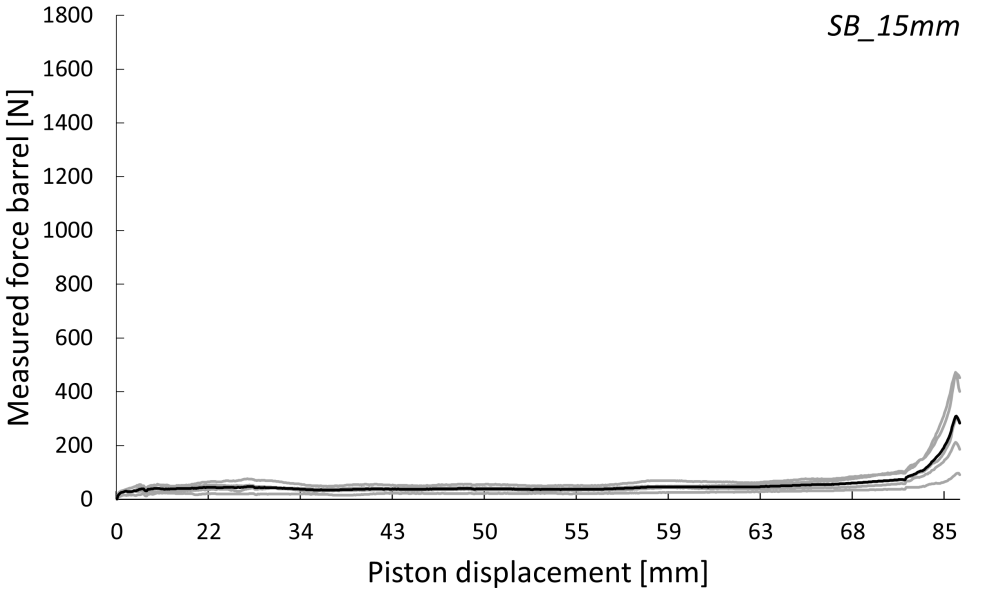
SB_15mm
Measured force barrel [N]
1800
1600
1400
1200
1000
800
600
400
200
0
0
22
34
43
50
55
59
63
68
85
Piston displacement [mm]

Volume fraction 0.52

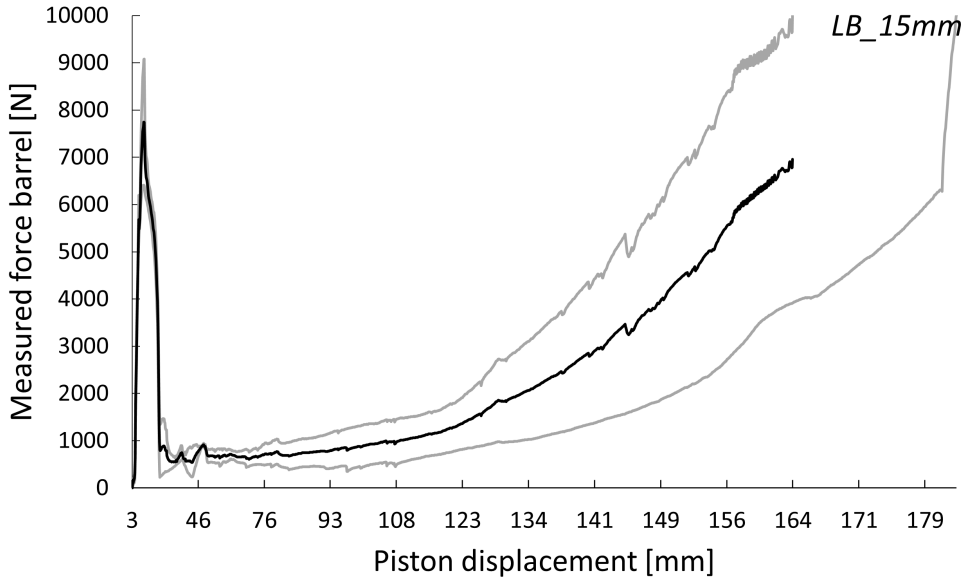

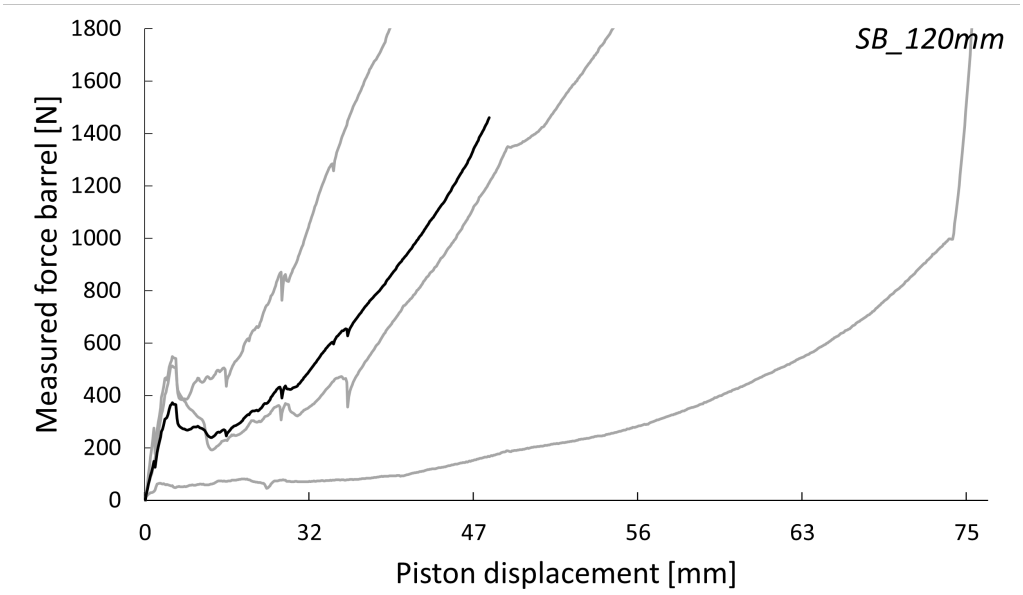

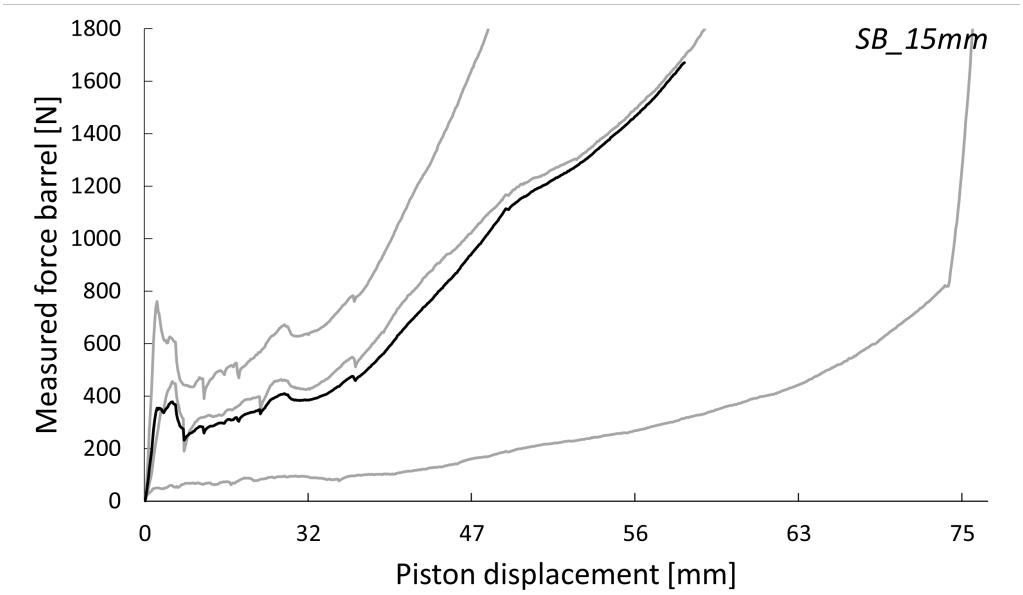

Mixture CG-2

Volume fraction 0.42

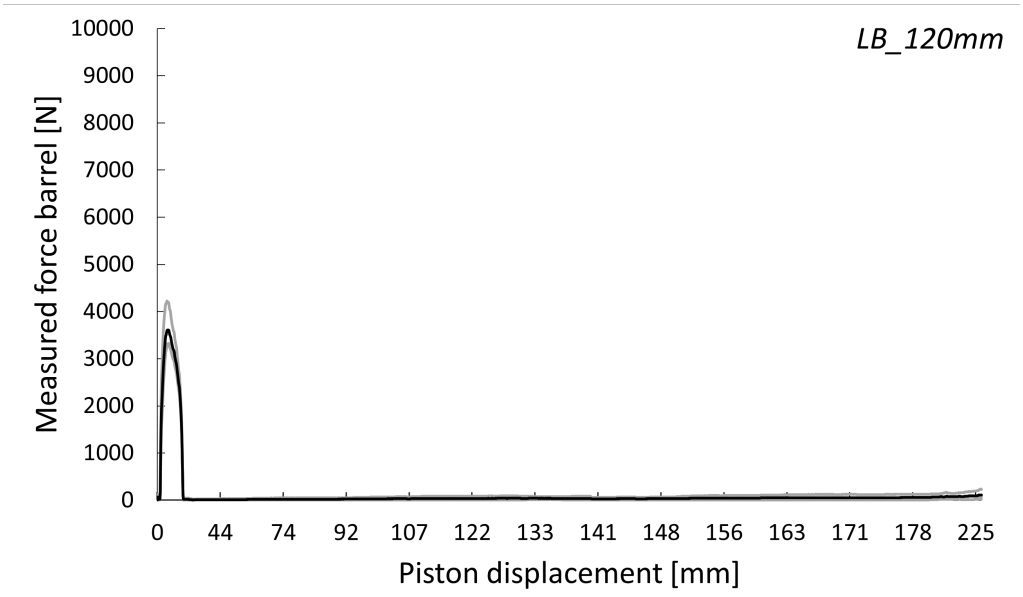

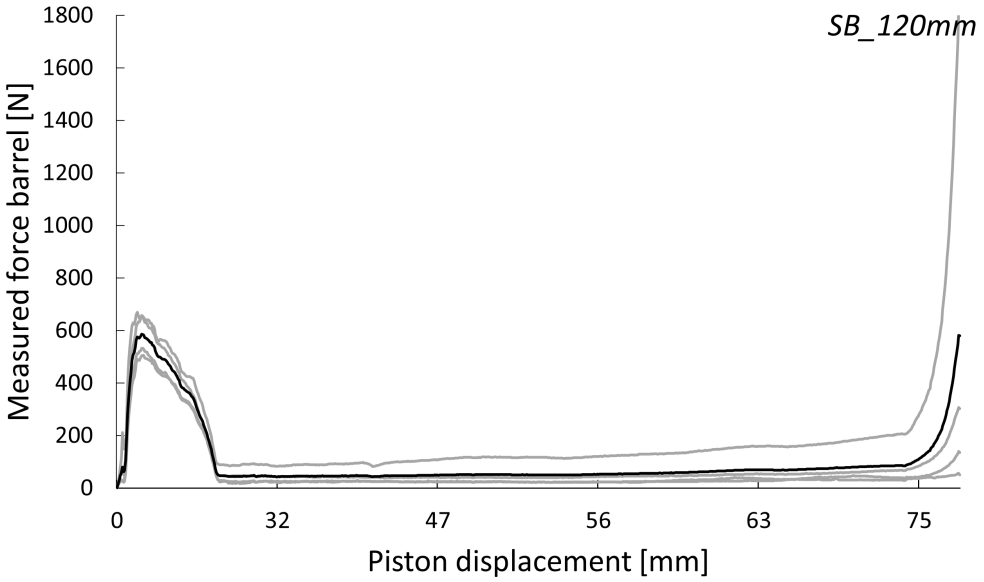
SB_120mm
Measured force barrel [N]
1800
1600
1400
1200
1000
800
600
400
200
0
0
32
47
56
63
75
Piston displacement [mm]

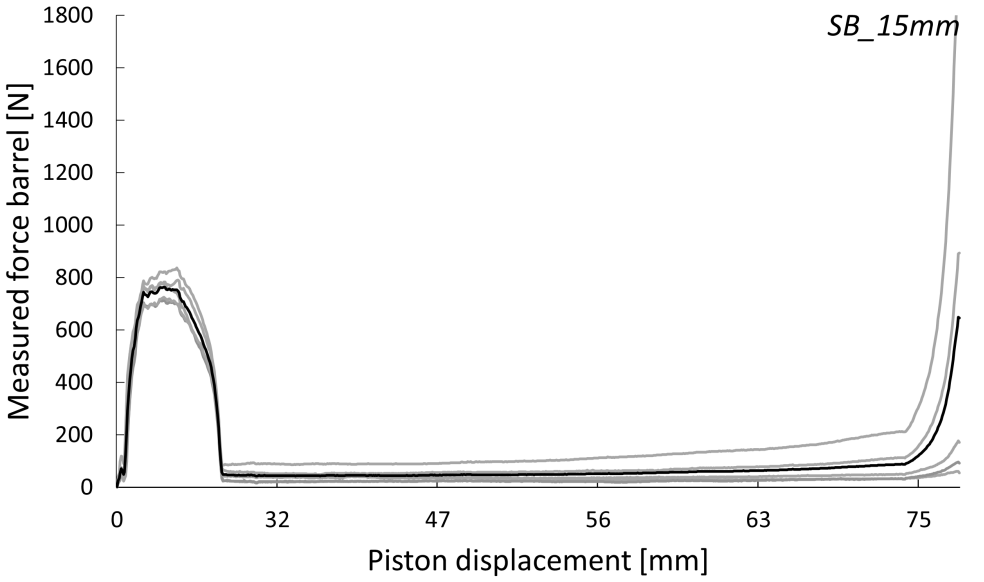
SB_15mm
Measured force barrel [N]
1800
1600
1400
1200
1000
800
600
400
200
0
0
32
47
56
63
75
Piston displacement [mm]

Volume fraction 0.44

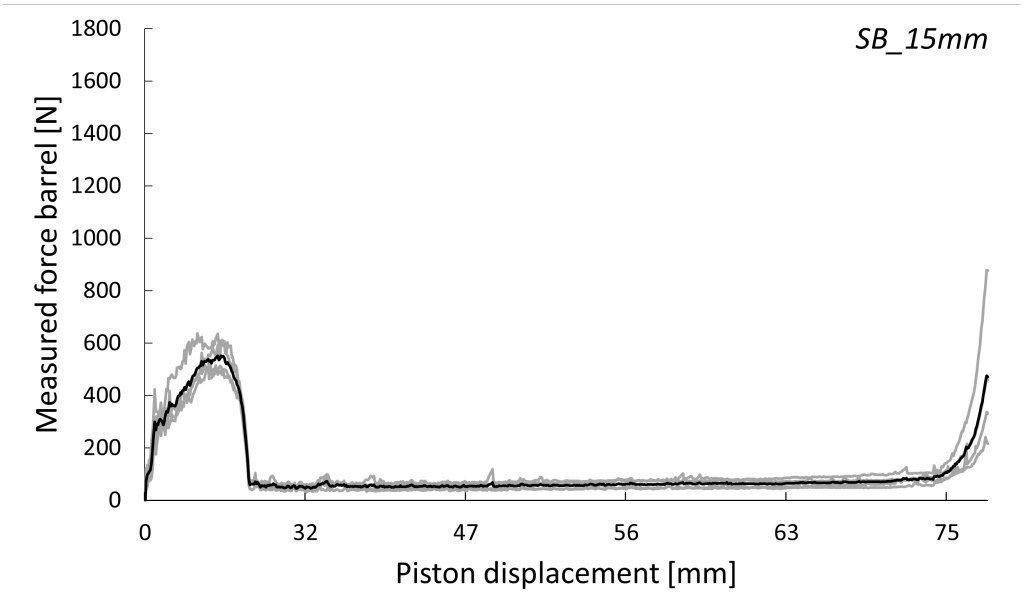

Volume fraction 0.48

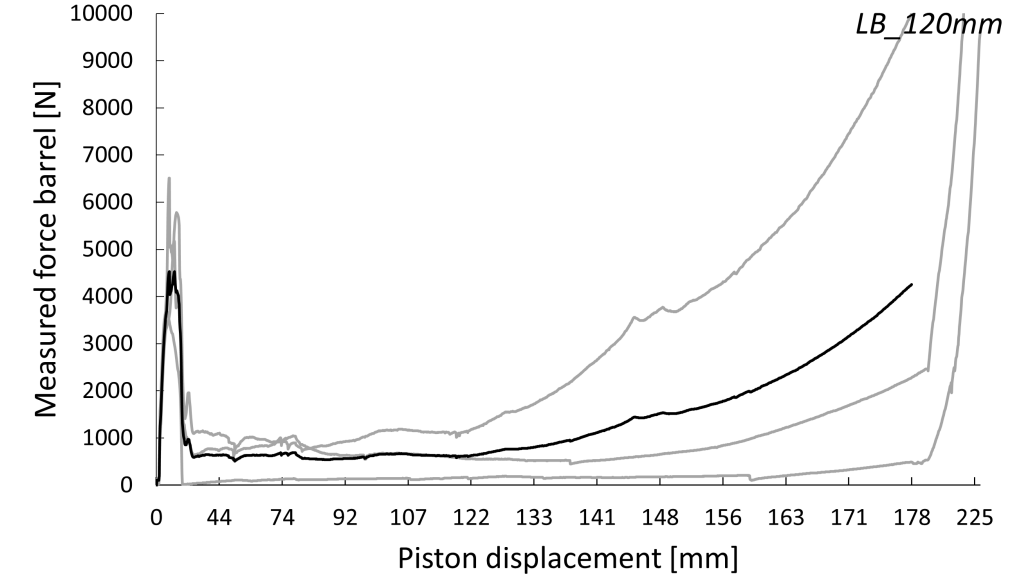

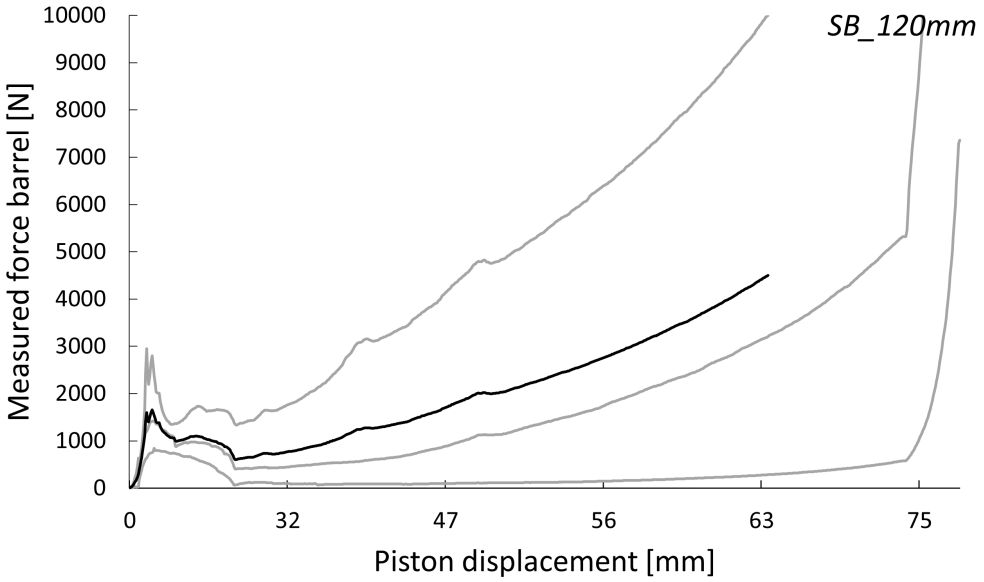

Mixture CS-2

Volume fraction 0.27

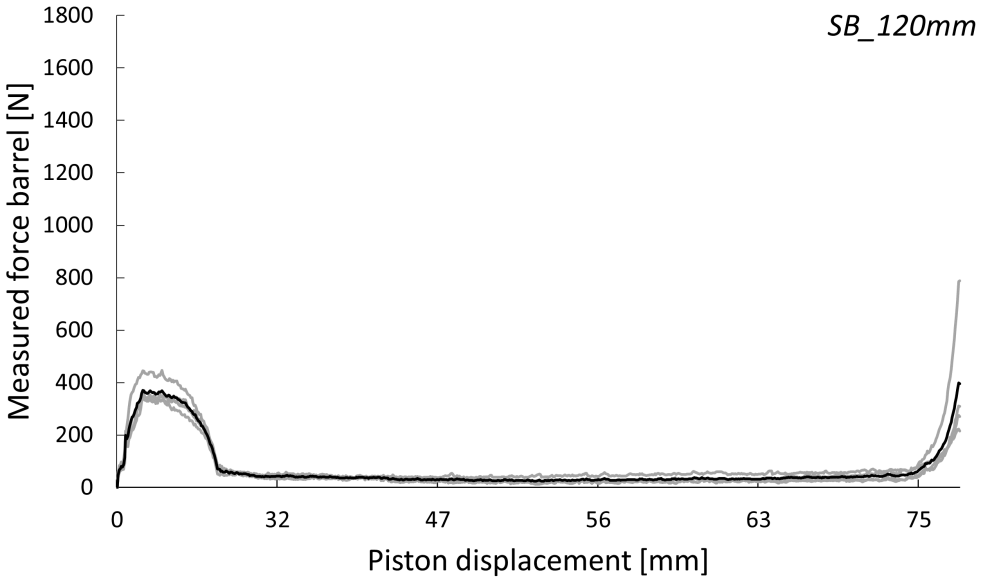

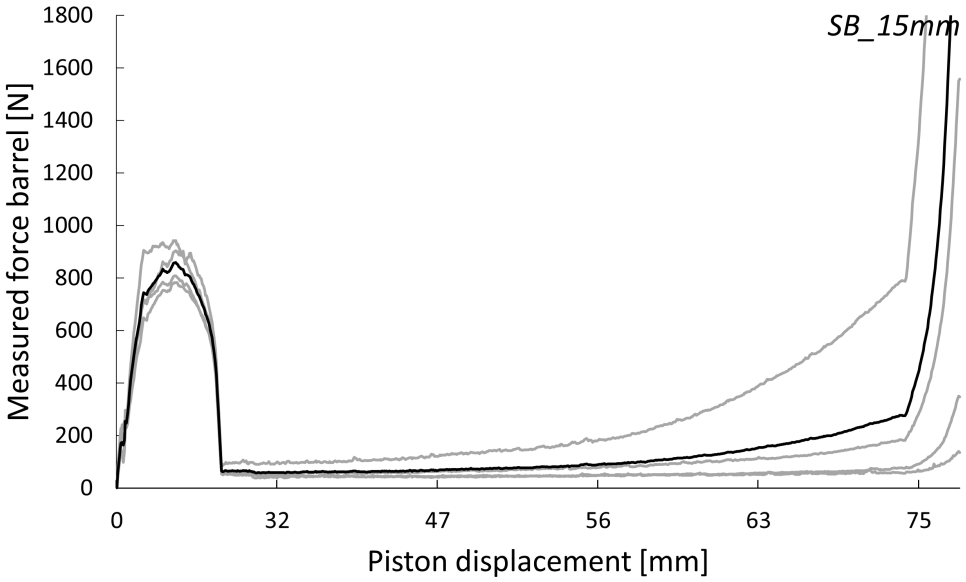
SB_15mm
Measured force barrel [N]
1800
1600
1400
1200
1000
800
600
400
200
0
0
32
47
56
63
75
Piston displacement [mm]

J

Results DST with varying heights

The influence of the height of the shear box in the Direct Shear Test has been researched. The height can have an influence on the forming of a local shear failure plane. Besides, the global shear stress could be measured over the local shear stress. Therefore, the height of the shear box is varied. The top and bottom plates have been varied in height. The explanation of the height is presented in Figure J.1. The heights of the top and bottom plates are given in Table J.1. The influence of the height of the plates in the DST has been researched for mixture CP, as presented in Table 3.1, for volume fractions 0.50, 0.53, and 0.56.

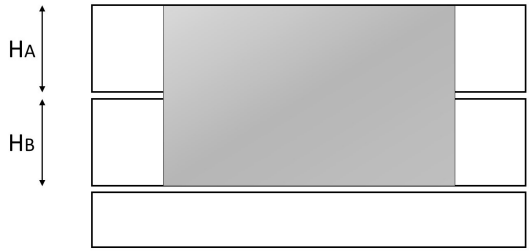

Figure J.1: Abstract explanation of varied heights in DST.

Table J.1: Varied tested heights of Direct Shear Test.

Type	Height top plate (H_A) [mm]	Height bottom plate (H_B) [mm]
18-18	18	18
18-12	18	12
18-6	18	6
12-12	12	12
6-6	6	6

Volume fraction 0.50

The results of the DST for mixture CP with volume fraction 0.50 are presented below. The heights of the plates do not change the behavior of the shear stress over the horizontal displacement. The height does not influence the measurement of a local shear plane failure for this mixture.

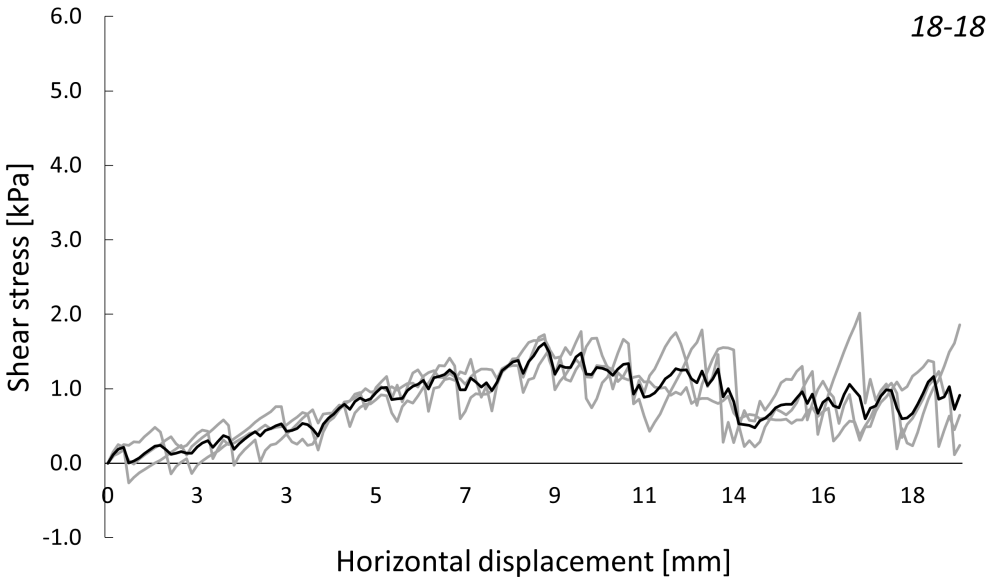
18-18
Shear stress [kPa]
6.0
5.0
4.0
3.0
2.0
1.0
0.0
-1.0
0
3
3
5
7
9
11
14
16
18
Horizontal displacement [mm]

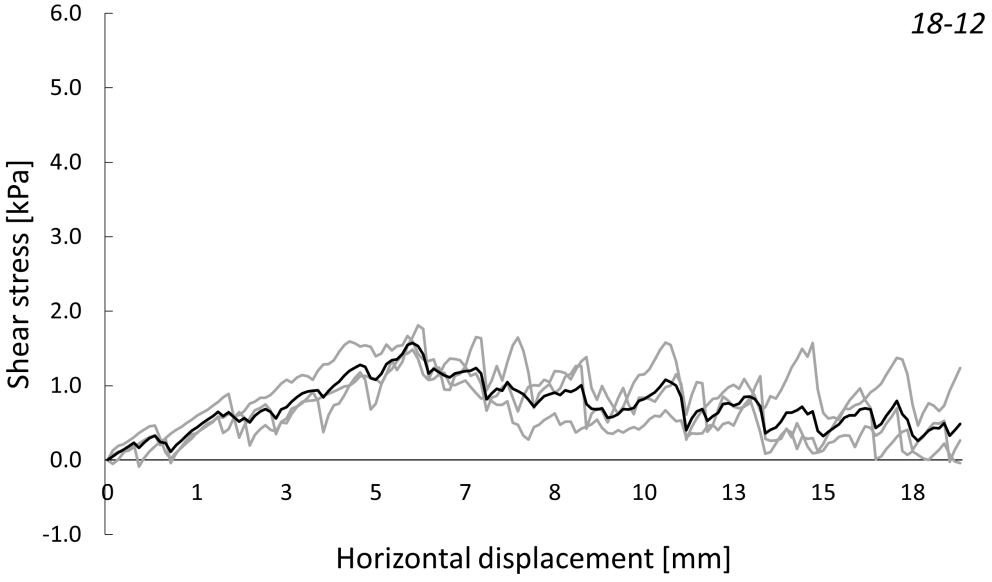
18-12
Shear stress [kPa]
6.0
5.0
4.0
3.0
2.0
1.0
0.0
-1.0
0
1
3
5
7
8
10
13
15
18
Horizontal displacement [mm]

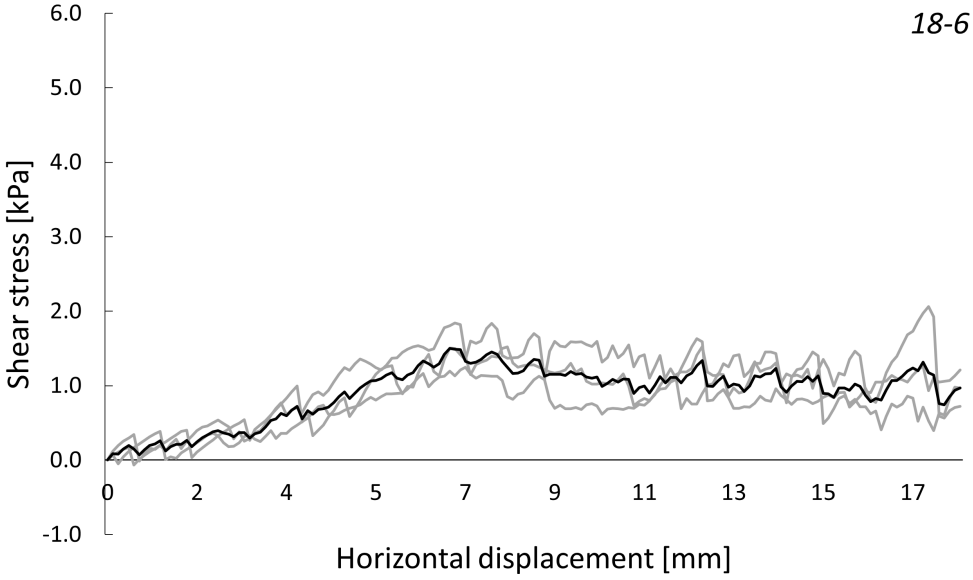
18-6
6.0
5.0
4.0
3.0
2.0
1.0
0.0
-1.0
Shear stress [kPa]
0
2
4
5
7
9
11
13
15
17
Horizontal displacement [mm]

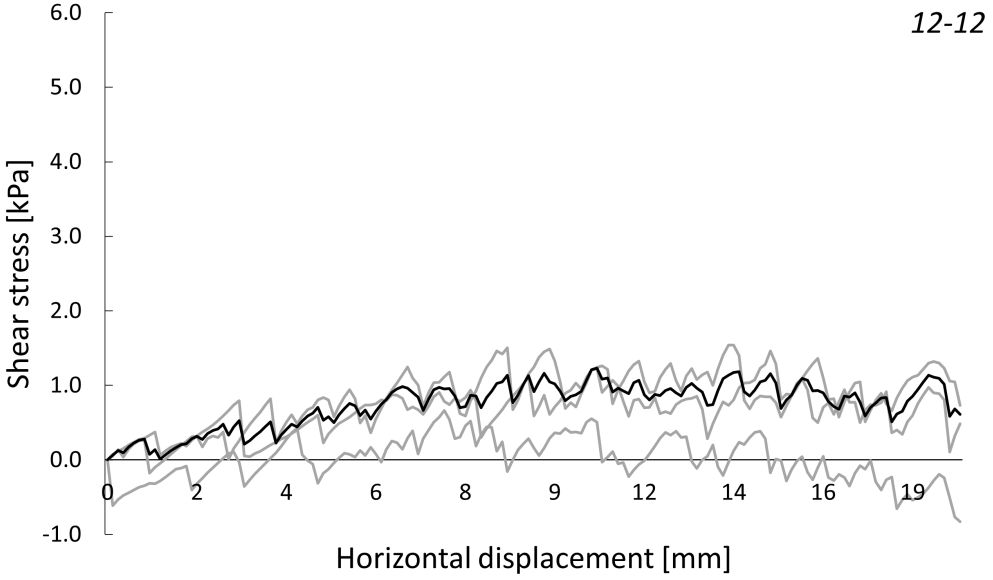
12-12
6.0
5.0
4.0
3.0
2.0
1.0
0.0
-1.0
Shear stress [kPa]
0
2
4
6
8
9
12
14
16
19
Horizontal displacement [mm]

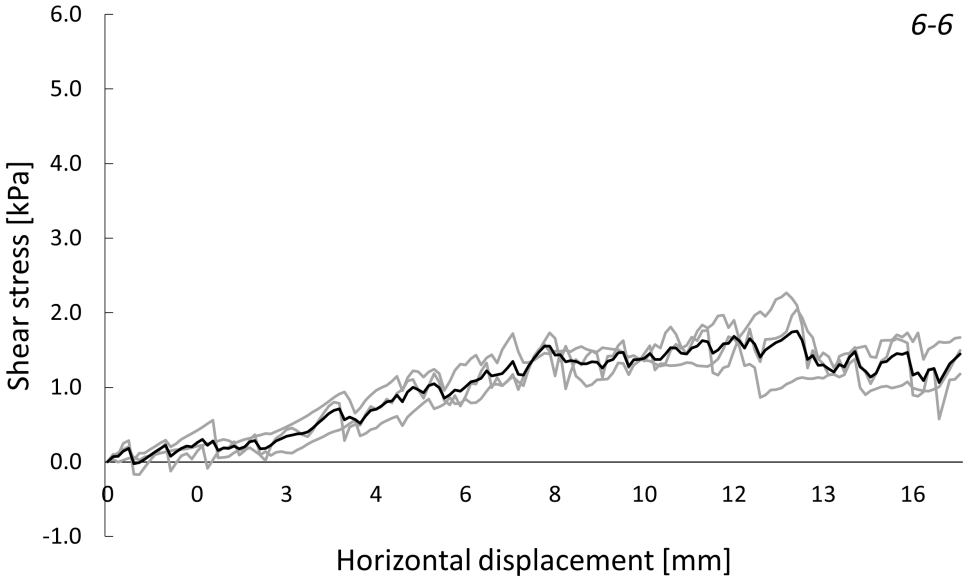
6-6
Shear stress [kPa]
6.0
5.0
4.0
3.0
2.0
1.0
0.0
-1.0
0
0
3
4
6
8
10
12
13
16
Horizontal displacement [mm]

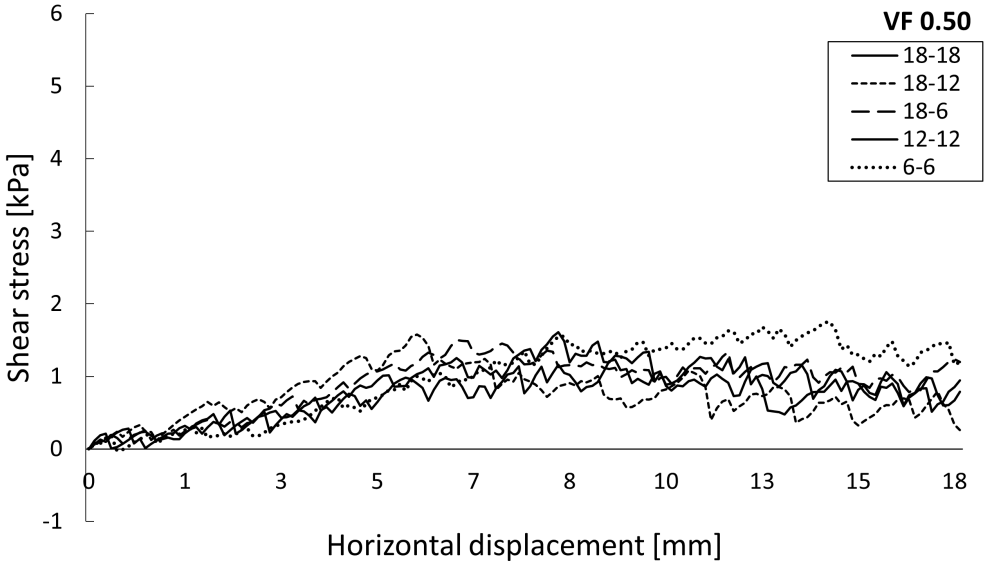
VF 0.50
18-18
18-12
18-6
12-12
6-6
Shear stress [kPa]
6
5
4
3
2
1
0
-1
0
1
3
5
7
8
10
13
15
18
Horizontal displacement [mm]

Volume fraction 0.53

The results of the DST for mixture CP with volume fraction 0.53 are presented below. The original shear box, with a height of bottom en top plate of 18 mm, shows an earlier static yield stress peak than the lower heights. The static yield stress peak of the lower heights, top and bottom plate, occurs with a larger horizontal displacement. However, the magnitude of shear stress does not vary for the original shear box compared to the lower heights of the plates.

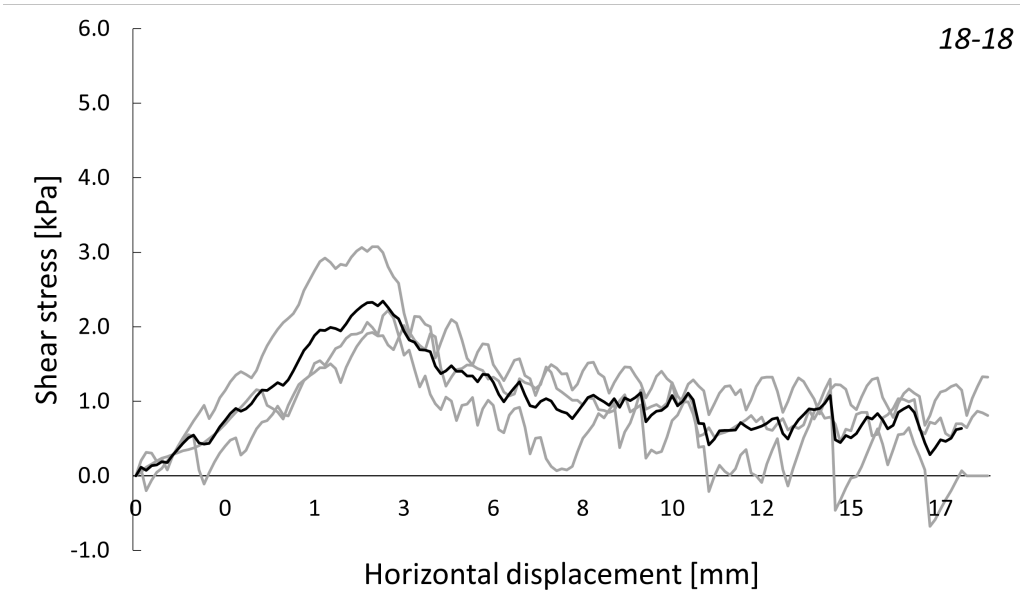

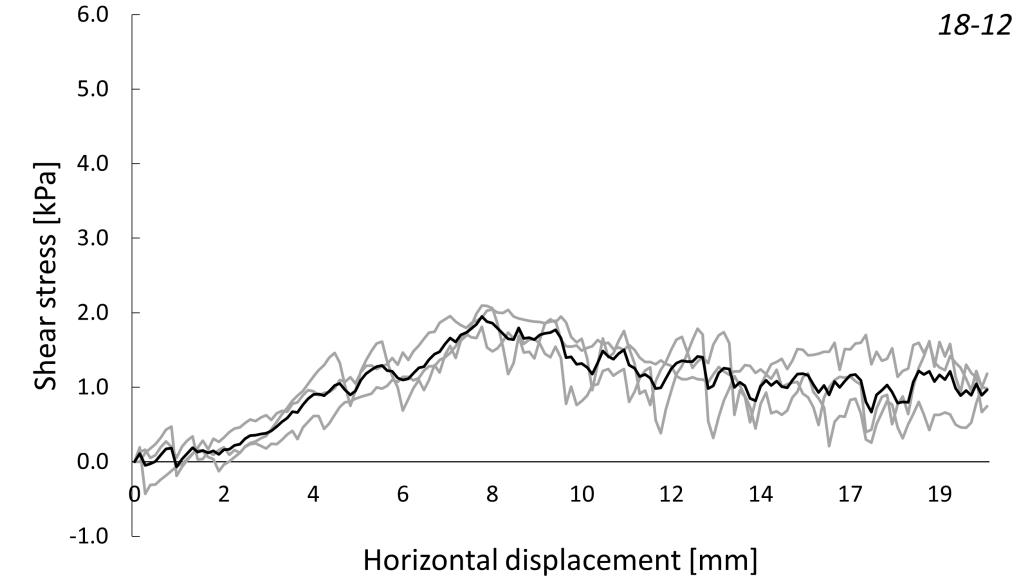

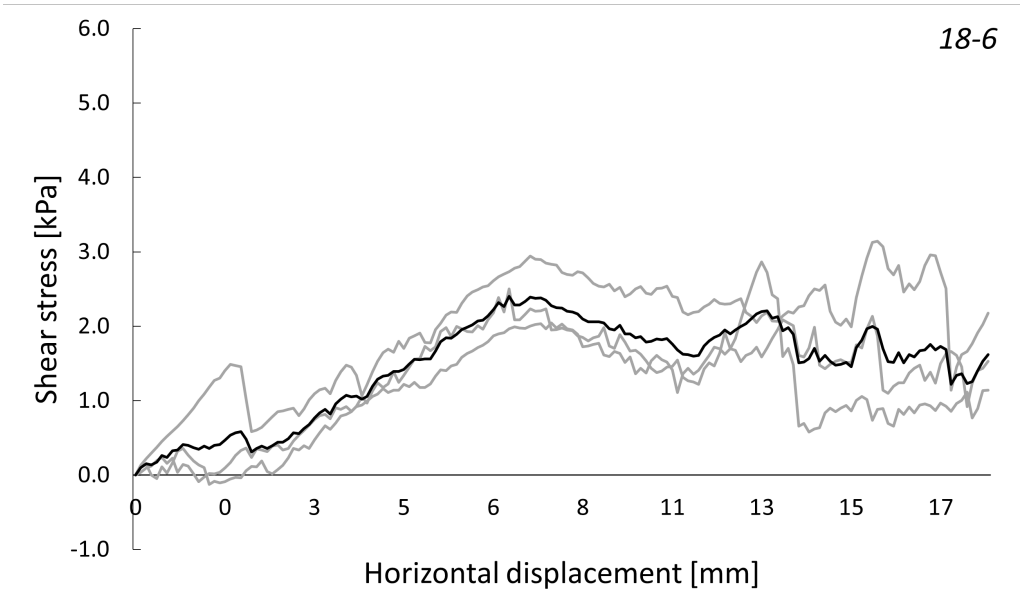
18-6
Shear stress [kPa]
6.0
5.0
4.0
3.0
2.0
1.0
0.0
-1.0
0
0
3
5
6
8
11
13
15
17
Horizontal displacement [mm]

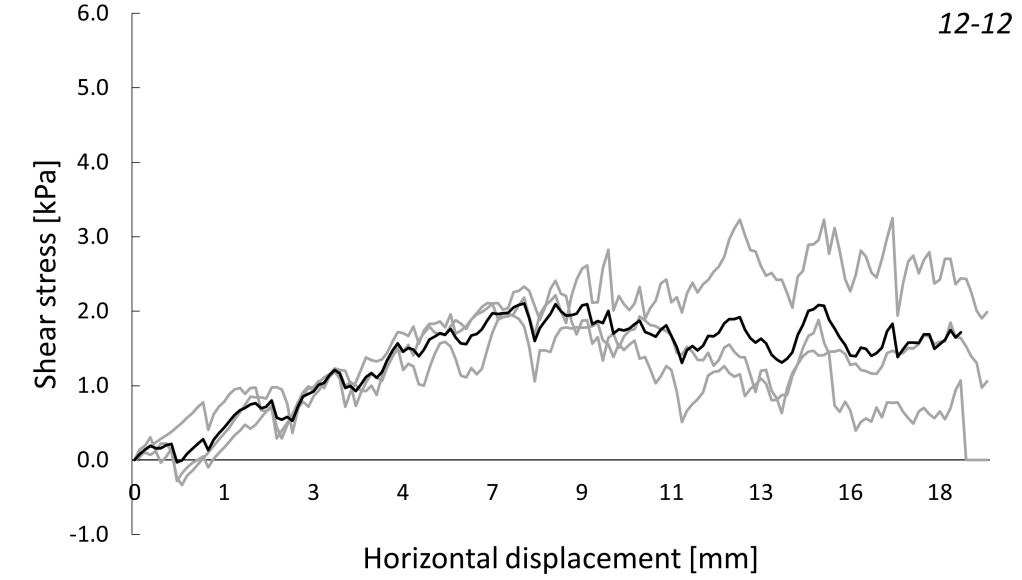
12-12
Shear stress [kPa]
6.0
5.0
4.0
3.0
2.0
1.0
0.0
-1.0
0
1
3
4
7
9
11
13
16
18
Horizontal displacement [mm]

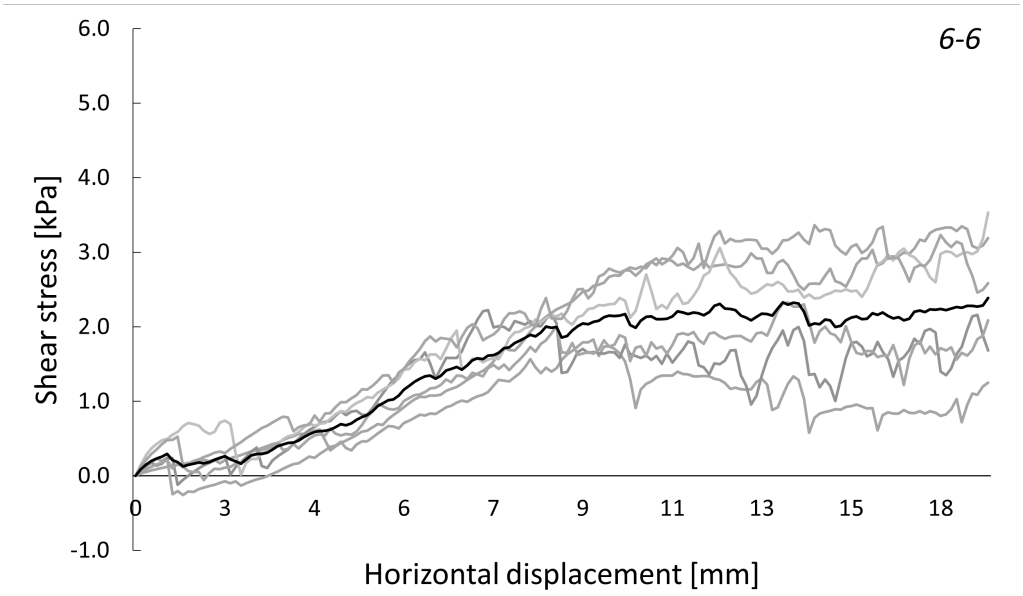
6-6
Shear stress [kPa]
6.0
5.0
4.0
3.0
2.0
1.0
0.0
-1.0
0
3
4
6
7
9
11
13
15
18
Horizontal displacement [mm]

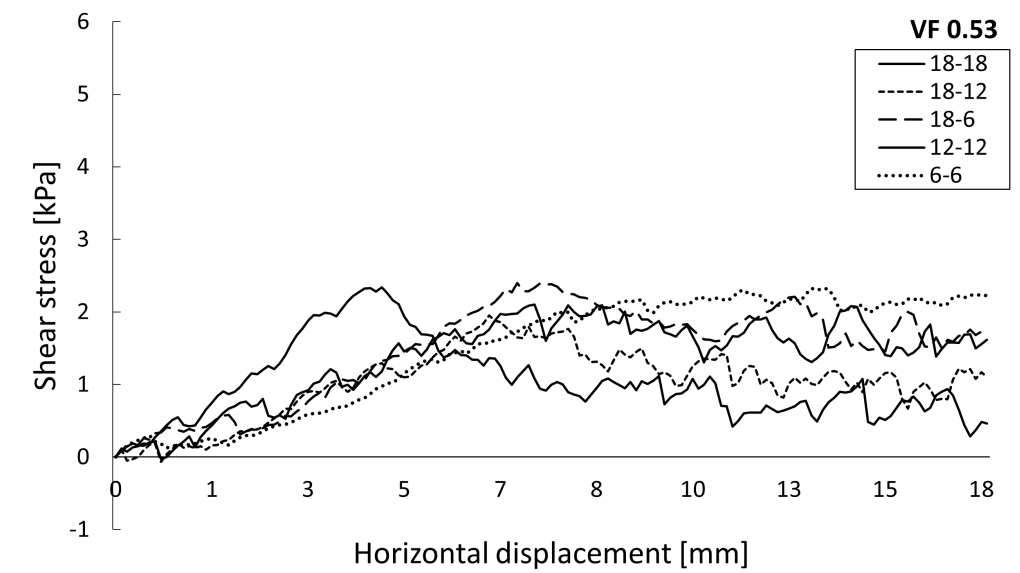
VF 0.53
18-18
18-12
18-6
12-12
6-6
Shear stress [kPa]
6
5
4
3
2
1
0
-1
0
1
3
5
7
8
10
13
15
18
Horizontal displacement [mm]

Volume fraction 0.56

The results of the DST for mixture CP with volume fraction 0.56 are presented below. The original setup of the DST, type 18-18, shows an earlier static yield stress peak than the lower height of the top and bottom plates. For the lower heights of the shear box, the static yield stress peak has been observed at a larger horizontal displacement. However, the magnitude of the shear stress does not vary for the original shear box compared to the lower heights of the shear box.

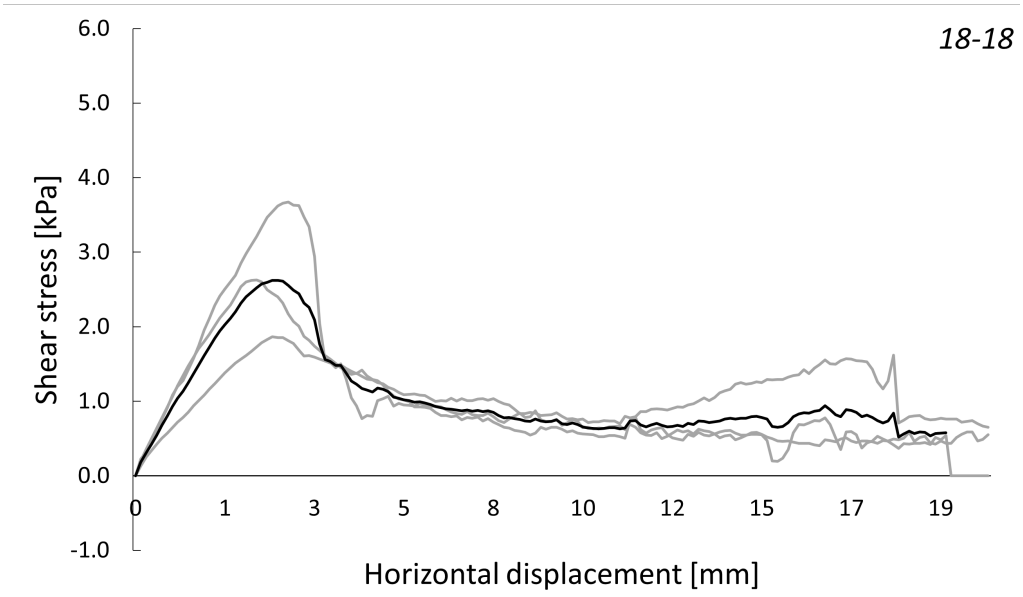

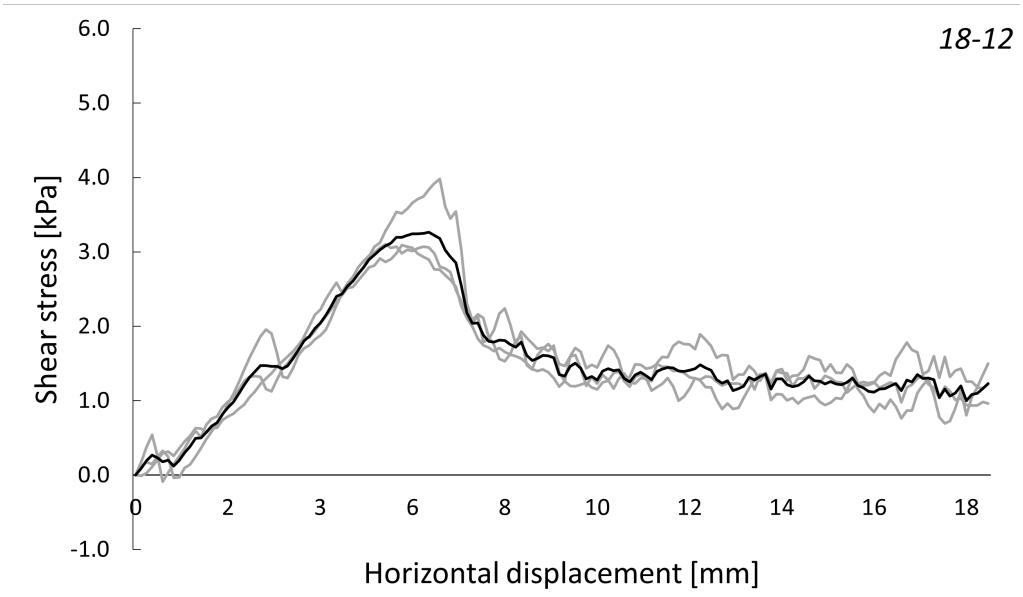

The height of the DST has an influence on the behavior of shear stress development over horizontal displacement, especially for mixtures with a higher volume fraction. This indicates that a global shear failure plane is measured over a local shear failure plane. However, the magnitude of the shear stress for the original shear box is in the same order of magnitude as the lower heights of the top and bottom

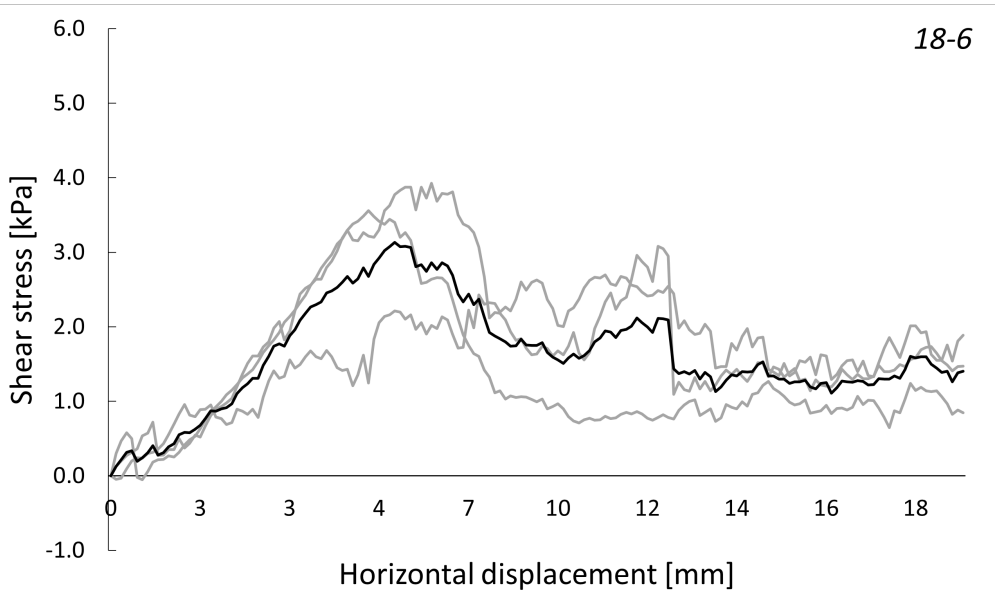

plates of the shear box. Therefore, the results of the original shear box, with an overall height of 36 mm, can be used to represent the local shear failure plane.

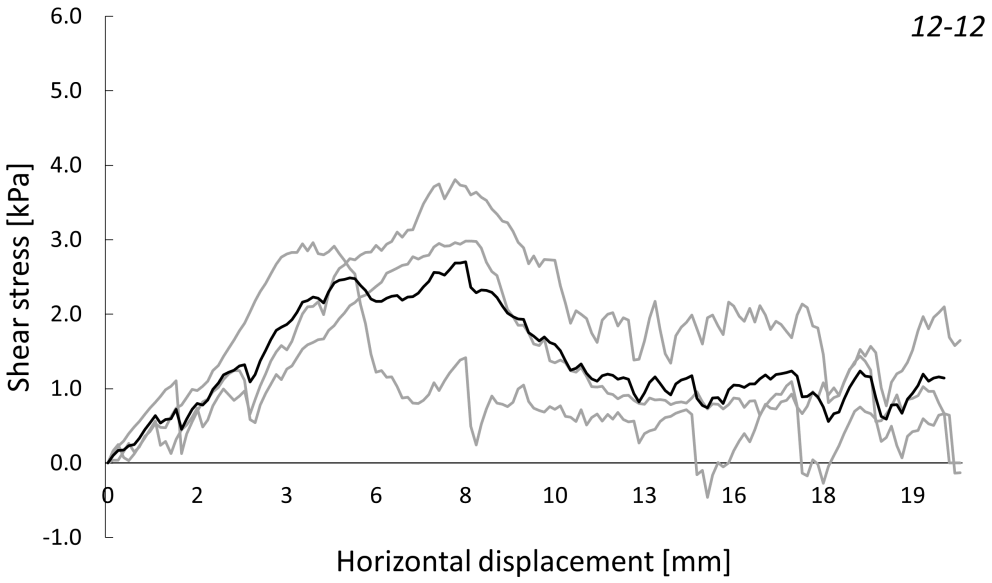
12-12
Shear stress [kPa]
6.0
5.0
4.0
3.0
2.0
1.0
0.0
-1.0
0
2
3
6
8
10
13
16
18
19
Horizontal displacement [mm]

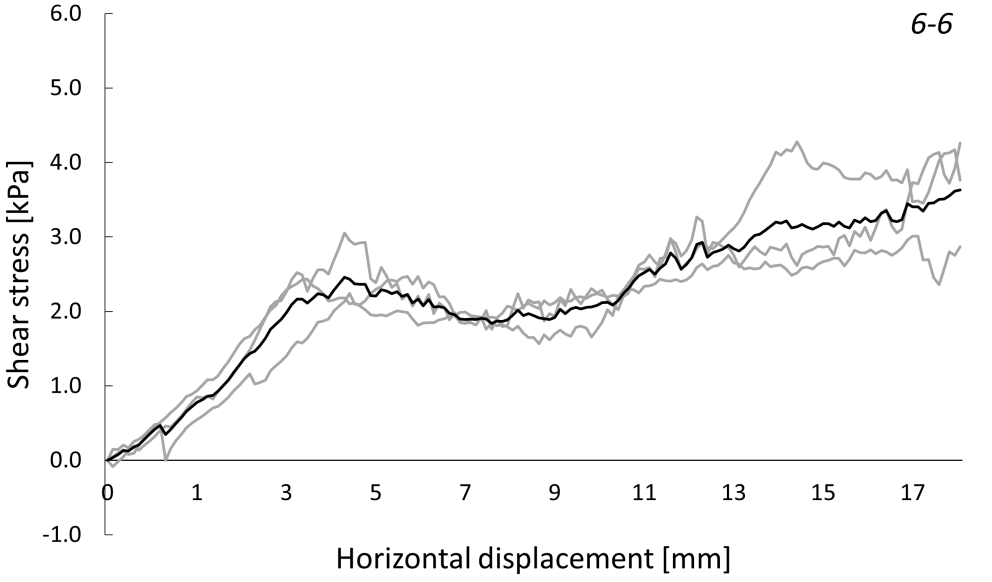
6-6
Shear stress [kPa]
6.0
5.0
4.0
3.0
2.0
1.0
0.0
-1.0
0
1
3
5
7
9
11
13
15
17
Horizontal displacement [mm]

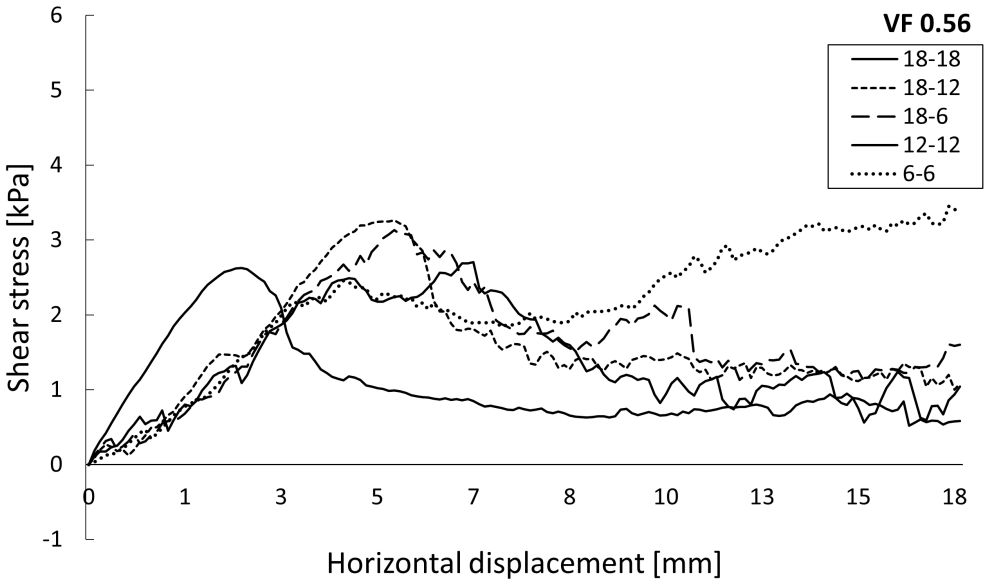
VF 0.56
18-18
18-12
18-6
12-12
6-6
Shear stress [kPa]
6
5
4
3
2
1
0
-1
0
1
3
5
7
8
10
13
15
18
Horizontal displacement [mm]

K

Results DST for other mixtures

The Direct Shear Test (DST) has also been performed for other mixtures than presented in Table 3.1. The DST has been performed for a cement paste mixture (CP-2) and a cement paste mixture with sand aggregates (CS-2). The mix proportions of the mixtures are presented in Table I.2. The DST is performed with various normal forces of 1.5 N (self-weight), 5.72 N, and 14.036 N, similar to the experimental program described in Section 3.2.

Mixture CP-2

Volume fraction 0.42

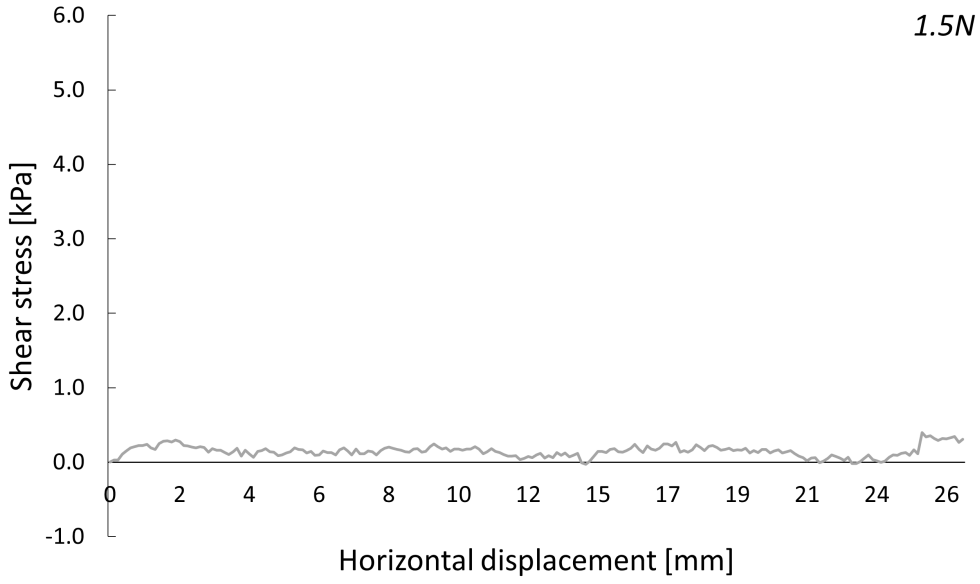

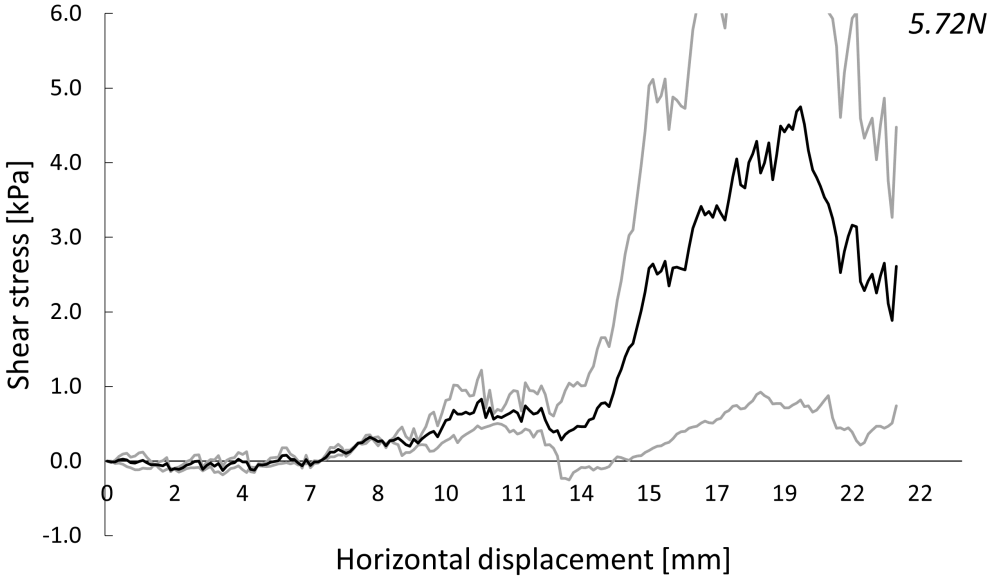
5.72N
Shear stress [kPa]
6.0
5.0
4.0
3.0
2.0
1.0
0.0
-1.0
0
2
4
7
8
10
11
14
15
17
19
22
22
Horizontal displacement [mm]

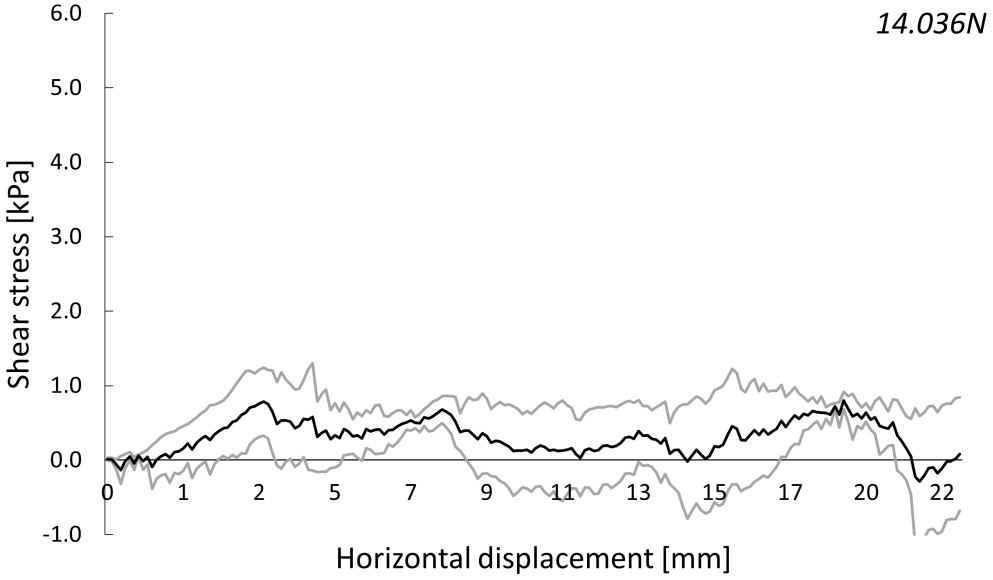
14.036N
Shear stress [kPa]
6.0
5.0
4.0
3.0
2.0
1.0
0.0
-1.0
0
1
2
5
7
9
11
13
15
17
20
22
Horizontal displacement [mm]

Volume fraction 0.44

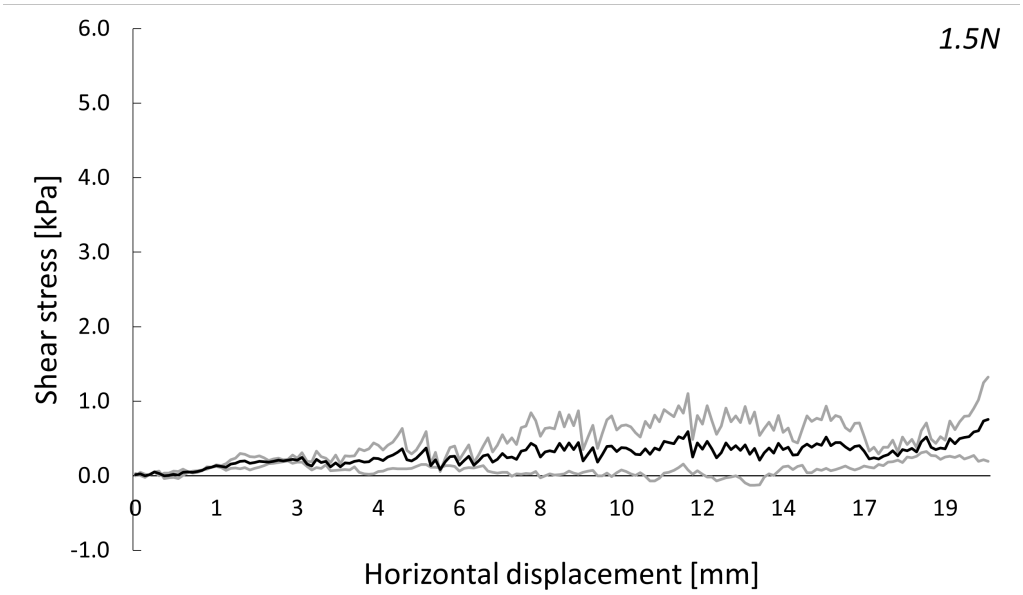

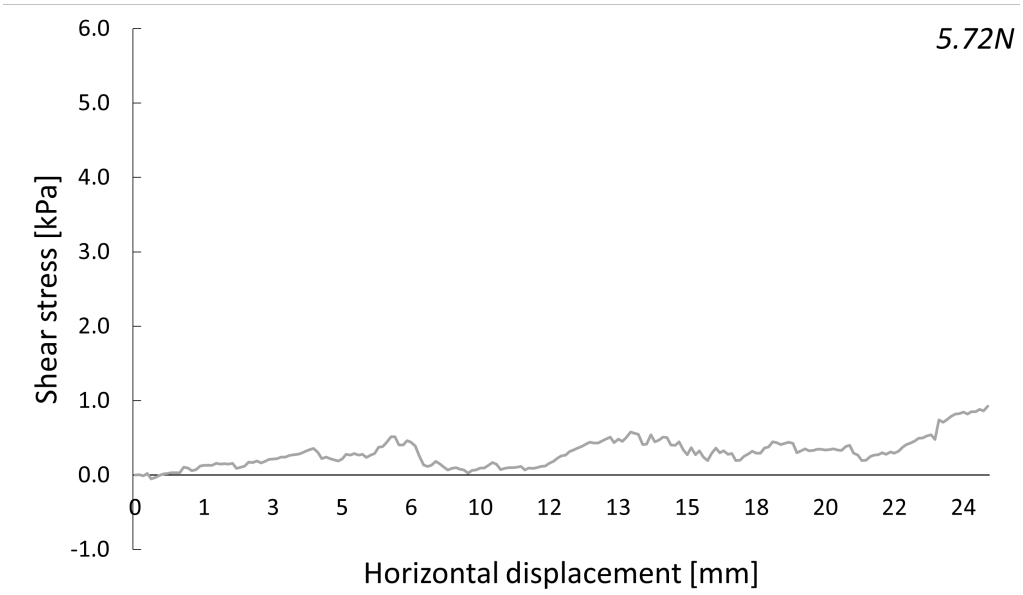

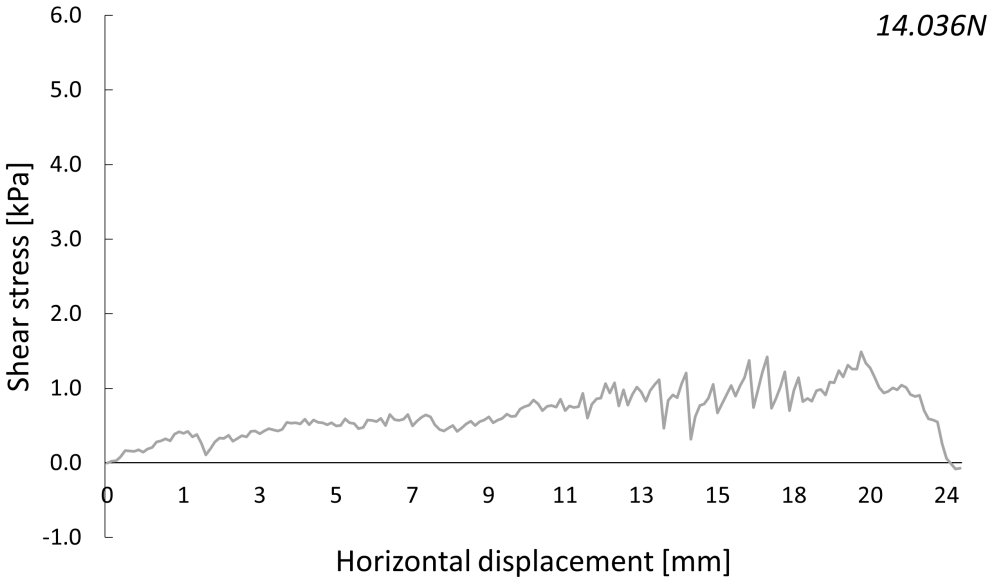

Volume fraction 0.48

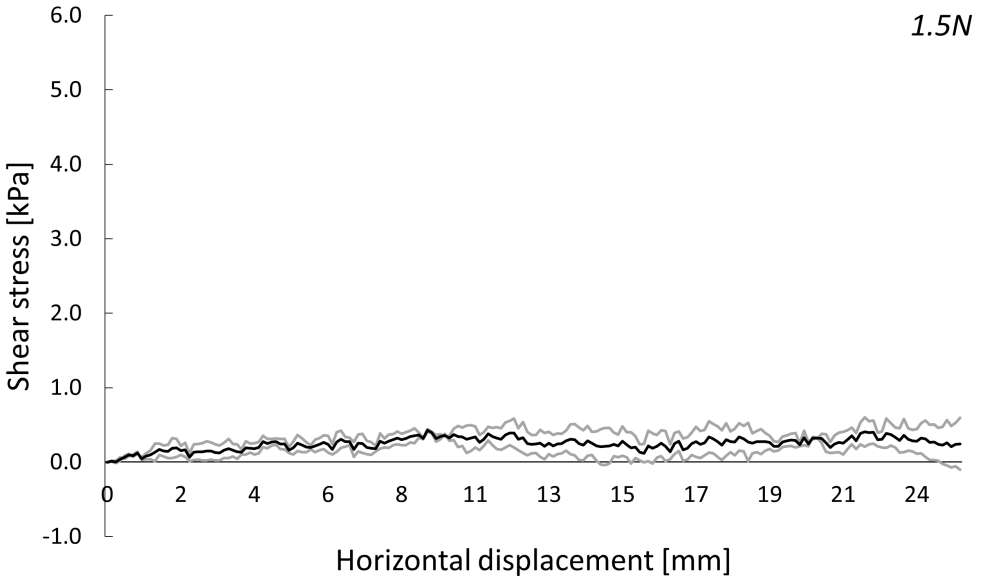

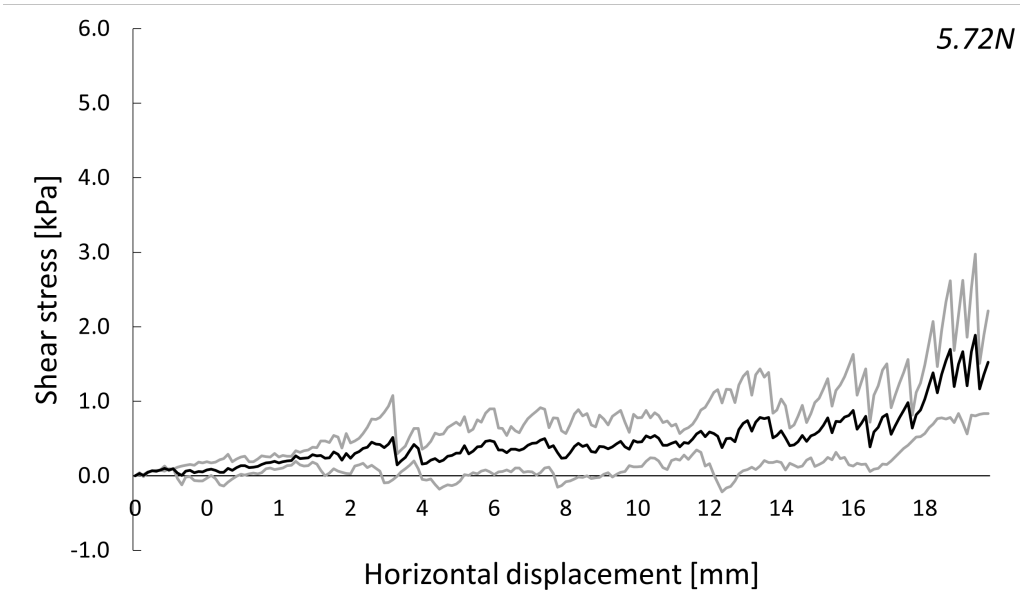
5.72N
Shear stress [kPa]
6.0
5.0
4.0
3.0
2.0
1.0
0.0
-1.0
0
0
1
2
4
6
8
10
12
14
16
18
Horizontal displacement [mm]

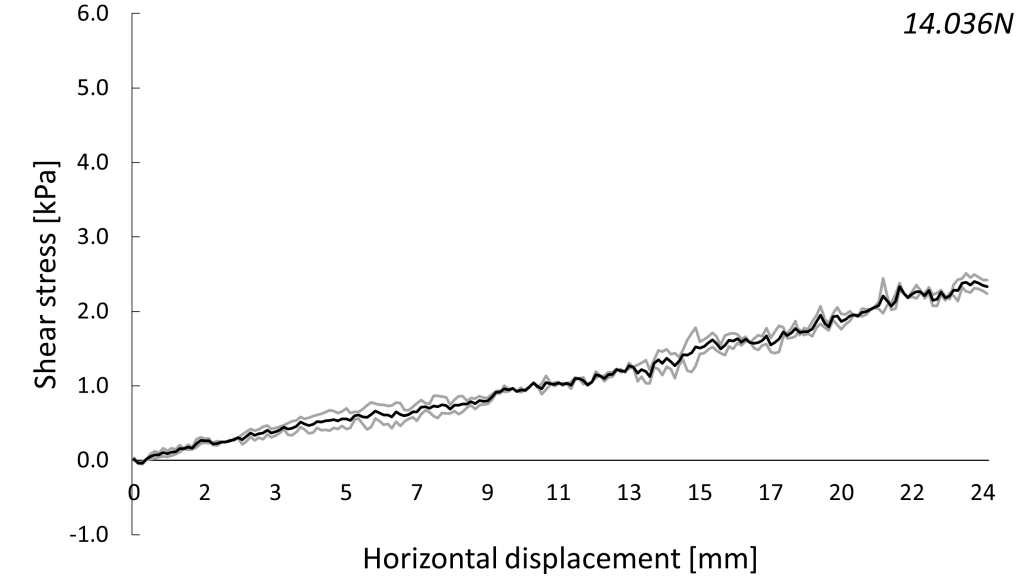
14.036N
Shear stress [kPa]
6.0
5.0
4.0
3.0
2.0
1.0
0.0
-1.0
0
2
3
5
7
9
11
13
15
17
20
22
24
Horizontal displacement [mm]

Volume fraction 0.52

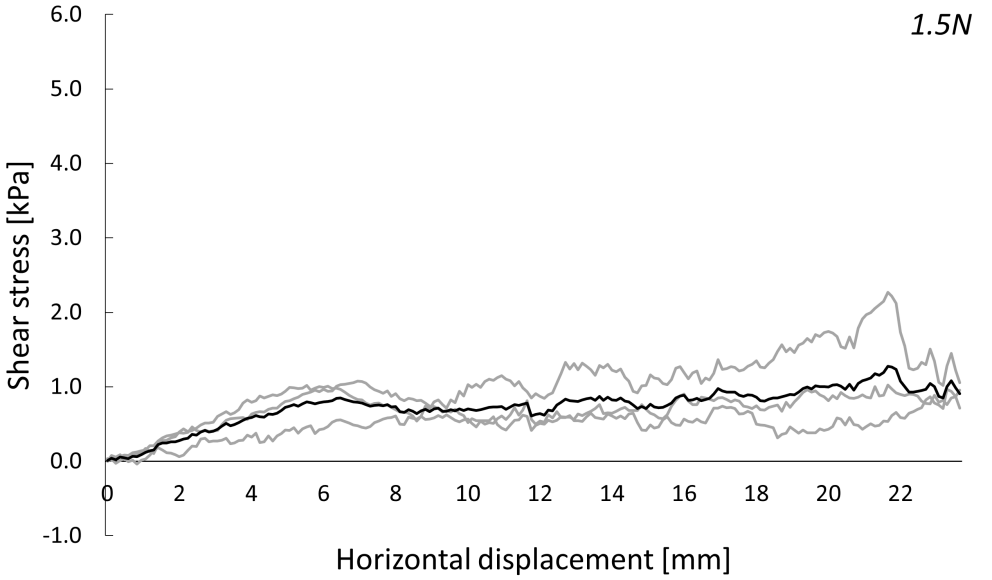

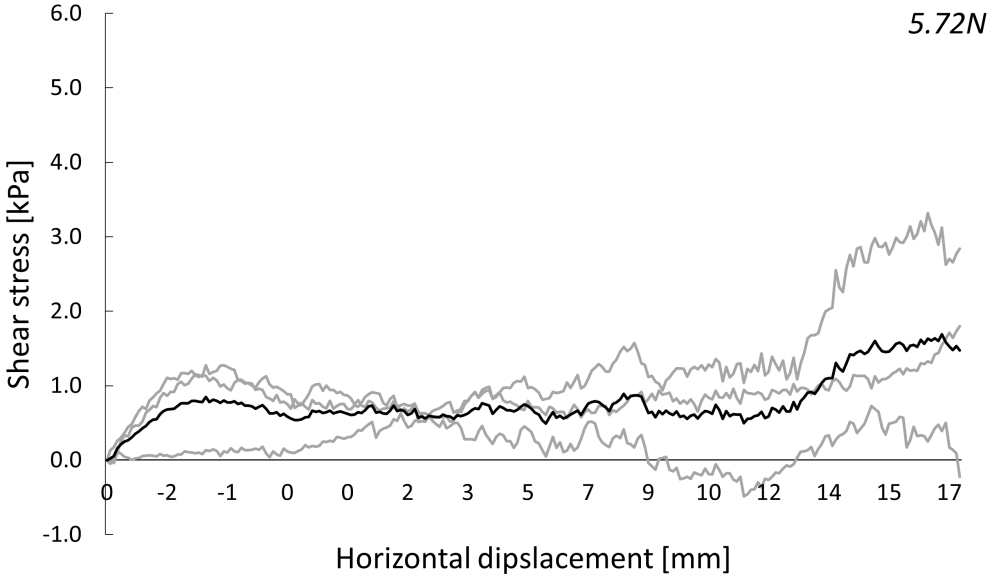

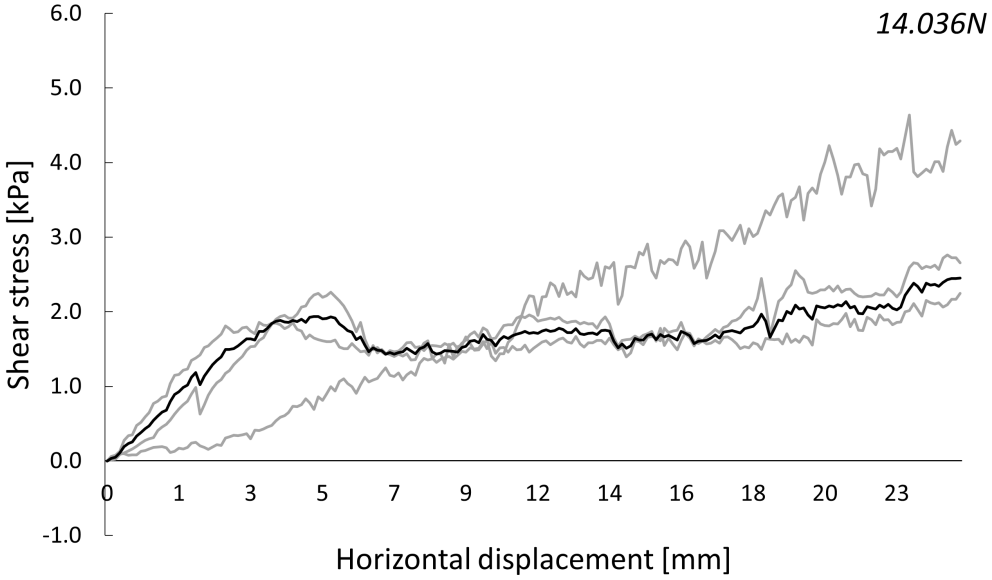

Volume fraction 0.55

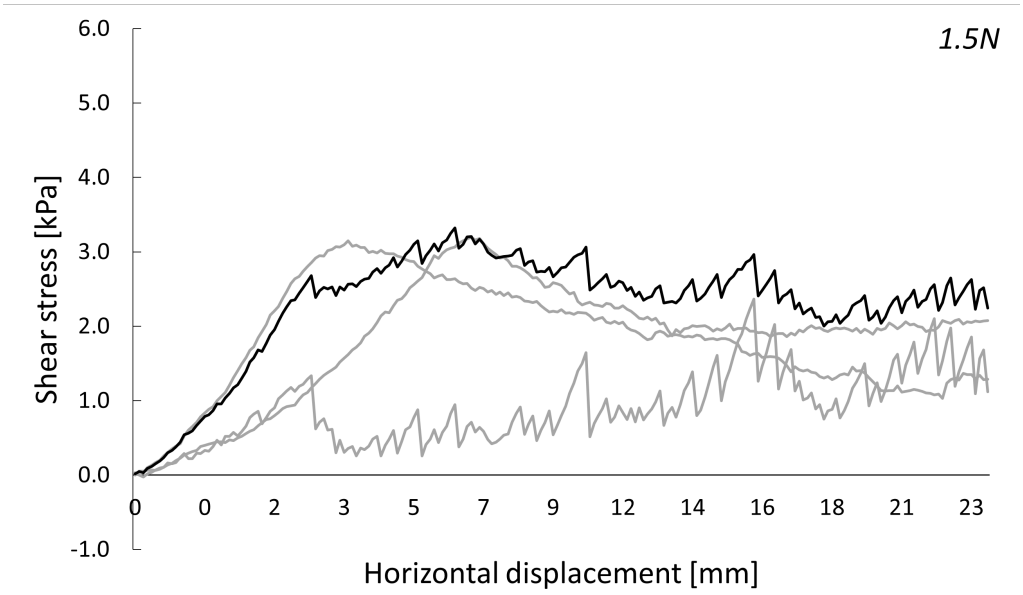

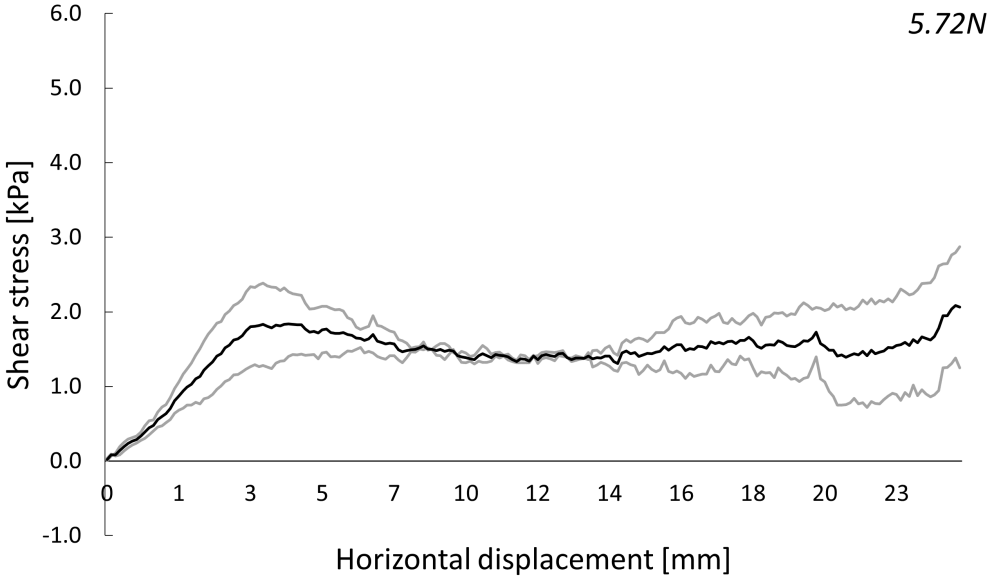
5.72N
Shear stress [kPa]
6.0
5.0
4.0
3.0
2.0
1.0
0.0
-1.0
0
1
3
5
7
10
12
14
16
18
20
23
Horizontal displacement [mm]

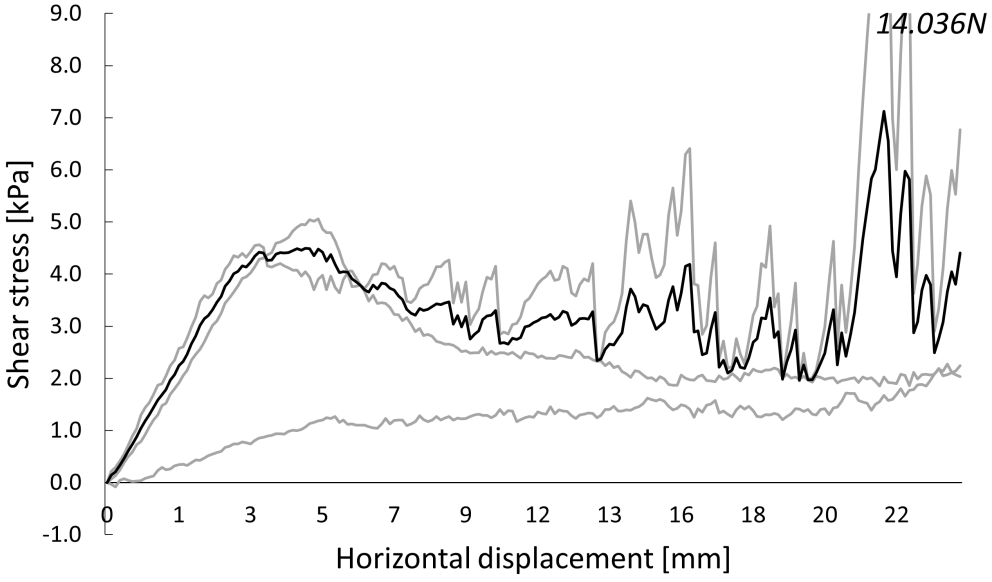
14.036N
Shear stress [kPa]
9.0
8.0
7.0
6.0
5.0
4.0
3.0
2.0
1.0
0.0
-1.0
0
1
3
5
7
9
12
13
16
18
20
22
Horizontal displacement [mm]

Mixture CS-2

Volume fraction 0.27

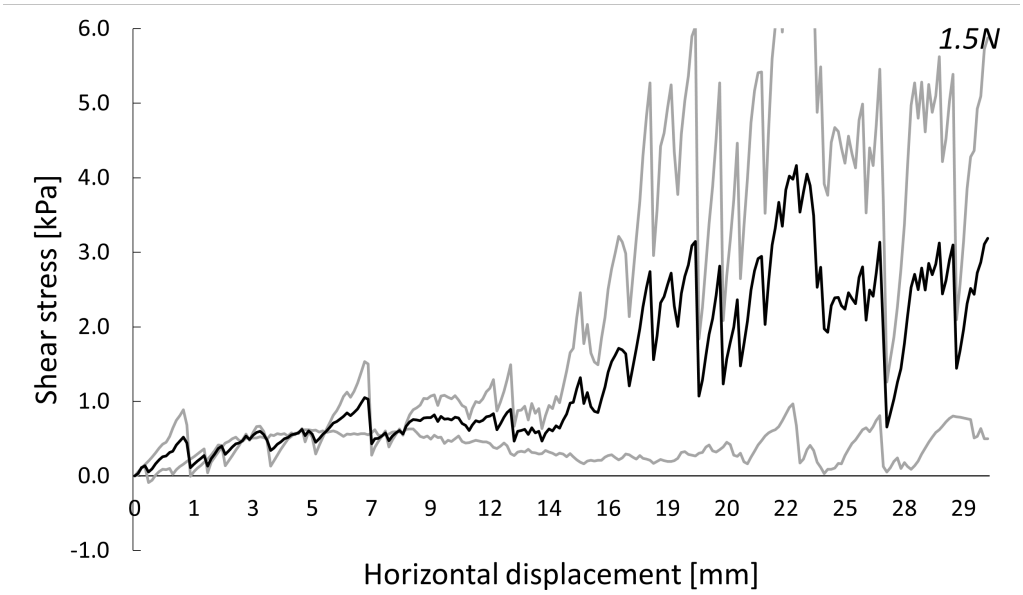

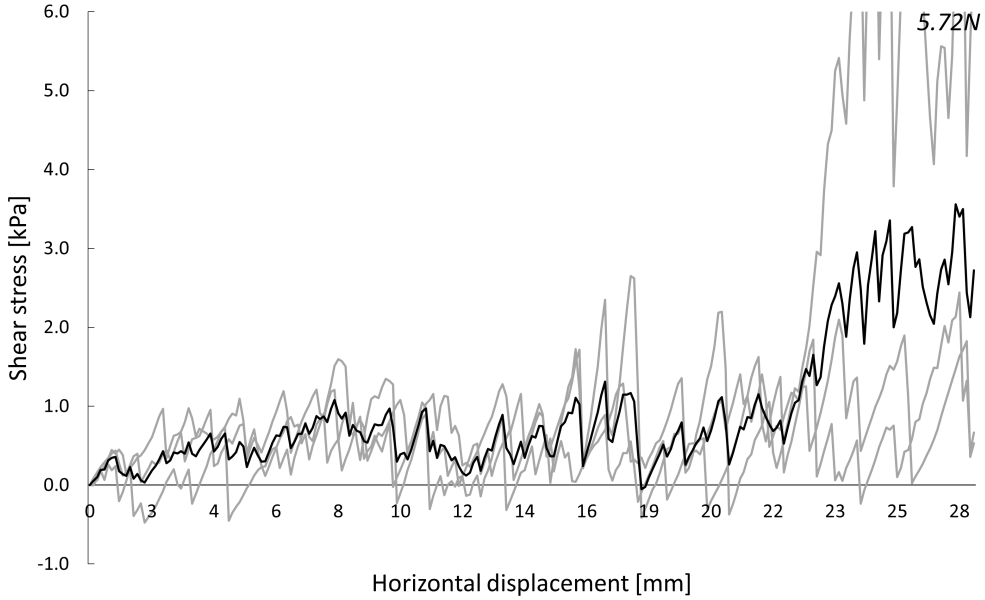

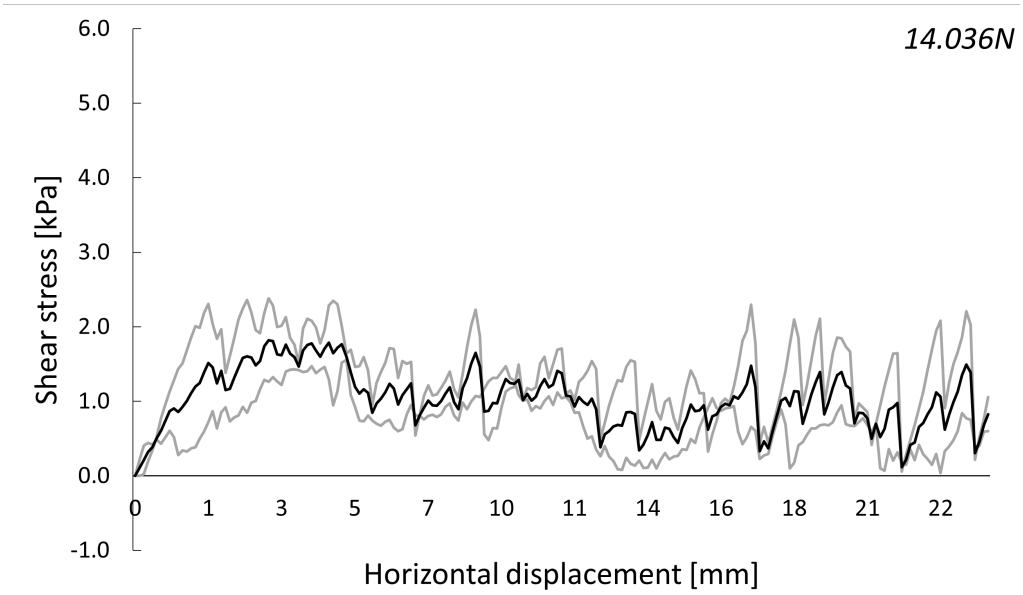

Volume fraction 0.35

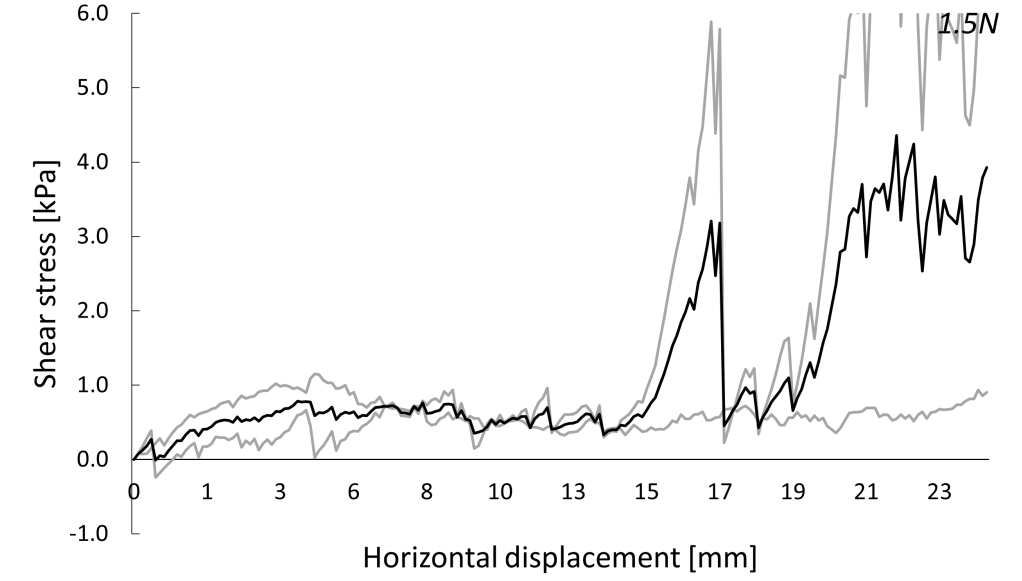

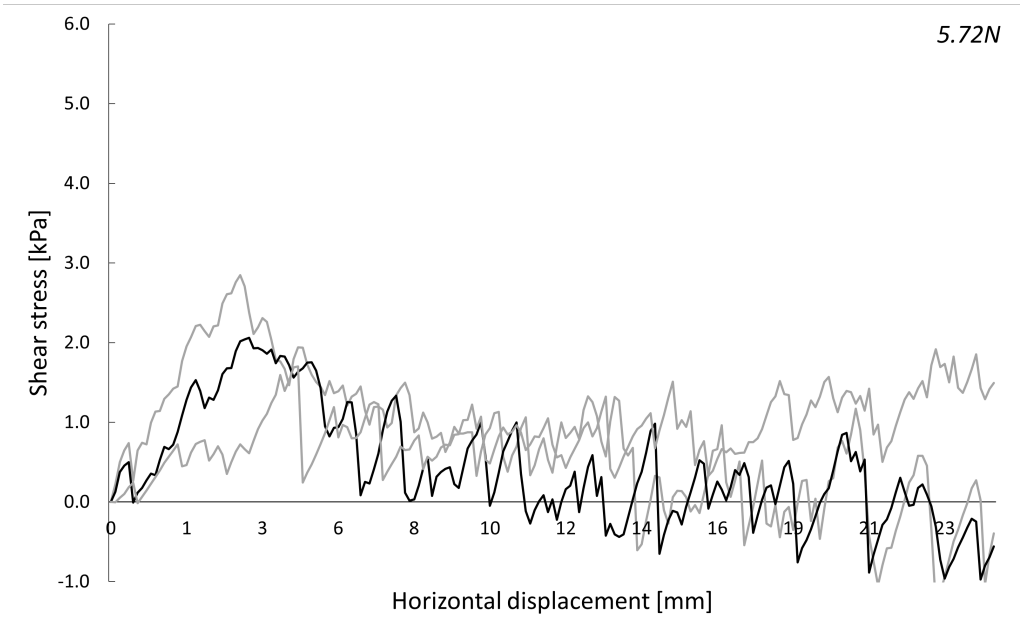
5.72N
Shear stress [kPa]
6.0
5.0
4.0
3.0
2.0
1.0
0.0
-1.0
0
1
3
6
8
10
12
14
16
19
21
23
Horizontal displacement [mm]

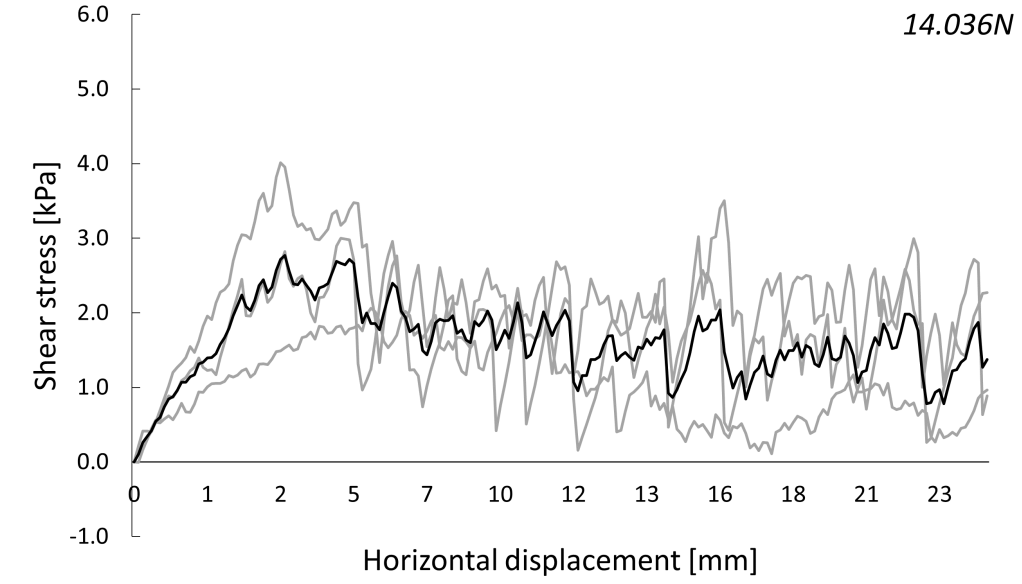
14.036N
Shear stress [kPa]
6.0
5.0
4.0
3.0
2.0
1.0
0.0
-1.0
0
1
2
5
7
10
12
13
16
18
21
23
Horizontal displacement [mm]

Volume fraction 0.40

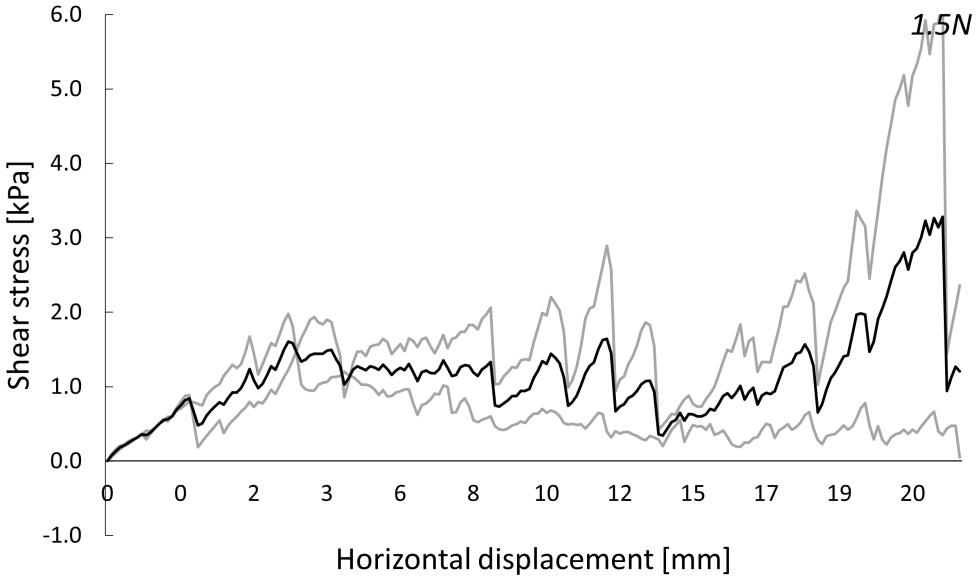

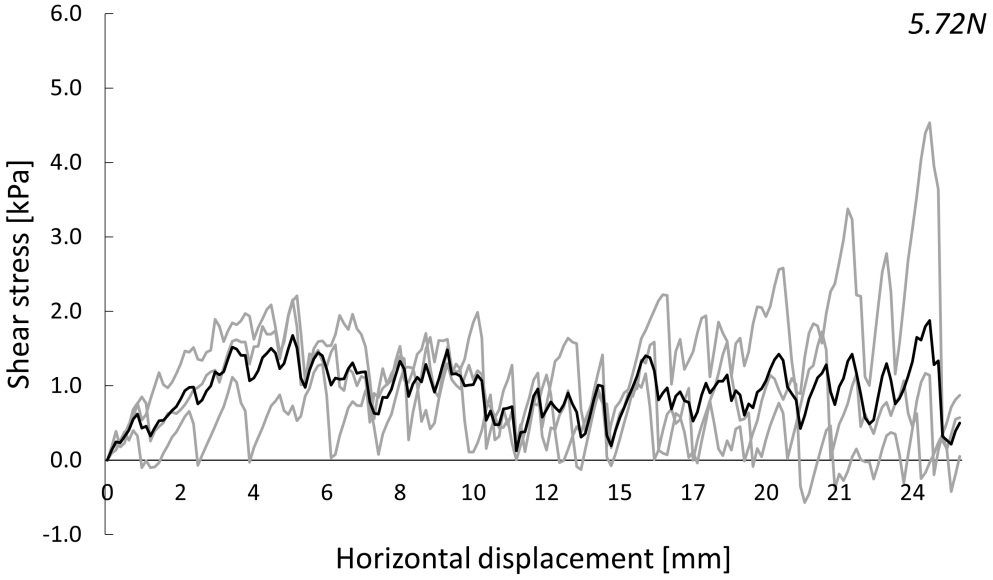

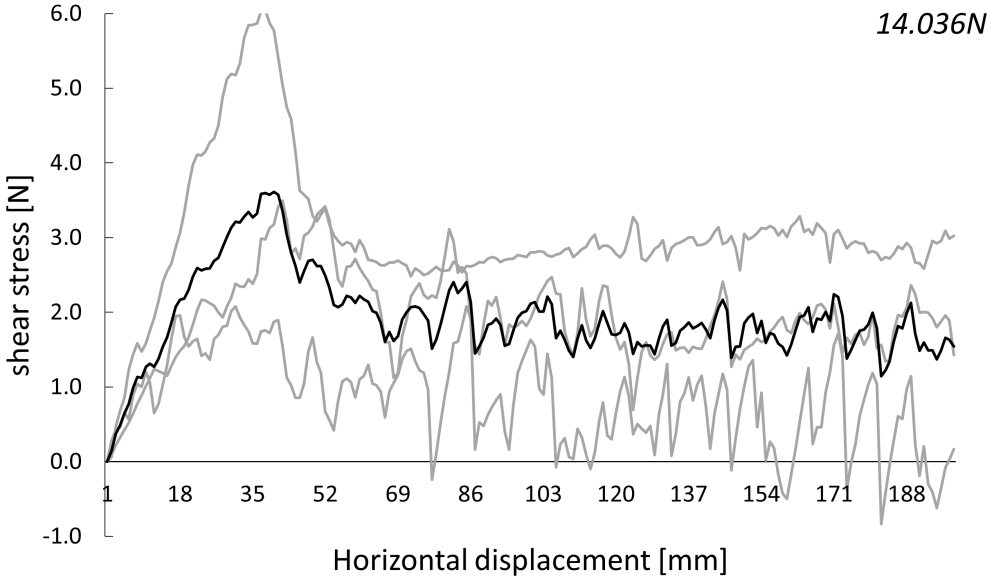

Volume fraction 0.47

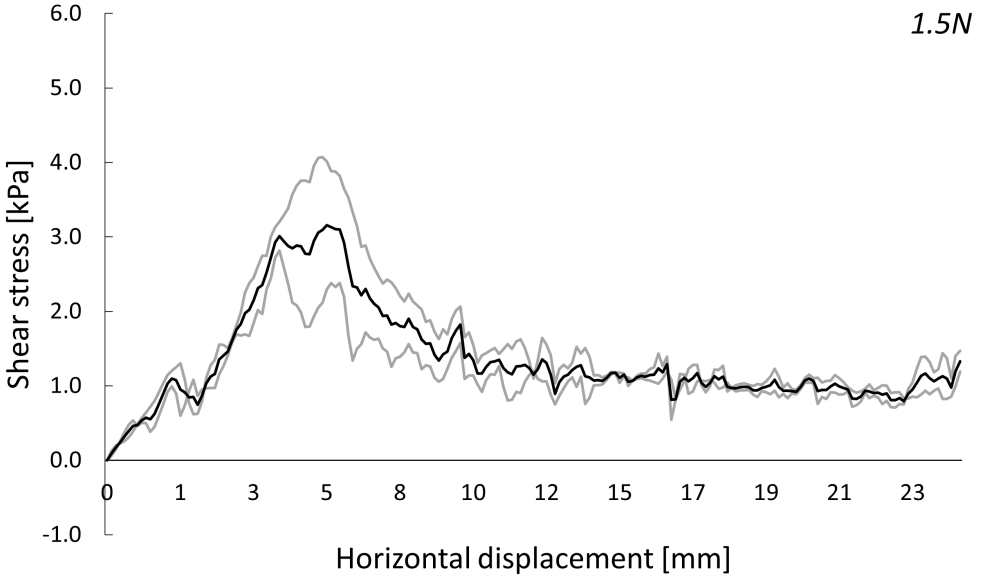

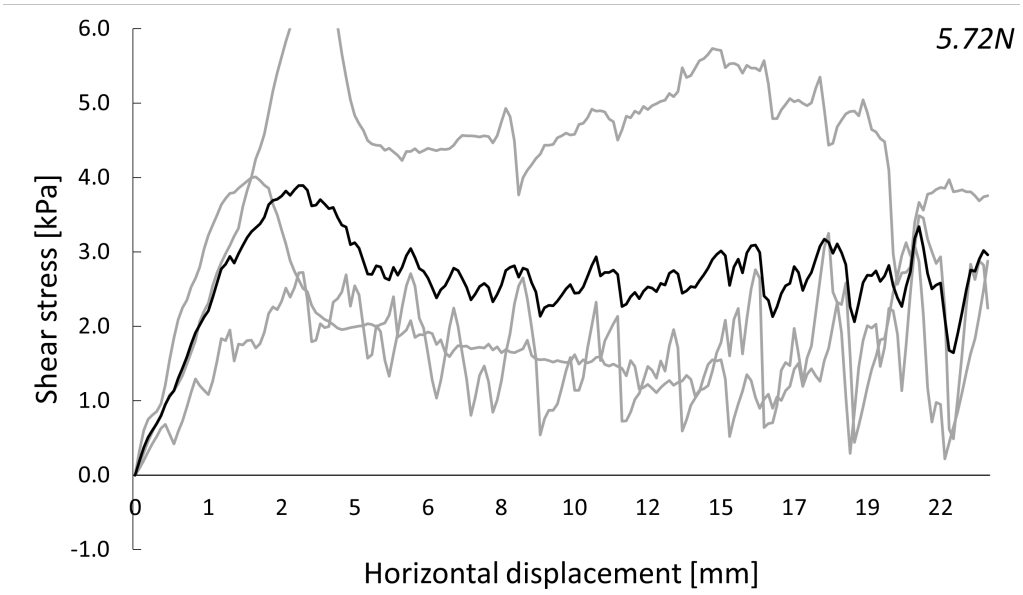
5.72N
Shear stress [kPa]
6.0
5.0
4.0
3.0
2.0
1.0
0.0
-1.0
0
1
2
5
6
8
10
12
15
17
19
22
Horizontal displacement [mm]

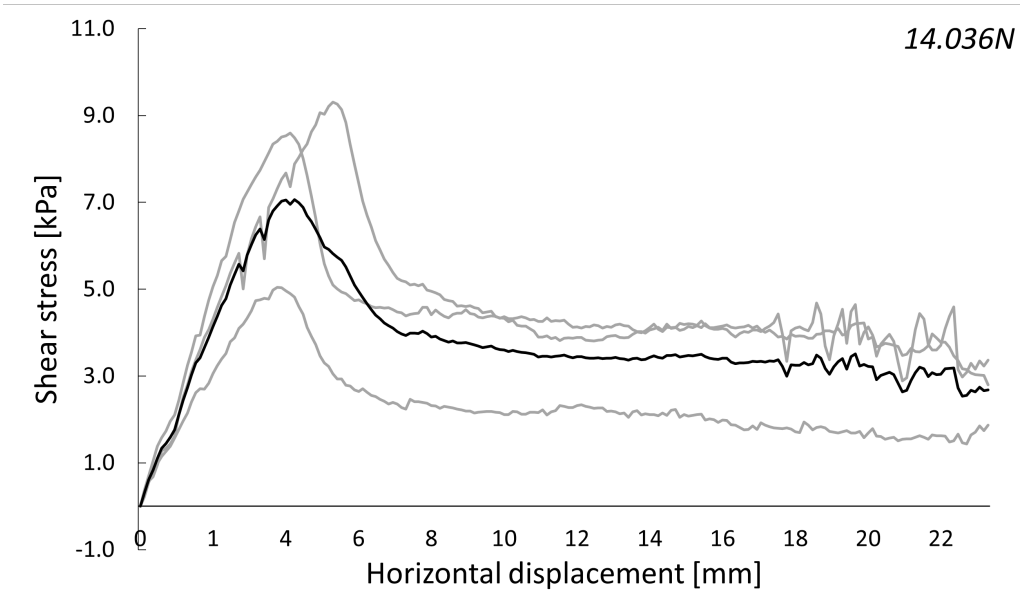
14.036N
Shear stress [kPa]
11.0
9.0
7.0
5.0
3.0
1.0
-1.0
0
1
4
6
8
10
12
14
16
18
20
22
Horizontal displacement [mm]

Volume fraction 0.55

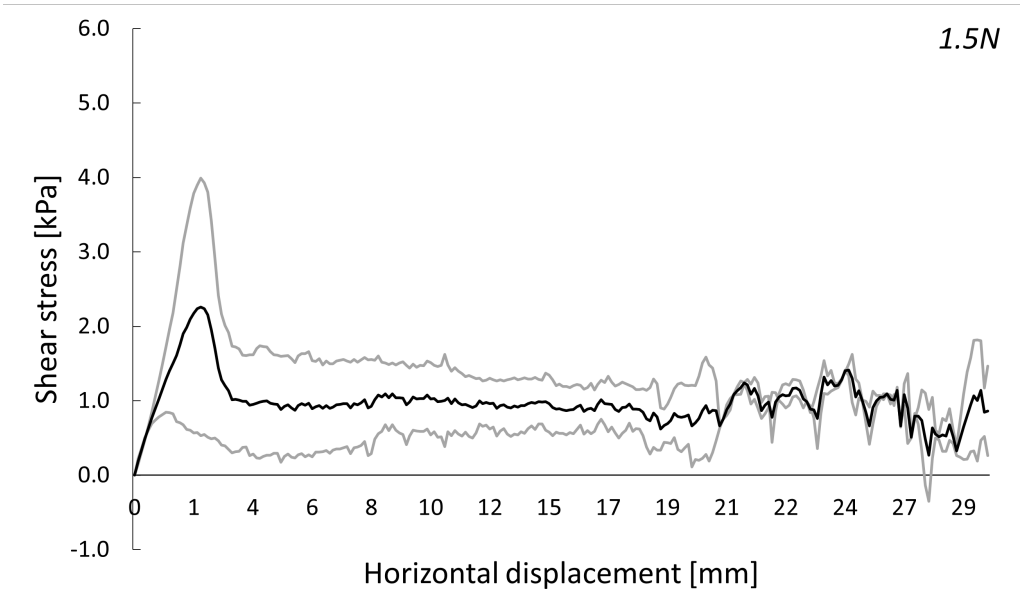

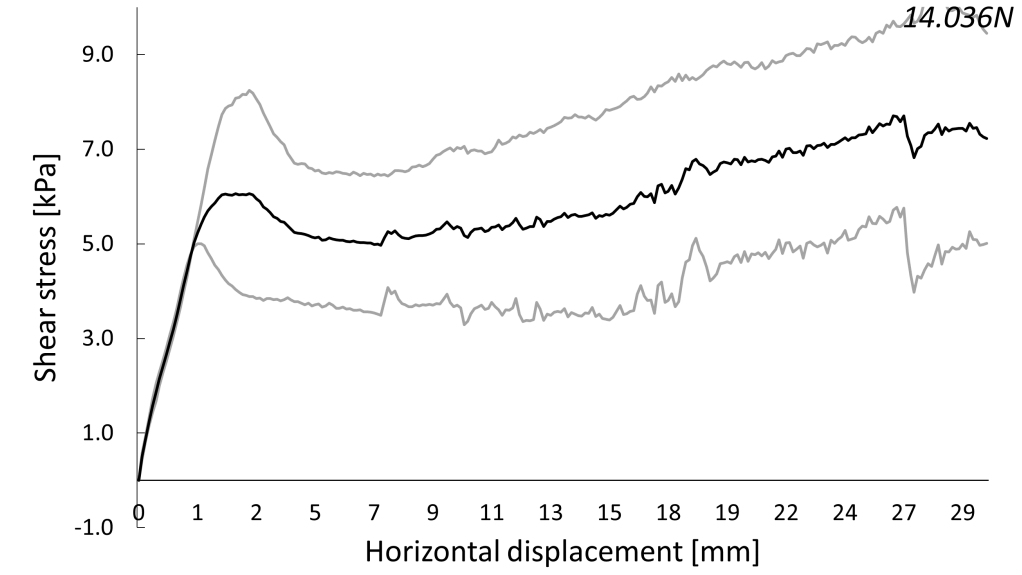

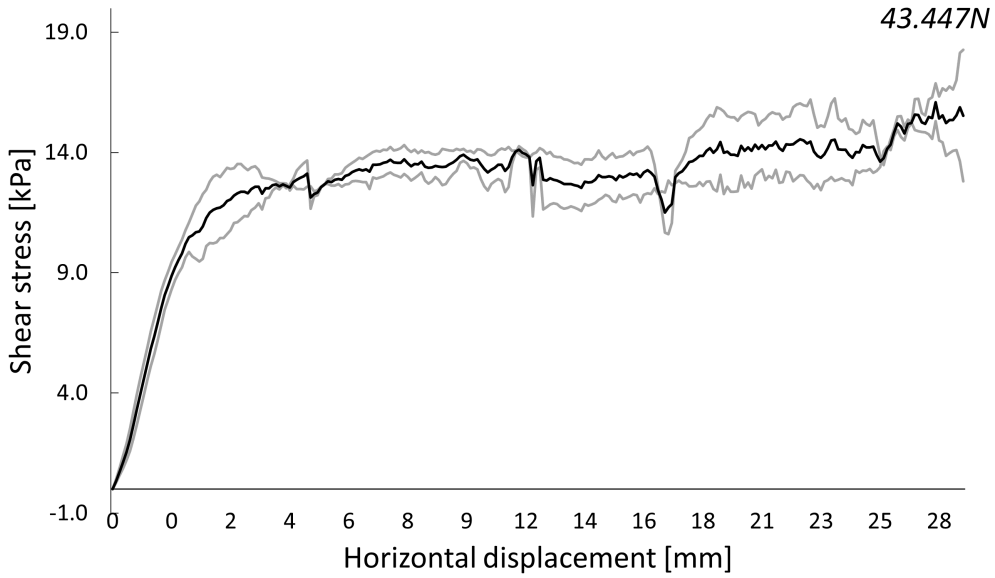
43.447N
19.0
14.0
9.0
4.0
-1.0
Shear stress [kPa]
0
0
2
4
6
8
9
12
14
16
18
21
23
25
28
Horizontal displacement [mm]